The interaction between climate and ice sheets: with special reference to the boundary layer of the ablation zone.

Alison Hall

PhD Thesis

1992

Department of Meteorology,
University of Edinburgh,
The King's Buildings,
Edinburgh,
EH9 3JZ

Declaration

This thesis has been composed by myself
and the work it contains is my own

Acknowledgements

I would like to acknowledge several people who have helped me with this thesis. Firstly my supervisors, Keith Weston for his advice, encouragement and meticulous checking of my work, and Geoffrey Boulton for setting up the project and guiding me in the right direction in the initial stages. Also Charles Duncan and Bob Harwood for their useful comments on my annual written reports.

Secondly, I would like to thank several people in the geology department for revealing the mysteries of ice sheets, particularly Richard Hindmarsh, Tony Payne, and Karen Dobbie, and Nick Hulton in the geography department.

I would also like to thank Rebecca Dale for painstakingly typing in alot of very boring numbers to the computer, and for supporting me and bringing me back into the real world when my thesis seemed to take over.

I would like to thank my friends outside of the department for their support and friendship throughout the 3 years I spent working on this thesis, without them it wouldn't exist.

This work was funded by the Natural Environment Research Council.

Contents

Abstract

1 Introduction and Background **11**

1.1 Mechanisms of Ice-Atmosphere Interaction 12

1.1.1 Ice-Albedo Feedback 15

1.1.2 Height-Mass Balance Feedback 16

1.1.3 Interaction with Mean Zonal Flow 17

1.1.4 Bedrock Adjustment 18

1.1.5 Carbon Dioxide and Ocean Circulation 18

1.2 How Can We Find Out More? 20

1.2.1 A Climatologists Perspective 20

1.2.2 Glaciologists Perspective 23

1.3 The Aims of the Thesis 29

1.3.1 What Does an Ice Sheet Need? 29

1.3.2 How these Needs will be Investigated. 30

2 The real climate over ice sheets **32**

2.1 The Climate of Antarctica 36

2.1.1 Radiation and Temperature 37

2.1.2 Mass Balance 50

2.1.3 Wind 52

2.2 The Climate of Greenland 58

2.2.1 Temperature and Radiation 62

2.2.2 Mass Balance 67

2.2.3 Wind 71

2.3 Summary 71

3 The Climate Over Model Ice Sheets **77**

3.1 Description of the GCM's. 78

3.1.1 The Met.O GCM 79

3.1.2 The NCAR CCM 80

3.2 The Simulated Climate over Antarctica 81

3.2.1 Surface Temperature and Radiation 84

3.2.2 Mass Balance 104

3.2.3 Wind and Pressure 108

3.3 The Simulated Climate over Greenland 111

3.3.1 Radiation 121

3.3.2 Mass Balance 124

3.4 Wind and Pressure 129

3.5 Does it matter? - Summary and Conclusion 129

4 A Slab Model over the Glacial Slopes **133**

4.1 Aim of the Model 133

4.1.1 Which boundary layer characteristics may be important? . 134

4.1.2 Previous Investigations of the Boundary Layer 135

4.2 Using the Observations as Constraints on a Slab Model 138

4.3 The Slab Model Formulation 142

4.3.1 The Idealised Boundary Layer 142

4.3.2 The Governing Equations 147

4.3.3 The Profile Factors 149

4.3.4 Parameterisation of Surface Friction 152

4.3.5 Entrainment with an Inverse Richardson Number Dependence153

4.3.6 Initialisation of the Model 154

4.4 Sensitivity Studies 155

4.4.1 Profile Factors $[S_1, S_2, S_3]$ 157

4.4.2 The Resolution of V 161

4.4.3 Drag coefficient$[C_d]$ 161

4.4.4 Sensitivity to Changes in the Initial Conditions 163

4.5 Summary and Conclusions 165

5 Results of the Experiments with the Slab Model 168

5.1 Sensitivity to Prescribed Boundary Conditions 169

5.1.1 The effect of the Geostrophic Wind [Vg] 169

5.1.2 The effect of Stability of the Air [γ] 171

5.1.3 The effect of Radiative Cooling 171

5.2 The Parameterisation of Entrainment 174

5.2.1 Type 1 Entrainment - The Turbulent Kinetic Energy Budget of the Whole Boundary Layer. 177

5.2.2 Type 2 entrainment - Entrainment Governed by Diffusion. 190

5.2.3 The Effect of Entrainment on the Evolution of the Boundary Layer 196

5.2.4 Comparison of the two methods 198

5.3 A Look at the Boundary Conditions from Different Ice Sheets . . 202

5.3.1 Changing the Surface Profile. 202

5.3.2 Past Ice Sheets 210

5.4 Conclusions 222

5.4.1 Summary 225

6 Conclusions **227**

6.1 Main Findings 227

6.1.1 Model Findings 229

6.2 Future Work 238

A Glossary of Terms 252

B Key to Mathematical Symbols 256

Abstract

Investigations of the interaction between climate and ice sheets were originally based on the orbital theory of the ice ages, and arose through a desire to understand the glacial cycles. More recently, interest has been stimulated in this field, with concern of global warming and the role of ice sheets with respect to future climatic change. The work of glaciologists shows that ice sheet models are very sensitive to the climate of the ablation zone. Studies by climatologists tend to look at the larger scale climate, concentrating on accumulation, rather than ablation patterns. This work looks at the way in which climate models can be used to simulate the climate over an ice sheet, in order to assess the climatic variables most sensitive to ice sheet evolution.

Data of the climate over the present day ice sheets in Antarctica and Greenland have been compiled and presented in a form suitable for comparison with GCM data. The work shows that GCM's cannot reproduce the temperature field, and boundary layer structure sufficiently accurately to provide boundary conditions for an ice sheet model.

A slab model is developed and used over the glacial slopes to investigate the way in which the boundary layer may affect the ablation of the ice. Over the glacial slopes, the boundary layer flow is turbulent and characterised by entrainment of warm air from above. The rate of entrainment governs the depth, temperature and wind regime of the boundary layer. Two new types of entrainment parameterisation are investigated, and compared to the laboratory derived formulation of Ellison & Turner (1959). Experiments show that the method of parameterisation of entrainment is not important, although the coefficients derived in the laboratory tend to be too high; this suggests that there is more loss of TKE from

the boundary layer on the glacial slopes, than empirical data from the laboratory suggests.

The model is run using surface profiles from present ice sheets, as well as reconstructed profiles from the Laurentide ice sheet at the last glacial maximum. The model is used to look at the climatic parameters which influence the ablation of ice, as well as the way in which the ice sheet itself may influence the climate of the boundary layer. Conclusions show that the evolution of ice depends on a balance between the upper geostrophic wind, the boundary layer development, ice sheet shape and surface radiation budget. If an ice sheet steepens as it retreats, the air accelerates, producing a warmer boundary layer via entrainment. This will enhance the steepening process, and increase the rate of retreat of the ice.

Chapter 1

Introduction and Background

The coupling between climate and ice sheets is a long established area of study. Over 100 years ago, Croll looked at the relationship betweeen the Earths orbit and the geological climate record. In 1941, Milankovitch proposed his orbital theory, which for many years was supported only by simple energy balance climate models. More recently, interest has been stimulated in this field with concern of global warming and the role of ice sheets with respect to future climate change. This requires an understanding of the way in which ice sheets have evolved in the past. Advances in numerical techniques and increased computer resources, endorsed by more accurate knowledge of the geochronological record, have lead to a greater understanding of the way in which ice sheets and climate have interacted in the past, and the way in which they may behave in the future. However, the large discrepancy in the timescales between the atmosphere and the cryosphere means that fully coupled models cannot be achieved, and the mechanisms of interaction are still poorly understood. The inaccessibility of present day ice sheets, means that ice sheet climates are not well documented, which is an added restriction when trying to understand the climates of the past. This thesis will look at the climate over present day ice sheets; in particular it will investigate the nature of

the atmospheric boundary layer in order to understand the way in which it may influence the evolution of ice. Due to the interdisciplinary nature of this work a glossary of terms has been included in appendix 5.4.1. Terms which are included in the glossary will be marked by a '† ' the first time they are used in each chapter. Appendix 2 gives a key to mathematical symbols used in the text.

1.1 Mechanisms of Ice-Atmosphere Interaction

The Milankovitch theory argues that ice ages are a response to orbital variations of the Earth around the sun, caused by changes in eccentricity, obliquity and precessional index. Support for the theory has been found in the palaeoclimatic record. Hays et al (1976) considered the Earth as a system which receives a forcing signal, the Milankovitch radiation variations (δQ), and produces an output signal, the geological climate record. There is much discussion as to the specific radiation parameters which characterise the input signal. Milankovitch considered the amount of summer insolation at 65°N to be critical for ice growth and this was used by Hays et al (1976) as their input signal, shown in fig. 1.1a. The output signal was provided from analysis of 3 palaeoclimatic indicators, one of which was the $\delta^{18}O$ record in deep sea sediment cores. The $\delta^{18}O$ record represents the ratio between the concentration of the heavy oxygen isotope ^{18}O to that of the lighter ^{16}O. This is considered to represent the changes in volume of ice as preferential evaporation of ^{16}O from the oceans becomes locked in the ice sheets, leaving the ocean anomalously rich in ^{18}O during an ice age. Since the investigations by Hays et al, Imbrie et al (1984) have constructed a more complete time series of the $\delta^{18}O$ spectrum, as part of the SPECMAP project, shown in fig. 1.1b. Regular cycles can clearly be seen in the climate signal. However whereas the dominant power of the climate signal is at 100k years (fig. 1.2b), the orbital variations have dominant

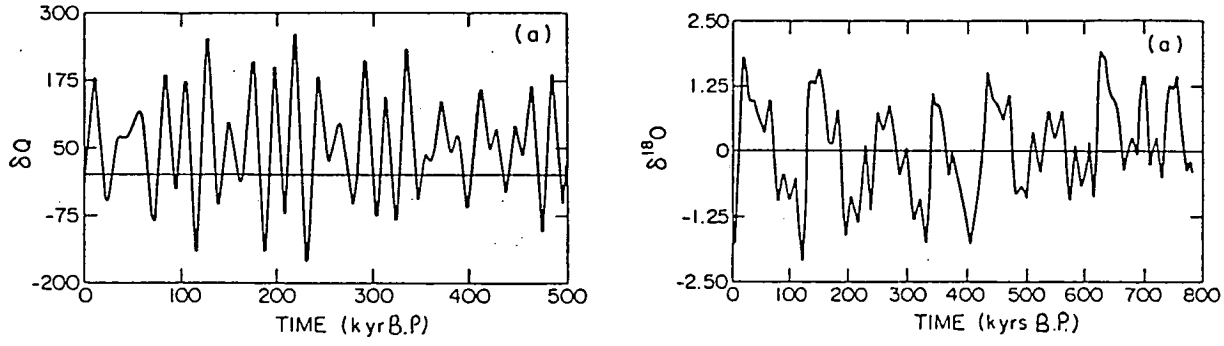

(a) (b)

Figure 1.1: (a)The forcing function of the climate system; Milankovitch summer insolation anomalies at 65°N results in the climatic signal given in (b); the $\delta^{18}O$ spectrum (Hyde & Peltier 1985, after Imbrie et al 1984).

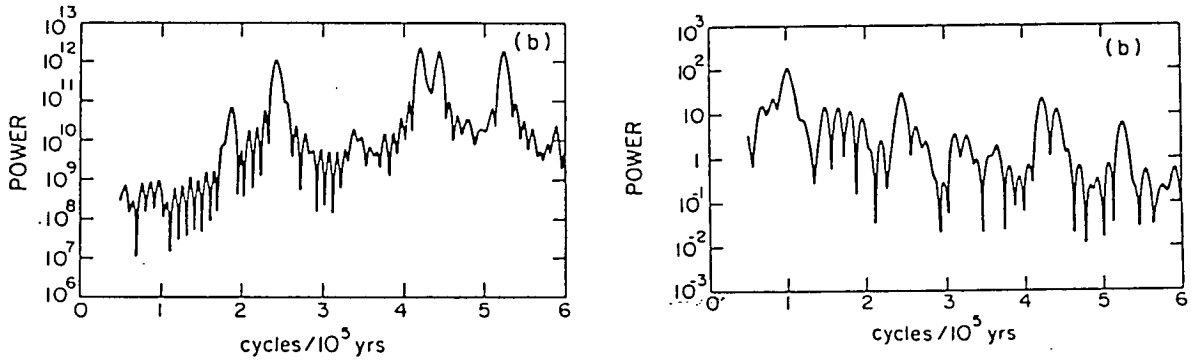

(a) Orbital Signal (b) Climate Signal

Figure 1.2: The power spectra of the climate (output) signal and the orbital (input) signal (Hyde & Peltier 1985).

powers at 41ky, 23ky and 19ky with a very weak signal at 100ky (fig. 1.2a). This has lead to discussions of non-linearity within the climate system and suggestions of other mechanisms which may be responsible for the 100ky signal. The existence of additional feedbacks within the climate system is made more apparent by the palaeoclimatic record, which suggests that the fall in temperature associated with an ice age is much greater than that produced by the orbital variations alone. The growth and decay of ice sheets is not symmetrical in time. The $\delta^{18}O$ series shows the 'sawtooth' nature of the evolution. This slow steady build up of ice followed by a rapid decay, although not apparent in every cycle, is present in the 2 most recent, and to a lesser extent between 300 and 500 kya. The variable nature of the evolution suggests that there is more than one mechanism, responsible for the observed pattern, producing more than one response time.

Ice sheet models have been shown to be extremely sensitive to climate parameterisation, particularly in the ablation zone.† Ablation† is primarily determined by boundary layer characteristics and the main area of interest for this work is therefore the boundary layer of the ablation zone. The boundary layer over ice sheets tend to be well defined, characterised by a strong inversion which, over the glacial slopes produces a buoyancy force to drive the strong winds which drain downslope and over the ice margin.† The flux of cold air from Antarctica is of the order of $2.2 \times 10^{10} m^3 s^{-1}$, such a large flux of cold air is an important component of the glacial climate. It removes the cold air from the interior of the ice influencing not only the climate of the glacial slopes but also that at, and beyond the margin where it mixes with relatively warm air.

The following section aims to review the main feedback mechanisms that have been suggested as being responsible for the advance and retreat of ice sheets. Some of the feedback mechanisms are postulated as acting independently of Milankovitch

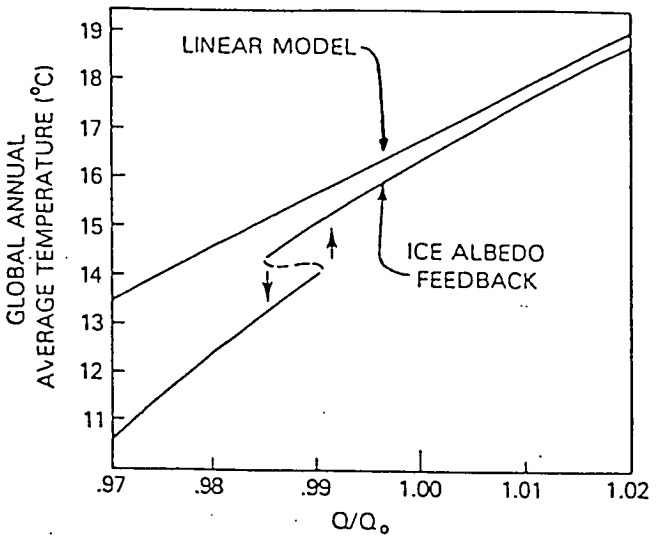

Figure 1.3: The variation of surface temperature with solar constant for a linear model and for the ice albedo feedback model of North et al (1983) showing the hysteresis effect.

forcing, while others are said to occur in direct response to the orbital variations, enhancing the response of the climate system. The final section of the chapter will look at the approaches which climatologists and glaciologists have taken in order to understand the interaction further, and the way in which this understanding can be used as a way forward in this study.

1.1.1 Ice-Albedo Feedback

The ice-albedo feedback has been investigated using climate models. When the surface temperature falls below freezing, precipitation falls as snow, which eventually forms land ice, and the ocean surface begins to freeze forming sea ice. This state persists while the temperatures remain low, leading to much higher albedos, so less solar radiation is absorbed, and the temperature falls further. The precise nature of this feedback within the atmosphere-cryosphere system is poorly understood. Experiments with energy balance climate models show a hysteresis effect (eg. North et al 1983), shown in fig. 1.3. When the solar constant is decreased, the temperature falls, and the ice slowly advances until the solar constant reaches 0.985 its present value. At this point the higher albedo produces a further drop in

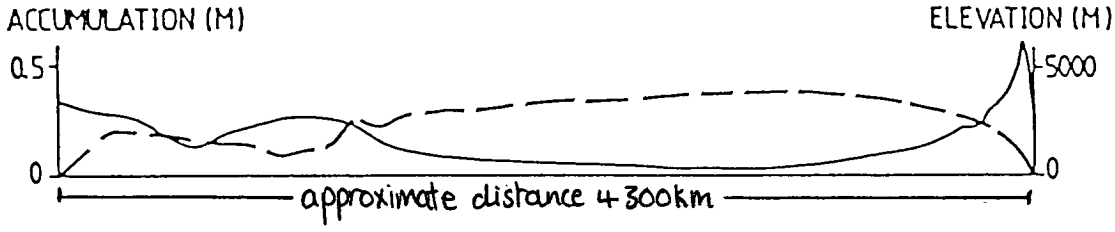

Figure 1.4: The accumulation profile for Antarctica, (Oerlemans & Van der Veen 1984): Ice elevation (— —): accumulation(———)

the temperature and the climate undergoes an abrupt transition to a lower state. Having reduced the solar constant to this extent, in order for the climate to return to the initial curve, the solar constant must be increased beyond 0.985 to 0.99 of its present value. Without the ice-albedo feedback the 0°C isotherm remains too far north compared to the palaeoclimatic evidence.

1.1.2 Height-Mass Balance Feedback

The interaction between height and mass balance† appears to be important in the early stages of growth of an ice sheet (Oerlemans 1980). Once the ice sheet begins to grow, enforced uplift of air increases precipitation and encourages growth into the prevailing winds (Oerlemans 1980, Oerlemans & Van der Veen 1984). The accumulation† profile for Antarctica shown in fig. 1.4 has a maximum at around 100km from the margin of the ice, falling rapidly inland, the profile for Greenland is similar, although the decrease in the centre of the ice sheet is less severe. This increased continentality of the climate in the interior is known as the 'elevation desert' effect,† and is an important negative feedback on ice sheet growth. (Budd & Smith 1979, Sugden 1977).

1.1.3 Interaction with Mean Zonal Flow

Continental ice sheets extend sufficiently high in the atmosphere that they are able to influence the upper atmospheric waves in a similar manner to the major mountain ranges of the present day climate. The results of experiments with climate models suggest that there is a strong atmospheric feedback initiated by the growth of large ice sheets (eg. Manabe & Brocolli 1985, Kutzbach & Guetter 1986), which may either enhance, or restrict further ice sheet growth. Lindemans & Oerlemans (1987) used the CLIMAP dataset as boundary conditions in a 2-layer steady state primitive equation model, and estimated that the waves produced in the atmosphere by the ice age topography would produce a lowering of the ELA[†] of between 400m and 500m. This is of the same order of magnitude required to initiate the large northern hemisphere ice sheets.

It is not only the generation of waves which is important, but also the location of the jet stream; GCM's show a split in the jet stream around major ice sheets (Kutzbach & Guetter 1986, Manabe & Brocolli 1985). The strong temperature gradient at the southern margin of the ice sheet and at the edge of the sea ice over the ocean, encourages a strengthening and equatorward displacement of the jet as the ice sheet advances, (Oerlemans & Vernaker 1981). This produces a zone of enhanced precipitation at the edge of the ice which encourages further advance of the ice sheet. Oerlemans & Vernaker (1981) found this positive feedback continued in their model until the margin reached 50°N. At this point the average mass balance over the whole ice sheet is reduced by the elevation desert effect to the extent that it causes retreat; 50°N corresponds to the latitude of maximum extent of the Laurentide ice sheet.

1.1.4 Bedrock Adjustment

Model experiments suggest that once ice sheets reach continental sizes the mass balance tends to dominate over ice dynamics, making it difficult to cause retreat of the ice in the time required by the paleoclimatic record (Budd & Smith 1979). A large continental ice sheet will tend to depress the bedrock on which it is lying. This isostatic[†] adjustment of the bed tends to lag the initiation of ice advance; if it is permitted to occur immediately in the model, the ice sheet remains below the snowline preventing ice growth, and if the lag is too great the ice sheet becomes too large. The change in elevation produced by isostatic adjustment, is of the same order of magnitude as the change in ELA responsible for the initial growth of the ice sheet (Budd & Smith 1979). In this manner bedrock adjustment is able to reproduce the rapid retreat of ice seen in the $\delta^{18}O$ record. Hyde & Peltier (1985) use a model of the atmosphere-cryosphere-lithosphere system to simulate ice age climate and demonstrate the important interactions between elevation desert, mass balance feedback, and bedrock adjustment. In the retreat of ice they found that the residual crustal depression to the south of the ice sheet encourages the ice to flow into this lower and warmer zone where ablation is high. The mass balance for the ice sheet becomes strongly negative and total collapse occurs before isostatic rebound is able to lift the ice sheet into colder air at greater elevations.

1.1.5 Carbon Dioxide and Ocean Circulation

The feedbacks mentioned above do not fully explain why the summer insolation at 65°N and the growth of ice sheets in the northern hemisphere appears to affect the global climate simultaneously, overriding the opposing effect of increased radiation in the southern hemisphere. It has been suggested that the radiational

changes which affect the atmospheric circulation are translated to large scale changes in the oceans. During the reorganisation of the ocean circulation the interaction of physical with biological and chemical processes produce a reduction in atmospheric carbon dioxide during a glacial period and an increase during the interglacial (Watson et al 1990). The actual mechanism by which the signal is translated to the oceans is still largely unknown. Broecker & Denton (1990), discuss the absence of North Atlantic Deep Water formation, which reduces the mixing of deep and surface waters, allowing greater depletion of carbon dioxide in the upper ocean by the photosynthesis of plant life. This in turn allows the ocean to absorb more carbon dioxide from the atmosphere. Thus, the initial reduction in summer radiation at 65°N peturbs the atmosphere, and is translated into a global reduction in atmospheric carbon dioxide via the oceans. Lower concentrations of atmospheric carbon dioxide lead to cooling of the atmosphere, through a reduction in the greenhouse effect, initiating a positive feedback. However, the reduction in carbon dioxide during the glacial period is not sufficient to account for the fall in temperature observed in the geological record. Palaeoclimatic evidence suggests a similar reduction in methane, also a greenhouse gas, and an increase in atmospheric dust particles, which would increase the amount of radiation reflected from the Earth. Both of these characteristics would increase the global cooling but not by the required amount. An additional problem is that the carbon dioxide curve appears to follow the $\delta^{18}O$ and therefore another forcing function is required which the carbon dioxide feedback may accentuate.

It is unclear how these effects and others, such as the cloud distributions, either individually or in combination produce the 100ky cycle of glaciations. The commonly held view is that the climate system 'flips' between modes of operation, in a similar way to the hysteresis described in section 1.1.1. Whether there are 2 or more states is not known, and whether a global warming in the future could

force a 'new' state is also a topic of discussion (Broecker & Denton 1990), but it appears that the interaction of the climate with ice sheets is a fundamental part of the system.

1.2 How Can We Find Out More?

Knowledge of the climate system has been increased by both glaciologists and climatologists. The different timescales of operation of the atmosphere and cryosphere are a barrier to fully coupled models and one of two approaches is generally taken. Glaciologists tend to have active ice sheets and a prescribed climate, while climatologists tend to look at a 'snap-shot' for the steady state climate over a fixed ice sheet. These two approaches are quite different, each has its own advantages and disadvantages and I will discuss each in turn below.

1.2.1 A Climatologists Perspective

The first verifications of the Milankovitch theory were carried out using energy balance climate models, which became more sophisticated as computer power increased. These models are useful for investigating the albedo feedback (eg. North et al 1981, 1984). At their most simple level they describe the rate of change of temperature T, in time t, for an air column of unit cross sectional area and mass m, using an energy balance equation of the form (Henderson-Sellers & McGuffie 1987),

$$mc_p \frac{\Delta T}{\Delta t} = \left(R_\downarrow - R^\uparrow\right) \tag{1.1}$$

(1.2)

$$\text{where } R_{\downarrow} = (1 - \alpha)\frac{S}{4} \text{ and } R_{\uparrow} = \epsilon\sigma T^4\tau_a$$

c_p is the specific heat capacity, $R_{\downarrow}$ is the incoming shortwave radiation, and $R_{\uparrow}$ is the outgoing longwave radiation, ϵ the emissivity of the surface, τ_a the transmissivity of the atmosphere, α the albedo and S the solar constant. So that

$$\frac{\Delta T}{\Delta t} = \frac{1}{mc_p}\left[\frac{S}{4}(1-\alpha) - \epsilon\tau\sigma T^4\right] \tag{1.3}$$

The equation can also be used over latitude zones, or for individual grid points in a model, in which case a diffusion and transport term must be introduced, and if the model is seasonal, a storage term. Over the range of temperatures experienced on Earth, the outgoing radiation can be linearised with respect to temperature such that;

$$R_{\uparrow} = \mathbf{A} + \mathbf{B}T \tag{1.4}$$

A and **B** are empirical constants which account for radiative properties of the atmosphere, cloud cover and the carbon dioxide and water vapour content etc. Incorporating these effects into the energy balance equation 1.3 gives an equation of the form (North et al 1981, 1984);

$$C(\hat{r})\frac{\partial T(\hat{r},t)}{\partial t} - \nabla\left[D_c(\lambda_s).\nabla T(\hat{r},t)\right] + \mathbf{A} + \mathbf{B}T(\hat{r},t) = Sa(\lambda_s,T)S_d(\lambda_s,T) \tag{1.5}$$

heating at the ground	Advection & Diffusion of Heat	longwave flux	shortwave inward and storage

$\hat{r}$ is a unit vector position on the Earths' surface, λ_s is the sine of the latitude, t the time of the year, T the surface temperature, C the effective heat capacity dependent on the type of surface, D_c the diffusion coefficient for heat transport,

A and **B** empirical constants (see equation 1.4), S is the solar constant, a is $(1 - \alpha)$ where α is the albedo, and S_d the solar insolation distribution function. This model was used by North et al (1983) to investigate the albedo feedback (see section 1.1.1). The land-sea distribution was prescribed and the heat capacity specified according to the surface (either land, ice or sea), in order to incorporate the ice albedo feedback, the albedo is prescribed according to latitude, but once the surface temperature falls below 0°C in the model, the albedo is given a fixed value for ice. The model is also useful for investigating the importance of the land sea distribution. For example the sea channels to the west of Greenland in the model, were critical for the maintainance of the present ice sheet. If the sea channel was removed, the continentality of the land mass was such that summer temperatures became too large and the ice retreated. These models have limitations; beyond the temperature of the surface, they do not give a great deal of insight into the climate evolution. There is no cloud variability, which is recognised as a strong influence of the surface energy balance, and in the case of the model of North et al there is no vertical variation in temperature.

General circulation models allow a much more comprehensive investigation of the climate to be carried out. However, because of the demands they make on computer time they are only able to look at the steady state conditions over fixed ice sheets (eg. Kutzbach & Guetter 1986, Manabe & Brocolli 1985, Mitchell et al 1988). These models are based on the primitive equations governing the fluxes of momentum, heat, mass and moisture. They have several layers within the atmosphere and grid points covering the whole globe. The NCAR Community Climate Model for example, has 9 sigma layers and a grid spacing of 4.4° latitude × 7.5° longitude (Kutzbach & Guetter 1986). The additional complexity of these models means they are able to give more information on the 3 dimensional structure of the atmosphere, in particular the topographic effect of ice sheets, and the influence

they have on planetary waves, discussed in section 1.1.3. The boundary conditions are prescribed for a specific climatic scenario, for which the GCM produces the steady state as output. The nature of these boundary conditions varies between models; the NCAR Community Climate Model has prescribed solar radiation, atmospheric composition, the location of ice sheets, land albedo, sea level, sea ice, and sea surface temperature (Kutzbach & Guetter 1986); other models have an interactive upper ocean eg. Manabe & Brocolli (1985), which allows sea ice locations and sea surface temperature to be determined within the model. The reliability of these steady state simulations of a transient climate system is debatable, but simulations of the present day climate illustrate the main features of the atmospheric circulation, and it seems that they are able to do the same for climates other than those of the present day, although the local variations in climate cannot be reliably predicted. Their main use is in investigating the influence of a large continental ice sheet on mean zonal flow and the splitting of the jet stream around large ice sheets, shown in fig. 1.5. The potential effect on precipitation and mass balance patterns has been discussed in section 1.1.3, but because the ice sheets of GCMs are fixed, due to limitations of computer power, the precise effect of the mass balance peturbations on the ice sheet evolution is difficult to determine.

1.2.2 Glaciologists Perspective

Models which incorporate an evolving ice sheet generally have a highly prescribed climate, and vary in complexity. The most simple follow a flow law, based on a perfectly plastic ice sheet. The work of Nye (1959) replaces the assumption of perfect plasticity with basal sliding at the bed, and a flow law acting within the main body of the ice. This gives a parabolic profile for the steady state ice sheet,

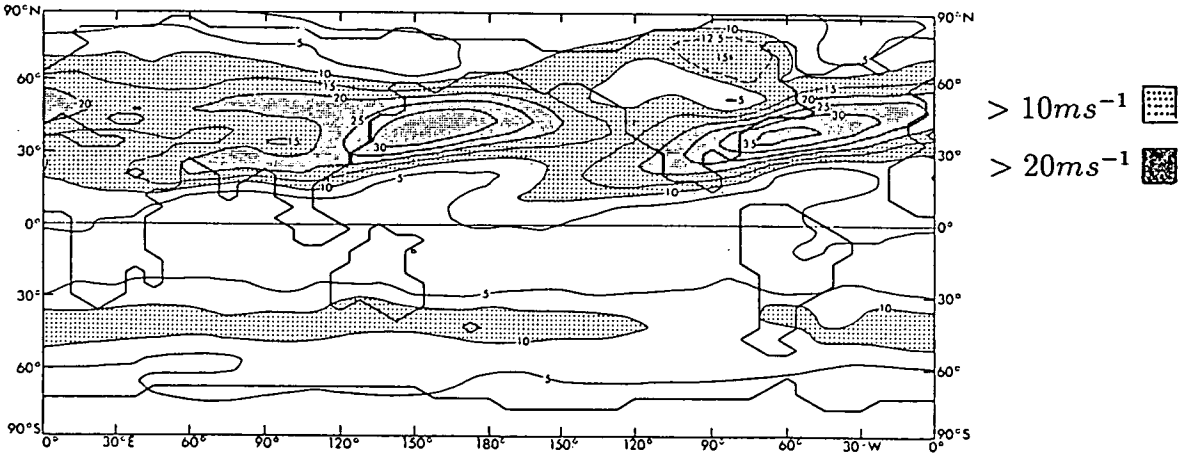

Figure 1.5: The split in the jet stream around the Laurentide ice sheet as predicted by the model of Manabe & Brocolli (1985) (Dec, Jan, Feb mean).

of the form:

$$H_i = h_d \left[1 - \left(\frac{x}{s_p} \right)^{\frac{n_g+1}{n_g}} \right]^{\frac{n_g}{2n_g+1}} \tag{1.6}$$

n_g is Glens' index, a constant with a value between 1.5 and 4.5. Stresses and strains and the temperature evolution of the ice are included in more complicated models.

The climate of an ice sheet model is present as an upper boundary condition and is conceptualised by the climate surface,† shown in fig. 1.6. This is an imaginary line sloping downwards to the pole, along which the mass balance is assumed to be zero. The point at which the line intersects the ground is the climate point,† and the point at which it intersects the ice sheet surface is the equilibrium line altitude. Above the equilibrium line altitude (ELA) there is a net accumulation on the surface of the ice and below the ELA there is net ablation. The most simple models prescribe an average value for accumulation

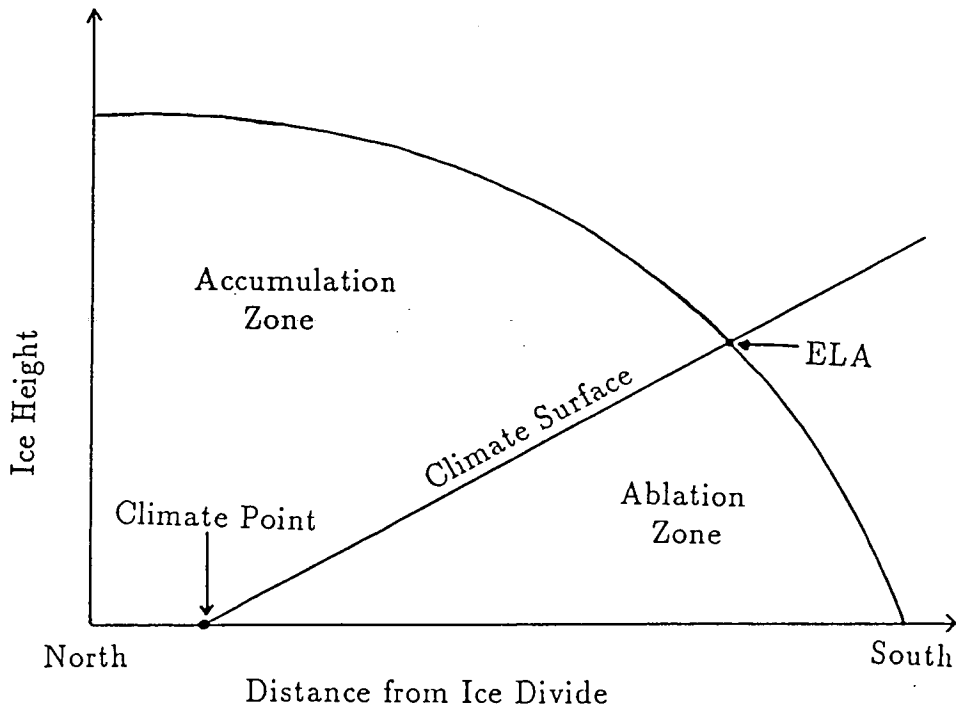

Figure 1.6: The parameterisation of climate in an ice sheet model.

over the ice sheet above the ELA and an average ablation below. However such models do not incorporate the elevation desert effect so it is difficult to cause the ice sheet to retreat. The observed accumulation profiles over Antarctica and Greenland, show a maximum accumulation about 100km from the margin, beyond which accumulation decreases to almost zero in the centre of Antarctica and is considerably reduced over Greenland. In order to account for the continentality of the climate in the centre of the ice sheet, the mass balance is parameterised as a function of distance above or below the ELA. For example Oerlemans (1981) prescribed mass balance (G) as a function of the distance from the ELA shown in fig. 1.7a and given by the following equation:

$$G = a(H^* - ELA) - b(H^* - ELA)^2 \tag{1.7}$$

where a and b are constants, h is the thickness of the ice and H the elevation of the bedrock and $H^* = H + h$. Hindmarsh et al (1989) incorporate a larger elevation desert effect by allowing the mass balance to decrease with distance above the ELA beyond some critical height. This is achieved by defining the accumulation

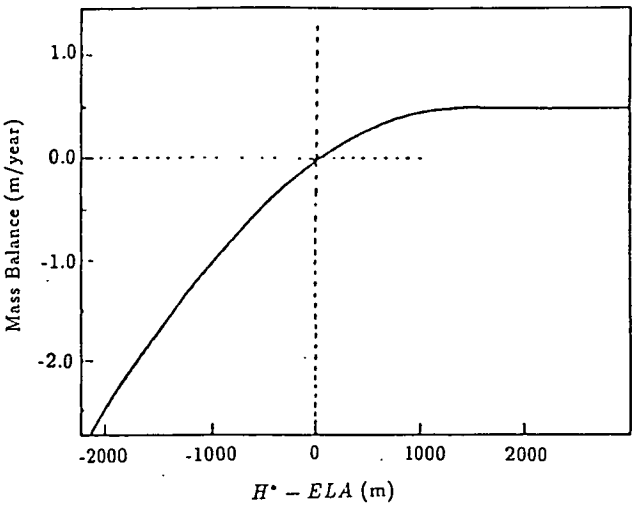

(a) Oerlemans (1981)

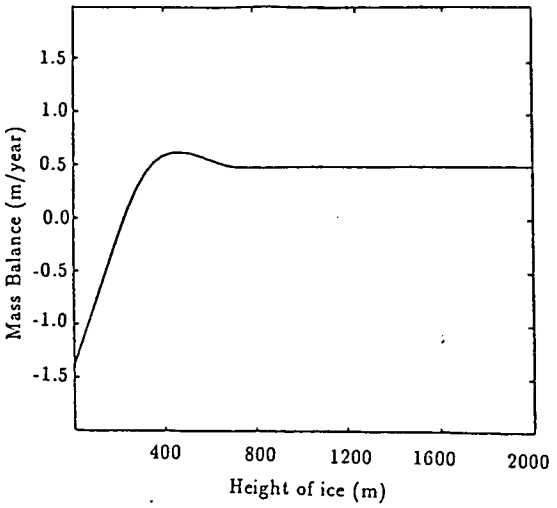

(b) Hindmarsh et al (1989).

Figure 1.7: The mass balance function used by Oerlemans (1981) and Hindmarsh to incorporate the elevation desert effect.

function ($Q(H_e)$), according to the following equations:

$$Q(0) = 0 \quad \text{and} \quad \frac{\partial Q(H_e)}{\partial H_e} = 12.5 \quad \text{for} \quad H_e < 0$$

$$Q(0.25) = 0.5 \quad \text{and} \quad \frac{\partial Q(H_e)}{\partial H_e} = 0 \quad \text{for} \quad H_e > 0.25 \qquad (1.8)$$

$H_e = h - ELA$ where h is the height of the ice. Between $H_e = 0$ and $H_e = 0.25$ $Q(H_e)$ is given by cubic interpolation of the points and slopes given in equation 1.8, as shown in fig. 1.7b. This is a thermomechanically coupled model which has been used to investigate the temperature evolution within the ice, and the sensitivity to the atmospheric temperature. It therefore has a temperature dependent rate factor in the flow law and a diffusion-advection-dissipation equation governs the temperature of the ice. The upper temperature is prescribed at the margin of the ice sheet (C_f) and a temperature gradient with altitude ($\frac{dT}{dz}$), imposed along the surface of the ice.[1] Experiments with these boundary conditions suggest that

[1]This is often referred to as lapse rate in the glaciological literature, but will be referred to as surface temperature gradient in this text, to avoid confusion with the more usual meterological definition of lapse rate, which is the rate of decrease of temperature with height at a particular location in the atmosphere.

the surface temperature gradient† is important in determining the shape of the ice sheet. When the ice sheet grows, the temperature just inside the margin rises rapidly, producing a warm based ice sheet. As the ice advances, cold ice is advected downwards reducing basal temperatures, particularly in the region at the base of the ice divide.† The result is that the warm patch appears to move outwards to the margin. The temperature gradient along the surface is important in determining the size of the warm patch at the base, which affects the shape of the ice sheet as shown in fig. 1.8; for a lower surface temperature gradient there is less downward advection of cold ice and the warm patch may extend inward as far as the divide producing a slightly lower and broader ice sheet. For the growth of a continental sized ice sheet a very stiff bed is required and a surface temperature gradient of at least -1°C/100m. This supports earlier work investigating the way in which air temperature affects the flow and shape of the ice sheet (eg. Paterson 1981). It is worth noting however, that the nature of the bed itself is also important in determining the flow regime and ice sheet shape. Ice flowing over a deformable bed, such as till, will tend to produce an ice sheet which is broader and flatter than ice flowing over non-deformable solid bedrock.

Models of ice sheets can be used to investigate the ice age cycles more closely, by including a climatic forcing function which causes the ice sheet to grow and retreat in the same run. This can be achieved by assuming that the climate surface has a constant gradient, and the climate point is moved in order to mirror the variations in summer insolation at 65°N. Hyde & Peltier (1985) determined the slope according to the gradient of the 0°C isotherm in a standard atmosphere, as $4000m.rad^{-1}$, and initiated glacial cycles according to some change in position of the climate point $\delta x(t)$, as caused by some insolation anomaly $\delta Q(t)$, incorporating

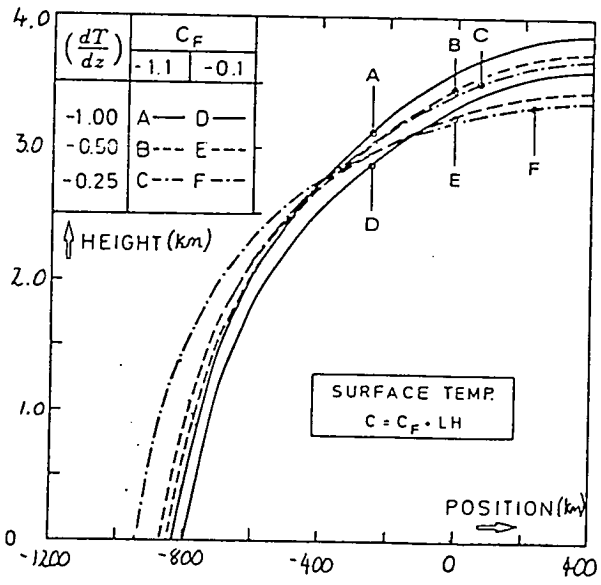

Figure 1.8: The effect of the surface temperature gradient on the profile of the ice sheet Hindmarsh et al (1989) (C_f is the temperature at the margin of the ice sheet).

a meteorological feedback parameter α_f, so that,

$$\delta x(t) = \alpha_f \delta Q(t) \left(\frac{dQ}{dx}\right)^{-1} \tag{1.9}$$

This is translated to a forcing function which follows the precessional component of the Milankovitch forcing. They take the calculated average position of the climate point over the last million years as 140km north of its present location, and the amplitude of oscillation as 490km, so the distance of the climate point north of the Arctic coast at time t is

$$y(t) = 140 - 490 \sin\left(\frac{2\pi t}{20}\right) \tag{1.10}$$

Thus as the climate point moves southward, more of the ice sheet moves into the accumulation zone† and the ice sheet grows; the reverse is true of a northerly displacement of the climate point.

The model of Hyde & Peltier is a zonal, annually averaged model of the northern hemisphere, coupled to a deforming lithosphere, the significance of which was

discussed in section 1.1.4. Hyde & Peltier also use their model to investigate more closely the sensitivity of the ice sheet model to climatic parameters. Their model is very sensitive to the values they assume for both ablation and accumulation, but particularly ablation; an increase in sea level accumulation of 5% causes a reduced period of oscillation from 100ky to 80ky, and a decrease of 5% results in a period of 160ky, both of the changes are accompanied by large changes in ice volume. The extreme sensitivity of the model to the prescribed climate suggests that the nature of the climate surface is fundamental to ice sheet growth, and that it is likely to change in response to the evolution of the ice sheet. In order to understand how this may occur it is necessary to understand more about the climate over present ice sheets, particularly the boundary layer towards the margins of the ice, which will affect the amount and extent of ablation. Only if we understand the extent to which this boundary layer is a response to changes in the ice sheet, as opposed to variations in the larger scale climate will it be possible to investigate the apparent sensitivity of ice sheets to the ablation regime more closely.

1.3 The Aims of the Thesis

1.3.1 What Does an Ice Sheet Need?

If climate and ice sheet models are ever to be coupled, we must be able to understand and simulate the climate above ice sheets of the present day, and in particular the components of the climate to which ice sheets are most sensitive. The needs of an ice sheet are

(i) A mass balance field determining the pattern of accumulation and ablation over the ice sheet. As explained in the work above it seems that ice sheets are more sensitive to ablation rather than accumulation.

(ii) A temperature field which influences the flow characteristics of the ice and therefore the ice sheet shape. This has been shown to be important on a long timescale (Hindmarsh et al 1989, Paterson 1981); a time lag of at least 5000 years is required before ice at the surface is advected into the main body of the glacier, in order that the atmospheric temperature may influence the flow regime and thus the shape of the ice sheet.

This work aims to concentrate on the first point concerning the mass balance field. This requires identifying the components of the climate which have most influence on ablation, and therefore are important for the ice sheet. They can be summarised as follows:

(i) Surface radiation balance.

(ii) Air temperature.

(iii) Wind speed.

1.3.2 How these Needs will be Investigated.

Many glaciologists have looked at the surface energy balance of ice sheets and the way in which it can be used to predict ablation. The climate of the ablation zone however is dependent on more than the radiation regime. The development of a strong boundary layer and consistent downslope winds has important consequences for ablation, through its influence on the temperature field, as well as the

increase in evaporation caused by higher wind speeds. Temperature is therefore critical to the ice sheet growth, not only through its influence on mass balance, but also through its influence on ice sheet dynamics. This thesis aims to increase understanding of the boundary layer climate over ice sheets and the way in which this may influence the evolution of the ice. This will be achieved as follows;

- The real climate over Antarctica and Greenland, will be investigated in chapter 2. This will draw on data from many sources in order to provide a reference for the remainder of the thesis.

- The climate simulated by GCM's will be compared to the real climatology in chapter 3. This will be used to assess the realism of the climate simulated by GCM's over ice sheets, and whether the models are capable of providing the parameters required by an ice sheet model. Data from two GCM's will be used the Meterological Office General Circulation Model (Met.O GCM) and the NCAR Community Climate Model (NCAR CCM).

- Chapters 4 and 5 will describe investigations of the boundary layer over the glacial slopes using a slab model. The model will be used to look at the way in which the boundary layer may affect ablation of ice, and the way in which the b.l itself responds to changes in the ice sheet. The results will be used to infer potential feedback mechanisms between the b.l and the evolution of ice.

Chapter 2

The real climate over ice sheets

In order to understand the way in which climates and ice sheets interact, it is important to first review the nature of the climate over an ice sheet, while at the same time remembering the evolution of an ice sheet has the potential to affect the climate on a global scale. This chapter will provide a basis for the analysis of the GCM simulations of the climate over ice sheets in chapter 3. It will describe the climate over the two main ice sheets present on the Earth today, the Antarctic ice sheet and the Greenland ice sheet. Ideally it would be possible to assess the simulations of past climates over ice sheets, but limitations of the palaeo-evidence would compound uncertainties in the model, rather than acting as a reliable comparison. Therefore it seems reasonable to concentrate the discussion on the ice sheets for which there are most observational data available, those of the present day.

There is no one data source which provides all the information required for an analysis of the GCM model climate. This work requires data on temperature, radiation, wind speed, boundary layer characteristics which have been attained by researching and collating data from many sources. Over Antarctica, a large

source of information is provided by Schwerdfeger (1970, 1984) in Volume 14 of the World Survey of Climatology and in 'The Climate of the Antarctic.' The work of Mather & Miller (1967) provides a detailed investigation of the wind regime over Antarctica. The work of Rusin (1964) presents a large amount of data on the radiational regime of Antarctica, but where cross checking of data and calculations were possible, it was frequently found to contain errors. The data from this source has therefore been used with caution. Other smaller texts have also been used and are referred to where appropriate. Over Greenland the work of Putnins (1970) in the World Survey of Climatology provides much of the background information, and Radok et al (1982) provides a more recent assessment of some climatic parameters. The mass balance† of Greenland is continuously being reassessed and therefore required an assessment of several works; the most recent is the study by Ohmura & Reeh (1991) and has been considered the most reliable, drawing on the findings of earlier work. The radiation regime is much harder to assess over Greenland and data more sparse, information has been obtained from ablation† studies of the ice sheet.

The data have been put into a form in which they can be used for comparison with the GCM data, as well to provide the boundary conditions of the slab model in chapter 4. This sometimes involved changing the units of contours which has lead to inconvenient contour spacing, which is particularly noticeable for the mass accumulation† data in sections 2.1.2 and 2.2.2. The data is only available as annual accumulation figures, whereas data from GCM's was available only for the months of January and July in units of mm water equivalent per day. Without the data for the remaining months of the year, this cannot be converted to annual figures. The maps of accumulation therefore show patterns rather than actual amounts that are directly comparible.

The Antarctic continent extends over an area of $14 \times 10^6 km^2$, over 97% of which is ice or snow covered. The continent is generally divided into the East Antarcitic Plateau in which the ice reaches elevations over 4000m, and the West Antarctic ice sheet that is dominated by the Ronne-Filchner Ice Shelf and the Ross Ice Shelf which float on the surface of the deep ocean (see fig. 2.1). East and West Antarctica are separated by the Trans Antarctic Mountains which protrude above the ice and reach over 5000m above sea level, and play an important role in the zonal atmospheric circulation of the southern polar latitudes. Surface slopes over the ice sheet are generally small, between 0.001 and 0.002, increasing rapidly towards the coast of the East Antarctic Ice Sheet where they may exceed 0.05. It will be seen in the following chapters, that the surface slope plays an important role in the climate of the continent.

The Greenland ice sheet is much smaller than that of the Antarctic, about $\frac{4}{5}$ of the continent is ice covered, an area of $1.726 \times 10^6 km^2$. The highest elevation of the ice cap is over 3000m above sea level and forms an elongated dome in the northern sector of the continent. A secondary dome to the south reaches just over 2500m.

Observations of the climate over ice sheets are still very limited due to the inaccessibility and the adverse weather of these regions. The Antarctic climate has been more consistently studied than that of Greenland, with several permanent stations in operation in the East Antarctic. Over Greenland, most observations are from expeditions and therefore last from several months to a few years. The map of Antarctica in fig. 2.1, illustrates the extent of the problem, and although the figure shows the best available coverage of ice sheet climate, it is still very sparse, particularly in the interior. The problems arising due to the wide scatter of the stations are increased because the periods of observation are often short,

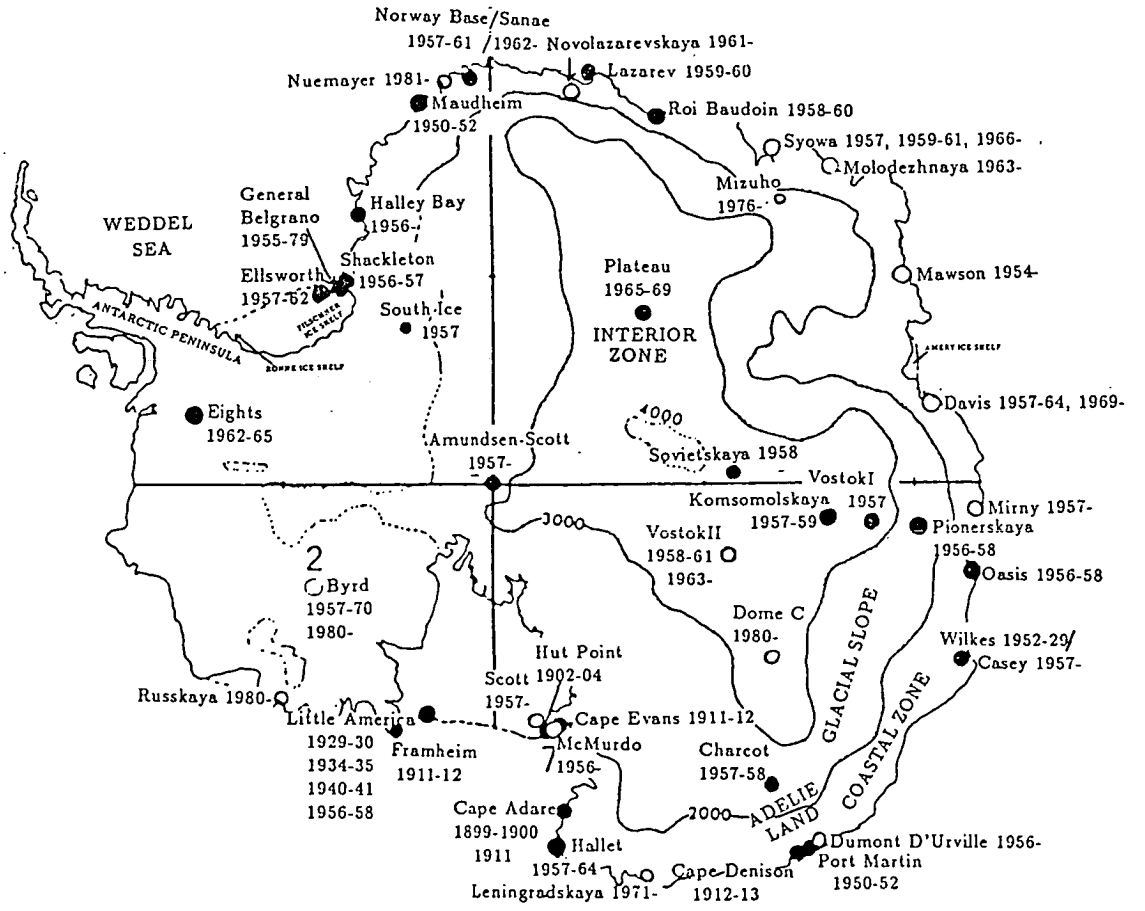

Figure 2.1: The distribution of observational stations over Antarctica

and do not always coincide, making comparisons of data between stations difficult. The following discussion will concentrate on the characteristics of the climate in winter and summer taking July and January as typically representative of each season. The data are used in chapter 3 as a comparison for the model simulations of the climate from the Meterological Office GCM and the NCAR Community Climate. Data specifically relevant to the boundary layer are summarised at the end of the chapter, and will be used in a modified form in chapter 4, to constrain a slab model.

2.1 The Climate of Antarctica

The climate over Antarctica is in may ways unique, its isolated location at extreme southern latitudes means that for a large part of the year the climate is dominated by the polar night and remains fairly stable;† even so it bears many of the characteristics observed in the climate over other ice sheets, such as a strong temperature inversion and strong katabatic winds. This makes it an ideal location in which to study the inversion and boundary layer structure which elsewhere, (eg Greenland or possibly past ice sheets) is interrupted, and destroyed periodically by synoptic disturbances. The Antarctic climate may be easily divided into 3 zones, shown in fig. 2.1; the interior, the glacial slope and the coastal zone. The classification is based on the nature of the winds and boundary layer in each zone, which will be discussed in section 2.1.3. First of all there will be an overview of the climatic data, particularly those relevent to ice sheet evolution.

As explained in chapter 1, the main link between the climate and an ice sheet is through the mass balance. The ablation requires a knowledge of the heat and radiation budget of the surface. Accumulation requires a knowledge of the moisture content of the atmosphere, and the large scale dynamics which result in precipitation on the ice sheet. The boundary layer is important, particularly over the glacial slopes and coastal zone, which constitute the ablation zone† over most ice sheets, Antarctica is the exception with no ablation zone. The work of Hyde & Peltier (1985) refered to in chapter 1, identified the ablation of ice to be the component of the ice mass budget to which the ice sheet is most sensitive. In this zone, high wind speeds develop in a distinct boundary layer, entraining warm air through the upper interface. The wind speed, or more specifically the rate of entrainment† of warm air, determines the temperature of the boundary layer, as well as the rate of removal of cold air from the interior, and therefore the flux of

cold air at the edge of the ice. The temperature of the boundary layer is important because of its influence on ablation; the flux of cold air is important because it may influence the large scale circulation, undercutting relatively warm air at the coast, encouraging the development of cyclones, which may ultimately feed into the accumulation over the ice sheet. Katabatic winds occur over most ice sheets, but over the Antarctic ice sheet, flow is relatively uninterrupted during the long winter, and it is therefore a useful location in which to understand the nature of the boundary layer producing the flow, which will be investigated further in chapters 4 and 5.

2.1.1 Radiation and Temperature

Radiation

The radiation regime of Antarctica is the dominant influence on the climate, responsible for the surface inversion and the long stable winter of 6 months, followed by the short summer, known as the coreless winter and peaked summer (Schwerdfeger 1970). Radiation is strongly influenced by cloud cover. Generally cloud tends to be high level and in thin semi-transparent layers, although they may be opaque at the coast where the fraction of cover increases, as shown in table 2.1. At Mirny and Lazareff (for locations see fig. 2.1), the respective mean cloud amounts are 6.6 and 7.9 tenths, compared to 4.6 and 4.2 at Komsomolskaya and VostokII in the interior; the lower ranges of cloud cover are more likely to be associated with low level cloud, 87% and 73% of the low cloud appears in the 0-2 tenths range at Komsomolskya and Mirny respectively. The low temperatures of the interior mean that when low cloud does form, it is often present as thin ice cloud in layers, rather than more dense water vapour cloud as is typical at lower latitudes. Table

Coastal Stations of East Antarctica														
Station	January							July						
	Total Cover tenths	frequency of each range of cover (%)						Total Cover tenths	frequency of each range of cover(%)					
		0-2		3-7		8-10			0-2		3-7		8-10	
		Tot	Low	Tot	Low	Tot	Low		Tot	Low	Tot	Low	Tot	Low
Mirny	6.6	27	73	10	3	63	24	7.0	26	61	10	3	64	36
Port Martin		4		18		78			46		25		29	
Oasis	7.0	23	61	13	13	64	26	7.2	23	60	10	10	77	30
Lazareff	7.9							7.1	19	74	19	3	62	23
Glacial Slope Stations														
Pionerskaya	6.5	31	73	10	7	59	30	6.2	32	81	13	0	55	19
VostokI								3.9	60	94	7	0	33	6
Interior Stations														
Komsomolskaya	4.6	42	87	22	3	36	10	3.4	58	100	16	0	26	0
VostokII	4.2	52	93	13	3	35	4	3.5	53	100	24	0	23	0

Table 2.1: Total mean cloud cover and % frequency of total and low level of cloud in each range of cover, at several Antarctic stations

Coastal Stations												
Station	Cu & Cb	Sc	St	Fs	Ns	Ac	As	Ci	Cs	Cc	0	un-known
Mirny	<1	14	<1	<1	9	16	12	12	7	3	19	7
Oasis	5	22	3	1	6	18	12	9	6	3	10	5
Lazareff	<1	13	1	0	2	4	20	11	14	<1	18	17
Glacial Slope												
Pion'ya	<1	1	0	<1	0	2	14	12	16	1	27	27
VostokI	-	-	-	0	0	5	15	22	19	3	30	6
Interior Stations												
Koms'ya	<1	2	1	0	0	2	2	28	20	<1	45	1
VostokII	<1	2	1	<1	0	30	9	16	26	6	8	2
Sov'ya	0	0	0	0	0	5	12	24	17	3	30	9

Cloud Types:

Low Level	Medium Level	High Level
Cu - Cumulus	Ns - Nimbostratus	Ci - Cirrus
Cb - Cumulonimbus	Ac - Altocumulus	Cs - Cirrostratus
Sc - Stratocumulus	As - Altostratus	Cc - Cirrocumulus
St - Stratus		
Fc - Fractostratus		

Table 2.2: Frequency of occurrence of cloud types at Antarctic stations (%)

2.2 shows the incidence of each cloud type over Antarctica. It can be seen that in the interior low level precipitation clouds are rare; most common are cirrus, cirrostratus and occasionally altostratus or altocumulus. At the coast, low level clouds become more common. This is particularly evident where there is a large influence from the sea. The occurrence of strong katabatic winds tends to lessen the influence of the sea so that at coastal stations such as Mirny and Mawson, which frequently experience katabatic flow, low level clouds once again become less common, compared to other coastal stations. However, at these sites, blowing snow may often obscure the sky producing white out conditions, which reduce the amount of radiation reaching the surface.

Shortwave Radiation Table 2.3 shows the fluxes of shortwave and longwave radiation at the surface of the ice, in January and July for several stations on the East Antarctic ice sheet. The downward shortwave fluxes, albedo, net shortwave and longwave balance have been taken from Schwerdfeger (1984), the upward longwave flux was calculated using Stefans law ($E_r = \sigma_{sb}T^4$)[1], and the remaining components calculated from the balance. The monthly mean values given for Plateau Station are taken from the 5 month averages, October to February and April to August. The values for VostokII, Sovietskaya, Komsomolskaya, Pionerskaya and South Pole have been taken from downward shortwave fluxes and the net total (SW and LW) balance given by Dalrymple (1966), assuming that the winter SW flux is zero. By comparing the two values at VostokII, the estimates of the net budget by Dalrymple (1966) are generally higher than those of Schwerdfeger (1984). This arises because measurements of radiation vary according to the method and equipment used. Despite these discrepancies the table provides a general outline of the radiation patterns over the continent. It will be seen in chapter 3 that the discrepancies between the data sources are small, compared to

[1] E_r=radiant emittance, T=surface temperature, σ_{sb}=Stefan-Boltzman constant

Stn	Mon	Shortwave down Wm^{-2}	Shortwave up Wm^{-2}	alb	surf temp °C	longwave up Wm^{-2}	longwave down Wm^{-2}	net SW Wm^{-2}	net LW Wm^{-2}	Å
Coastal Stations										
Hal	Jan	284.5	230.4	.81	-4.8	293.4	253.8	54.1	-39.6	.13
	Jul	0	-	-	-28.9	201.3	178.9	-	-22.4	.11
Mir	Jan	314.7	245.5	.78	-1.6	307.6	269.1	69.1	-38.5	.13
	Jul	3.7	3	.81	-16.6	245.1	213.0	0.7	-32.1	.13
Mol	Jan	309.5	58.2	.19	-0.5	312.6	220.8	251.3	-91.8	.30
	Jul	1.9	1.2	.63	-18.0	239.7	207.6	0.7	-32.1	.13
Nov	Jan	310.6	61.9	.20	-0.7	311.7	213.1	248.7	-98.6	.32
	Jul	-	-	-	-17.7	240.9	195.0	-	-45.9	.19
Glacial Slope										
Miz	Jan	336.8	272.6	.81	-18.6	237.5	180.0	64.2	-57.5	.24
	Jul	<0.2	≈0.17	.85	-39.1	169.7	136.8	<0.03	-32.9	.19
Interior Stations										
Pla	O-F	312.1	263.6	.84	-33.9	185.3	139.0	48.5	-46.3	.25
	A-A	1.5	1.3	.86	-68.0	100.1	85.2	0.2	-14.9	.15
VII	Jan	405.8	336.7	.83	-32.3	190.3	141.4	69.1	-48.9	.26
	Jul	-	-	-	-67.0	102.1	84.9	-	-17.2	.17
(Data from Dalrymple 1966)										
VII	Jan	316.3	237.2	.72	-32.3	190.3	114.7	79.1	-75.6	.4
	Jul	-	-	-	-67.0	102.1	87.1	0	-15.1	.15
Sov	Jul	-	-	-	-69.6	96.5	86.0	0	-10.5	.11
Kom	Jan	362.9	283.1	.78	-32.2	190.6	115.5	79.8	-75.1	.39
	Jul	-	-	-	-62.0	112.4	79.8	0	-32.6	.29
Pio	Jul	-	-	-	-38.0	172.9	156.6	-	-16.3	.09
S.P	Jul	-	-	-	-59.9	116.9	89.0	-	-27.9	.24

Table 2.3: Radiation budget at several stations in Antarctica. Station abreviations; Hal-Halley, Mir-Mirny, Mol-Molodheznaya, Nov-Novolarevskaya, Miz-Mizhuo, Pla-Plateau, VII-VostokII, Sov-Sovietskaya, Kom-Komsomolskaya, Pio-Pionerskaya, S.P-South Pole.

the difference between the observations and the model predictions.

The most notable feature of the radiation budget is the polar night, affecting the pole for 6 months of the year. In the summer, the decreasing amounts of cloud with distance from the coast, combined with the shorter atmospheric path at high elevations in the interior, allows much more shortwave radiation to reach the surface in the interior; this can be seen by comparing a downward flux at Mirny of $314.7 Wm^{-2}$with that at VostokII of $405.8 Wm^{-2}$. However, large albedos over the whole ice sheet, mean that most radiation is reflected, and the net SW fluxes are almost uniform over the ice sheet, and much smaller than the individual components. It can be seen from table 2.3 that the net fluxes at most stations are less than $100 Wm^{-2}$, whereas the upward and downward components range from the $230.4 Wm^{-2}$outgoing flux from Mirny to the $405.8 Wm^{-2}$incoming flux at VostokII. The exceptions are Molodezhnaya and Novolazarevskaya, both of which are located where bedrock protrudes from the snow and ice cover, lowering the albedo, so the surface absorbs much more radiation.

Longwave Radiation The longwave fluxes of radiation determine the temperature field and therefore the climate for most of the year. The downward flux during the summer exceeds that of the winter. The upward longwave flux reflects the pattern of isotherms, being greatest at the coast during the summer; according to Stefans law, the upward longwave flux at the surface is proportional to T^4. The effective longwave radation is more conveniently shown by the Ångström ratio ($\mathring{A} = R_N/R_\uparrow$)[2]. This gives an indication of the extent to which the downward atmospheric flux compensates for the loss at the surface. A small value indicates that the downward flux compensates for most of the loss. Referring back to table 2.3, values tend to be largest in the interior (Schwerdfeger 1984),

[2] R_N = net longwave flux, $R\uparrow$ = upward longwave radiation

and although they may decrease during the winter, they generally remain greater than those at the coast. At Komsomolskaya the January Å ratio is 0.39, whereas in July it is 0.29 for example, compared to 0.13 in both January and July at Mirny. A decrease of the Å ratio in the winter is the opposite of what might be expected, since in winter cloud amounts tend to be less which, acting on its own, would reduce the downward LW flux and increase Å. However in the interior it is not cloud amounts, but the temperature inversion that determines back radiation (Schwerdfeger 1984). Large amounts of cooling at the surface result in a strong inversion over the continent. Warm air advection between the coast and interior means there is a layer of warm, moist air overlying the cold surface, without which downward longwave radiation would be considerably reduced. This, coupled with low surface temperatures which reduce the upward fluxes, results in small values of Å. The result is that a balance is struck in the interior between the components of the longwave radiation budget and this prevents the continent becoming increasingly cold, and the inversion stronger, during the winter. This is known as the coreless winter and will be returned to later in this section.

Sensible Heat Flux The other component of the surface energy budget which will be discussed here is the sensible heat flux. Beneath the inversion this is a negative flux, transporting heat downward to the surface at a rate proportional to the stability of the layer (inversion strength) and vertical wind shear in the layer. The flux may be important in an ablation zone (Braithwaite & Olesen 1990a), but in Antarctica it has very little influence on the climate, although it plays a small role in maintaining the coreless winter. Dalrymple et al(1966) estimate the flux to be $5.3 Wm^{-2}$in January and $12.1 Wm^{-2}$in July at Maudheim on the coast, and $27 Wm^{-2}$in July at the South Pole where the inversion is stronger.

Temperature

Temperatures over the Antarctic continent are consistently the lowest on the Earth. The mean January and July surface temperatures are shown in fig. 2.2 (Schwerdfeger 1970). It can be seen that the temperature remains below zero throughout the year apart from a very narrow strip around part of the coast during the summer. It is also significant that the isotherms are not symmetrical about the pole, but are centred over the very high Eastern Plateau region. Towards the coast the surface temperature gradient† increases slightly, the reason for this will be discussed later. Since the temperatures are constantly below freezing, excluding the possibility of extensive ice melt, the temperature is most important for the evolution of the ice. If there is a large surface temperature gradient,† and the temperatures in the centre of the ice are very cold, as explained in chapter 1 this will, over time influence the flow regime of the ice and therefore the ice sheet shape. Surface temperature gradients have been calculated by various authors (eg Schwerdfeger 1970, Rusin 1964) and are generally found to be more than the DALR.† The January and July values have been calculated in table 2.4. The table of surface temperature gradients shows the July values to be greatest. Some authors subtract a latitudinal temperature gradient from the temperature gradient along the surface (eg. Rusin 1964). However as the boundary layer is almost completely decoupled from the upper atmosphere this does not seem to be necessary. Variations of temperature with latitude occur due to interchange and modification of air masses, so that rather than being a gradual gradient between the poles and the equator there are large temperature gradients in regions where the exchange of air masses is greatest; the air which flows over the Antarctic ice sheet originates from the cold interior and under the prevailing wind regime, there is no interchange at the surface with warmer airmasses from the north.

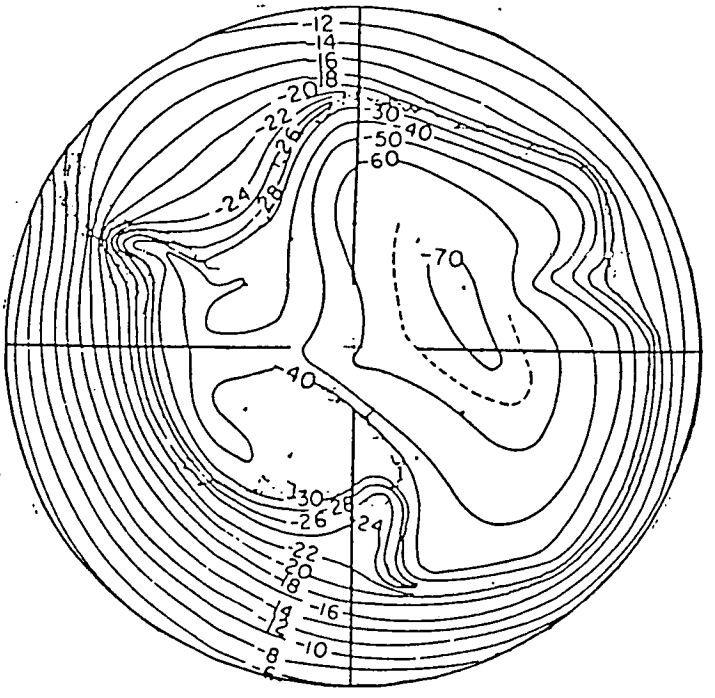

(a) July

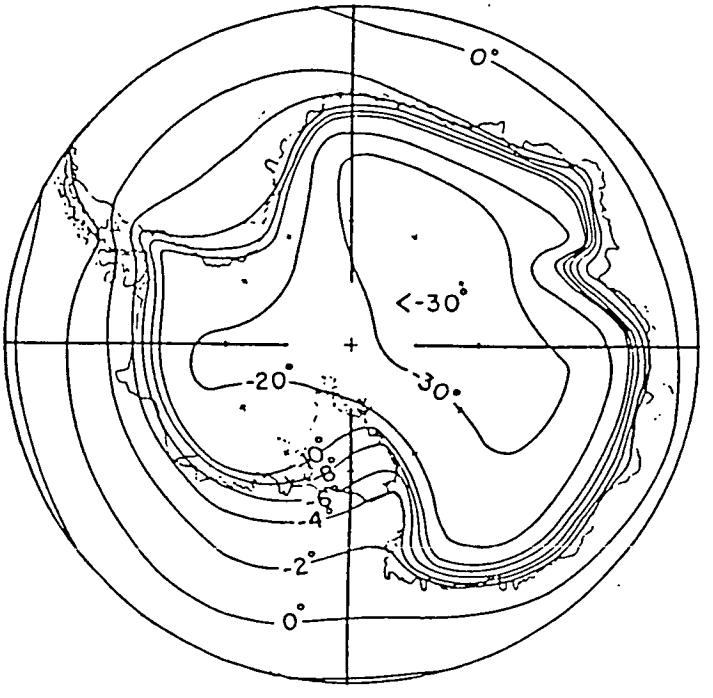

(b) January

Figure 2.2: The mean surface temperature in the Antarctic for January and July. (Schwerdfeger 1970)

Stations	Temp °C		ΔT °C		Height	ΔH	temp grad °C/100m	
	Jan	Jul	Jan	Jul	(m)	(m)	Jan	Jul
Mirny	-1.6	-16.6			35			
-			21.8	30.7		2665	0.81	1.15
Pionerskaya	-23.4	-47.3			2700			
Pionerskaya	-23.4	-47.3			2700			
-			-	10.7		550	-	1.9
VostokI	-	-58.0			3250			
Pionerskaya	-23.4	-47.3			2700			
-			8.8	14.7		800	1.1	1.8
Komsomolskaya	-32.2	-62.0			3500			
Pionerskaya	-23.4	-47.3			2700			
-			8.9	19.7		800	1.1	2.5
VostokII	-32.3	-67.0			3500			
Pionerskaya	-23.4	-47.3			2700			
-			-	22.6		950	-	2.4
Sovietskaya	-	-69.9			3650			
Komsomolskaya	-32.2	-62.0			3500			
-			-	7.9		150	-	5.2
Sovietskaya	-	-69.9			3650			

Table 2.4: Surface temperature gradients between Antarctic stations

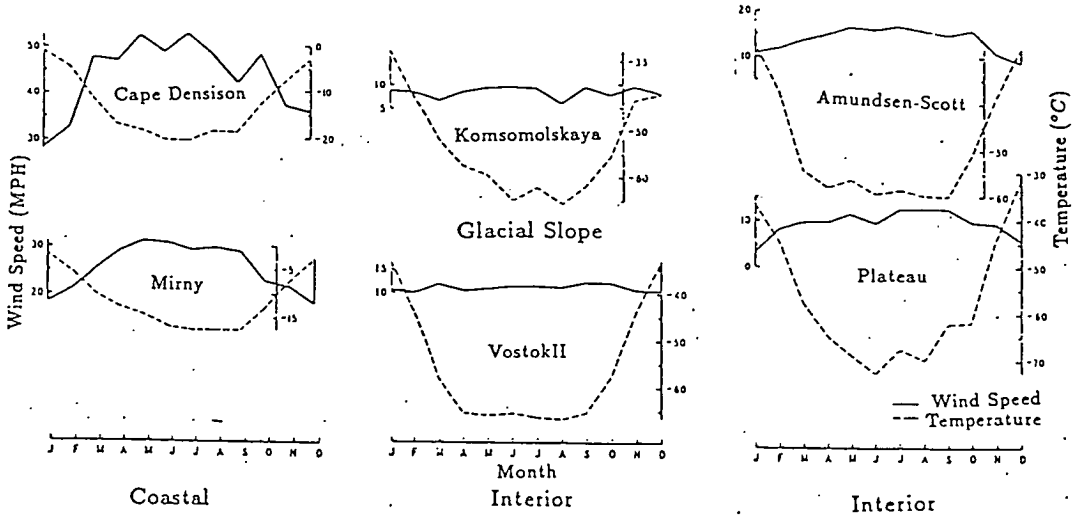

Figure 2.3: The 'coreless winter' in Antarctica: mean monthly variation in surface temperature at several Stations on the Eastern Ice Sheet.

The surface temperature gradient depends on the rate of radiational cooling of the air compared to the rate at which warm air from above the boundary layer is entrained. Air in the interior is cooled by radiation and then flows away down the slopes warming at the DALR. In the winter when winds are stronger there is entrainment of air from above the boundary layer, which further increases the b.l temperature, and consequently the the surface temperature gradient, although at the bottom of the slope the gradient may decrease due to stagnation of air on the ice shelves (Fortuin & Oerlemans 1990). In summer, low wind speeds cause the advective timescale to become smaller relative to the radiative timescale, consequently there is more radiational cooling of the air before it flows downslope, and a reduction in the surface temperature gradient.

Coreless Winter The radiation budget of Antarctica results in a very long winter and short summer. This is most clearly illustrated by the monthly variation in surface temperatures at several stations in fig. 2.3. After an initial cooling at the start of the winter, low Å ratios in the interior, and the downward flux of

sensible heat during the winter, prevent the surface becoming progressively colder throughout the whole of the winter period. Once the balance is attained at the beginning of the winter it is maintained, and temperatures remain steady until the sun is sufficiently high above the horizon for the downward solar flux to disturb the balance. The nearer the pole, the longer this takes, and hence the longer winter experienced by this region. From fig. 2.3 it can be seen that Amundsen-Scott (South Pole), Plateau and VostokII located in the interior, experience the longest and deepest winters - up to 8 months duration. The winters become progressively shorter and more shallow over the glacial slope to the coastal zone, at Cape Denison and Mirny.

Temperature Inversion The other major feature attributable to the radiation balance is the surface temperature inversion. Again, once established at the beginning of the winter this tends to remain fairly constant, maintained by the radiative processes, advection and adiabatic sinking of warm moist air from low latitudes (Schwerdfeger 1984). Fig. 2.4 shows the isolines of inversion strength after Phillpot and Zillman (1970). The strength of the inversion was measured by soundings recording the maximum temperature in the radiosonde ascent. The depth of the inversion varies from 100-200m at the coast, to between 500 and 1000m in the interior (Phillpot & Zillman 1969). Fig. 2.5 shows a typical inversion structure at VostokII in the interior (Schwerdfeger 1970); the inversion can be seen to be strongest in the layer nearest to the ground, and topped by a layer 1000-2000m deep in which temperature changes little with height, even so the temperature at 7km is still greater than that at the surface. The figure clearly shows that the temperature change is very gradual, so that exact height of the inversion above the interior is difficult to determine. On the glacial slopes and coastal strip where the wind speed increases, the boundary layer becomes more well-mixed and more clearly defined.

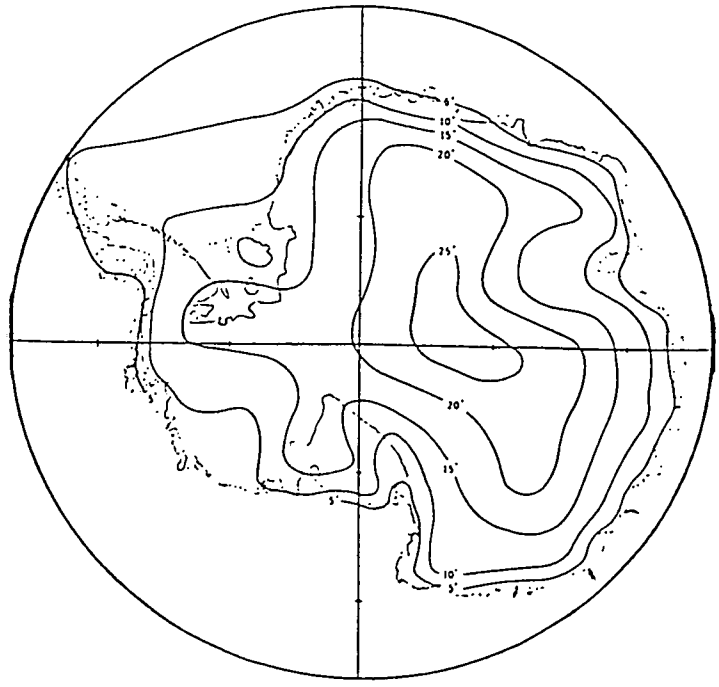

Figure 2.4: Isolines of inversion strength over Antarctica (Phillpot & Zillman 1969)

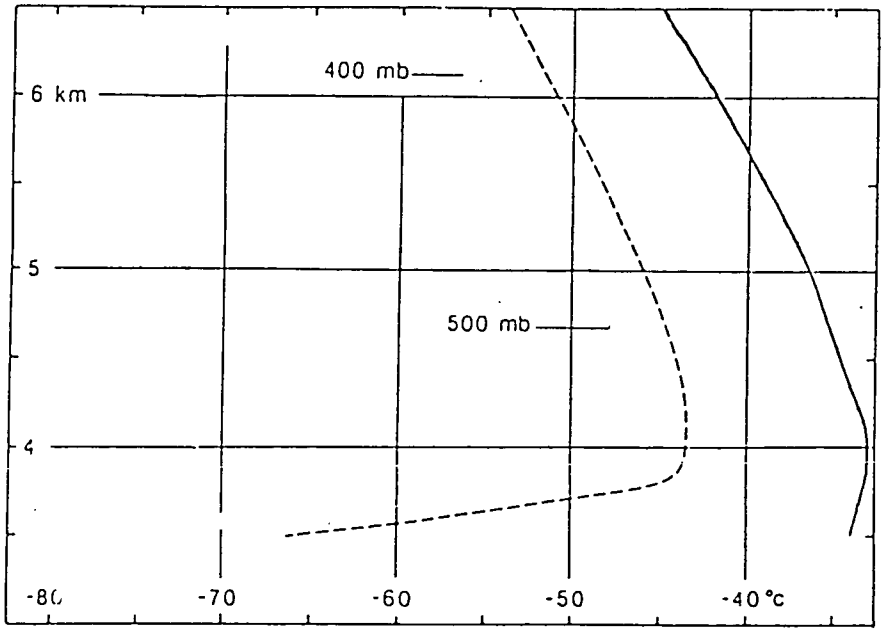

Figure 2.5: The inversion strength at Vostok I: Average winter [April-September] (----); Average summer [December-January](——) Average for the years 1958-1960 and 1964-1973. (Schwerdfeger 1984).

2.1.2 Mass Balance

There is much uncertainty surrounding the estimates of the mass balance of Antarctica, even so far as to whether the net budget is positive or negative (Schwerdfeger 1984). These arise because of problems in determining loss by iceberg calving, runoff, sublimation/evaporation and deposition. It is generally taken that south of 85°S deposition of hoar frost during the winter, is approximately equal to the removal of mass by sublimation during the short summer, therefore any precipitation at these latitudes adds to the ice mass, replenishing the ice lost at the coast by calving (Schwerdfeger 1984). At lower latitudes, deposition is less and sublimation is more, so there may be a slight deficit. However, neither of these processes has a significant effect on the mass balance of the ice sheet. In Antarctica the main loss is through iceberg calving. Gain in ice is by precipitation, or more specifically ice-crystal precipitation beneath clear skies. This is primarily a winter phenomena, fed by the layer of warm moist air 1000-2000m thick, and situated several hundred metres above the surface of the interior in winter. This layer of air, advected from lower latitudes, cools and becomes super-saturated with respect to ice, but not water. The ice crystals grow by diffusion and fall from a clear sky. During the summer, the inversion is considerably weaker and warm air advection is less, so that whether or not ice crystals fall from clear skies depends on whether the air is ascending or descending. If the air descends then it warms, leading to less supersaturation. Fig. 2.6 shows the accumulation over Antarctica, which should be used as an indication of the precipitation patterns rather than an absolute representation of the amounts (Schwerdfeger 1984). Notable is the greater precipitation in the west compared to the east. On the western ice shelf, terrain is much flatter allowing moist air masses to penetrate further inland. Particularly noticeable is the maximum to the E of the Ross Ice Shelf, caused by stable air masses approaching the trans-Antarctic Mountain barrier from the east

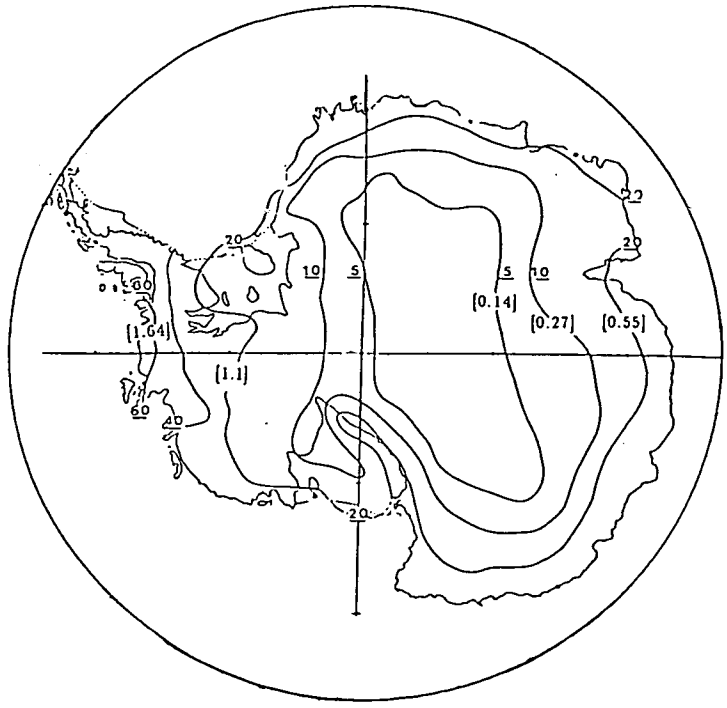

Figure 2.6: The accumulation on the Antarctic Ice Sheet in grams cm^{-2} $year^{-1}$, [numbers in square brackets mm water equivalent day^{-1}].

or south-east. As the air builds up on the windward side of the mountains it is forced to rise, cooling as it does so producing orographic precipitation. The result is that precipitation increases by more than 1/3 between the centre of the Ross ice shelf and the mountains (Schwerdfeger 1984).

The seasonal distribution of accumulation is less clear. The tables 2.7, 2.8 and 2.9 at the end of this chapter seem to show a winter maximum of precipitation, consistent with the above analysis. However, at the coast there may be a summer maximum, where precipitation is more likely to be caused by synoptic disturbances, the activity of which is greatest in summer in the region of the ice sheet margin.† The data presented in the tables do not make any allowances for the effects of blowing snow, so estimates in areas of strong winds, towards the coast and during the winter, will be subject to large errors. The high values recorded at Pionerskaya are a good example, the station experiences consistently high winds and has a precipitation over ten times greater than suggested in fig. 2.6.

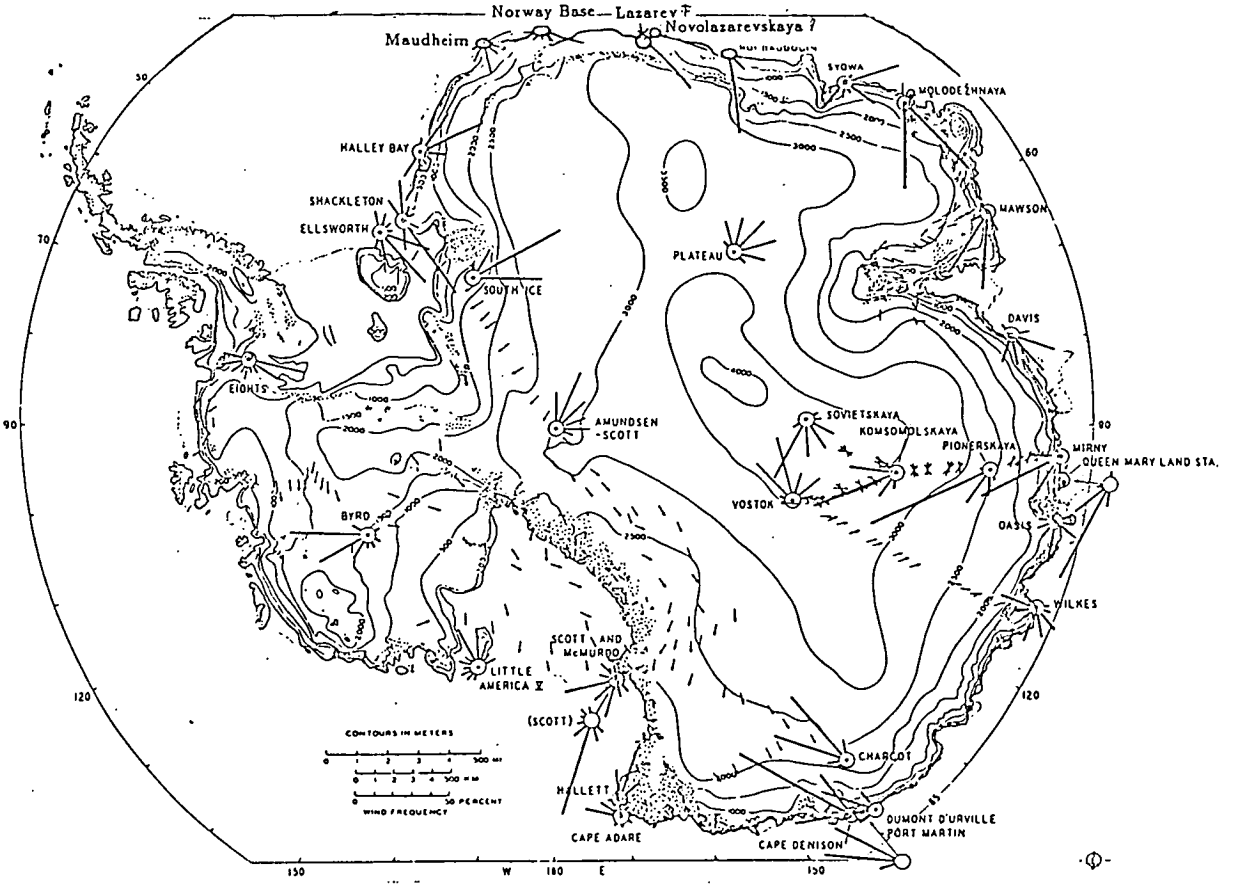

Figure 2.7: Wind roses and traverse data for the Antarctic Ice Sheet (Mather & Miller 1964).

2.1.3 Wind

The temperature structure of the boundary layer is responsible for the generation of remarkably constant winds over the ice sheet. Pionerskaya in the interior for example reports 85% of the winds between 110°-160°in 1958, with just 0.06% of days experiencing calm for the same period. Mirny at the coast receives 88% of its winds from the south-east quadrant, and the depth of the flow was observed to be 200-500m. Fig. 2.7 (Mather & Miller 1967) shows the wind roses for various stations and additional information obtained from traverses across the ice sheet where the orientation of sastrugi on the ice show the prevailing wind direction. This has been used by Mather and Miller to construct the pattern of streamlines shown in fig. 2.8. The figure shows that on the East Antarctic Ice Sheet the

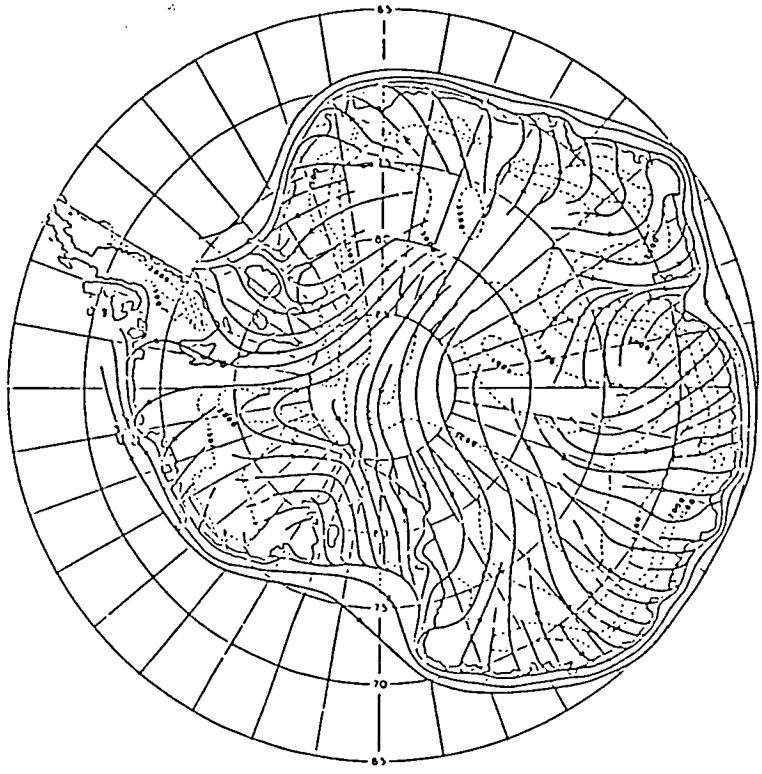

Figure 2.8: The pattern of streamlines for the surface winds in Antarctica (Mather & Miller 1967). This is time-averaged behaviour determined according to the predominant wind frequencies at each station.

winds blow at approximately 45° to the relief contours in the interior, and become perpendicular nearer the coast. These winds are a result of the negative buoyancy of the air, the mesoscale pressure gradient force, the coriolis force and friction. The relative importance of each term varies over the ice sheet and will be discussed separately for the Western ice shelf and the Eastern ice sheet. The winds on the East Antarctic ice sheet will be further divided into 3 zones;

1.Interior
2.Glacial Slope
3.Coastal Zone

The boundary layer over the glacial slope and coastal zone is fed by cool air from the interior. The structure of the boundary layer, which is important in determining the temperature at the surface of the ice, will be studied using a slab model in chapters 4 and 5. The following section will provide a framework for the model describing the characteristics of the boundary layer in each zone. A summary of data for several stations in each zone can be found at the end of this chapter in tables 2.7, 2.8 and 2.9

The East Antarctic Ice Sheet

Interior. Slopes in the interior are very small, typically 0.001. The buoyancy effect therefore is insufficient to account for the wind speeds of 3-5ms^{-1}observed (table 2.7). These winds are actually the geostrophic wind† modified by friction. This was first observed by Dalrymple et al (1966) and Lettau and Schwerdfeger (1967) in studies at the South Pole station, but has since been verified for other

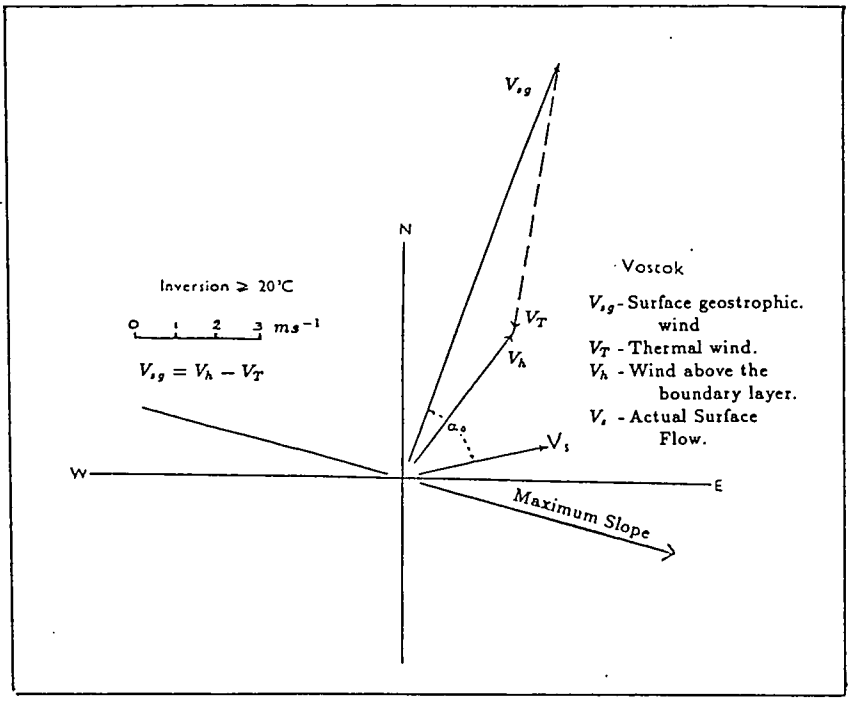

(a) Vector diagram of the winds: (V_{sg}) surface geostrophic wind; (V_T) thermal wind; (V_h) wind above the boundary layer; (V_s) actual surface flow.

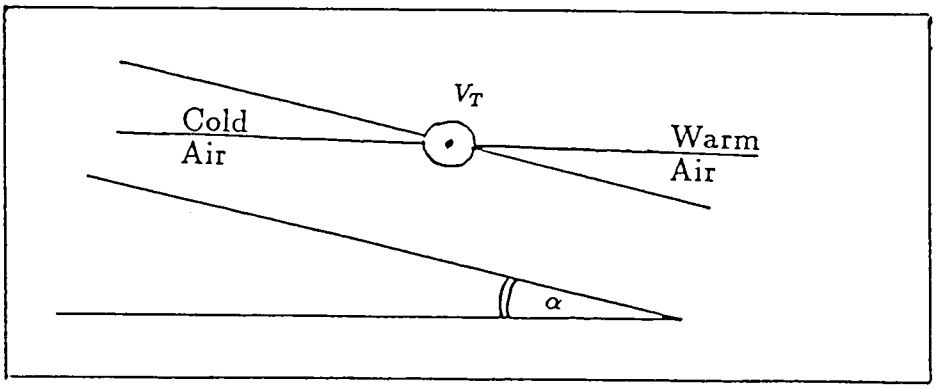

(b) Cross-section of the sloped inversion, showing the horizontal temperature gradient and the thermal wind.

Figure 2.9: The nature of the thermal wind due to the sloped inversion. The driving force behind the winds of the interior (Schwerdfeger & Mahrt 1968b).

stations of the Antarctic interior (eg. Schwerdfeger and Mahrt 1968a, 1968b and Lettau et al 1977). Fig. 2.9 shows how the sloped inversion produces a horizontal

temperature gradient implying a thermal wind parallel to the contours. Subtracting this from the geostrophic wind at the top of the b.l., gives the geostrophic surface wind, which is considerably larger than the upper geostrophic flow. Frictional deviation at the ground causes the resultant wind to blow at between 30° to 60° to the fall line. The net effect is an anticlockwise rotation of wind direction accompanied by a decrease, or at least no significant increase in wind velocity with height. Above the b.l, the actual wind approximates the geostrophic flow and is almost parallel to the contours of surface relief. Under lapse conditions (during the daytime in summer), the effect of the thermal wind is removed and there is an increase of wind velocity with height in the lower atmosphere.

Glacial Slope The glacial slope is a broad band extending from approximately 700km inland to between 100 and 200km from the coast. Slopes tend to be greater than in the interior plateau region, and are around 0.0025 (table 2.8). Here the buoyancy force is more significant and the corresponding wind speeds greater, between 5-10ms^{-1}, and directed closer to the fall line. Profiles taken in the nighttime during the summer under inversion conditions in fig. 2.10 (Kodama et al 1989), show very strong winds in the b.l, decreasing rapidly to the top, and driven primarily by the buoyancy of the air, modified by the coriolis force. This low level jet does not disappear under lapse conditions, eg. at 1500 hours, as might be expected. Observations taken during the daytime in the summer (Kodama et al 1989) suggest that a geostrophic wind is set up, similar to that of the interior, only now the baroclinicity† originates from the strong ice-ocean temperature gradient, rather than the sloped inversion.

Coastal Zone At the coast the ice sheet falls away rapidly and slopes may be as large as 0.05 (table 2.9). This enhances the buoyancy force and frequently

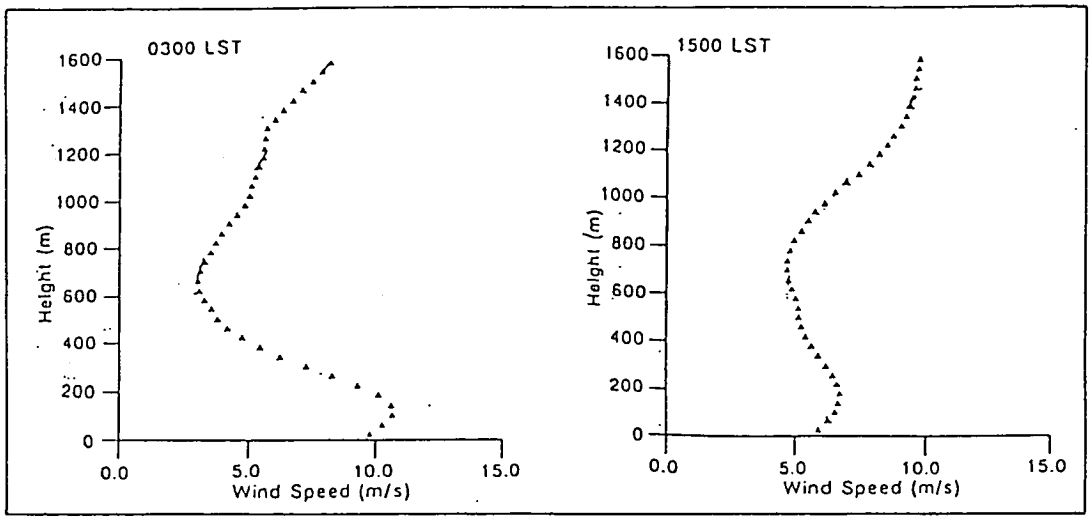

Figure 2.10: The measured profiles of wind speed in Adelie Land, Antarctica (Kodama et al 1989).

produces wind velocities up to $20ms^{-1}$. Here the winds are truely katabatic, which means they may be more sporadic in nature compared to elsewhere on the ice sheet. Upslope topography is also important, particularly where it leads to confluence, and thus acceleration of the air flow as the slopes increase, as may be seen in fig. 2.11, (Parish 1984); air flow over Adelie Land converges at Port Martin and Cape Denison producing very high wind speeds.

The West Antarctic Ice Shelf

The winds in the West Antarctic Ice shelf bear many of the characteristics of the winds of the interior region of the eastern ice sheet. Quasi-geostrophic flow has been observed at Byrd station for example (Schwerdfeger & Mahrt 1968a,b). However the other type of winds prevalent on the ice shelf are the barrier winds of the Ross ice shelf and the Antarctic Peninsula. These arise when a stable flow approaches a mountain barrier. In this situation the stable flow is unable to cross the barrier and results in a build up of stable air on the windward side of the mountain range, this then creates a horizontal temperature gradient, shown

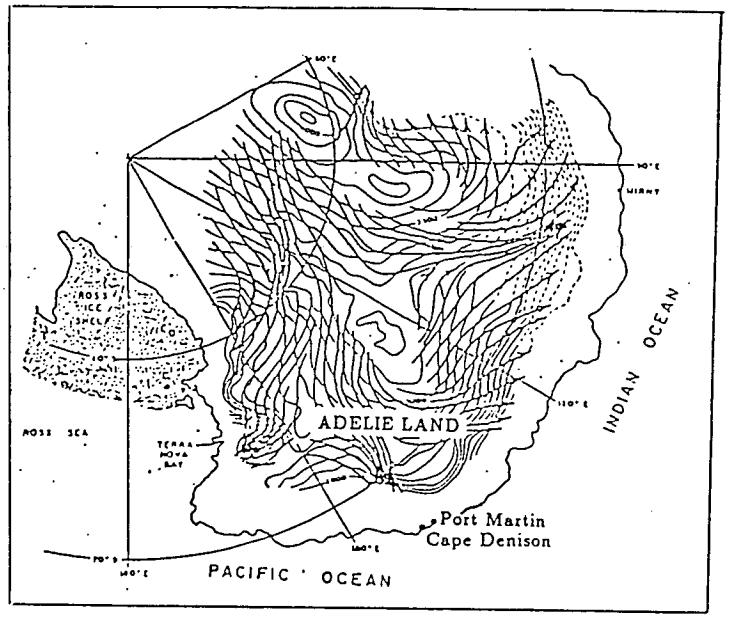

Figure 2.11: The flow lines based on model wind calculations over Adelie Land by Parish (1984).

in fig. 2.12, and an associated thermal wind, which when subtracted from the geostrophic wind above the stable layer produces a surface wind parallel to the mountain range. Over the Antarctic continent this is the southerly flow over the Ross ice shelf, which arises from stable air masses approaching the Trans Antarctic Mountains from the east. There is a similar phenomena to the east of the Antarctic Peninsula caused by easterly flow over the Filchner and Ronne Ice Shelves, but which is not shown on fig. 2.8.

2.2 The Climate of Greenland

Greenland is located in the zone of maximum westerly flow and therefore its climate is much less isolated than that of Antarctica. The climate of Greenland both affects, and is affected by, the global atmospheric dynamics in a more direct

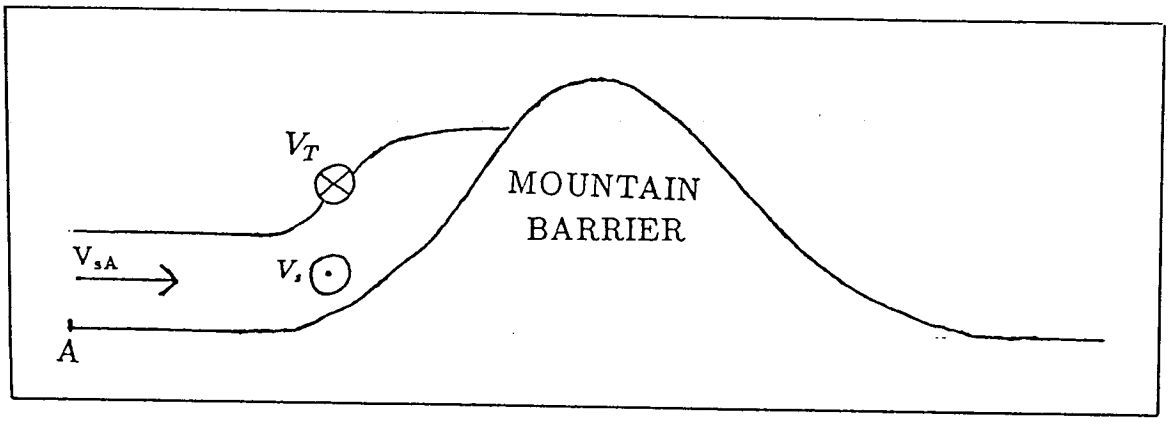

(a)The build up of cold stable air on the windward side of the mountain range and the associated thermal wind.

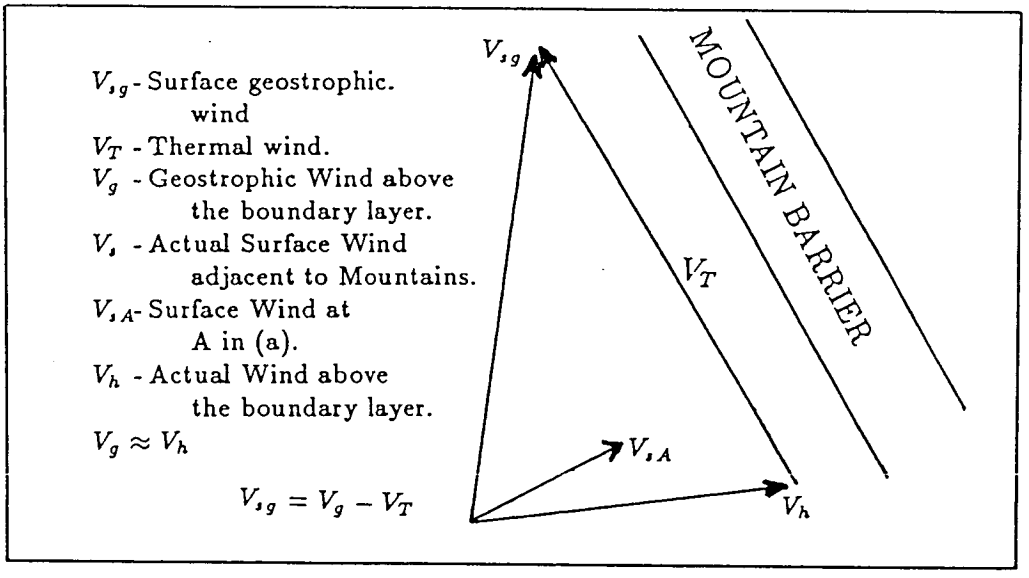

(b) The geostrophic wind above the inversion (V_g), the thermal wind due to the temperature gradient A-B in (a) (V_T), and the resultant surface wind (V_s).

Figure 2.12: The formation of barrier winds in the East Antarctic.

way than that of Antarctica. The ice sheet, at over 3000m, is a barrier to the mean zonal flow, and along with the Rocky mountains and the Urals, generates waves and pressure disturbances in the flow, increasing the meridional exchange of air masses. The main centres of exchange are the warm air flowing northwards on the west of the continent in the Davis Strait, and cold air travelling south on the east coast, the Denmark Strait (for locations see fig. 2.13). In addition to this, the strong winds that are deflected to the right as they flow off the ice sheet generate ideal conditions for cyclogenesis in both the Davis Strait-Baffin Bay area, and the Denmark Strait-Iceland area, when the cold polar southeasterly flow at the west coast, or the northwesterly flow on the east coast meets the relatively warm ocean water (Radok et al 1982). The distribution of sea ice, complicates the climate yet further; in particular, from December to March, when the Davis Straits are almost completely iced over, the Smith Sound is ice-free. This large area of open sea to the north-west of the Thule Peninsula destabalises the air, increasing the activity of cyclogenesis to the west (Putnins 1970).

Despite the differences of the Greenland climate in its role in the global dynamics, the climate of the ice cap itself is very similar to that of the Antarctic; it is dominated by the surface inversion. However, cyclonic influences are generally greater, and lows approaching the southern tip of Greenland may split, with one low moving north into Baffin Bay and the other half travelling in a north-easterly direction across the ice sheet to the Greenland Sea in the west. Sometimes a low pressure centre may cross the ice sheet as an upper level wave disturbance, disrupting the inversion and boundary layer structure, before undergoing regeneration at the east coast. Complete low centres rarely penetrate into the interior and cross the ice sheet, unless there is strong zonal flow and conditions for regeneration at the coast by the flux of cold air from the ice cap.

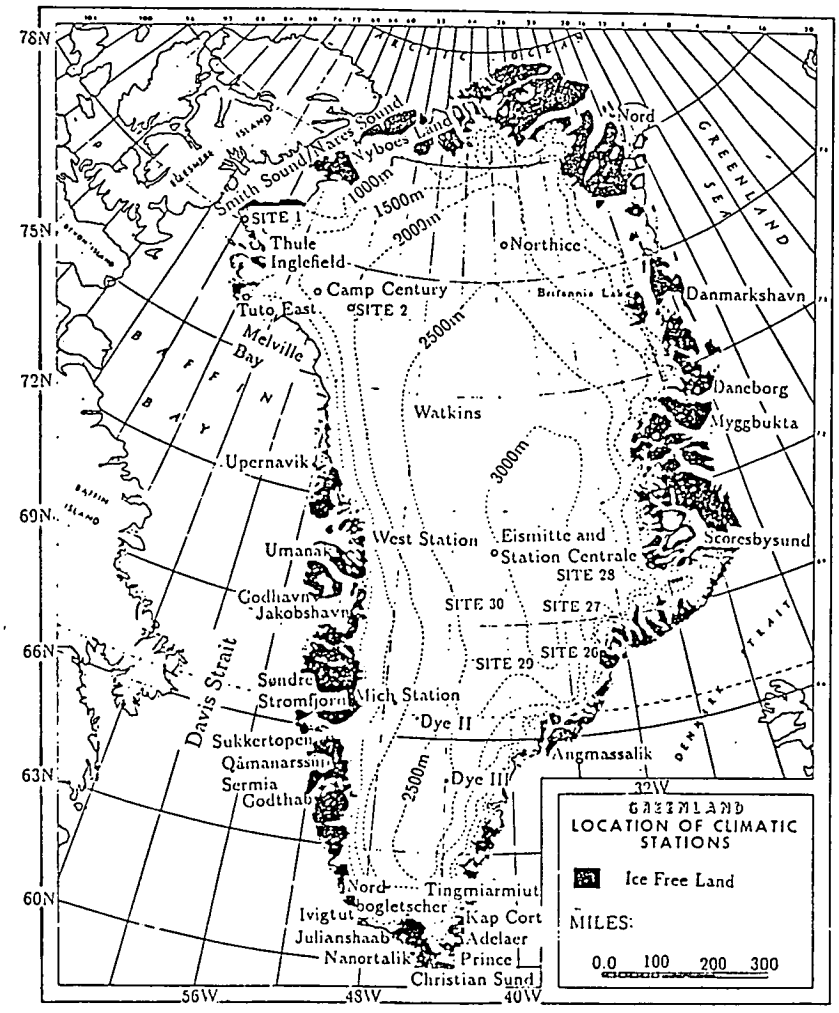

Figure 2.13: The observation sites and the elevation of the Greenland Ice Sheet, compiled from information from Radok et al (1982) and Ohmura & Reeh (1991).

There are very few observations available for Greenland, particularly inland from the coast where only a few permanent stations have been set up; Eismitte or Station Centrale and Northice in the centre of the ice sheet, offer most information about the interior. Other information is available from expedition traverses and, for mean annual temperature and accumulation, pit sites.† Fig. 2.13 shows the main sites of observations, traverses and elevation of the ice sheet.

2.2.1 Temperature and Radiation

Radiation

Measurements of radiation are rare in Greenland, most have been obtained during ablation studies and therefore concentrate on the coastal ablation zone. Estimates that have been made of the radiation budget at the surface are shown in table 2.5. The estimates suggest a net loss of radiation from the surface of the ice in the interior; as in the Antarctic, high albedos mean that the ice reflects most of the incoming solar radiation, and longwave cooling of the surface is the dominant radiational component. In contrast to Antarctica, Greenland has an ablation zone, and once ice begins to melt, the albedo decreases, from about 0.8 to 0.6 in the example in the table. This initiates a positive feedback in the ablation process, since as the albedo decreases, more solar radiation is absorbed, and more ice melts which decreases the albedo yet further. The short wave balance is much greater therefore in the summer than during the winter.

Fig 2.14 (Radok et al 1982) shows the mean surface temperature of the Greenland ice sheet, constructed from the 10m depth measurements in pits. It has been consistently shown that the temperature of the ice 10m below the surface approximates the mean annual surface temperature (Benson 1962, Radok et al 1982). The lack of stations makes it difficult to construct mean monthly isotherm maps since data from pit sites are useless in this instance. Fig. 2.15 shows the mean air temperature of Greenland after Prik (1959) (Vowinckel & Orvig 1970). The pattern common to all 3 maps is the low temperatures over the Plateau, -50°C in January and -10°C in July. In contrast to Antarctica temperatures at the coast are above freezing in the summer, as would be expected in the region where the net surface radiation exceeds zero, the ablation zone.

Flux	(annual)		(summer)			
	Loewe(1964)[a]		Ambach 1979		Braithwaite Olesen (1990b)	
	interior	margin	Ac Zone Carrefour	Ab. Zone CampIV	Ablation Zone	
					Nordbog-letscher	Qamanârssûp Sermia
SW down	72	72	-	-	-	-
SW up	59	42.5	-	-	-	-
net SW	13	27.5	51	157	123.3	$156.6 Wm^{-2}$
net LW	-20	-20	-45	-42	-24.1	$-32 Wm^{-2}$
Sen.Heat			2	22	26	$52 Wm^{-2}$
Lat.Heat					-0.8	$-15.9 Wm^{-2}$
Balance	-7	7.5	-8	137	114.4	160.7

[a]given by Radok et al (1982)

Table 2.5: Estimates of the surface radation balance over Greenland (Wm^{-2})

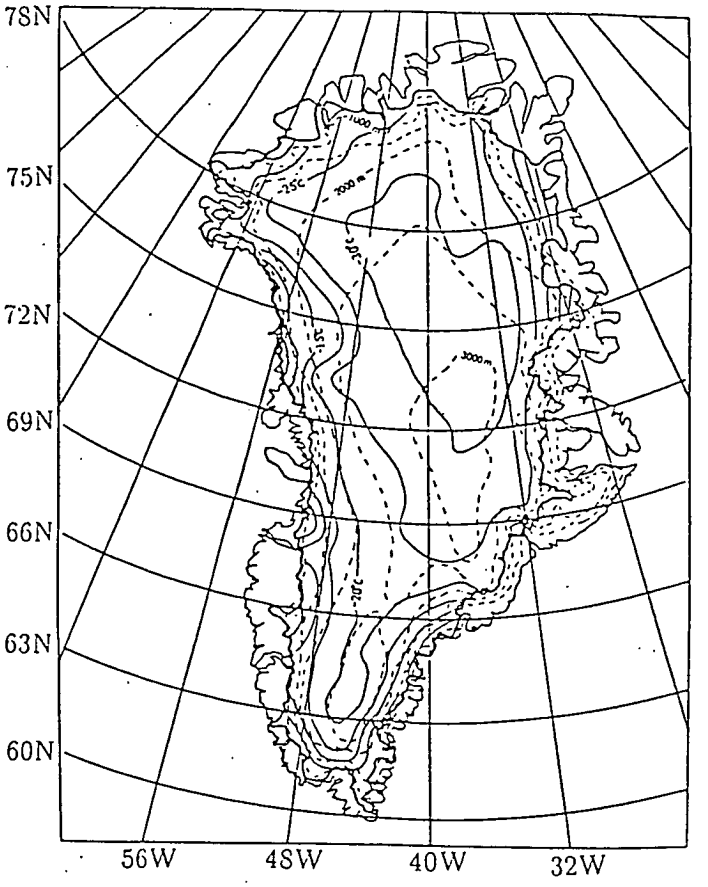

Figure 2.14: The mean annual surface temperature over Greenland constructed from snow pit sites (Radok et al 1982).

Surface Temperature Gradients The surface temperature gradient in Greenland has been investigated by several authors. Diamond (1960) estimated that the mean annual temperature gradient along the surface of the ice is between 0.6 and 0.8°C/100m. The lower values being found on the Thule Peninsula, which was previously mentioned as an area affected by frequent low pressure invasions from the ice-free sea to the north-west. Langway (1959) asserts that the temperature gradient in Greenland varies according to the orientation of the slope and found the low surface temperature gradients on the north-west facing slopes of Nyboes Land of 0.6°C/100m to be largely the result of saturated air from the Polar Seas rising over the land at the saturated adiabatic lapse rate.† Therefore it is important to distinguish between the surface temperature gradients near to the coast, which may be influenced by advection of moist air from the sea, the gradients of the interior and gradients of E-W facing slopes dominated by katabatic flow off

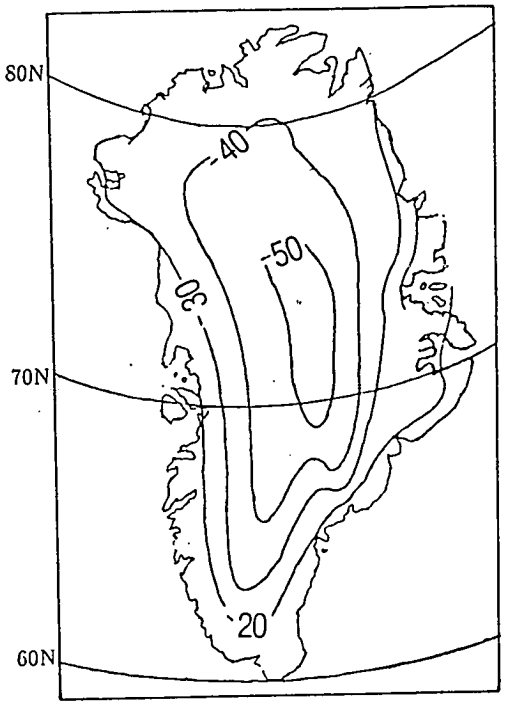

(a) January

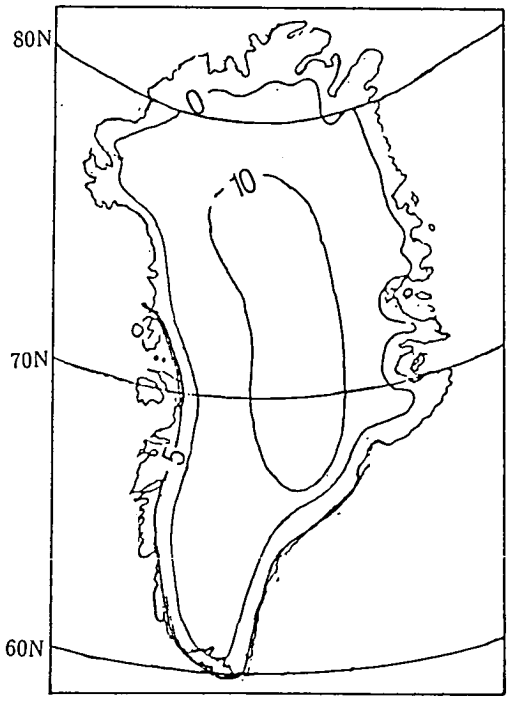

(b) July

Figure 2.15: The mean monthly surface temperature over Greenland (Vowinckel & Orvig 1970 after Prik 1959).

the central plateau. Bensons' (1962) analysis confirms this, and cites 3 additional reasons for deviations from adiabatic temperature gradients.

(i) Radiational cooling may be greater at high elevations where the water vapour content of the air is less. This may lead to superadiabatic temperature gradients between the interior and the coast.

(ii) Melting at low elevations; in Benson (1962) this is given as a reason for the temperature gradient being greater than adiabatic. In fact the process of melting takes in latent heat which would have the effect of decreasing the temperature gradient.

(iii) As the air becomes warmer downslope it can absorb more moisture from the snow which, depending on the wind speed may decrease the surface temperature gradient.

These explanations are supported by observations on the traverse described by Benson(1962), east of the Thule Peninsula. The gradient was slightly less than adiabatic in the summer (0.91°C/100m) when storm wind penetration over the continent is more likely, and in winter when the katabatic flow is strongest, they exceeded the DALR (1.05°C/100m). A further process which may increase the surface temperature gradient on the slopes was put forward by Fortuin & Oerlemans (1990) in relation to the Antarctic, but may also apply over Greenland; this was the entrainment of warm air from above the boundary layer, which increases as the katabatic wind speed increases.

Vertical Temperature Structure During the winter an inversion exists almost permanently over the ice sheet. This has been noted as a feature of the climate of the north Polar region (Vowinckel & Orvig 1970), but a lack of data

means it is difficult to assess the temperature structure in detail. Observations at Station Centrale indicate a mean January inversion depth betweeen 1949 and 1951 of 329m with a strength of 9.9°C, and overlain by a thin isothermal layer. In the summer the inversion is weakened. At the coast warm air advection may mean it is destroyed completely, but in the interior there is generally a weak raised inversion. At Station Centrale in July, observations for the same period mentioned above, found a mean inversion to extend from 705m to 968m above the surface but the temperature increase was just 0.8°C.

2.2.2 Mass Balance

Accumulation Many authors have made estimates of accumulation over Greenland (eg. Bader (1961), Benson (1962), Langway (1959)) Fig. 2.16a shows a recent assessment of the accumulation over the Greenland ice sheet by Ohmura & Reeh (1991). The sporadic nature of the climatic data over Greenland means that the observations aren't all taken from the same year, so the values over the ice sheet are not strictly comparable (Radok 1982). However Radok states that the inter-annual variations are probably small, and the figures give a reasonable overview of the accumulation pattern, and Ohmura & Reeh (1991) excluded data from stations with short records or those contaminated by melt. Most precipitation over Greenland is orographically induced, and may be enhanced by cyclogenesis, particularly at the coast. As shown in fig. 2.16, maximum accumulation occurs on the south east facing slope of the southern dome, decreasing rapidly eastwards. A secondary maximum occurs on the west facing slope and on the south facing slopes around Baffin Bay. The smallest accumulation is in the north eastern sector of the ice sheet and a small area of the west coast around 66°N.,

The precipitation pattern may be explained according to the circulation of the air over the ice sheet, shown in fig. 2.17 (Ohmura & Reeh 1991). The circulation is dominated by the Icelandic low to the south east and the Baffin Bay low in the west. During the winter, the easterly flow from the Atlantic is very moist after a long ocean trajectory, therefore producing the high precipitation observed on the south east of the southern ice dome. Radok et al (1982) suggests the precipitation may be enhanced in this region due to cyclogensis encouraged by the cold air flowing off the ice cap undercutting the relatively warm air over the ocean. The western side of the ice cap is under the influence of modified continental air from North America. This air has a much lower water vapour content, hence the lower values of precipitation observed in this region compared to the southern dome. Most precipitation in the west is caused by cyclones from the Atlantic Ocean travelling north into Baffin Bay. During the summer the influence of the Icelandic and Baffin Bay lows is weakened and a pressure ridge exists orientated towards the centre of the ice sheet from the north east in a south easterly direction. This reduces the precipitation in the south east, but the air entering Baffin Bay has a slightly greater southerly component, and therefore a longer ocean passage, with higher water vapour content than during the winter. Thus, the west coast tends to experience a summer maximum of precipitation compared to a winter maximum on the south east sector of the southern dome, Radok et al (1982) suggests the maximum on the west coast occurs in the autumn rather than the summer. The low in the Polar Basin encourages precipitation to fall on the north west facing slopes, creating a summer maximum in this region. The north east slopes, however remain in the rain shadow throughout the year.

Ablation and Mass Balance The equilibrium line altitude (ELA)† has been estimated to be at around 1390m, and many estimates have been made of the total balance for the whole ice sheet, both positive and negative. It is thought

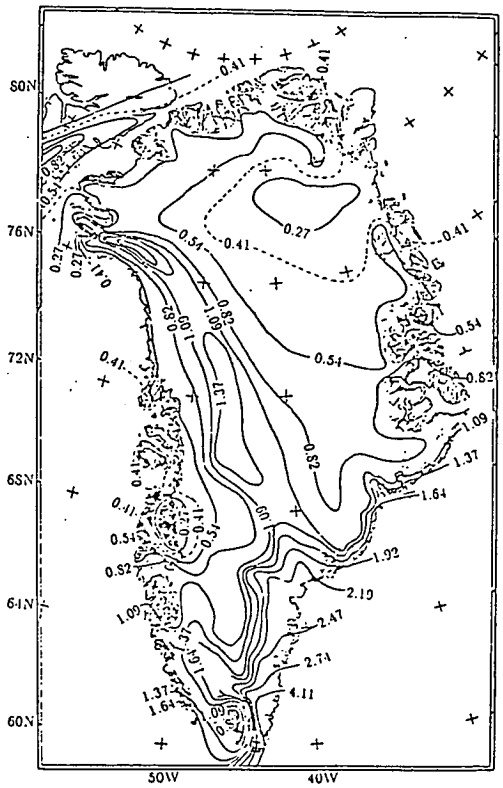

(a) Accumulation taken from Ohmura & Reeh (1991).

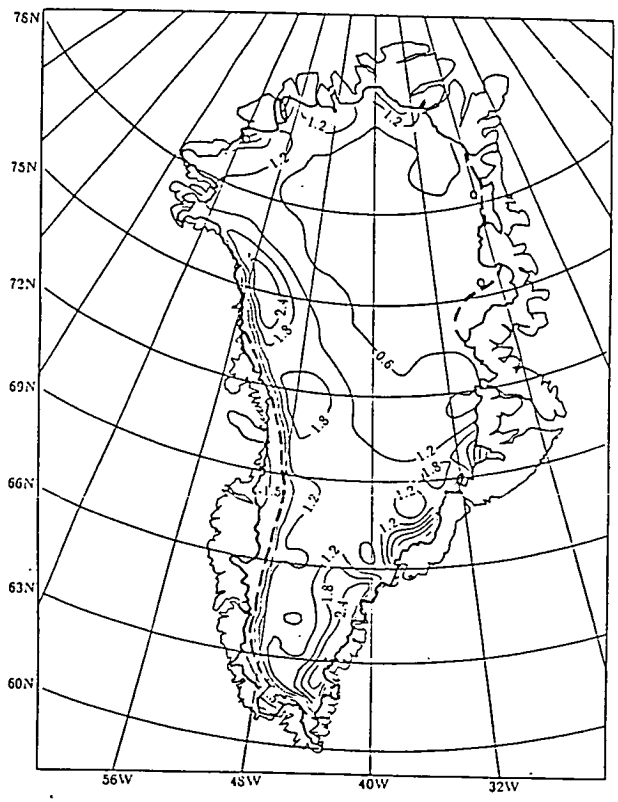

(b)Net Mass Balance taken from Radok et al (1982).

Figure 2.16: The accumulation and mass balance of ice over the Greenland ice sheet in $mmday^{-1}$ water equivalent.

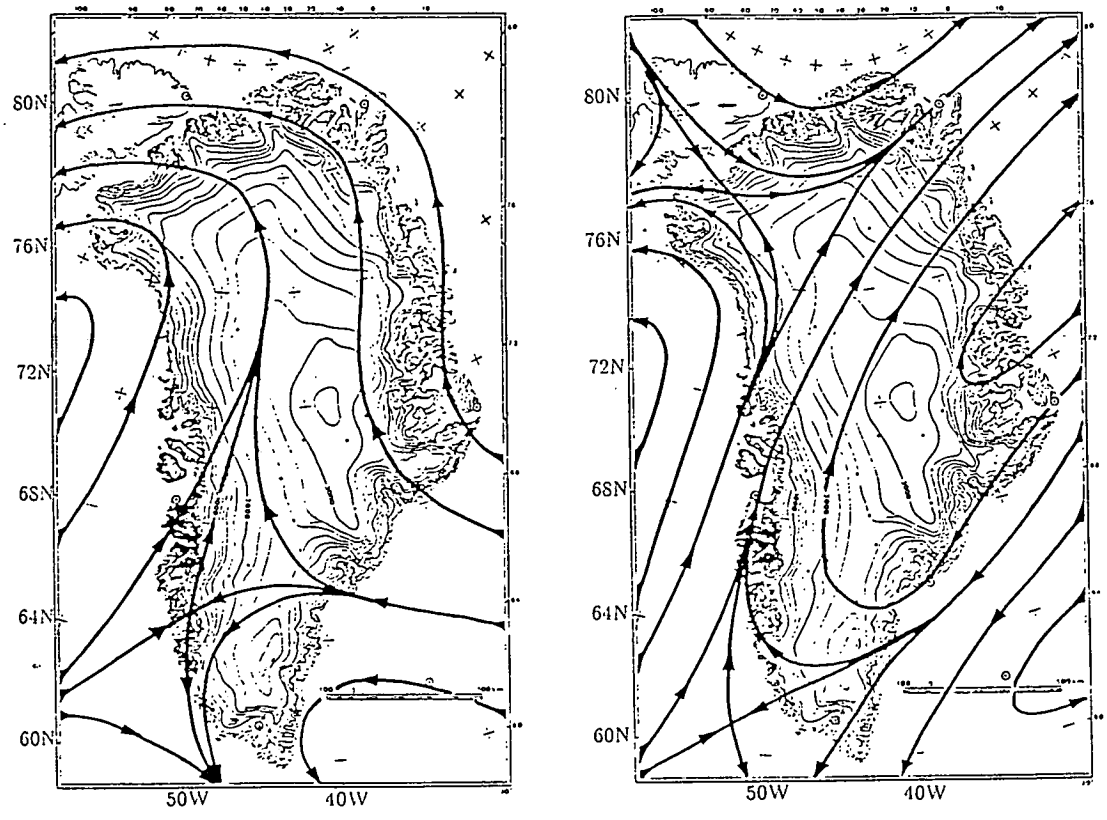

(a) January (b) July

Figure 2.17: The resultant wind over Greenland at 850mb (Ohmura & Reeh 1991).

to be approximately zero at present, but the rate of retreat of ice at the margins is expected to increase if there is climatic warming (Letregully et al 1991). Fig. 2.16b shows the mass balance as estimated by Radok et al (1982); the line of zero mass balance is the equilibrium line altitude. The pattern of contours is similar to those of accumulation, the large positive mass balance occuring where accumulation (fig. 2.16a) is large. The actual amount of ablation is uncertain and spatially variable, locally on the coast it may be much higher than the contours indicate. Braithwaite & Olesen (1990a,b) used radiation budgets to assess ablation at two coastal sites Nordbogletscher and Qamanârssûp Sermia, they give estimates of 26.4mm water/day and 33.4mm water/day respectively. They found the budget to be dominated by the radiation balance accounting for 2/3 of the mean ablation, mainly due to the SW radiation, the turbulent heat fluxes contributed much less to melting, of the order of 1/3.

Station	Wind Speed ms^{-2}		wind direction	
	Jan	Jul		
West Station	8.9	4.1	$> 10ms^{-2}$ 110°	$> 15ms^{-2}$ 108°
Eismitte	4.7	4.2	$> 8ms^{-2}$ 141°	$> 12ms^{-2}$ 152°

Table 2.6: The wind speed and direction at Westation and Eismitte in Greenland

2.2.3 Wind

Data for wind speed and direction are limited, but table 2.6 (Putnins 1970) shows the January and July wind speeds and the most common wind direction for the highest wind speeds at 2 stations, one in the interior (Eismitte) and one at the coast (West Station). As may be expected the winds tend to be strongest in the winter, and weaker in the central region where the depth of flow may only be 100m. Consistent with the theory of drainage flow and katabatic winds the predominant direction is easterly, on the western facing slopes, although with a large component parallel to the relief contours (which run approximately north - south) in the interior (Putnins 1970).

2.3 Summary

This chapter gives a general outline of the characteristics of the climate over the Antarctic and Greenland ice sheet. The main findings can be summarised as follows:

- The climate of ice sheets is dominated by the negative radiation balance which produces a temperature inversion over the ice.
- In Antarctica the temperature structure and surface slope characterise the wind regime in 3 zones over the ice sheet, the interior zone, the glacial slopes and the coastal zone.
- In the interior flow is quasi-geostrophic, a result of the thermal wind created by the inversion over the shallow slopes.
- On the glacial slopes the increase in buoyancy of the air causes acceleration, and the development of a more distinct boundary layer where the flow is governed by buoyancy, the geostrophic wind, coriolis force and friction.
- At the coast flow is more sporadic, driven by the buoyancy force and dependent on the nature of upslope conditions.
- There is very little precipitation over Antarctica, ablation is mainly by ice calving, the net mass balance is approximately zero.
- The climate of Greenland is also characterised by a surface temperature inversion.
- Boundary layer winds exist in Greenland in a similar way to those of Antarctica, but the plateau is much smaller and the flow frequently interupted by the mean zonal flow.
- Precipitation over Greenland is greater than Antarctica; it is a result of the orography of the ice sheet and general circulation of the region. It is enhanced in regions of cyclogenesis at the coast, which may be fed by the cold drainage flow from the ice sheet.

- The Greenland ice sheet has an ablation zone, where ice is lost due to evaporation/melt during the summer months. There is also loss of ice due to ice calving. The net mass balance is approximately zero at present, but it is thought to be sensitive to climatic warming.

This information will be used as a comparison for the data from GCM simulations in chapter 3. The nature of the boundary layer, as the layer of air adjacent to the ice, plays a critical role in determining the temperature at the surface of the ice sheet and the rate of removal of cold air from the centre of the ice sheet. If climate and ice sheets are to be successfully coupled, accurate representation of these processes, which may potentially affect the mass balance of the ice sheet, is essential. Boundary layer processes are particularly important because of their influence on ablation, which appears to be an important component of ice sheet models (Hyde & Peltier 1985). The data specific to the boundary layer, summarised in the following 3 tables and explained in section 2.1.3, will be used in chapter 4 to provide constraints on a slab model used to investigate the evolution of the atmospheric boundary layer over an ice sheet.

INTERIOR STATIONS													
Station & location	altitude (m)	slope	slope direction	wind direction	deviation of wind from slope	wind speed (ms^{-1})	surface temp (°C)	inversion (°C) Mean Jan July	humidity	cloud amount (tenths)	ppn (mm/day) (includes blown snow)	pressure (mb)
VostokII 78.45°S 106.9°E	3500	0.0011	285°	250° range 200-250	35°	Mean5.1 Jan 4.4 Jul 5.3	Mean-55.6 Jan -32.3 Jul -67.0	15.7 1.0 22.6 av. ΔT to 4km (512m above ground)	Mean75% Jan 78% Jul 73%	Mean4.2 Jan 4.2 Jul 3.5	Mean0.15 Jan 0.02 Jul 0.19	Mean624.2 Jan 632.7 Jul 624.4
Plateau 79.25°S 40.5°E	3620	no reliable data		10° range 320-040	n.a	Mean(4.3) Jan 3.0 Jul 5.8	Mean-56.4 Jan -33.9 Jul -68.0	——no data available——				Mean609.2 Jan 619.0 Jul 605.3
South Pole 90°S	2800	complex 0.00176 $\pm$0.0026	110-150°	20°	100°	Mean6.21 Jan 4.2 Jul 7.4	Mean-49.3 Jan -27.9 Jul -59.9	13.0 1.3 17.4 [14.1] [-0.5] [20.2] to 650mb[to 600mb]	n.a	Mean3.7	Mean0.49 Jan0.07 Jul0.02	Mean680.9 Jan 687.8 Jul 677.4
Sovietskaya 78.4°S 87.6°E	3650	0.0015	140°	110°	30°	Mean3.6 Jan 2.5 Jul 4.4	Mean(-56.0) Jan n.a Jul -69.9	no data available		Mean(2.5) Jan n.a Jul 1.6	Mean(0.14) Jan n.a July0.21	Mean(608.6) Jan n.a Jul 610.8
Komsomolskaya 74.1°S 97.5°E	3500	0.0011	210°	110°	50°	Mean3.75 Jan 5.0 Jul 4.1	Mean-52.2 Jan -32.2 Jul -62.0	no data available	Mean72% Jan 70% Jul 77%	Mean3.9 Jan 4.6 Jul 3.4	Mean0.13 Jan0.03 Jul0.12	Mean624.0 Jan 632.8 Jul 613.7
Byrd 80.0°S 119.5°W	1533	0.001- 0.002	60°	20°	40°	Mean8.2 Jan 6.0 Jul 9.9	Mean-27.7 Jan -14.7 Jul -35.6	6.4 0.4 9.4 av. ΔT to 750mb at 04h LMT	n.a	Mean6.6 Jan 6.9 Jul 5.9	Jan0.48	Mean805.8 Jan 813.3 Jul 802.7

Table 2.7: Summarised data for the interior stations

Table 2.8: Summarised data for the glacial slope stations

GLACIAL SLOPE												
Station & location	altitude (m)	slope	slope direction	wind direction	deviation of wind from slope	wind speed (ms^{-1})	surface temp (°C)	inversion (°C) Mean Jan July	humidity	cloud amount (tenths)	ppn (mm/day) (includes blown snow)	pressure (mb)
Pionerskaya 69.74°S 95.32°S	2700	0.0025	185°	140 ° range 110-160°	45°	Mean10.6 Jan 10.6 Jul 10.5	Mean-38.0 Jan -23.4 Jul -47.3	no data available	Mean76% Jan 76% Jul 74%	Mean6.0 Jan 6.5 Jul 6.2	Mean2.64 Jan 1.45 Jul 3.32	Mean690.0 Jan 698.5 Jul 687.4
Vostokl 72.15°S 96.62°E	3250	0.0023	200°	range 140-160°	50°	Station only operative Apr-Nov 1957						
						Jul 5.3	Jul -58.0		Jul 71%	Jul3.9	Jul 0.20	Jul 640.0
Charcot 69.03°S 139.02°E	2400	0.0023	210°	170° range 140-190°	40°	Mean9.61 Jan n.a Jul 9.3	Mean n.a Jan n.a Jul -48.6	no data available		Mean2.5		
Eights[a] 75.23°S 77.17°E	430	0.005	350°	185° 330-360°[b] 170-200°[c]	10-30° 165°	Mean5.24 Jan 4.9 Jul 5.4	Mean-26.0 Jan -10.0 Jul -33.5	no data available		Mean5.9 Jan n.a Jul n.a	no data	Mean942.5 Jan 942.3 Jul 949.0

[a] Actually located on the ice shelf but bears many characteristics of stations on the slope
[b] katabatic flow
[c] cyclonic flow

COASTAL STATIONS

Station & location	altitude (m)	slope	slope direction	wind direction	deviation of wind from slope	wind speed (ms^{-1})	surface temp (°C)	inversion (°C) Mean Jan July	humidity	cloud amount (tenths)	ppn (mm/day) (includes blown snow)	pressure (mb)
Cape Denison 67.9°S 142.7°E	6	0.067	180°	165°	15°	Mean22.1 Jan17.8 Jul25.0	Mean-12.8 Jan -0.9 Jul -19.6	no data available	Mean73% Jan 73% Jul 75%	Mean5.1 Jan 7.4 Jul 3.7	n.a	Mean988.2 Jan 988.6 Jul 986.8
Port Martin 66.8°S 141.4°E	14	0.065	140°	145°	5°	Mean18.5 Jan 12.8 Jul 19.5	Mean-12.2 Jan -1.6 Jul -19.0	no data available	Mean64% Jan 68% Jul 66%	Mean4.8 Jan n.a Jul n.a	n.a	Mean988.2 Jan 988.6 Jul 986.8
Maudheim 71.05°S 10.9°W	38	flat		80° 2°peak 180°		Mean7.7 Jan n.a Jul n.a	Mean-17.4 Jan -4.0 Jul -27.2	no data available		Mean5.2 Jan n.a Jul n.a	n.a	Mean989.9 Jan 989.4 Jul 988.4
Novolazarevskaya 70.8°S 11.8°E	87	0.04 - 0.05	190°	135°?	55°?	Mean10.3 Jan 7.4 Jul 10.7	Mean-10.6 Jan -0.7 Jul -17.7	no data available	Mean52% Jan 58% Jul 51%	Mean5.9 Jan 5.6 Jul 5.5	Mean0.83 Jan 0.42 Jul 0.94	Mean976.1 Jan 978.4 Jul 978.4
Roi Baudoin 70.43°S 24.32°E	37	flat		165°		Mean8.1 Jan n.a Jul9.3	Mean-15.2 Jan -4.5 Jul -23.1	no data available		Mean4.8 Jan n.a Jul n.a	no data available	
Syowa Base 69°S 39.6°S	15	0.056	100°	55° 2°peak 180°	45°/ 80°	Mean5.9 Jan 4.7 Jul 6.6	Mean-10.5 Jan -0.6 Jul -18.0	no data available	Mean73% Jan 71% Jul 72%	Mean6.6 Jan 6.5 Jul 6.0	n.a	Mean985.5 Jan 987.0 Jul 985.1
Dumont D'Urville 66.7°S 140.0°E	41	offshore island		130°	not a large katabatic component	Mean10.9 Jan 10.2 Jul 9.7	Mean-10.7 Jan -0.7 Jul -16.2	no data available		Mean5.0 Jan n.a Jul n.a	n.a	Mean988.0 Jan 989.3 Jul 992.6
Hallet 72.3°S 170.3°E	5	On Peninsula		210°	not katabatic	Mean3.6 Jan 3.1 Jul3.4	Mean-15.3 Jan -1.1 Jul -26.4	no data available		Mean4.9 Jan n.a Jul 6.5	n.a	Mean988.2 Jan 990.0 Jul 987.4
McMurdo 77.85°S 166.62°W	40	Ice Shelf flat/gentle		90°		Mean6.5 Jan 5.3 Jul 6.5	Mean-17.4 Jan -3.1 Jul -25.8	no data available		Mean6.1 Jan 6.4 Jul 4.8	n.a	Mean987.8 Jan 990.5 Jul 989.2
Halley Bay 75.52°S 26.62°W	29	Ice Shelf flat/gentle		80° 2°peak 240°		Mean4.8 Jan 4.5 Jul 5.1	Mean-18.5 Jan -4.8 Jul -28.9	no data available	Mean1.5mb[a] Jan 3.5mb Jul 0.6mb	Mean6.6 Jan 7.5 Jul 5.8	n.a	Mean989.3 Jan 991.2 Jul 989.7
Mawson 67.6°S 62.9°E	8	0.05	140°	135°	5°	Mean10.9 Jan 8.8 Jul 11.7	Mean-11.3 Jan +0.1 Jul -17.8	no data available	Mean-17.5°C[b] Jan -6.9°C Jul -24.1°C	Mean7.2 Jan 8.0 Jul 7.0	Mean1.44 Jan 0.32 Jul 3.5	Mean987.7 Jan 989.2 Jul 989.1
Molodezhnaya 67.7°S 45.9°E	42			115°		Mean10.3 Jan 5.4 Jul 11.1	Mean-10.9 Jan -0.5 Jul -18.0	no data available	Mean66% Jan 65% Jul 66%	Mean6.7 Jan 7.2 Jul 6.0	n.a	Mean983.1 Jan 988.8 Jul 986.5
Mirny 66.6°S 93.0°E	35	0.05 - 0.06	180°	150°	30°	Mean11.5 Jan 7.9 Jul 13.1	Mean-11.3 Jan -1.6 Jul -16.6	-0.3 -2.2 -0.1 increase in T to 470m above ground	Mean70% Jan 69% Jul 73%	Mean6.4 Jan 6.6 Jul 6.8	Mean1.7 Jan 0.42 Jul 2.48	Mean984.0 Jan 986.2 Jul 984.3
Davis 68.58°S 77.97°E	14	at satellite station 0.04 | 90° on rocky outcrop		45°	45°?	Mean4.9 Jan 4.7 Jul 4.9	Mean-10.3 Jan +0.6 Jul -17.3	no data available	Mean-16.2°[b] Jan -7.1°C Jul -21.8°C	Mean6.5 Jan 6.2 Jul 6.5	n.a	Mean985.5 Jan 987.4 Jul 986.9
Oasis 66.27°S 100.75°E	29	0.05 - 0.08	rocky outcrop	90°		Mean7.2 Jan 6.4 Jul 7.4	Mean-9.1 Jan +1.8 Jul -16.8	no data available	Mean56% Jan 46% Jul 70%	Mean7.0 Jan 7.0 Jul 7.2	Mean0.59 Jan 0.1 Jul 0.9	Mean983.1 Jan 986.3 Jul 985.1
Wilkes/Casey 66.25°S 110.53°E	12	0.5	110°	90° & 180°	20° (& 170°)	Mean6.9 Jan 5.1 Jul 8.0	Mean-9.2 Jan +0.1 Jul -14.6	no data available	Mean-13.2[b] Jan -4.3 Jul -18.5	Mean5.5 Jan n.a Jul 7.8	Mean0.85 Jan 0.32 Jul 0.32	Mean983.2 Jan 985.7 Jul 984.8

[a] vapourpressure
[b] Dew point

Table 2.9: Summarised data for the coastal stations

Chapter 3

The Climate Over Model Ice Sheets

In chapter 1, it was stated that this thesis aims to investigate the climate over ice sheets, and particularly the way in which models can be used to simulate the components of the climate system to which ice sheets are most sensitive. The work of Hyde & Peltier (1985), and Oerlemans (1981) showed that evolution of ice in models is extremely sensitive to the climatic upper boundary conditions, particularly in the ablation zone,† yet the climate of ice sheet models is generally very crudely prescribed. Furthermore there is evidence that the change in mass balance† produced by an external forcing on the climate, is not independent of altitude. Oerlemans & Hoogendoorn (1989) and Braithwaite & Olesen (1990b) both found the largest change to occur at the margin, therefore the technique outlined in chapter 1, commonly used to drive models of the glacial cycles, by moving a theoretical climate point† north and south but maintaining a constant slope of the climate surface† (eg. Hyde & Peltier 1985), is not necessarily realistic. Introducing a more detailed climate to ice sheet models causes problems, due to the disparate timescales between climate and ice sheets and a lack of detailed knowledge of the real climate over ice sheets, highlighted in chapter 2. There has been very little work which has attempted to assess the model climate over

ice sheets. When GCM's have been used to investigate 'snap-shot' pictures of ice age climate the accuracy of the model climate over the ice sheet is not always considered, (eg. Kutzbach & Guetter 1986), despite model evidence that ice sheets are very sensitive to its variation. The models must be able to simulate the climate over the ice sheet in order that they can drive a model of an ice sheet, causing it to grow and retreat in a manner that is consistent with the palaeoclimatic evidence.

This chapter is therefore an attempt to address this problem. Based on the descriptions of chapter 2, a comparison will be made between the GCM climates, and the observed climate over ice sheets. The two models which have been chosen are the Meteorological Office (Met.O) General Circulation Model and the NCAR Community Climate Model 1. The Met.O model is a large grid scale model referred to widely in the climatological literature as a 'state-of-the-art' model. The NCAR model on the other hand, is a spectral model, and therefore provides a useful comparison to a grid point model. GCM's have limitations in their resolution, which make it difficult to represent the boundary layer realistically. In the ablation zone it is boundary layer processes which largely determine the amount of ablation;† chapters 4 and 5 will look at a simple way in which the boundary layer of the ablation zone can be investigated in more detail.

3.1 Description of the GCM's.

A brief description of each of the models taken from the handbooks is given below; because this information is repeated in other sources the description does not include the details of model equations. For this, the original work should be referred to, which for the Met.O model is the Handbook of the Met.O GCM by Slingo (1985), and for the NCAR model is the Description of the NCAR CCM1

by Williamson et al (1985).

3.1.1 The Met.O GCM

The Met.O GCM is an 11-layer grid point model with a $2.75^o \times 3.5^o$ latitude longitude grid and a 10 minute timestep. The model has coordinates (x, y, σ) where $\sigma = p/p_*; p_*$ is the surface pressure. It is governed by the conservation of mass, momentum, heat and moisture, so the variables are surface pressure, wind velocity, temperature, and moisture content. The model has an interactive radiation scheme and is therefore not constrained by parameters based on present day climate (Slingo 1985). Cloud is predicted by the model, allowing random overlapping of 3 layers, and 1 convective tower, which may extend through one or more layers, depending on the extent of convection. The radiative properties of the cloud are prescribed. The radiatively active gases CO_2, O_3,and $H_2O(g)$ are prescribed. For the shortwave fluxes, the albedo is prescribed from the global dataset for land according to Wilson and Henderson-Sellers (1985) (quoted from Slingo 1985); snow covered land albedo is prescribed according to snow depth; sea-ice albedo is prescribed as a function of temperature. The albedo of ice sheets is held constant at 0.8. Longwave radiation is treated in 6 spectral bands and the contributions from each of the bands, are calculated at each layer boundary, with emissivities and absorptivities for each layer calculated assuming a constant mass mixing ratio of each gas within a layer. Clouds, with the exception of high cloud, are treated as black bodies emitting at the temperature of the cloud boundary.

The boundary layer is the lowest 3 layers of the model with eddy diffusivity representing the turbulent exchanges of momentum, sensible heat and water vapour, over a surface of sea, sea-ice, land-ice or land. The sea surface temperature is

prescribed, and over land-ice, sea-ice and land the temperature is calculated from a surface energy balance equation. Sea-ice forms when the temperature falls below 271.2K and land ice at temperatures lower than 273K. Snow depth and soil moisture content vary according to the water vapour, snow and heat budgets.

Precipitation forms in the model when the specific humidity exceeds the saturation specific humidity for the layer temperature, and latent heat is released due to condensation; if the temperature is less than freezing, latent heat of fusion is released as the precipitation is allowed to freeze. The snow is melted if it enters a layer greater than 273K. The precipitation is summed through the layers to determine the precipitation at the ground. A penetrative convection scheme is used; convection is initiated when a parcel of small excess buoyancy becomes more buoyant after rising to the layer above. In the convection process, buoyant plumes are allowed to rise and entrain environmental air, until they cannot rise to the next layer and remain buoyant, at which point detrainment is assumed to occur until the residual parcel can rise and remain buoyant at the next level. Once the mass of the plume is less than a defined lower limit it is assumed that it will be destroyed by entrainment.[†]

3.1.2 The NCAR CCM

The NCAR model is a spectral GCM with 9 sigma levels and a timestep of 30 minutes. It solves the primitive equations conserving mass, momentum, heat and moisture in spectral space, but the physical parameterisations are carried out in grid point space, with a latitude longitude spacing of $4.4^o \times 7.5^o$. As with the Met.O model there is an interactive cloud scheme, clouds forming whenever the air becomes saturated, with random overlapping of layers, but no cloud in the

layer near the surface or the top two layers. Multiple reflections of radiation are permitted between layers of cloud and between the lowest layer and the ground. The shortwave radiation scheme requires prescribed O_3, CO_2 and H_2O mixing ratios and prescribed surface albedo. This is constant over land, based on the Matthews (1983) (quoted from Williamson et al 1985) dataset, with a dependence on solar-zenith angle. The snow albedo is weighted using 50% land albedo and 50% snow albedo, ice is prescribed an albedo of 0.8 and sea-ice 0.7. The longwave radiation is solved using emissivities and absorptivities of each layer; the emissivity of convective cloud is given as 1 and that of non-convective cloud (formed under stable† conditions) according to moisture content.

The boundary layer treatment is similar to the Met.O model using a bulk aerodynamic parameterisation up to the first model layer, and surface temperature is calculated from an energy balance equation. Sea surface temperatures, sea ice locations and snow cover are prescribed according to their seasonal variation.

3.2 The Simulated Climate over Antarctica

In chapter 2 it was explained that the seasonal evolution of Antarctic climate is strongly influenced by the polar night, which produces the characteristic 'coreless winter' (eg.Schwerdfeger 1970). This is a useful starting point for any comparison of the model climate over the ice sheet to that which is observed. Fig. 3.1 shows the mean monthly surface temperature for the Met.O model at latitudes 71.25°S and 81.25°S between longitudes 60°W and 120°W. Comparing fig. 3.1 to the temperature regime of Cape Denison and Vostok II in fig 2.3, it can be seen that the coreless winter is reproduced fairly well, with temperatures falling to a minimum value by April, and remaining low for 6 months before beginning to rise

Figure 3.1: The mean monthly temperature variation of the Met.O model along latitudes 81.25°S (——x——) and 71.25°S (——·——) between 60°W & 120°W

again. The model does not appear to reproduce the latitudinal difference in the length of the coreless winter. Referring back to chapter 2 it will be remembered that closer to the interior a longer winter is observed; temperatures may remain consistently low for 8 months of the year. The failure of the model to reproduce this, suggests that the balance between the downward atmospheric radiation beneath the inversion and the upward flux from the ground, which is responsible for the maintenance of the coreless winter, is not accurately reproduced by the model. This will be investigated in the following sections. The climate of Antarctica is strongly influenced by surface topography. The resolution of both models requires that the model topography is smoothed, and this is an important consideration to make in any assessment of the model climate. The topography for each of the models is shown in fig. 3.2.

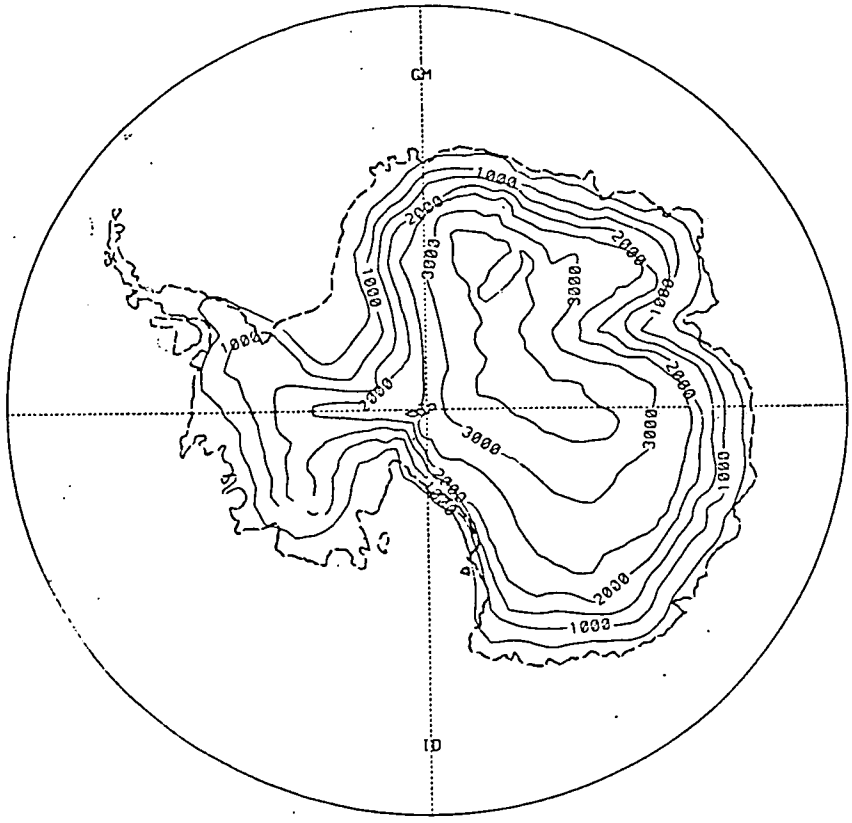

(a) Met.O model

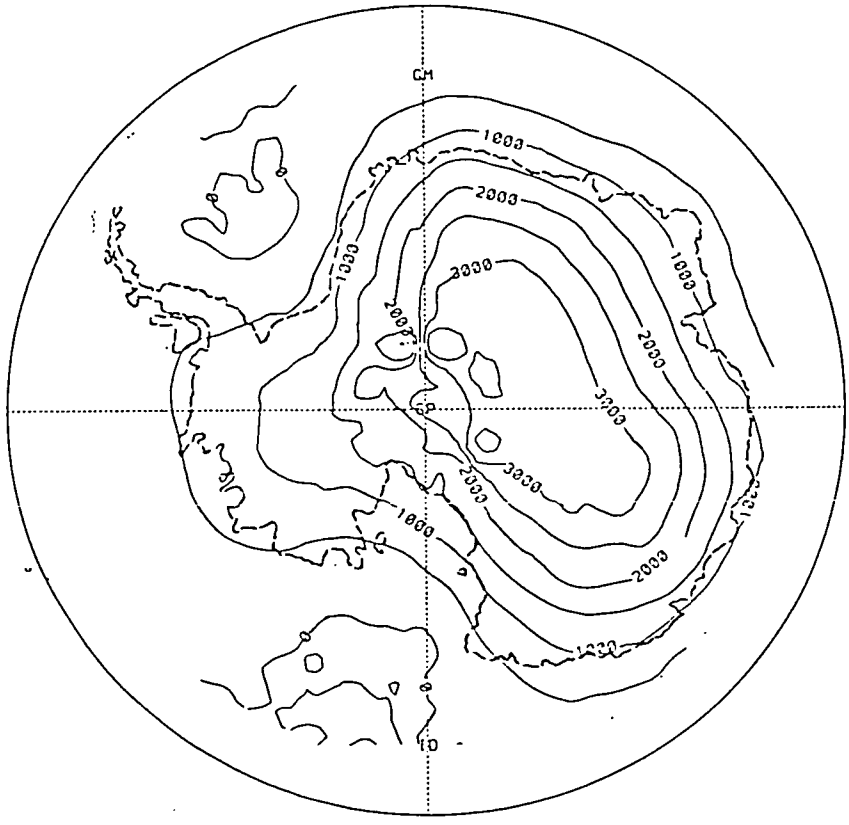

(b) NCAR model

Figure 3.2: Surface topography over Antarctica for each of the models.

3.2.1 Surface Temperature and Radiation

A realistic simulation of the temperature and radiation balance for a GCM is critical if the model is to be able to predict ablation accurately. On the Antarctic ice sheet this isn't strictly applicable as the temperature remains below freezing throughout the year. However, Antarctica is the largest area of ice with a reasonably known radiation and temperature regime and therefore provides an essential indicator of the models ability to predict these variables over ice.

Temperature

The surface temperature of the models over Antarctica are shown in figures 3.3 and 3.4. Both models reproduce the assymetry of the contours over the continent, shown in fig. 2.2, such that rather than being centred on the pole, the coldest region is the East Antarctic Plateau. Neither of the models reproduce the very cold core in the centre of the continent in July, where temperatures on the very high plateau fall to -70°C. The NCAR model is closest with a similar area of ice enclosed by the -60°C isotherm. The Met.O model only reaches -60°C at a location much further west than the lowest observed temperatures. Over the central plateau the temperature only falls to -55°C. The coastal region on the other hand is too cold, the -30°C contour which lies inside the boundary of Antarctica in July is at the coast or over the sea-ice in both models.

The summer (January) simulation is better for the NCAR model, reaching -30°C; the Met.O model is reasonable but remains slightly too warm over the central Plateau, where the minimum contour is -25°C. Both models produce temperatures which are slightly low at the coast. The -2°C contour which follows the coast in

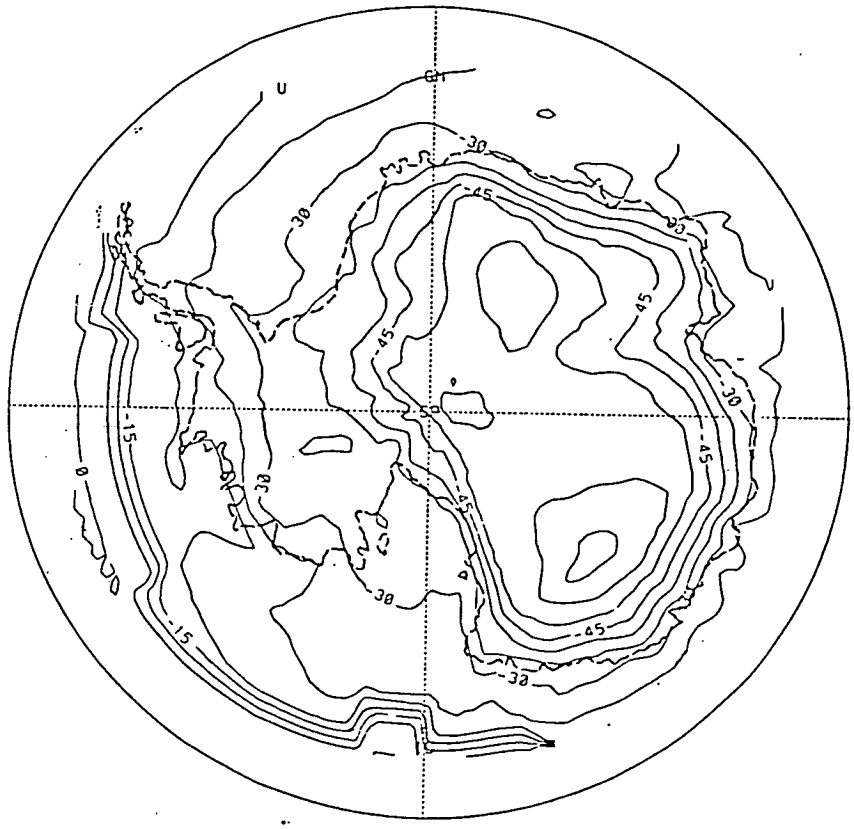

(a) July (contours at 5°C intervals).

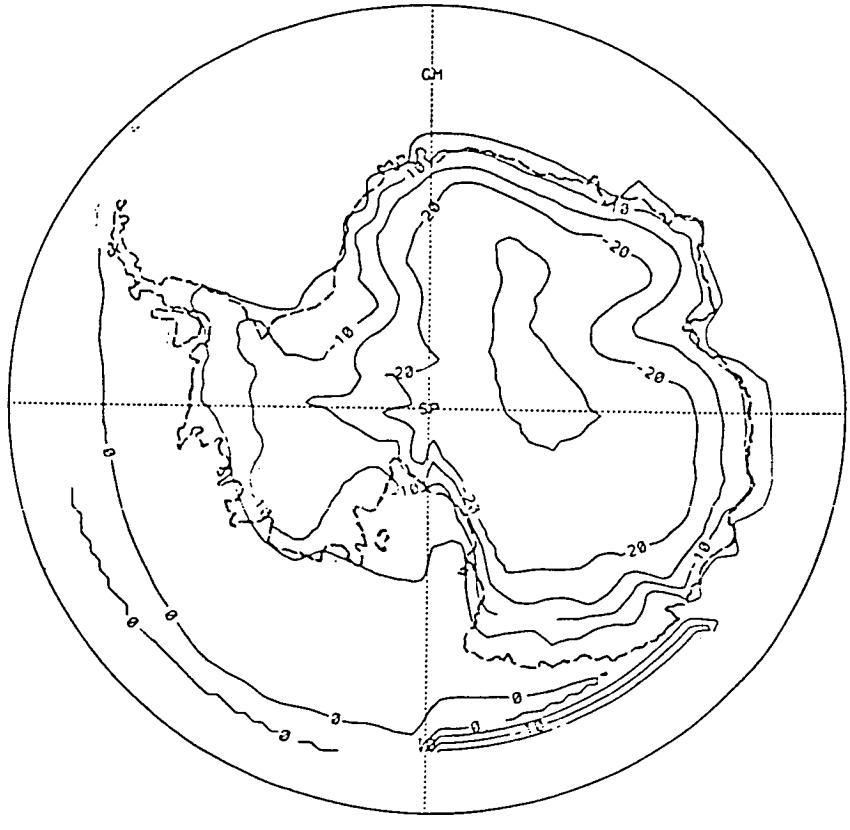

(b) January (contours at 5°C intervals).

Figure 3.3: Variation in the monthly mean temperatures of the Met.O model

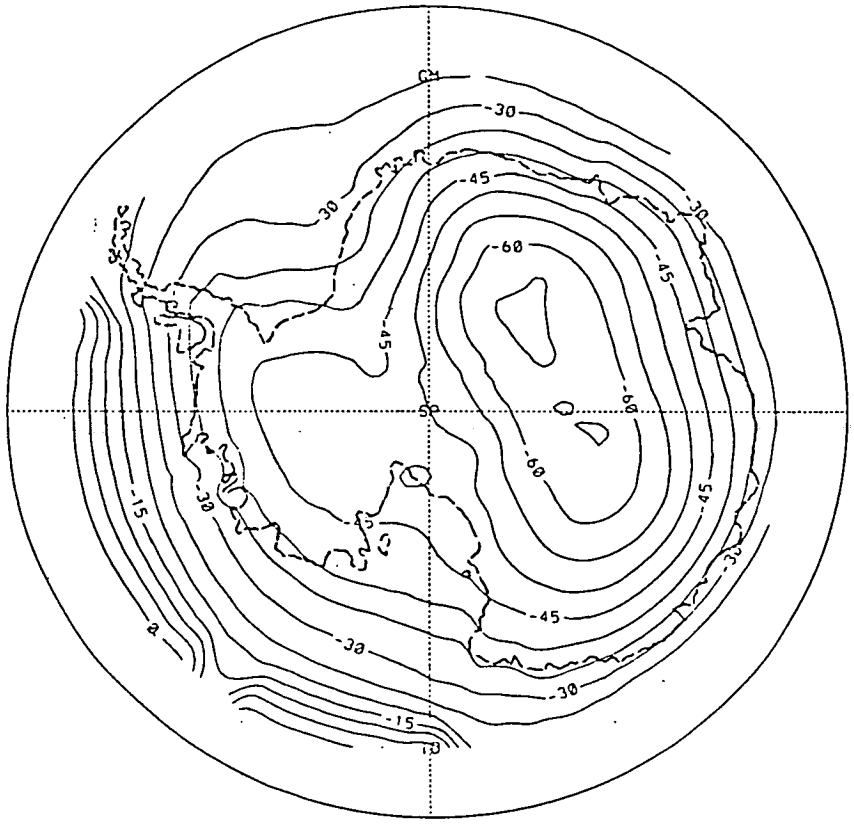

(a) July (contours at 5°C intervals).

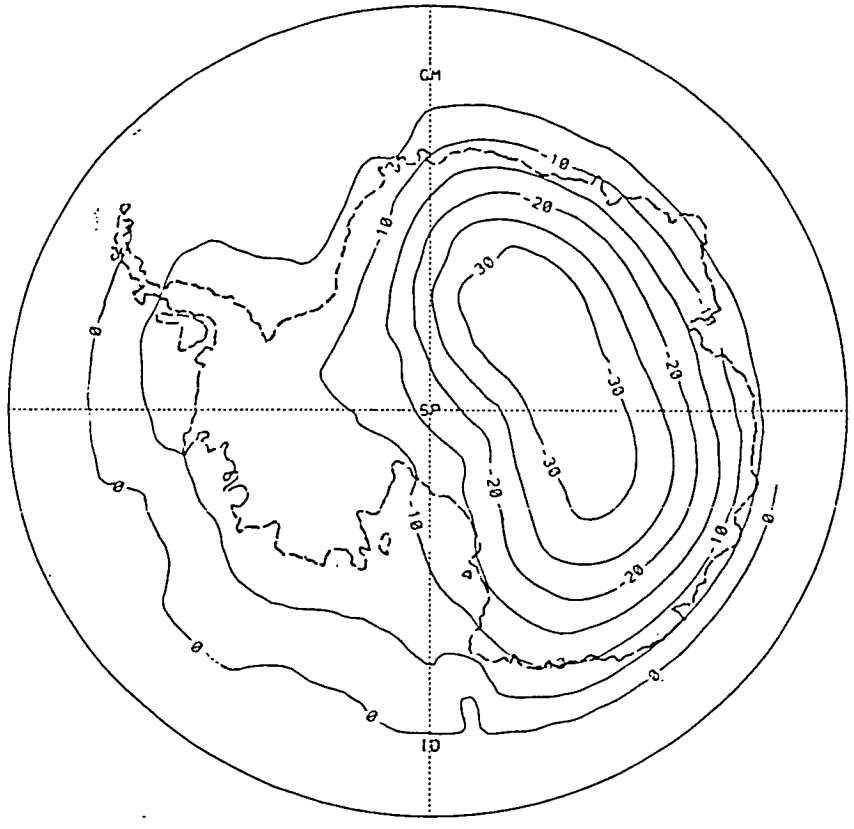

(b) January (contours at 5°C intervals).

Figure 3.4: Variation in the monthly mean temperatures of the NCAR model

Met.O surface temperature gradients.							
Position	ΔH (m)	July			January		
		Temp °C	ΔT °C	L.R °C/100m	Temp °C	ΔT °C	L.R °C/100m
76.875E 76.25S 76.875E 73.75S	500	222.160 226.866	4.706	0.94	251.153 253.204	2.051	0.41
140.625E 73.75S 136.875E 68.75S	1400	212.484 227.358	14.874	1.06	250.541 257.206	6.665	0.48
140.625E 81.25S 155.625E 81.25S 159.375E 81.25S	500 500	221.515 225.353 231.759	3.838 6.406	0.79 1.28	250.842 252.248 256.690	1.406 4.442	0.28 0.89
5.625E 76.25S 1.875E 73.75S	1500	222.337 229.448	7.111	0.47	250.354 252.098	1.744	0.12
mean				0.91			0.38

Table 3.1: Temperature gradients along the surface of the ice for the Met.O model.

fig. 2.2 lies some distance north of the coast in both models.

Surface Temperature Gradients.† The temperature pattern observed in both winter and summer, of a warm model interior and cold coast has important consequences for the temperature gradient along the surface of the ice sheet, shown in table 3.1 and 3.2.

The temperature gradients along the surface of the ice are lower for January than

NCAR surface temperature gradients.							
60.0E		209.210			241.418		
77.8S	1000		9.376	0.94		9.16	0.92
60.0E		218.586			250.578		
73.3S	1000		13.111	1.31		12.55	1.25
60.0E		231.697			263.123		
68.9S							
15.0E		214.241			244.072		
77.8S	1000		7.988	0.80		8.518	0.85
15.0E		222.229			252.590		
73.3S	1000		14.138	1.41		11.15	1.11
15.0E		236.367			263.738		
68.9S							
mean				1.12			1.0

Table 3.2: Temperature gradients along the surface of the ice for the NCAR model.

July, this follows the same trend as the observations, although actual values are less than observed. For the Met.O model in January they vary between $0.12°C/100m$, and $0.89°C/100m$ compared to the observed value of $0.8°C/100m$ to $1.00°C/100m$. The NCAR model appears to be much better, although possibly slightly too high, with a summer gradient between $0.85°C/100m$ and $1.25°C/100m$. As would be expected from the discussion of figs. 3.3 and 3.4. the July temperature gradients, particularly for the Met.O model are too low varying between $0.47°C/100m$ and $1.28°C/100m$, the average is $0.91°C/100m$, whereas observations suggest values in the winter exceed $1°C/100m$ (Rusin 1964). The NCAR model has an average temperature gradient which is more reasonable, 1.12°C/100m, but there is a large variability of 0.84°C/100m to 1.41°C/100m.

From the above discussion it would appear that the climate predicted by the Met.O model is not conducive to the growth of a large ice sheet, which requires a surface temperature gradient of greater than 1°C/100m (Hindmarsh & Boulton 1989). The climate of the NCAR model initially appears more favourable, but the low resolution of the model and smoothing of the topography, means that the results must be treated cautiously. The temperatures seem to be consistently high in the interior and low at the coast, which suggests problems with the dynamics of the model air flow. As described in the previous chapter, radiational processes dominate in the interior. The air flow has its major component parallel to the contours, so the air has time to cool before reaching the glacial slope. On the slopes the air velocity increases, and the downslope component becomes larger. At this point turbulent processes acting on the air become more important and the temperature of the air increases at the dry adiabatic lapse rate† (DALR). Deviations from the DALR are caused by entrainment of warmer air from above the b.l which may increase the temperature gradient, particularly over the glacial slope and coastal strip. If the flow is slow however, there may be additional

radiational cooling of the air which results in a slightly lower temperature gradient. Thus the temperature gradient is affected by both the radiation and wind regimes of the climate and these will be investigated for each of the models in following sections. First, however there will be an assessment of the vertical temperature structure of the atmosphere as this is an indicator of the effectiveness of the radiation regime, as well as being a driving force for the winds over the ice sheet.

The Temperature Inversion. As explained in chapter 2, the climate over an ice sheet is characterised by a strong temperature inversion caused by radiational cooling from the ground. This process is enhanced in Antarctica during the winter because there is no shortwave heating of the ground. Data were available for σ level 1 at between 84m and 90m, level 2 between 420m and 470m and level 3 between 1100m and 1150m above the surface of the Met.O model. For the NCAR model, σ level 1 at 60-64m and level 5 between 4.2 and 4.6km above the ground. Neither model reproduces the depth or strength of the inversion, which may be as high as $14°C$ over the central plateau in the lowest 60m of the atmosphere, and extend upwards several kilometres above the ground. Fig. 2.5 in chapter 2 shows the inversion to be strongest close to the ground in July, and even at 7km the temperature is still greater than that at the surface.

Fig 3.5 shows that in the lowest layer of the Met.O model the inversion is absent over most of the central plateau in July, and is only weakly present on the glacial slope, shown by the shaded regions, around the Ross ice shelf, to the south-west of the Weddel sea, along the coast of the East Antarctic ice sheet and the low land to the south of the Amery ice shelf (for locations see fig. 2.1). This is the reverse of the observed pattern which has the strongest inversion in the centre of the ice sheet. At higher levels in the model the inversion is present, but the strength and location of the centre are still considerably different to the observed pattern. Fig.

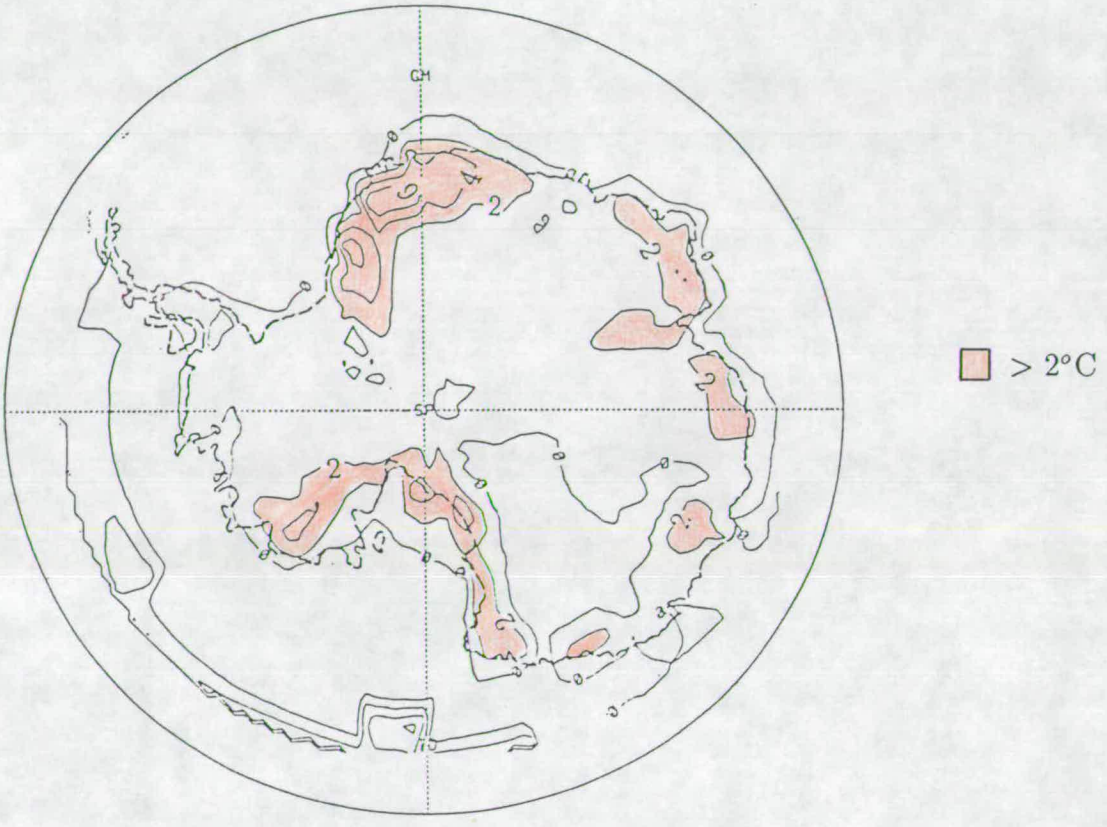

Figure 3.5: The temperature at level 1 minus the Surface Temperature for the Met.O model in July (contour interval of 2°C).

Figure 3.6: The temperature at level 3 minus the Surface Temperature for the Met.O model in July (contour interval of 4°C).

3.6 shows the difference in temperature between the surface and level 3; again this shows the reverse trend of the observations. Over the south pole and in the eastern longitudes where the observed inversion is strongest the inversion only reaches $4°C$, it is stronger towards the coast and particularly on the glacial slope of Adelie Land, between 110°-160°, where the anomalous cold core was observed in the surface temperature fig. 3.3a. Comparing actual temperatures to the temperatures at higher model layers, it seems that the inaccuracies in predicting the inversion strength arise due to predicted temperatures which are too high on the central plateau, rather than temperatures which are too low at upper levels.

The NCAR model reproduces the pattern of the inversion in July much better, (fig. 3.7); the lowest level of the inversion up to approximately 60m is fairly good reaching 14°C in the interior, however the inversion is too shallow and by level 5,

(a) Level 1 temperature minus surface temperature.

(b) Level 5 temperature minus surface temperature.

Figure 3.7: The temperature inversion in the NCAR model in July (contour interval of 2°C).

4.2km above the ice, the temperatures are lower than those at the surface.

In January the inversion may often be absent so lapse conditions may exist, although a weak inversion may be visible over the central plateau at night, (fig. 2.5 in chapter 2). The deviations from the observed pattern is similar to that of the July simulations and therefore the maps of the data have been omitted. The Met.O data show a weak inversion between levels 1 and 2 in the model over Adelie Land, but over the central plateau there is no change, or a decrease of temperature with height. Again the NCAR model reproduces the pattern more accurately in the lower layers, showing an inversion over the central plateau to level 1,but the temperature of the layers above tends to decrease too rapidly up to level 5 where temperatures are 22-28°C colder than the surface.

Radiation

The net SW and LW fluxes were available for both models, for the Met.O model the upward and downward components of each flux were also available.

Short-wave Fluxes. Chapter 2 explained that the downward SW flux tends to be larger in the interior than on the slope, because of the short atmospheric path of radiation arriving there. This trend is eventually masked further north by the higher solar elevations, so that the downward flux at the coast is not always lower than the flux on the glacial slope. High albedos mean that most incoming radiation is reflected away from the surface and the net downward flux is of the order of $60Wm^{-2}$-$80Wm^{-2}$, tending to be slightly less than the interior, towards the coast. Therefore typically Vostok II in the interior has a net SW budget of $79.1Wm^{-2}$, whereas Mizuho on the glacial slope has a budget of $64.2Wm^{-2}$, and at the coast

(a) Met.O Model

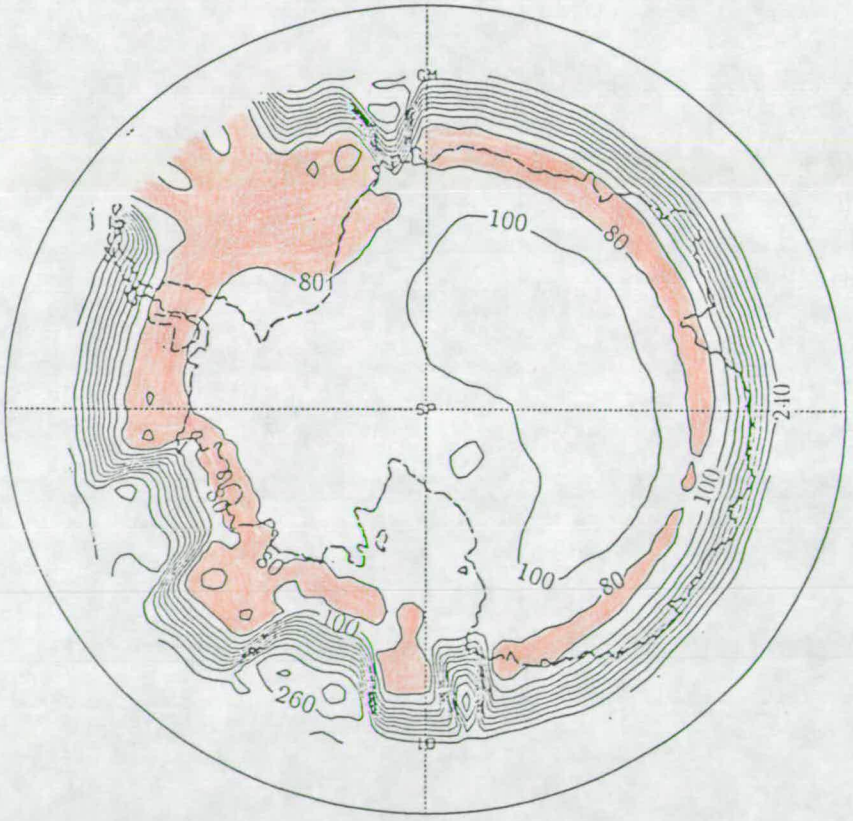

$< 80 W m^{-2}$

(b) NCAR Model

Figure 3.8: The net shortwave fluxes for each of the models at the surface in January over Antarctica (contour interval of $20 W m^{-2}$).

the flux for Mirny is $69.1 Wm^{-2}$. Data are sparse and discrepancies between stations at the same latitude are often greater than those along a longitudinal section. However compared to the differences to the model predictions inter-observational variations are small.

Fig. 3.8, shows the net short-wave fluxes of radiation for each model (July SW fluxes are zero). The NCAR model predicts the minimum flux along the glacial slopes, (depicted by the shading), but the actual values tend to be greater than those which are observed. The model predicts values of $100 Wm^{-2}$ in the interior, decreasing to less than $80 Wm^{-2}$around 70°S, and then increasing to the coast. The pattern of the Met.O model is less clear. There is no minimum on the glacial slopes, over most of the ice sheet the flux is around $40 Wm^{-2}$and only begins to increase significantly, north of the coast of Antarctica in the zone of higher solar elevation. Cattle & Roberts (1988) have looked at the high latitude climatology of the Met.O model and mention misrepresentation of the cloud cover as the reason for gross inaccuracies in the radiation of the model. The model tends to predict too much cloud, which is too thick, so that the predicted downward flux of solar radiation is as much as $100 Wm^{-2}$too low, which also leads to under predictions of the upward and net fluxes. The effect is particularly noticeable in the interior where low clouds are rare and cloud cover is almost always less than 4/8.

Longwave Fluxes. Fig. 3.9 and fig. 3.10 show the net longwave fluxes for the models. The long-wave budget is also dependent on accurate representation of cloud in the model. The predicted net upward flux of between 0 and $15 Wm^{-2}$in July by the Met.O model is reasonable compared to the observed net fluxes in July, when VostokII records a flux of $17.2 Wm^{-2}$and Mirny $32.1 Wm^{-2}$. The January fluxes of the model however are not so good; in the interior the observations show the flux at Vostok II may reach $75.6 Wm^{-2}$according to Dalrymple (1966), and

(a) January

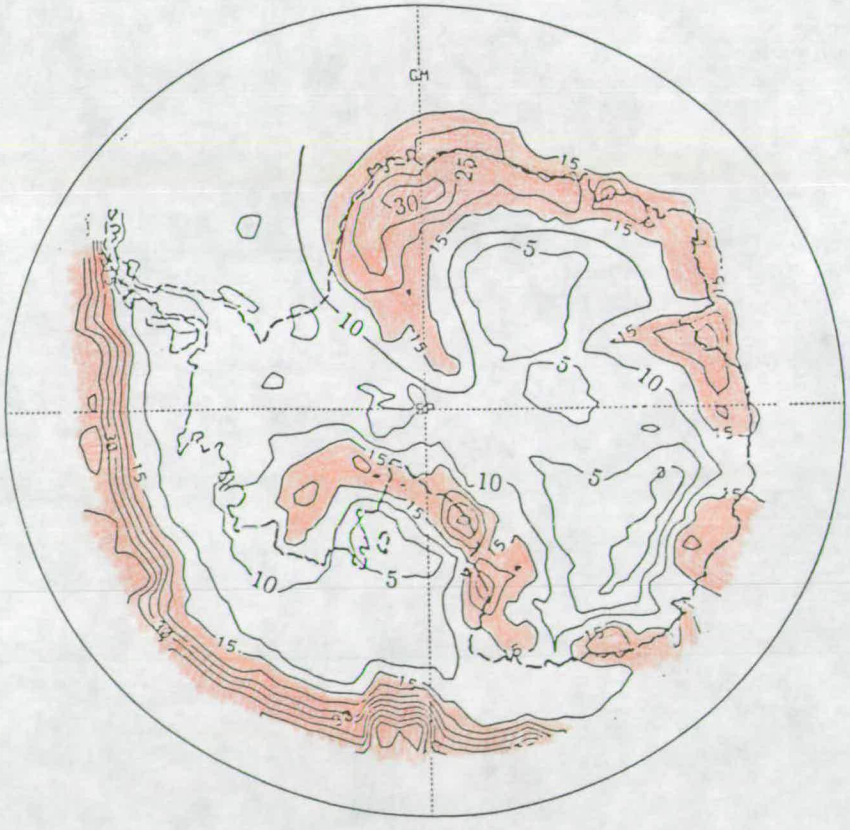

(b) July

Figure 3.9: The net longwave fluxes at the surface of the Met.O model (positive upwards, contour interval of $5Wm^{-2}$).

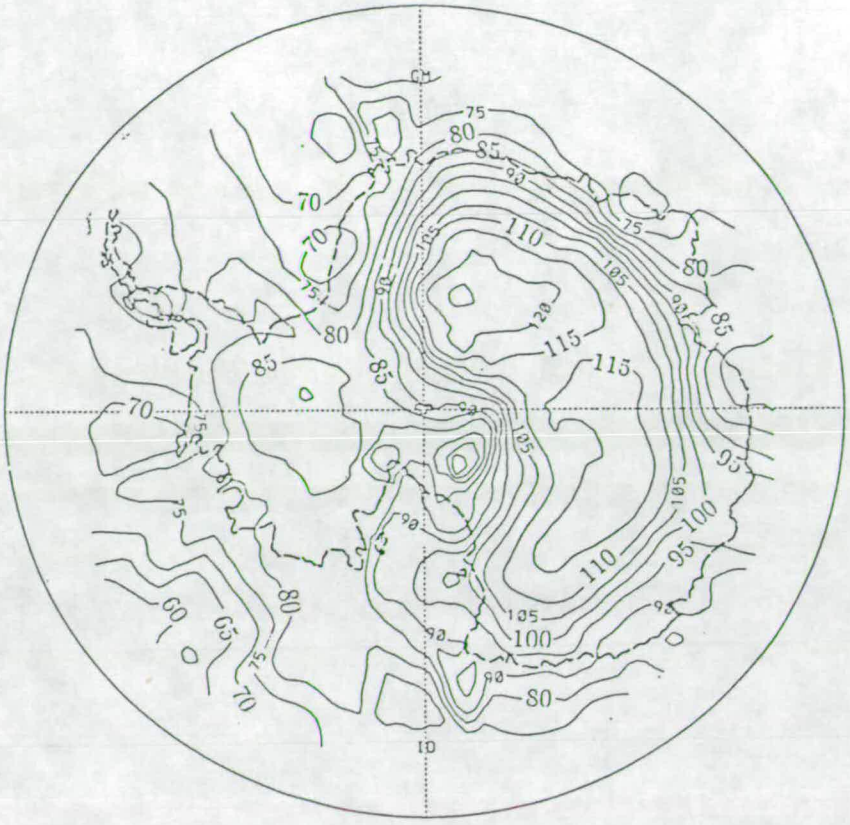

(a) January

(b) July

Figure 3.10: The net longwave fluxes at the surface of the NCAR model (contour interval of $5Wm^{-2}$).

at the coast Mirny has a flux of $38.5Wm^{-2}$, whereas the flux in the model is comparatively low at $20Wm^{-2}$, with the maximum cooling at the coast, rather than in the interior. In contrast, the NCAR model tends to predict fluxes which are too high, although they do decrease towards the coast. In the winter the net longwave flux from the surface is $60Wm^{-2}$and in the summer values decrease from $120Wm^{-2}$in the interior to to $70Wm^{-2}$at the coast.

Cloud amounts can again account for the discrepancy of the Met.O model, since too much cloud increases the amount of atmospheric radiation received by the surface. This is illustrated by the downward component of the LW flux in the Met.O model shown in fig. 3.11; the predicted downward flux is much higher than that which is observed, particularly in the winter. In January for example the simulated downward longwave flux of the Met.O model increases from $200Wm^{-2}$to $260Wm^{-2}$between the interior and the coast, while in July the increase is from $120Wm^{-2}$to $160Wm^{-2}$, these correspond to increases of $80Wm^{-2}$-$250Wm^{-2}$and $70Wm^{-2}$-$200Wm^{-2}$respectively in the observations. The additional downward flux from the cloud tends to offset any effect of the high surface temperatures which lead to excessive upward fluxes in the infra-red. This is reflected in the low Ångström ratio of the Met.O model, which is 0.05 in the summmer and 0.1 in the winter. These values are much lower than those observed, which tend to be between 0.2 and 0.4, because the cloud in the model produces much more downward radiation than is produced by either the cloud or the warm moist layer of air above the surface of the Antarctic ice sheet. Thus the downward radiation of the model is more effective at counteracting the loss than is realistic. Inadequacies in the longwave radiation can be used to explain the discrepancies between the model and the actual inversion pattern. The NCAR model has the greatest net upward flux and achieves the greatest surface cooling with a strong inversion close to the ground. The increase in LW cooling from the interior to the coast in the

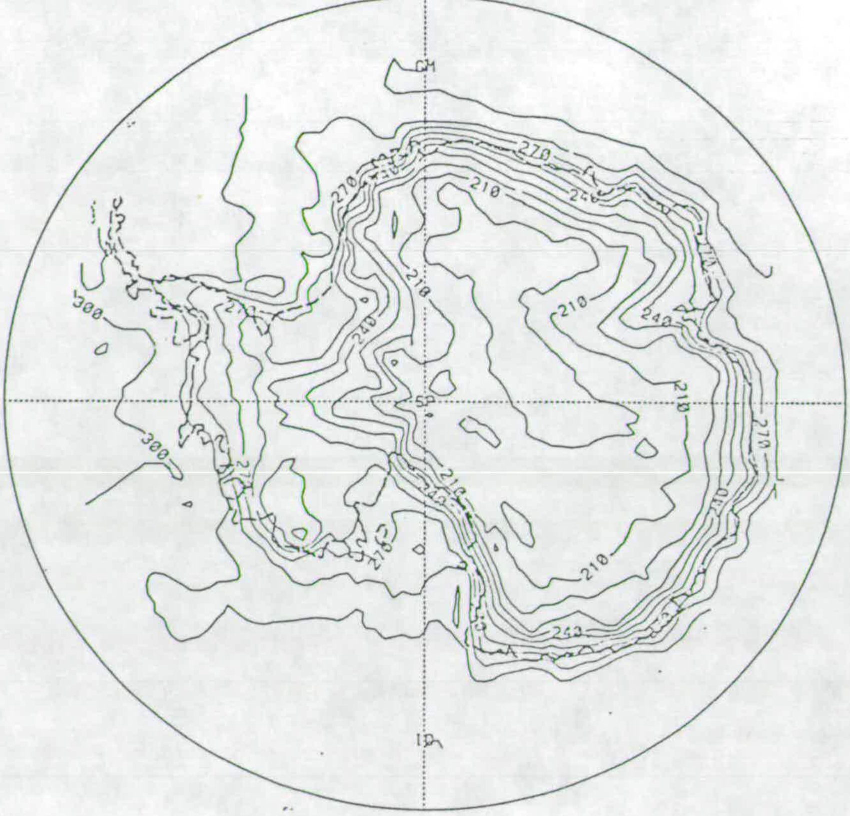

(a) January

(b) July

Figure 3.11: The downward component of the longwave flux at the surface of the Met.O Model (contour interval of $10 Wm^{-2}$).

Met.O model, is consistent with the location of the strongest surface inversion. This can be seen by the shaded regions of fig. 3.5 and fig. 3.6. Neither model reproduces the cloud cover of the interior or the layer of warm air at upper levels which is advected from lower latitudes and helps maintain the deep inversion and the coreless winter as described in section 2.1.1. In both models the high values of downward radiation caused by inaccurate parameterisation of polar cloud means that the longwave balance is achieved at a higher temperature than on the actual ice sheet.

Sensible Heat Flux. The sensible heat flux is the other significant component of the energy balance determining the surface temperature. Over an ice sheet because of the cold surface this is a negative flux, directed into the ice, mirroring the upward longwave flux. The eddy diffusivity which is used to parameterise boundary layer turbulent fluxes, uses the temperature difference across a layer to parameterise the sensible heat flux. Therefore without accurate prediction of the net radiation budget is is unlikely that the sensible heat flux will be sufficiently large.

This is confirmed in fig. 3.12, which shows the Met.O model sensible heat flux. In January the flux is in the wrong direction and in July, it is negative (ie. into the ground), but it is too small. This is consistent with the earlier discussion about the lack of surface cooling and the weakness of the inversion. As would be expected the sensible heat flux is smallest where there is a small upward flux of LW radiation and weak inversion. In July the location of the shaded region, showing the largest negative flux, coincides with the strongest inversion and greatest LW radiational cooling.

The NCAR model, which seems to reproduce the longwave cooling more accu-

(a) January

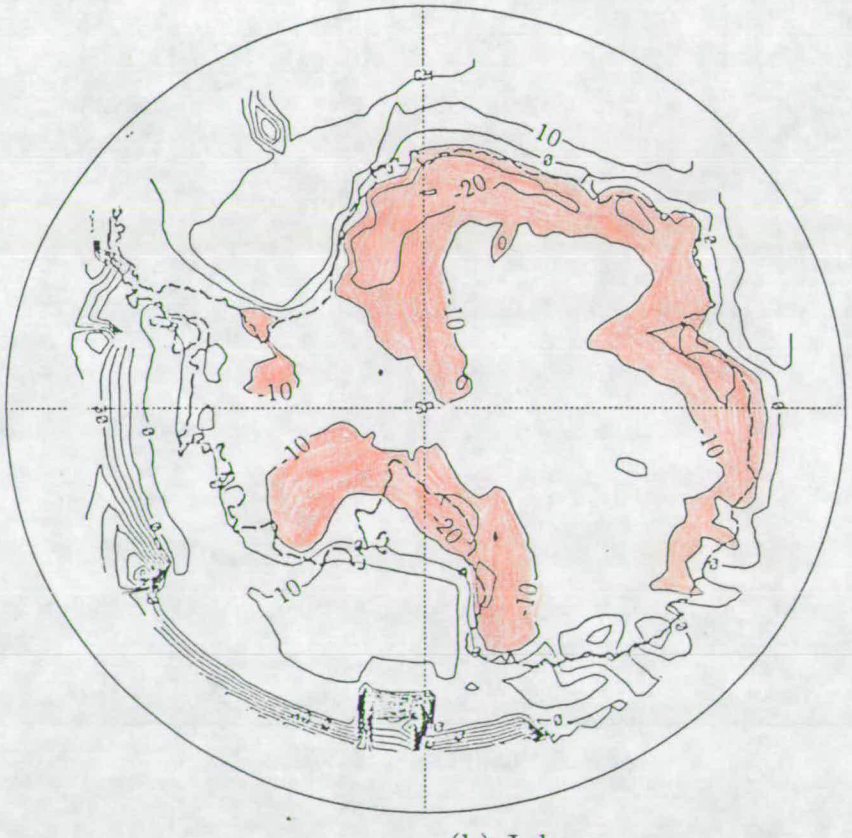

(b) July

Figure 3.12: The sensible heat flux in the Met.O Model over Antarctica (contour interval of $10Wm^{-2}$).

(a) January

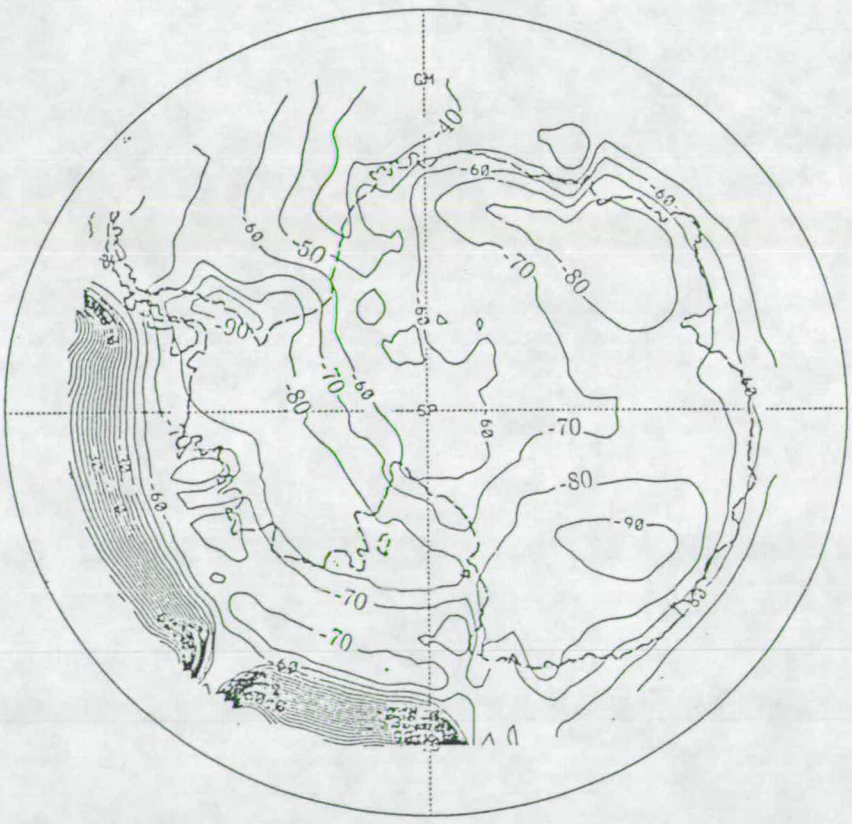

(b) July

Figure 3.13: The sensible heat flux in the NCAR model over Antarctica (contour interval of $10 W m^{-2}$).

rately, predicts a higher and more realistic sensible heat flux, shown in fig. 3.13, but it tends to be too low on the coast between 90°and 120°E in January, so that whereas Mirny has an observed value of -15.9Wm^{-2}it is the 0Wm^{-2}contour of the model that passes through the station location. In July the sensible heat flux of the NCAR model is too high, consistent with the high upward LW flux and strong temperature inversion in the lowest model layer.

The discussion in this section indicates clearly that the parameterisation of cloud is critical to the prediction of the radiative fluxes over the ice sheet and therefore surface temperature. The clouds over Antarctica are generally fairly high and in thin layers, which isn't typical of cloud cover globally, which tend to be much thicker and lower. Clouds in the models are given radiative properties typical for the globe rather than ice sheets and it is this, combined with problems of resolution that causes discrepancies in the predictions.

3.2.2 Mass Balance

The second important component of the climate for the ice sheet is the mass balance. This is the accumulation† minus the ablation. Ablation is the loss of ice due to melting and runoff, wind removal and calving of icebergs where the ice sheet meets the coast. From the GCM's, snowmelt is the only variable that can be obtained directly from the data, since the other processes require a knowledge of the snow and ice dynamics. The Antarctic ice sheet is unique in this respect, in that it does not have a distinct ablation zone as the temperature remains below freezing throughout the year. Ablation, or snowmelt will therefore be disregarded in this section.

Accumulation is predominantly precipitation, which in Antarctica means snow-

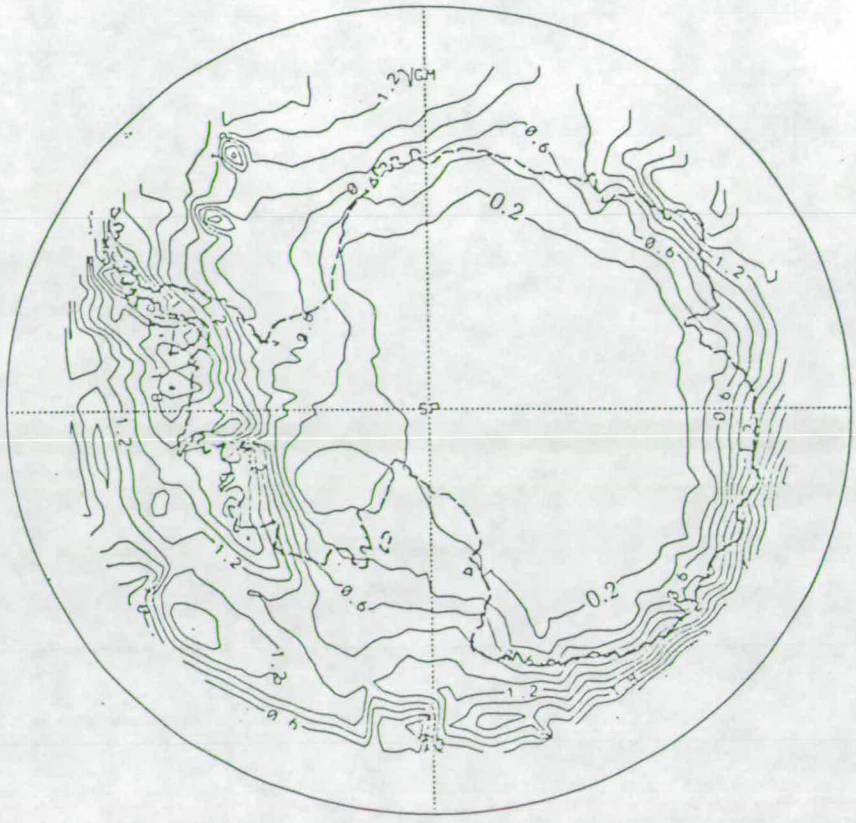

Figure 3.14: Precipitation minus evaporation over Antarctica for the Met.O model in July (contour interval of 0.2mm/day).

fall. There are little data available on precipitation in the Antarctic as explained in chapter 2, the best is total annual accumulation shown in fig. 2.6; this can be used to compare trends in the seasonal simulations of accumulation, rather than concentrating on absolute values. Figs. 3.14 and 3.15 shows the net accumulation, as given by precipitation minus the evaporation over the ice sheet, for the models. The January simulation of the Met.O model has been omitted because values tend to be uniformly low (less than 0.2mm/day). Comparing the figures to fig. 2.6 suggests that the observed pattern of increasing accumulation towards the west over the ice shelf is almost reproduced by the Met.O model in July, although there is an extended region of low accumulation to the west of the Ross ice shelf, which isn't present in the observations. The ridge of very high accumulation over the trans-Antarctic mountains to the east of the Ross ice shelf is absent, probably due to smoothing of the topography, which lessens the orographic effect of the mountain barrier. The NCAR model also has low accumulation in the central

(a) January

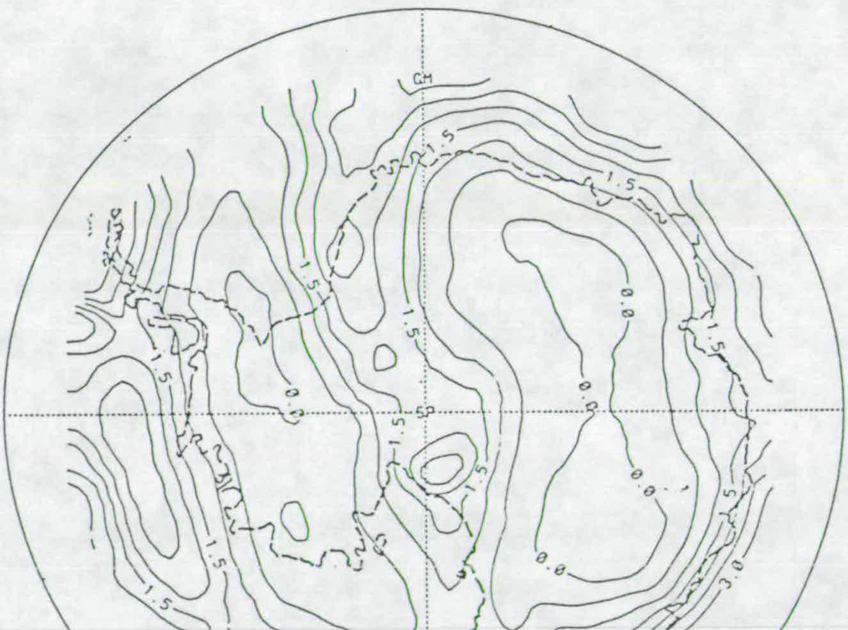

(b) July

Figure 3.15: Precipitation minus evaporation over Antarctica for the NCAR model (contour interval of 0.5mm/day).

plateau but rather than increasing over the western ice shelf there is a ridge of high accumulation values across the centre of the continent from the SE Weddel Sea to the S Ross ice shelf, with particularly high values to the S of the Ross ice shelf of 3mm/day in January and 2.5mm/day in July. The problem of accurate precipitation predictions of the NCAR model was also noted by Pitcher et al (1983), as being largely due to the resolution of the model, which is unable to reproduce variables with large temporal and spatial variability, such as precipitation. In contrast to the Met.O model the NCAR model suggests a summer maximum of precipitation. Rusin(1964) has recorded the precipitation at various gauges over the ice sheet, these show a maximum of precipitation in July. However the gauges were also collecting blowing snow, so high wind velocities at the coast may make the seasonal differences appear much larger than they really are. It is possible that at the coast there is a summer maximum of precipitation as it is mainly produced by cyclonic activity. In the interior values of 0.02mm/day in January increase to 0.19mm/day in July. This is more likely to be due to a real increase in snowfall, as most precipitation in the interior is in the form of ice needles from a clear sky, which has been observed to be primarily a winter phenomena (see chapter 2). The summer maximum and ridge across the continent in the NCAR model, could be arising because the weak storm track between the Ross and Weddel Seas is intensified by the model and the smoother contours of orography allow cyclonic disturbances to penetrate too far inland. This region of high predicted precipitation coincides with the line of weaker inversions described earlier suggesting greater mixing of the air in this area which may be expected under the influence of cyclonic disturbances.

3.2.3 Wind and Pressure

Pressure

There is little information about surface pressure other than spot observations at individual stations. The height of the ice sheet means that the pressure tends to be very low which is reproduced by both models. January pressures tend to be slightly higher, but still less than 650mb. It is possible that the models are slightly high in their predictions. However this is more likely to be a facet of the smoothing of the topography rather than a real feature of pressure in the model. This becomes obvious if the two models are compared; the Met.O model produces a slightly more elongated region of low pressure than the NCAR model, corresponding to the 3000m contour line in each model.

Wind

Section 2.1.3 explained the nature of the wind in Antarctica. There are no data available for the NCAR model so this section will only discuss the simulation of the Met.O model. Predictions of wind are important because of their role in turbulent entrainment of warm air into the boundary layer, a process which is important in determining both the absolute temperatures and temperature gradient over the ice sheet on the glacial slope. They may also be of secondary importance if there is a significant amount of ablation by blowing snow.

Comparing fig. 3.16 to fig. 2.8, wind direction appears reasonable, with the streamlines emanating from the central plateau and strongest over Adelie Land in July, strengthening towards the coast. It will be noticed that off the west coast

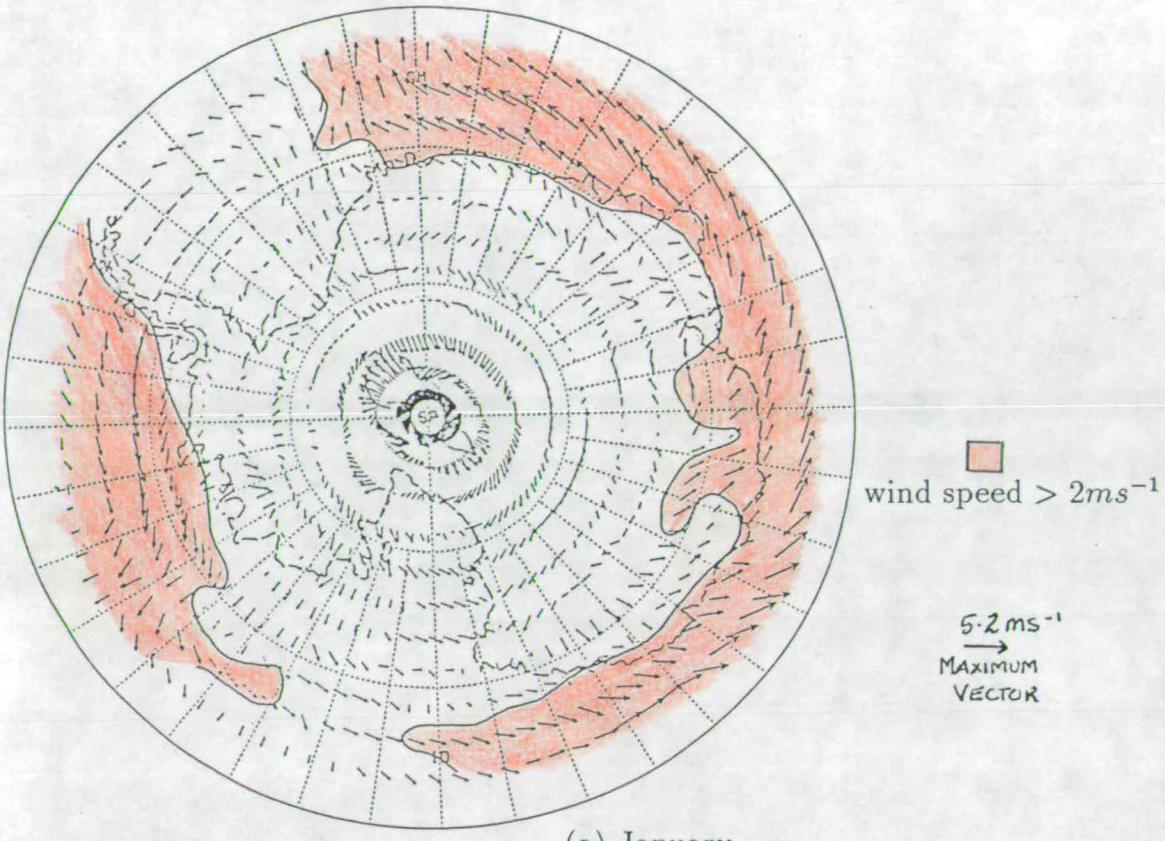

(a) January

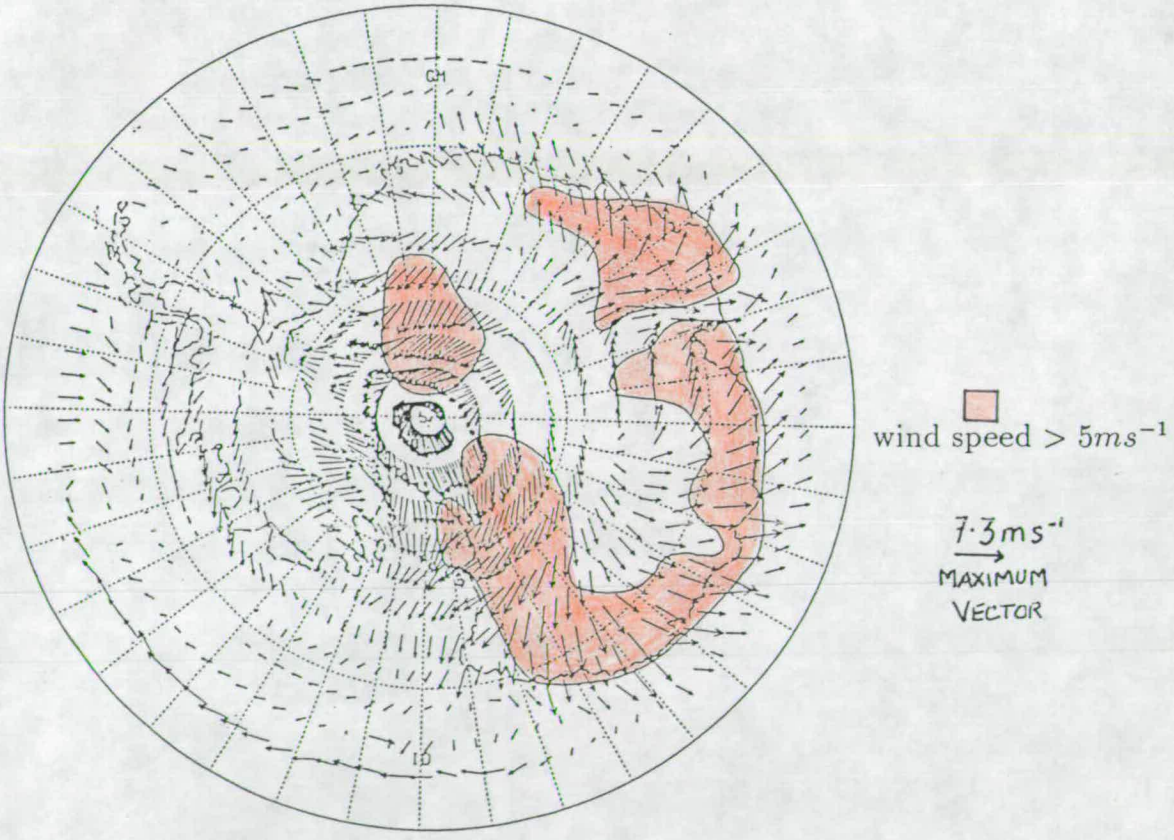

(b) July

Figure 3.16: Wind vectors over Antarctica for the Met.O model.

the easterly flow is weak in July and becomes westerly further from the ice. This is consistent with observations off the west coast of Antarctica whereas strong easterlies are consistently observed off the coast of Antarctica facing the Indian Ocean around 40°E.

The wind speed over the ice sheet is largely determined by the strength of the inversion, be it the gradient wind of the interior or the katabatic drainage flow over the slopes and coastal zone. Therefore the under representation of the inversion discussed previously, also has implications for the wind velocity predicted by the model. The shading on fig. 3.16a shows wind speeds greater than $1ms^{-1}$and on fig. 3.16b the shaded region has a wind speed greater than $6ms^{-1}$. These wind speeds are much lower than those which are observed; Cape Denison is located within the $6ms^{-1}$ isotach of the model in July, yet the observed wind speeds at this station can reach $20ms^{-1}$, elsewhere in the coastal zone wind speeds consistently reach 9 or $10ms^{-1}$, which is nowhere achieved by the model.

The wind speeds in the interior seem to be more accurately reproduced by the model, although the predictions are still slightly too low. For example, Plateau station at 78.5°S and 106.9°E records a mean January wind speed of $3ms^{-1}$and a mean July speed of $5.8ms^{-1}$, whereas the model calculates speeds of $2ms^{-1}$and $4ms^{-1}$respectively, for a similar location. The discrepancy in the predictions of wind speed between the interior and the coast can be accounted for by the way in which the GCM treats the forcing mechanisms of the wind. In the interior, the winds are dependent not only on the inversion strength, but also the pressure field of the upper atmosphere, which the model simulates more realistically than the conditions within the boundary layer. In contrast, the winds of the glacial slope and coastal zone are dependent on the state of the boundary layer, and it has been shown the model does not simulate these features well.

3.3 The Simulated Climate over Greenland

The assessment of the climate over the Greenland ice sheet is in many ways more significant for the coupling of climate and ice sheets than the Antarctic, because of the dynamics of the Greenland climate. The ice sheet, which is much smaller than that in the Antarctic, is located within the northern hemisphere westerly flow and extends sufficiently far south for significant melting to occur to create an ablation zone. The Greenland ice sheet, therefore bears many more of the characteristics of the large ice sheets that formed over North America and Europe during the last ice age. However the analysis is hindered by the lack of a coherent set of meteorological observations, and the fact that the ice sheet is much smaller than the Antarctic means it is covered by fewer model grid points and is very poorly represented. This is particularly the case of the NCAR model which has only 49 grid points in the area 60°W to 15°W and 86.6°N to 60°N, which covers the Greenland ice sheet. The ice sheet is more adequately represented by the Met.O model and the difference may be best illustrated by comparing the respective topographies, fig. 3.17. Smoothing has been carried out to such an extent that the ice sheet in the NCAR model does not exceed 1000m, which compares to 2500m of the Met.O model and 3000m over the real ice sheet. The height of the ice sheet means that it acts as a barrier to the mean westerly flow, which as explained in chapter 2 determines the dynamics of the climatic regime for the ice sheet. It will be seen that this is particularly noticeable in the predictions of precipitation by the models.

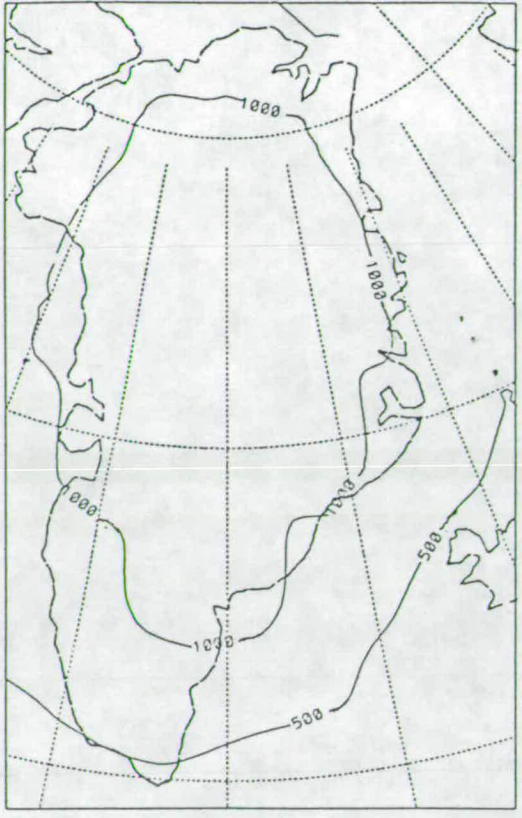

(a) NCAR

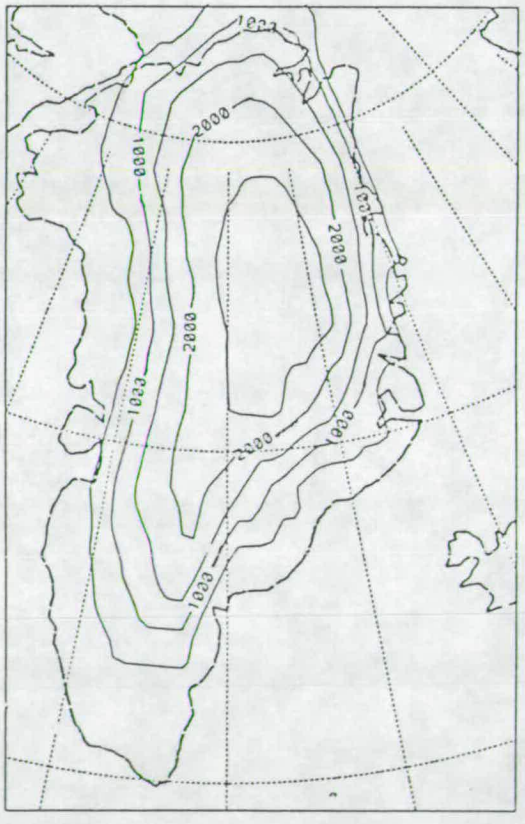

(b) Met.O

Figure 3.17: Topography of the Greenland ice sheet in the models (contours at 500m intervals).

Temperature

The effect of the smoothing of the surface orography on the climate is apparent in the maps of surface temperature figs 3.18 and 3.19. As mentioned in the introduction to this section the effect is especially noticeable for the NCAR model. In July, although the NCAR model has a minimum temperature closer to the observations (fig. 2.15), than the Met.O model, the minimum lies over the Thule Peninsula in the NW of the ice sheet, rather than slightly north of the high plateau. The shape of the Met.O model contours is slightly better, with secondary minimum delineated by the $-20°C$ and $-25°C$ contours over the plateau, but even so the lowest temperatures are again over the NW, and at -30°C are much warmer than the observations. In both models, the temperature gradient increases to the coast and the location of the 0°C isotherm in each of the figures shows the temperatures at the coast to be generally higher than those which are observed.

In the summer the simulation of the Met.O model is much better (fig. 3.19); the -12°C isotherm encloses an area to the north of the high plateau, but at the coast the temperature of 4°C is slightly less than the observations. The map of the NCAR model again shows the limitations of resolution, particularly at the southern tip of the continent where the absence of high ground has lead to much higher temperatures, greater than 7°C. Further north the model still manages to attain a minimum of -8°C, even without accurate topography, which suggests that the radiation regime may be compensating for the smoothing of the topography by increasing the amount of cooling at the surface. This will be discussed in greater detail in section 3.3.1.

Surface Temperature Gradients. The analysis of the previous section makes it clear that neither model attains temperatures as low as the observations. How-

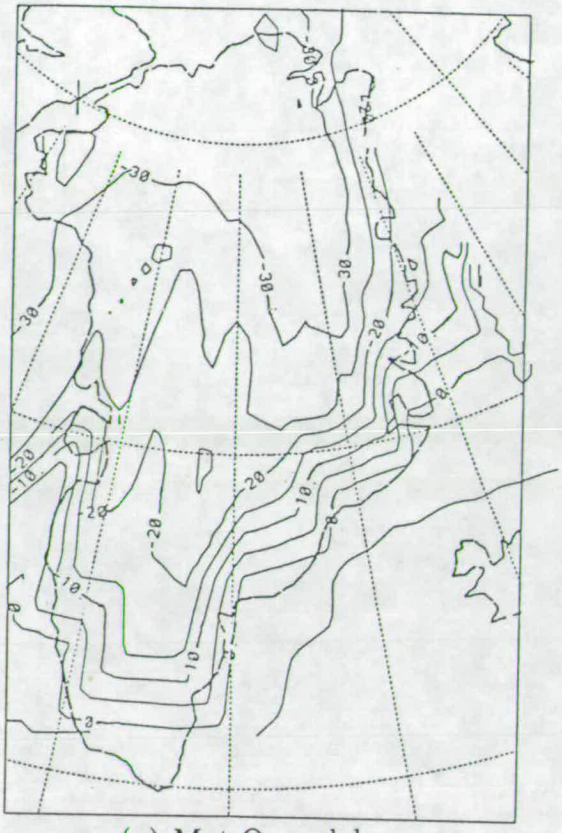

(a) Met.O model

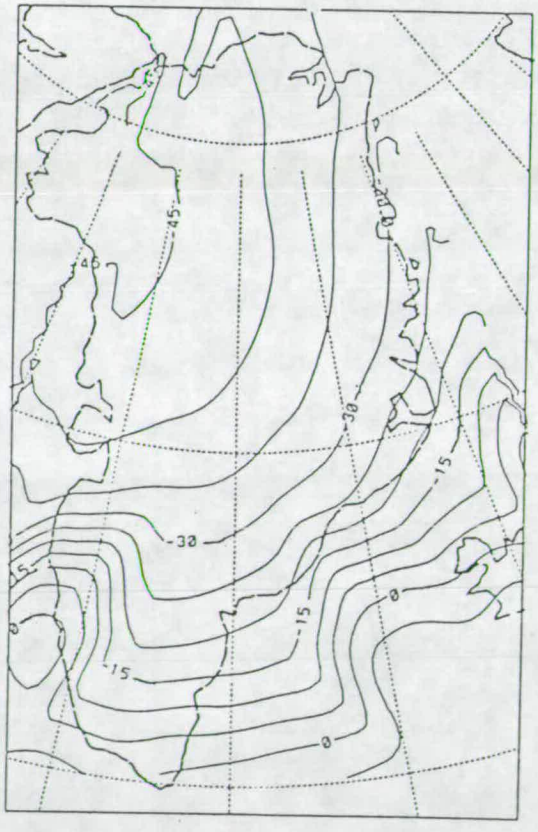

(b) NCAR model

Figure 3.18: The surface temperature of the models over Greenland in January, contour interval 5°C.

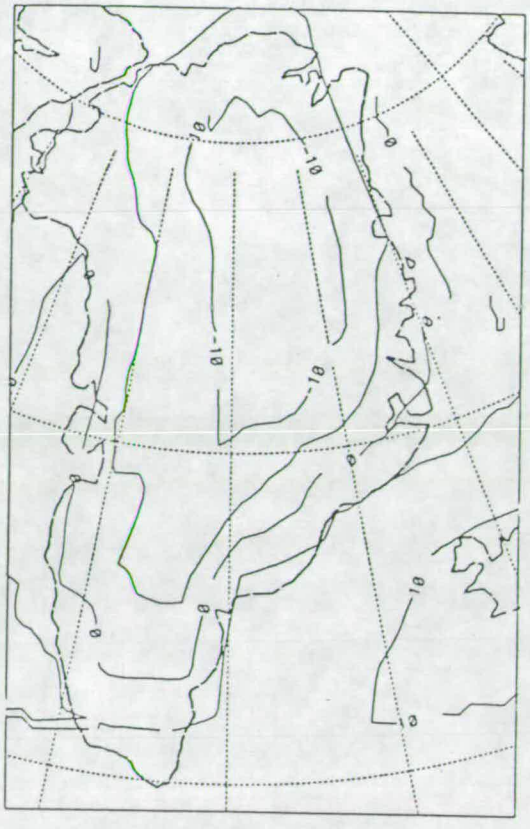

(a) Met.O model

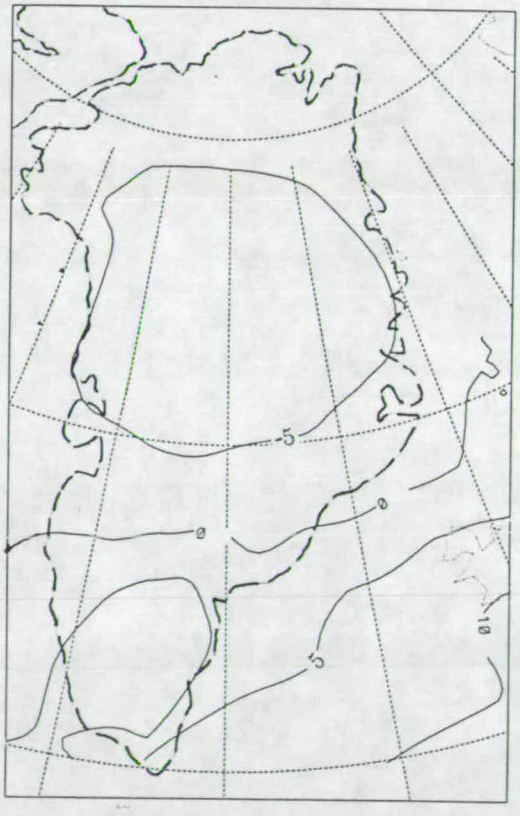

(b) NCAR model

Figure 3.19: The surface temperature of the models over Greenland in July, (contour interval 5°C).

ever if the temperatures are consistently higher, it may be that temperature gradients along the surface of the ice sheet are much closer to the actual temperature gradients.

Poor topography of the NCAR model means that temperature gradients are difficult to calculate, and are generally low, particularly in summer; in the January simulation the lowest temperatures do not coincide with the highest land. In July the temperature gradients appear to be higher; on the west facing slope they are 1°C/100m at 77.8°N and at 68.9°N they are 0.87°C/100m, however these estimates have been made over very small changes in altitude and are therefore subject to large errors.

It seems more meaningful to discuss the temperature gradient of the Met.O model. These are illustrated by the linear regression lines of fig. 3.20 for latitudes 71.25°N and 78.75°N. On the west coast values are considerably lower than the observed surface temperature gradients, which in the winter tend to equal or exceed the DALR (dry adiabatic lapse rate) and in the summer may be slightly less, being between 0.6°C/100m and 0.8°C/100m (Diamond 1959). As in Antarctica it is the strength of the katabatic regime which is the important determining factor of the temperature gradient. At the coast cyclonic influences increase in importance so in some of the figures coastal grid points are excluded from the calculations. However even allowing for this, it seems the July surface temperature gradients are higher than those in January, which suggests the model is particularly poor at reproducing the katabatic effect in the winter; 0.5°C/100m is reasonable, if a little low for the summer when synoptic influences are greater. The resolution of the model makes it difficult to determine the surface temperature gradients on the eastern facing slopes, this is shown in the figure for January at 78.75°N. This suggests that higher gradients are achieved on these slopes, where the mean

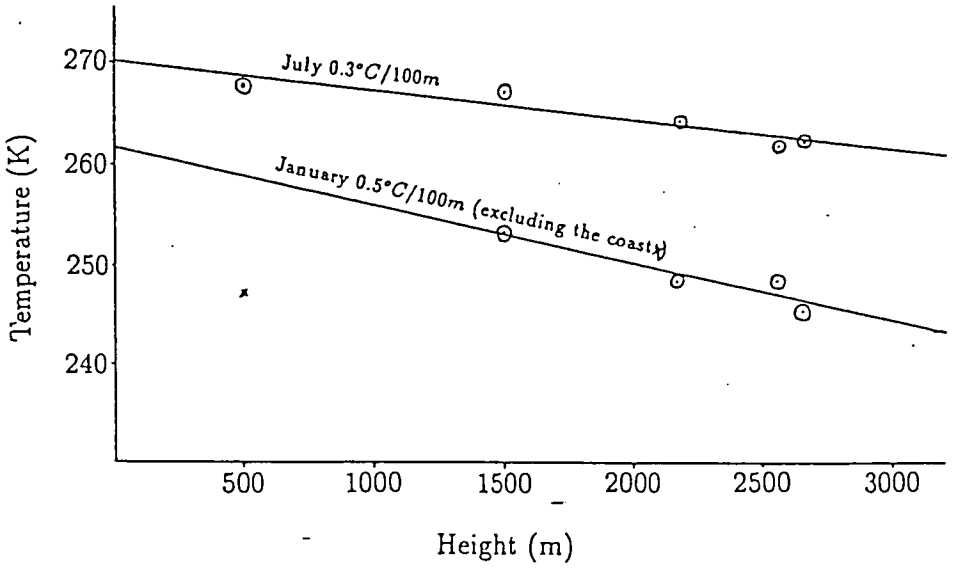

(a)71.25°N

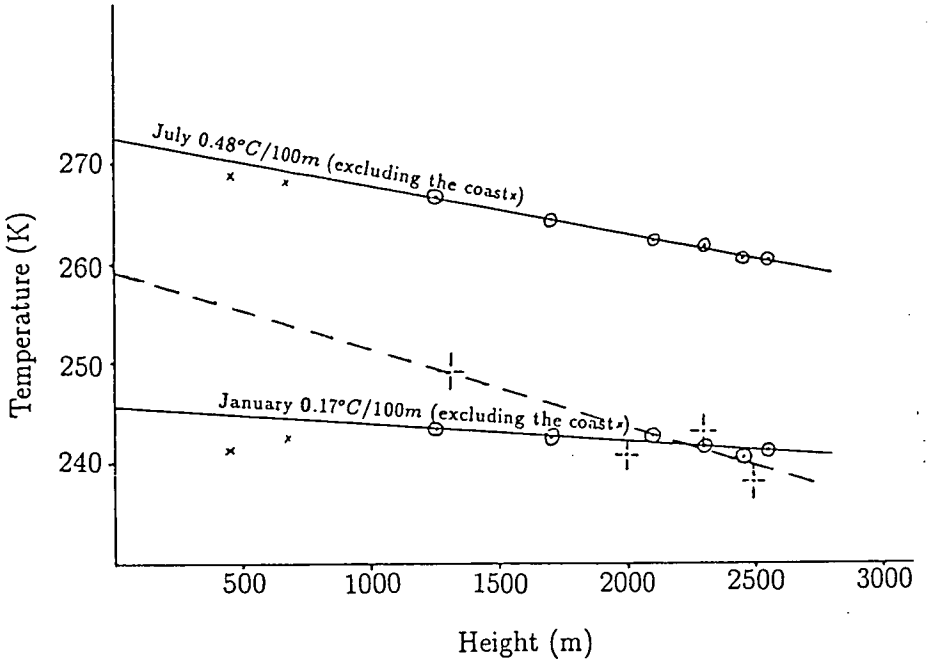

(b)78.75°N

Figure 3.20: The surface temperature Gradients over the Greenland ice sheet as predicted by the Met.O model,(———);west facing slopes. (- - - -);east facing slope.

zonal flow is directed in the same direction as the slope of the terrain, encouraging the development of drainage flow in the model. The higher surface temperature gradients on these slopes is most likely to be due to a foehn effect,† rather than the presence of true katabatic winds.

Vertical Temperature Structure. The limitations in the model climate are reflected in the vertical temperature structure, which is particularly significant in winter when an inversion is present over most of the ice sheet. Fig. 3.21 shows the low level winter inversions for each of the models. Observations in the North Polar Basin show an almost permanent inversion during the winter months (Vowinckel & Orvig 1970), which tends to increase in strength over Greenland according to Putnins (1970) who notes a mean January inversion strength at Eismitte station on the ice cap of of 9.6°C and extending to 329m above the surface. The Met.O predictions, therefore are too weak with the inversion of 6°C extending to level 2 at approximately 500m. The NCAR model however, in spite of limitations of model resolution simulates a much stronger inversion over the western half of the ice sheet; 14°C at 64m above the ground. Thus once again the NCAR model is closer to the observed climate than the Met.O model, which is an indication that the resolution of the model is not exclusively responsible for the poor simulations, but that the treatment of the parameterisations, particularly cloud and radiation are equally significant. This will be discussed in the following section.

Fig. 3.22 shows that the elevated inversion that tends to be present in the summer is not reproduced by either model. In July the NCAR model still has a weak inversion in the lowest layer and the Met.O model has a weak (2°C) inversion to level 2.

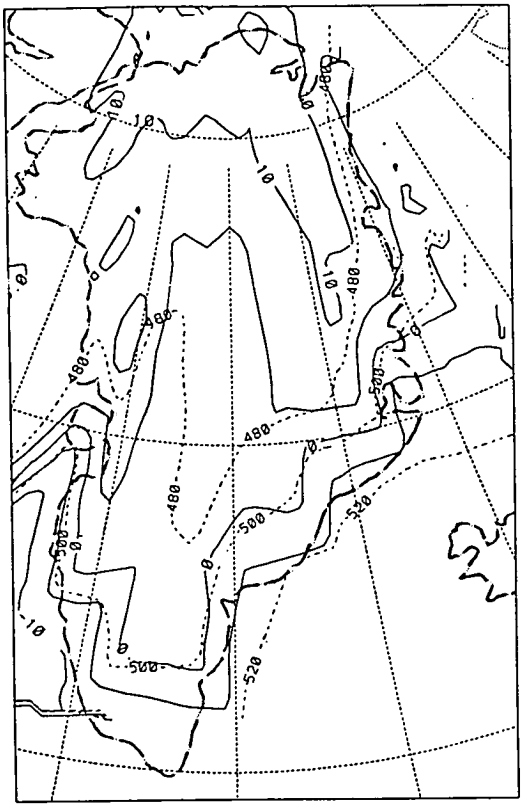

(a) Met.O Model (level 2)

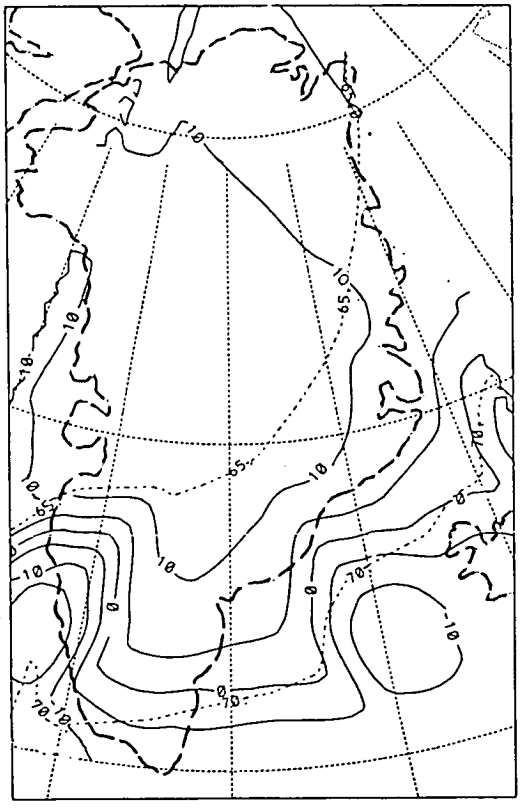

(b) NCAR Model (level 1)

Figure 3.21: The temperature inversion of each model for January, contour interval of 2°C (dotted lines indicate the height, in metres, of the level above the surface).

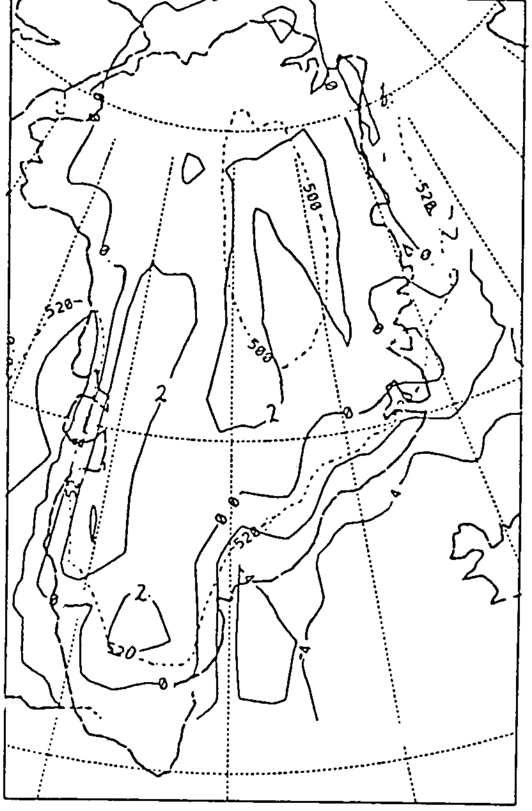

(a) Met.O Model (level 2)

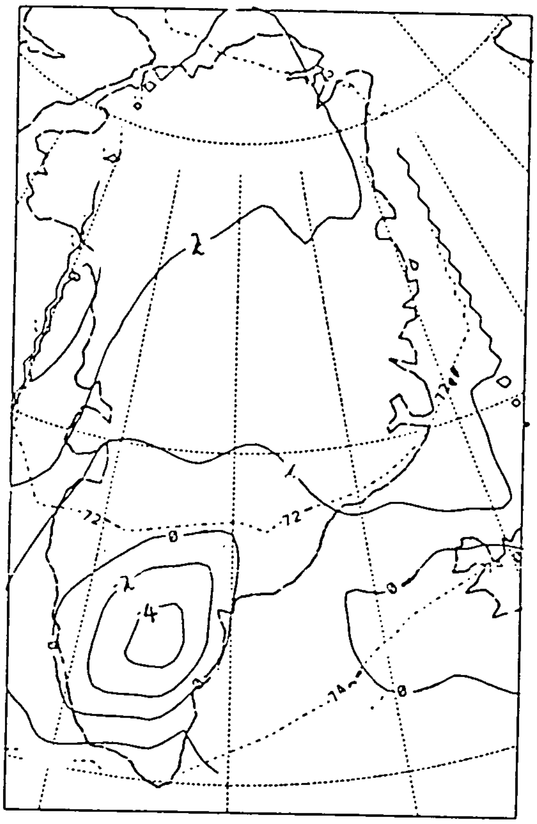

(b) NCAR Model (level 1)

Figure 3.22: The temperature inversion in each model for July, contour interval of 5°C (dotted lines indicate the height (m) of the level above the surface).

3.3.1 Radiation

Longwave Fluxes. It has already been suggested that the errors in the predictions of surface temperature by the models are not wholly attributable to the resolution and smoothing the orography in the models, since the NCAR model reproduces the winter inversion and low winter temperatures more closely than the higher resolution Met.O model. The other important factor in predicting temperature is the radiation budget. From the discussion of temperature, it would be expected that the radiative fluxes of the NCAR model reproduce the actual climate most closely than the much more limited cooling of the Met.O model. This may be caused by different predicted cloud amounts of the models, and results in the higher than observed temperatures and weaker inversions shown in figs. 3.19, 3.18 and 3.21. A comparison of the net cooling of the models suggests this may be the case. The net upward longwave fluxes are shown in figs. 3.23 and 3.24. The Met.O model has a net upward longwave flux of only $20 Wm^{-2}$over most of the ice sheet in January, compared to 60-$70 Wm^{-2}$for the NCAR model. It is expected that the observed flux would lie somewhere between the two, but without observations this is difficult to verify. This is easier to do for the summer as most observational studies of the radiation budget over Greenland have been conducted as part of summer ablation studies. In the summer, the longwave fluxes of the models show similar discrepancies to those of the winter, the NCAR fluxes being the larger of the two. In this case it can be verified that the actual fluxes lie between the predictions using the observations of Ambach (1979) for example. These show a net longwave flux downward at the surface of $42 Wm^{-2}$at CampIV in the ablation zone (1013m) and $45 Wm^{-2}$at Carrefour in the accumulation zone† (1850m).

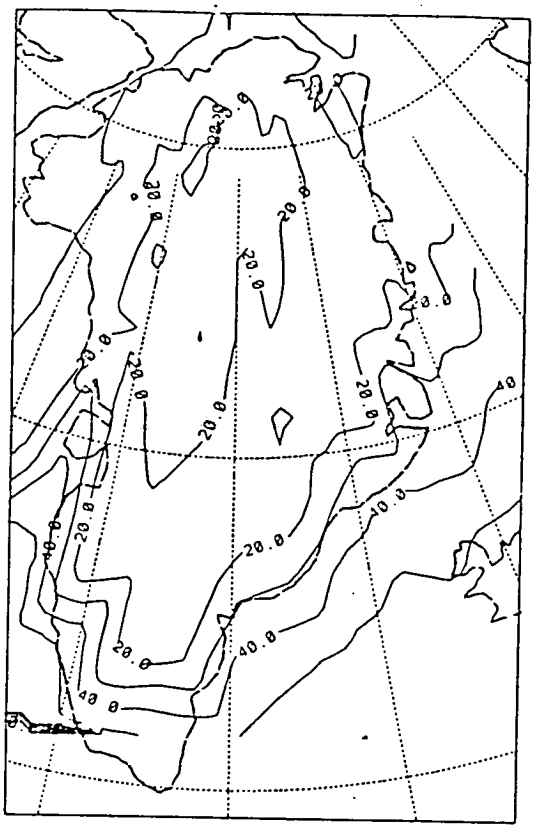

(a) Met.O model

(b) NCAR model

Figure 3.23: Longwave fluxes over Greenland in the model winter (contour interval of $10 W m^{-2}$).

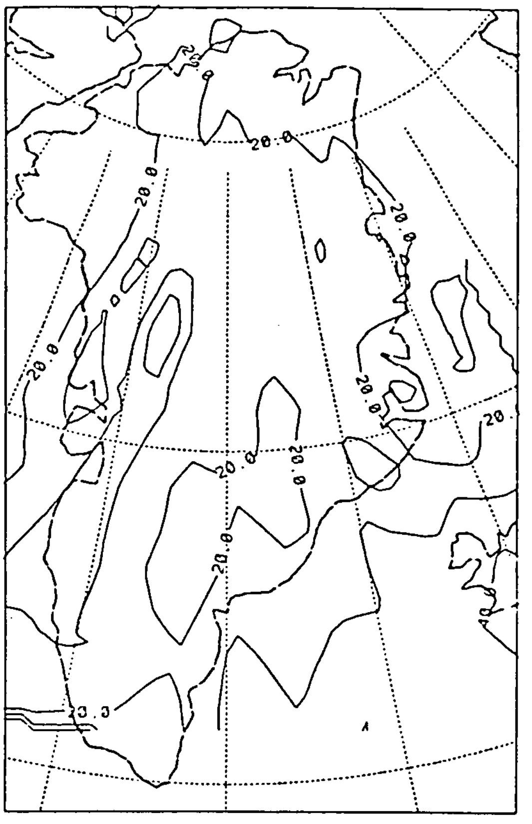

(a) Met.O model

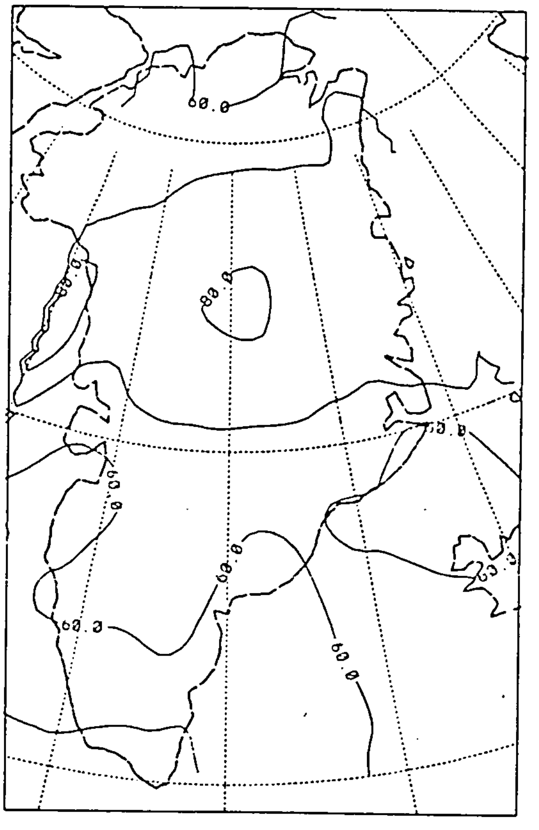

(b) NCAR model

Figure 3.24: Longwave fluxes over Greenland in the model summer (contour interval of $10Wm^{-2}$).

Shortwave Fluxes. The net shortwave flux downward has a much greater spatial variation. It is particularly high in the summer ablation zone where melting rapidly reduces the albedo of the ice. The NCAR model tends to over estimate the shortwave flux, particularly at the coast, compared to large underestimates by the Met.O model, (fig. 3.25). Neither model incorporates the effect of decreasing albedo of melting ice, although the Met.O model parameterises the albedo according to snow depth and the NCAR model prescribes the albedo at the edge of the ice sheet as 0.25 instead of 0.8 as over the main body of ice. The observed fluxes of $51 W m^{-2}$in the accumulation zone and $157 W m^{-2}$in the ablation zone are reproduced by neither.

Sensible Heat Flux. The inaccuracies of the short and long wave fluxes again place limitations on the sensible heat flux of the model. As shown in fig. 3.26, the flux is predicted to be strongest in the winter of the NCAR model where there is most surface cooling and a strong inversion. It can be seen in fig. 3.27 that the observed fluxes of $36 W m^{-2}$in the ablation zone and $15 W m^{-2}$of the accumulation zone in July are not captured in either model. In the NCAR model the flux becomes large and positive in the south coinciding with the strong vertical lapse rate† in the atmosphere and high surface temperature. In the Met.O model the flux is uniformly low.

3.3.2 Mass Balance

The limited amount of data makes the mass balance a difficult quantity to assess. Snowmelt for the Met.O model is small and at no place exceeds accumulation making it impossible to delineate an ablation zone from the model climate. In the south of Greenland, the grid spaces are approximately 200km apart in the Met.O

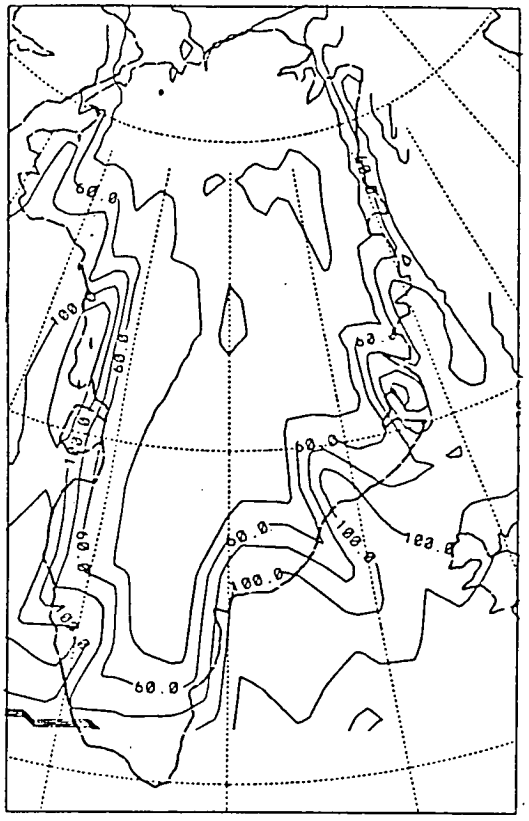

(a) Met.O model

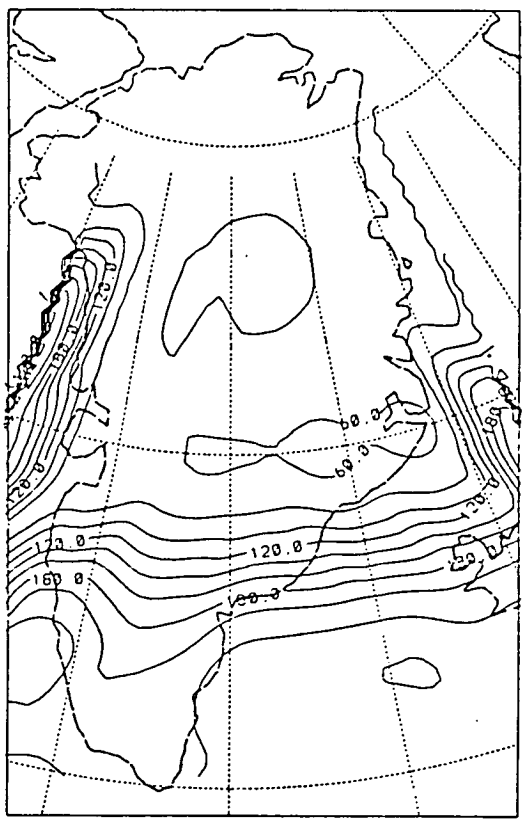

(b) NCAR model

Figure 3.25: Shortwave fluxes in the model summer over Greenland (contour interval of $20 W m^{-2}$).

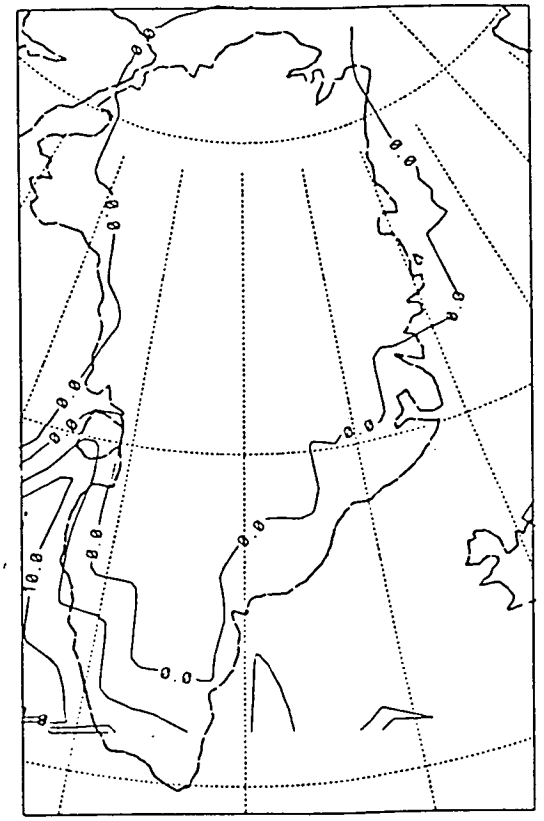

(a) Met.O model (contour interval of $5Wm^{-2}$).

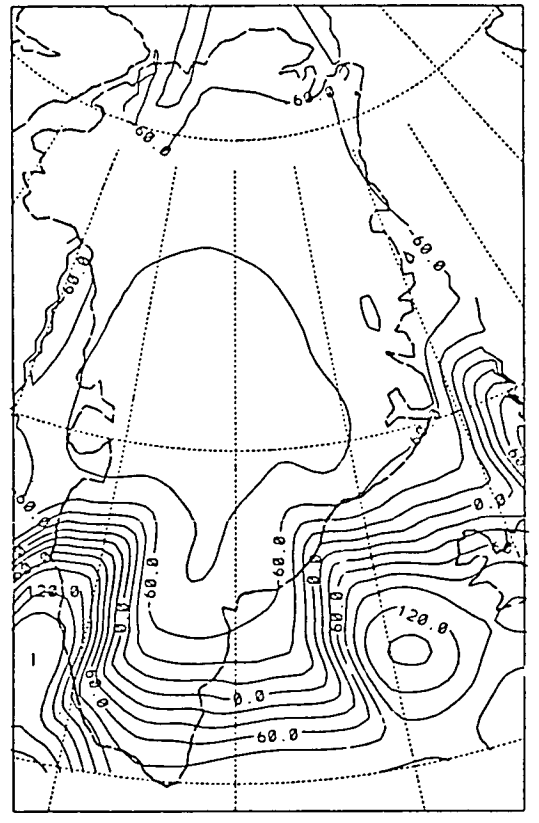

(b) NCAR model (contour interval of $20Wm^{-2}$).

Figure 3.26: Sensible heat flux over Greenland in January in each of the models.

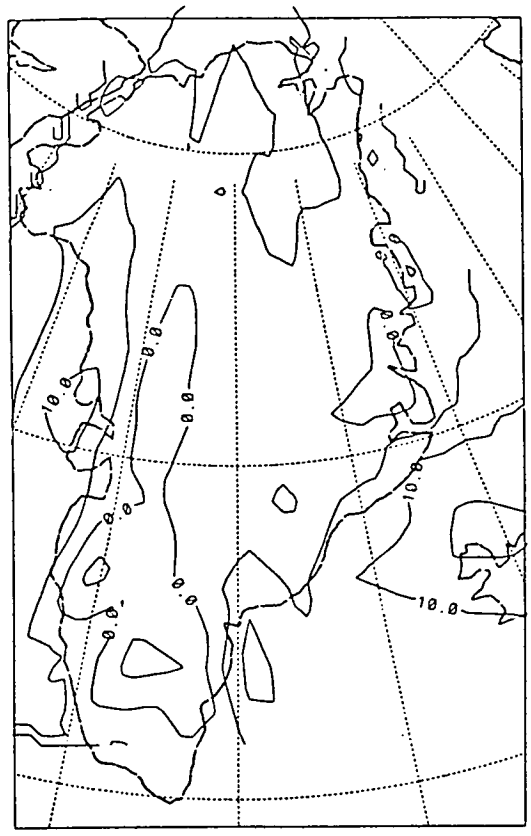

(a) Met.O model (contour interval of $5Wm^{-2}$)

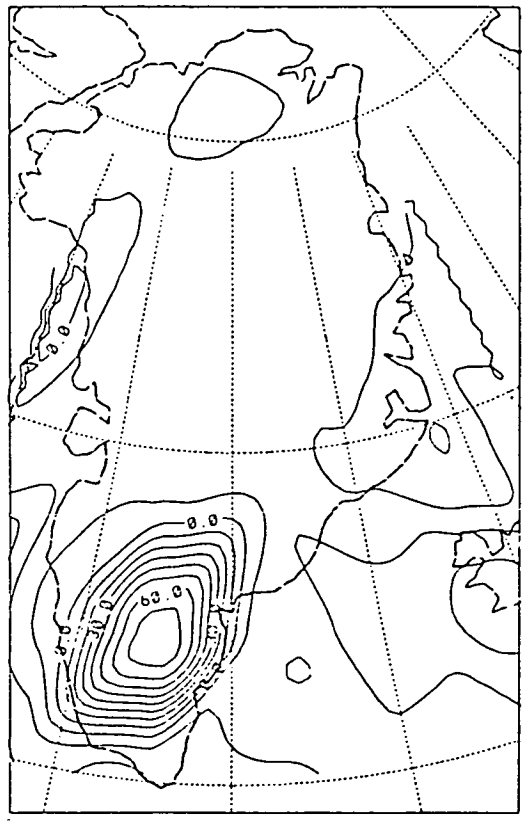

(b) NCAR model (contour interval of $10Wm^{-2}$)

Figure 3.27: Sensible heat flux over Greenland in July in each of the models.

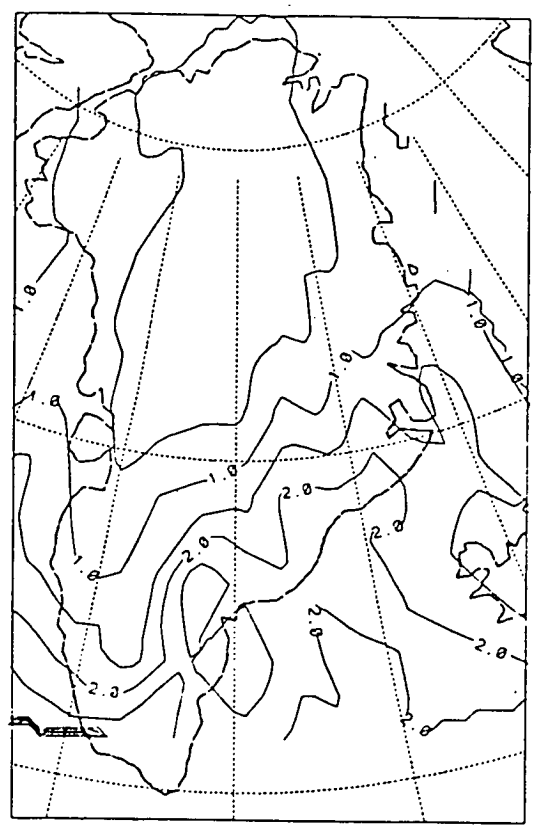

Figure 3.28: July precipitation for the Met.O model (contour interval 0.5mm/day).

grid; the ablation zone is of the order of 100km wide from the margin so once again the resolution of the models presents limitations on its potential use.

The accumulation over Greenland is predominantly snow, falling as a result of the orographic effect of the ice sheet and the general circulation of the region. As shown in fig. 2.16 the amount of snowfall tends to be greatest on the east facing slopes of the southern dome and on the west coast, decreasing rapidly inland. The pattern shown in fig. 3.28 compares reasonably well to that of Ohmura & Reeh (1991), although the accumulation is too low on the southeast coast and too high on the east coast around 70°N.

3.4 Wind and Pressure

The effect produced by the surface pressure, as explained in the first section, tends to reveal more about the topography than it does about the pressure distribution in the model so it will not be discussed.

The wind speed data are only available for the Met.O model which shows stronger winds in January than July, see fig. 3.29. The maximum speed occurs over the high land, indicating the winds are not katabatic in the model. The observations show an increase of wind speed downslope (West Station on the edge of the ice cap has a mean January wind speed of $9.3ms^{-1}$and Esmitte in the centre $4.3ms^{-1}$). The cold air flows downslope under the influence of gravity producing easterly winds on the west facing slopes, and westerly winds on the east facing slope. In the model however the winds of the west facing slopes are predominantly westerly, thus bearing more characteristics of the large scale flow than the regional flow over the ice sheet. The summer winds, which tend to be more uniform when the katabatic effect is weakened are still underpredicted by the model, which has a maximum summer wind speed of $2ms^{-1}$at the coast compared to observations between 4 and 5 ms^{-1}.

3.5 Does it matter? - Summary and Conclusion

The significance of the analysis presented in this chapter is only apparent when considered alongside the requirements of an ice sheet. The climate provides an ice sheet with a mass balance field, and the ice sheet is most sensitive to the climate

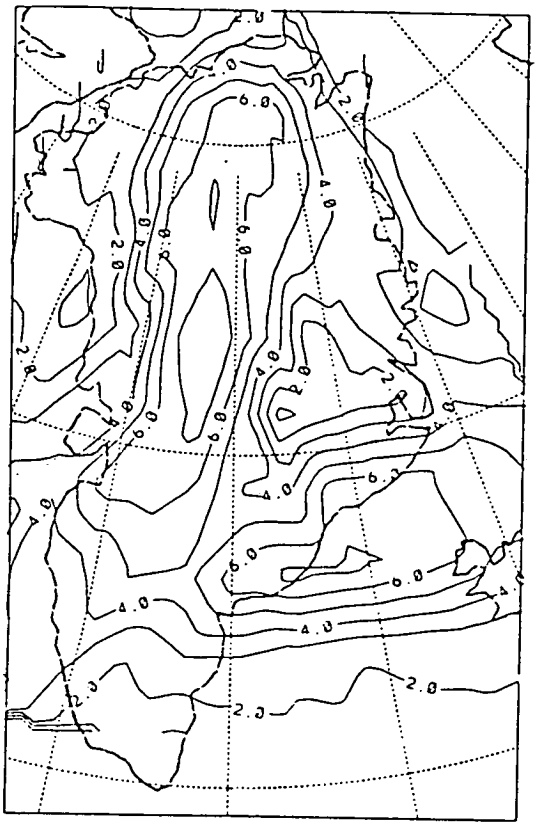

(a) January

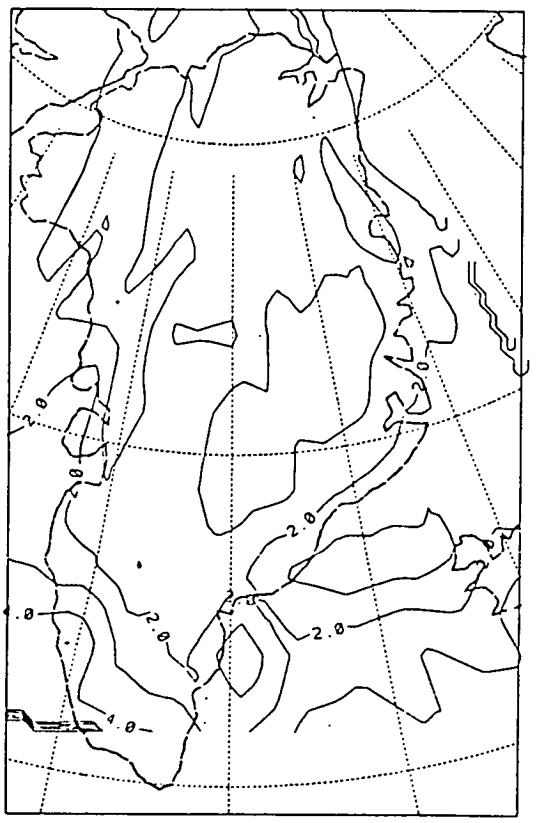

(b) July

Figure 3.29: The wind speed predicted by the Met.O model (contour interval of $1ms^{-1}$).

of the ablation zone. Ablation is largely governed by boundary layer processes which are not well reproduced by a GCM which has a poor resolution on this scale. Further limitations arise over ice sheets due to inaccurate parameterisation of polar cloud, which is important for the radiation regime. The main findings of this chapter can be summerised as follows.

- The radiation balance is poorly reproduced, resulting in temperatures which are too high, largely due to the increase in downward longwave radation caused by too much cloud in the Met.O model. The NCAR model has larger fluxes of LW radiation but tends to overestimate the net SW flux, contributing to higher than observed temperatures.

- The inversion in both models is too weak and too shallow. It is slightly better at the surface of the NCAR model which has less polar cloud and therefore less back radiation.

- Neither model reproduces the layer of warm air above the inversion, advected from lower latitudes over Antarctica.

- The wind direction of the Met.O model is good, but the wind speeds tend to be low.

- GCM's cannot simulate the boundary layer well due to problems of resolution.

- Neither model is able to reproduce the accumulation field. The Met.O model is slightly better than the NCAR model over Greenland due to the resolution of topography.

- It is impossible to delineate an ablation zone over Greenland in either model, due to low resolution.

The treatment of the boundary layer and the large grid scale of GCM's means they cannot adequately describe the climate of the ablation zone, the climatic parameter to which ice sheet models are most sensitive. The remainder of this thesis therefore will look at an alternative approach to understanding the climate of the ablation zone. Here, it is the characteristics of the boundary layer that are important. In this region, where slopes tend to be greater than in the interior, advective processes tend to dominate over the radiative ones. Thus the temperature of the boundary layer is determined by the nature of the air at the top of the slope, modified by the dynamics of the wind and turbulence induced entrainment of warm air into the top of the boundary layer. The next chapter describes a slab model which is used to investigate this boundary layer evolution more closely.

Chapter 4

A Slab Model over the Glacial Slopes

4.1 Aim of the Model

The aim of the next two chapters is to investigate the boundary layer climate over an ice sheet using a slab model. This chapter will present the formulation of the model and the sensitivity of the steady state boundary layer to variations in model parameters. In chapter 3 it was shown that GCM's are unable to reproduce the boundary layer climate over an ice sheet, which limits their ability to provide upper boundary conditions for ice sheet models. This work aims to investigate the evolution of the atmospheric boundary layer over ice sheets, and which parameters are most important in determining the properties of the boundary layer to which the ice sheet is most sensitive. This essentially means those which contribute to the mass balance† of the ice sheet. In chapter 1 it was stated that the results of experiments with ice sheet models indicate that the component of the mass balance to which the evolution of ice is most sensitive, is the ablation.† Ablation tends to be governed by boundary layer characteristics, rather than the dynamics of the large scale atmosphere which is the case for the accumulation† field. This chapter

will describe a slab model of the atmospheric boundary layer over an ice sheet, and the results of sensitivity experiments with the model parameters. In chapter 5, the model will be used to look at the effect changes in the boundary layer may have on the ablation of ice. This is a potential feedback in the atmosphere-cryosphere interaction and so the way in which the ice affects the boundary layer will also be considered.

4.1.1 Which boundary layer characteristics may be important?

Temperature is probably the most obvious climatic characteristic of the boundary layer that will influence the ablation. Its role has been investigated by several authors. Ablation can be calculated by the surface energy balance of the ice, which requires an estimate of the surface temperature (eg.Braithwaite & Olesen 1990b, Ambach 1989). Over most of the ablation zone,† slopes are large, so that advective processes dominate over radiative ones in determining the surface temperature, making it appropriate to consider the dynamics of the air flow in an investigation of the surface temperature. Ambach (1989) used a heat balance model to look at the change in the equilibium line altitude (ELA)† over Greenland due to variations in atmospheric temperature, absolute humidity, cloudiness and annual accumulation. He found the height of the ELA to be most sensitive to variations in temperature. In a study of the Greenland ice sheet, Braithwaite & Olesen (1990a) found temperature to correlate to ablation at Nordbogletscher and Qamanârssûp Sermia with correlation coefficients of 0.68 and 0.76 respectively. Temperature is also important due to the interplay between the surface temperature gradient† of the ice, the temperature at the base of the ice, and the shape of the ice sheet.

The importance of wind for the mass balance of the ice sheet seems to vary according to the location; the study by Braithwaite & Olesen (1990a) over Greenland found wind ablation to be small compared to the ablation due to snow and ice melt. They suggest that wind speed is likely to be more significant because of its enhancement of evaporation. Wendler(1989), in a study of blowing snow over Antarctica, suggests that the strong winds experienced near the coast are responsible for a snow flux of 6.3 x $10^6 kgm^{-1}a^{-1}$. If the length of the glacial slope where strong winds occur is assumed to be between 200km and 500km in length, the total annual flux of blown snow over Antarctica varies from 1 x 10^{12} to 3 x $10^{12}kg$. These fluxes are comparable in magnitude to the loss due to evaporation and runoff, but the loss by bottom melting of ice shelves is 20-30 times greater and loss due to iceberg calving over 1000 times greater, therefore the removal by wind is a relatively small component of the mass budget in Antarctica. However, for a land based ice sheet where there would be no loss due to calving or bottom melting of ice shelves, if the katabatic winds are strong enough, wind removal has the potential to be a large component of the ice mass budget.

4.1.2 Previous Investigations of the Boundary Layer

There have been several model investigations of the boundary layer over ice sheets ranging from simple slab models to the more complex numerical grid point models. The sparse dataset over Greenland means that most investigations tend to be based on Antarctic data. Fortuin and Oerlemans (1990) carried out regression analyses on the temperature and mass balance data of Antarctica. They found superadiabatic surface temperature gradients in the interior where radiational cooling is greatest, and subadiabatic surface temperature gradients between the glacial slopes and the ice shelves. However they present a physical analysis that is

somewhat simplified. They considered the Antarctic continent to be covered by a surface inversion overlain by a warm moist layer from which the precipitation falls. The inversion layer consisted of a slab of air, cooled in the interior and flowing over the ice sheet, warming adiabatically. The geometry of the ice sheet was assumed to cause divergence of the air, which leads to a halving of the inversion height between the interior and the coast. The large temperature gradients along the surface in the interior were attributed to the large amount of radiative cooling, which is greater nearer the centre of the ice sheet, and the low gradients at the base of the slopes explained by the stagnation of air on the ice shelves, lowering the temperature at the base of the slope. Although both of these processes are occurring over the Antarctic ice sheet the explanation seems to be an over simplification of the dynamical processes involved, and is not entirely consistent with observational studies and numerical grid point model investigations of the boundary layer over Antarctica (eg. Parish 1984, Parish & Waight 1987, Gosink 1990, Kodama et al 1989). Along a large part of the glacial slopes, away from the stagnant air of the ice shelves, the surface temperature gradient may be superadiabatic, not due to radiational cooling, but due to entrainment† of warm air from above the boundary layer (see chapter 2).

Work by Parish & Waight (1987) using a numerical grid point model, confirms that the boundary layer is not completely decoupled from the free atmosphere, and divergence of the air on the glacial slopes is to some extent compensated for by the entrainment of air from above. Over the glacial slopes the boundary layer therefore may not change in depth significantly, or may even deepen if there is sufficient turbulent entrainment. The model of Parish & Waight (1987) demonstrated the importance of topography in generating the large wind speeds on the glacial slopes. The results of the model show a reasonable agreement to the observations available, but the apparent upslope flow above the boundary layer shows the re-

turn flow to the centre of the ice sheet at rather a low level. This phenomenon of models is discussed by James (1989), as arising because the model is reaching a steady state which is never attained by the atmosphere. They argue that the downslope flow over the real ice sheet is maintained by removal of cyclonic vorticity by decaying mid-latitude cyclones and drag exerted by gravity waves propagating at right angles to the downslope flow, weakening the circumpolar vortex.

The objective of this work is to investigate the flow using the most simple approach that can predict the components of the boundary layer climate most likely to produce changes in the ice sheet. This will be used to infer mechanisms by which this may feed-back to the boundary layer. A slab model will be used, which is quick and easy to run, and can therefore be used to investigate changes at various stages in the ice sheet evolution, a process which takes several thousand years. A forward stepping, numerical integration of the model will be used, which means it can only be used to investigate shooting flow. This means that the flow at any point is determined exclusively by upslope conditions. Over an ice sheet this can only be said to be true of the flow on the glacial slopes and in the coastal zone; it cannot be extended to the interior, where the winds are not governed by boundary layer processes but driven by the geostrophic[†] flow above the inversion. This is appropriate for this work, which aims to study the climate of the ablation zone. Lalaurette & Andre (1985) compared the analytic solution of Manins & Sawford (1979), which implies initiation from a crest, to the earlier work of Ball (1956) and found a numerical integration to be a more realistic method to use in an investigation of the dynamics of katabatic flow. This requires the specification of initial values for the 4 variables U_1, V_1, h_1 and $\Delta\theta_1$, which represent the conditions at the top of the glacial slope. The scarcity of data in this region means that model results, such as those presented by Parish & Waight (1987), will be used to complement the actual data in providing a basis for the constraints on a slab

model. The possibility of discrepancies between the actual observations and the results of a model must be acknowledged.

4.2 Using the Observations as Constraints on a Slab Model

Inversion strength and wind speed. Ideally to constrain a slab model of the boundary layer we would use a series of observations taken along a profile of an ice sheet. However as explained in chapter 2 and shown in fig. 2.1, the distribution of stations makes this difficult. The best available profile is on the East Antarctic Ice Sheet between VostokII, Komsomolskaya, VostokI, Pionerskaya and Mirny. Bearing in mind this covers a distance of over 1000km, much detail will be unresolved. Observations made in July have been used, and fig. 4.2 shows the wind roses at each station (Mather & Miller 1967), and the mean monthly surface temperatures for July. The inversion strength has been calculated from the figures given by Phillpot & Zillman (1970) at Mirny and VostokII, but for the remaining stations there are no direct data available and the inversion has been calculated using the 500mb temperature interpolated from the map given by Schwerdfeger (1970), assuming a vertical potential temperature gradient of 6.7°C/km (lapse rate† of 3.1°C/km). The value for the vertical temperature gradient is the same as that given by Gosink (1989) and that of a standard Polar atmosphere. This seems reasonable from the profile given in fig. 2.5. but the profiles given by Kodama et al (1989) indicate a slightly lower value may be applicable and the numerical model results of Parish & Waight (1987)suggest that over the glacial slopes and coast the potential temperature gradient is close to zero. From fig. 4.4 it would appear a surface temperature gradient of 3.1°C/km is appropriate

in the interior, but that the stability of the air decreases over the glacial slopes and the coastal zone; the surface temperature gradient of 3.1°C/km results in a predicted inversion strength close to the values which can be interpolated from fig. 2.4[1] in the interior, but further down the glacial slope, and particularly at the coast, the difference between the 500mb temperature and the temperature above the boundary layer given by the observed strength of the inversion and surface temperature imply a much higher surface temperature gradient. This would be expected in a region where advection of relatively warm, unstable air from the ocean is more likely.

Boundary layer depth The observations of Gosink (1982, 1989) suggest a depth for the boundary layer of 400m. This is in close agreement with the observations presented by Kodama et al (1989) in the nighttime during the summer, which suggest a depth of around 400m, and possibly up to 600m. Although the actual depth is uncertain, it is unlikely that it decreases significantly over the glacial slopes. Much depends on the definition of the boundary layer. In the interior it is generally defined according to the inversion depth, which according to Phillpot and Zillman (1970) is between 500 and 600m but may be up to 1000m (Schwerdfeger 1984). As explained in chapter 2, the shape of the temperature profile in the interior zone, makes the absolute depth difficult to determine. Over the glacial slopes however, the boundary layer depth is more conveniently defined according to the depth of the katabatic flow which, because this tends to result in a more well mixed boundary layer, approximately coincides with the height of the lowest level of the inversion. Therefore at the top of the glacial slope, where there is a transition from a radiatively-produced boundary layer to a katabatic boundary layer, it would be expected that the depth will decrease slightly, and the upper boundary will become more well defined. There are no real data which shows the

[1]Komsomolskaya=21°C, VostokI=18°C, Pionerskaya=13°C

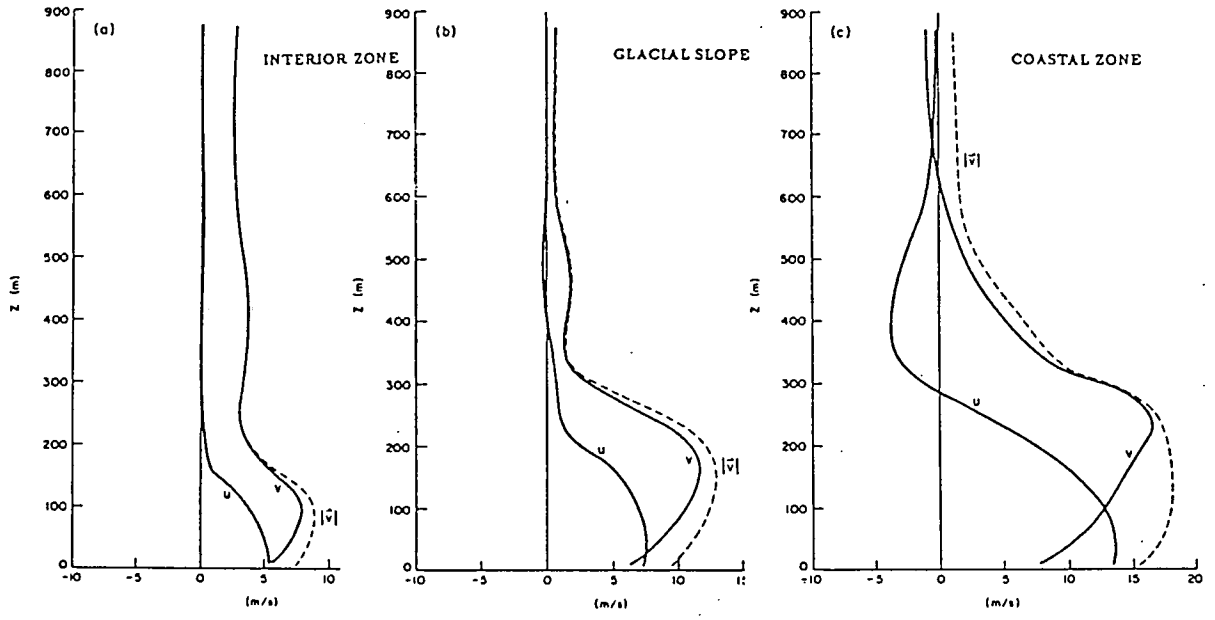

Figure 4.1: The variation in the depth of flow from the interior to the coast of Antarctica (Parish & Waight 1987).

depth evolution of the flow downslope once the katabatic layer is established, so the results of the numerical model of Parish & Waight (1987), which show the depth of flow to increase downslope as shown in fig. 4.1, have been used.

Geostrophic wind speed. There are very little data with which to assess the magnitude of the geostrophic wind above the inversion so it will be assumed to be constant; it is recognised that this may not be truely realistic. The height of the 500mb surface indicates a decrease in the pressure gradient between the interior of the East Antarctic ice sheet and the coast, but there are no data which allow the gradient to be reliably determined. Since the model is located over the glacial slopes where the geostrophic wind gradient is small, it seems reasonable to assume a constant value for Vg.

Schwerdfeger & Mahrt (1968a,b) calculated the geostrophic wind at VostokII, Byrd, and South Pole and found values between 2 and $5.1 ms^{-1}$. The results of the numerical model of Parish & Waight shown in fig. 4.3 show the value to vary

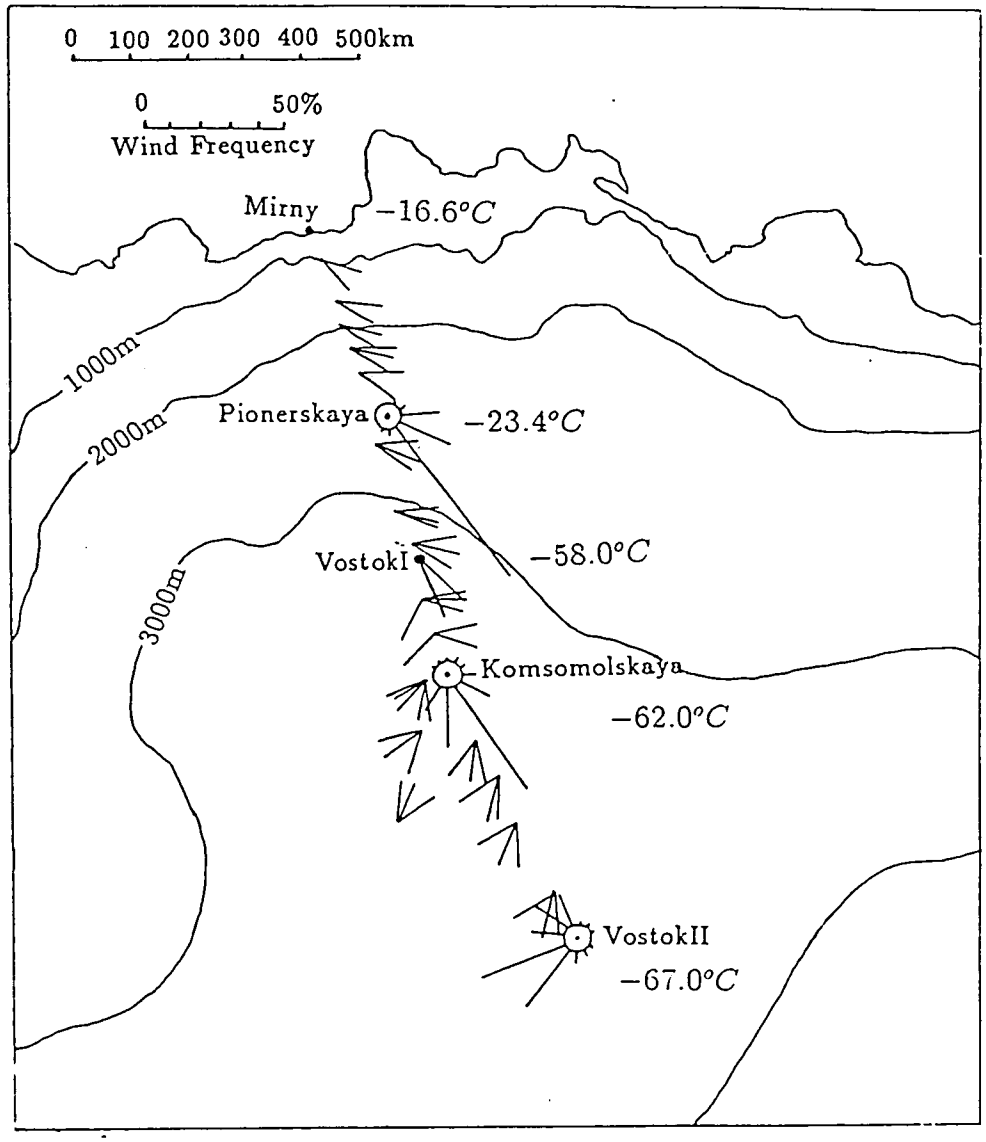

Figure 4.2: The wind roses and mean July temperature for each of the stations discussed in section 4.2.

from around $4ms^{-1}$in the interior to 2-$3ms^{-1}$over the glacial slope.

The data of this section are summarised in fig. 4.4 in a form suitable for constraining a slab model of the boundary layer. The figure shows the strength of the inversion decreasing from 25K in the interior to 12K at the top of the slope, and to be minimal or absent at the coast. At the same time the wind speed increases and becomes oriented more directly downslope.

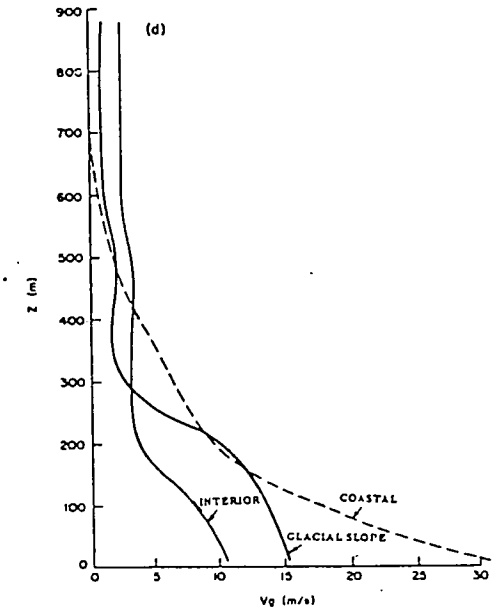

Figure 4.3: The geostrophic wind in the boundary layer from the numerical grid point model of Parish & Waight (1987).

4.3 The Slab Model Formulation

4.3.1 The Idealised Boundary Layer

The concepts of the model are shown in graphical form in fig. 4.5. The boundary layer is treated as a layer of cold air flowing over a dome shaped ice sheet, and with a prescribed surface profile given by equation 4.11, defining the slope angle α, at the lower boundary so that, $\tan\alpha = \frac{dH_i(x)}{dx}$.

$$H_i = h_d \left[1 - \left(\frac{x}{s_p} \right)^{\frac{n_g+1}{n_g}} \right]^{\frac{n_g}{2n_g+1}} \tag{4.11}$$

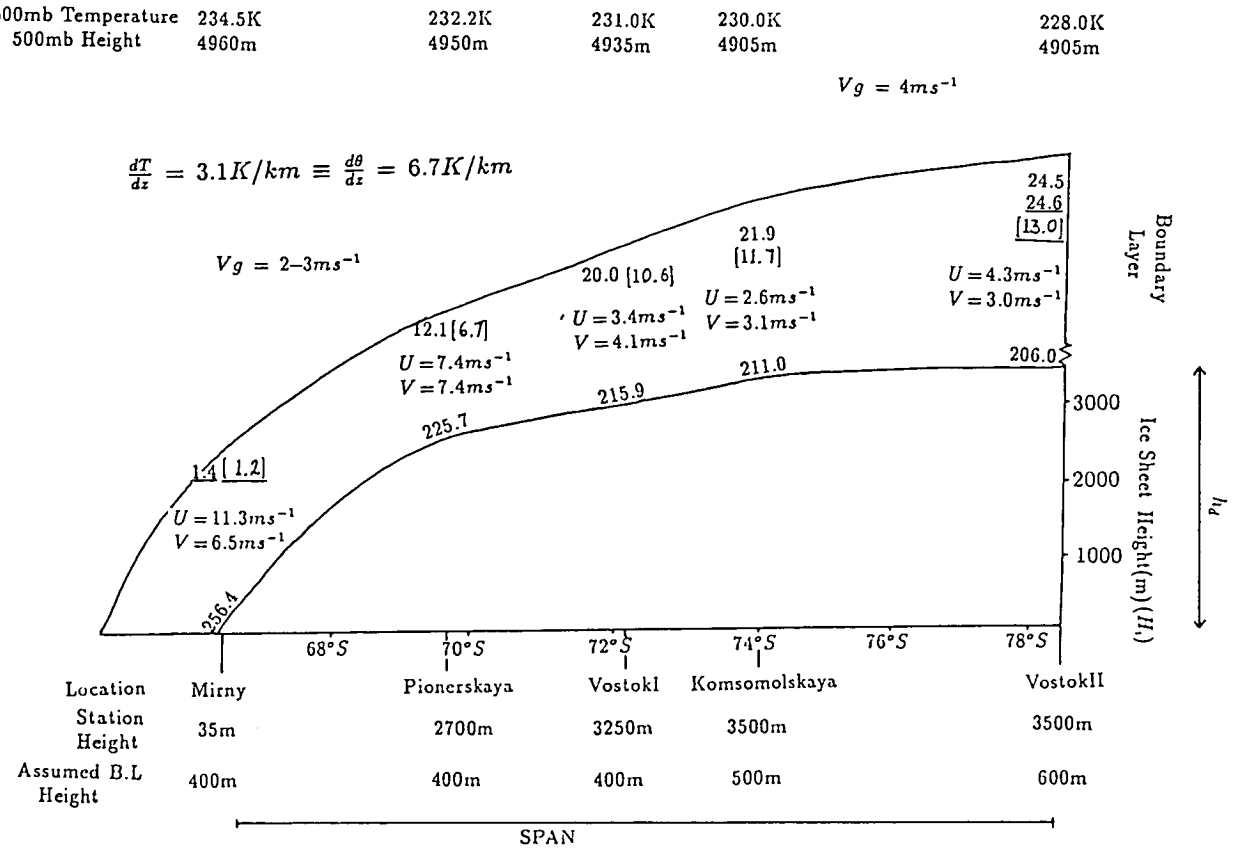

Figure 4.4: The constraints on a slab model as given by the observations from VostokII to Mirny. Mean July surface temperature is shown along the surface of the ice, the figures within the boundary layer represent the calculated inversion strength, with the equivalent potential temperature deficit for the layer in square brackets. Underlined values indicate observations from Phillpot & Zillman (1970).

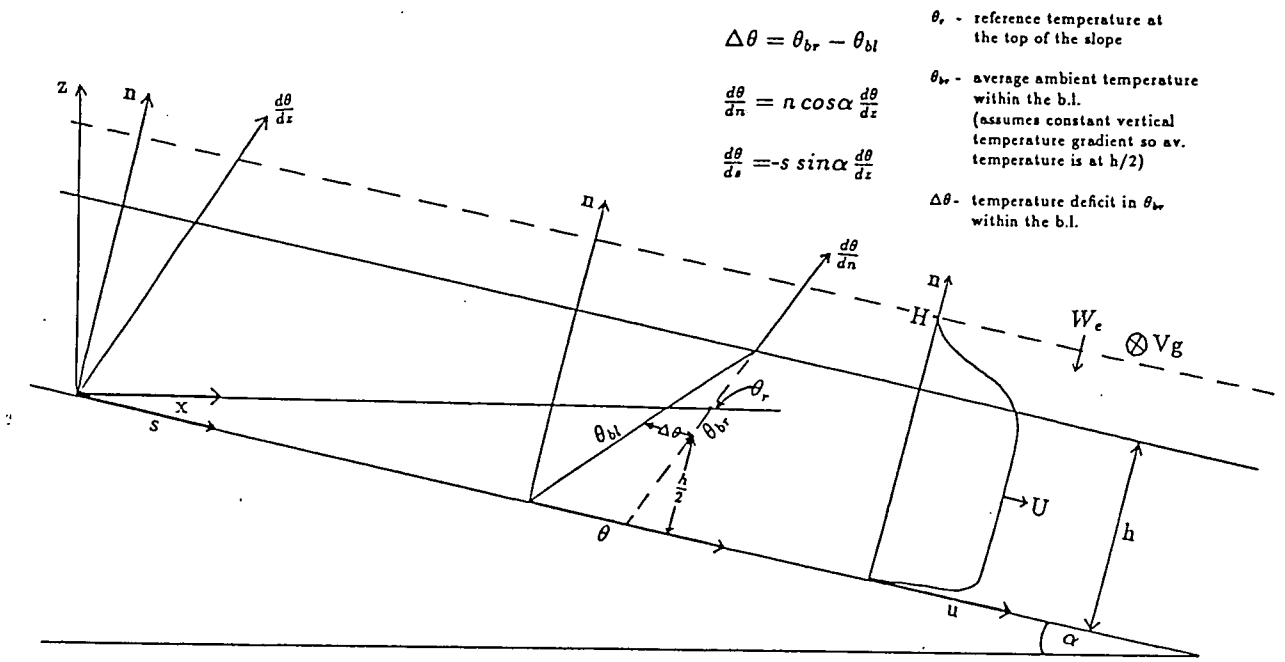

Figure 4.5: The idealised boundary layer of the slab model.

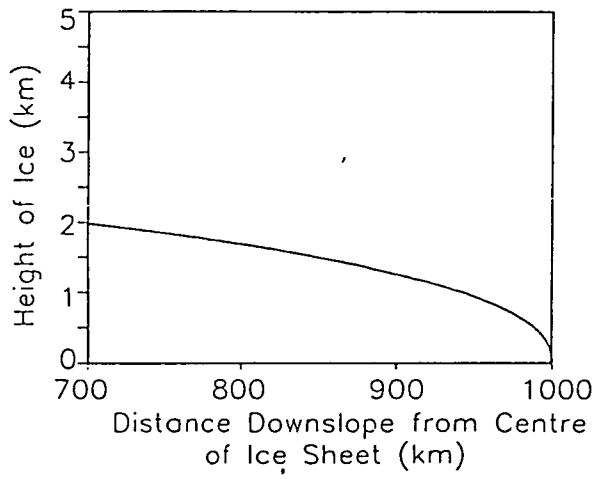

Figure 4.6: The shape of the surface profile described by equation 4.11.

Where H_i is the height of the ice sheet, h_d the height at the divide† and s_p the span,† The constant n_g is defined according to Glens' flow law and is generally taken to be 3. This profile is based on Glens' Flow Law for ice and is generally taken to represent an idealised profile of an ice sheet (Glen 1955) shown in fig. 4.6. The s-axis follows the surface of the ice sheet in the direction of maximum slope, parallel to the direction of flow component u, the y axes is directed perpendicularly to the left, in the direction of flow component v, parallel to the contours, and the n axis is orientated normal to the $s - y$ plane. The air is treated as a Boussinesq fluid, so that variations in density are ignored except for those producing a buoyancy force when combined with gravity (Manins and Sawford 1979); this approximation is reasonable for heights of a few hundred metres. The upper boundary of the model is constrained by a prescribed potential temperature gradient ($\frac{d\theta}{dz}$) and wind speed (Vg). The temperature gradient implies a Brunt-Vaisalla buoyancy frequency, the velocity of propagation of small amplitude gravity waves, which in a stable† layer is defined as,

$$N^2 = \frac{g}{\theta_r}\frac{d\theta}{dz} \tag{4.12}$$

The wind above the boundary layer is assumed to be geostrophic and in the y direction. Surface cooling is prescribed according to a constant net radiative divergence of the boundary layer (R_n). The air within the boundary layer is acted on by a buoyancy force due to the potential temperature deficit ($\Delta\theta$), in the ambient temperature field (θ_{br}), and flows downslope under the influence of this force combined with the overriding pressure gradient force ($\frac{dp}{ds}$) and the coriolis force. Friction acts at the interface with the ice sheet, and entrainment is permitted with the warmer air above the b.l. The profiles of θ, w, and u and v, are given in fig. 4.7. H is defined as being the level unaffected by the katabatic flow and h is the scaled depth of the boundary layer. The profile of θ generally shows a gradual linear increase with height. The gradient ($\frac{d\Delta\theta}{dz}$) within the boundary layer

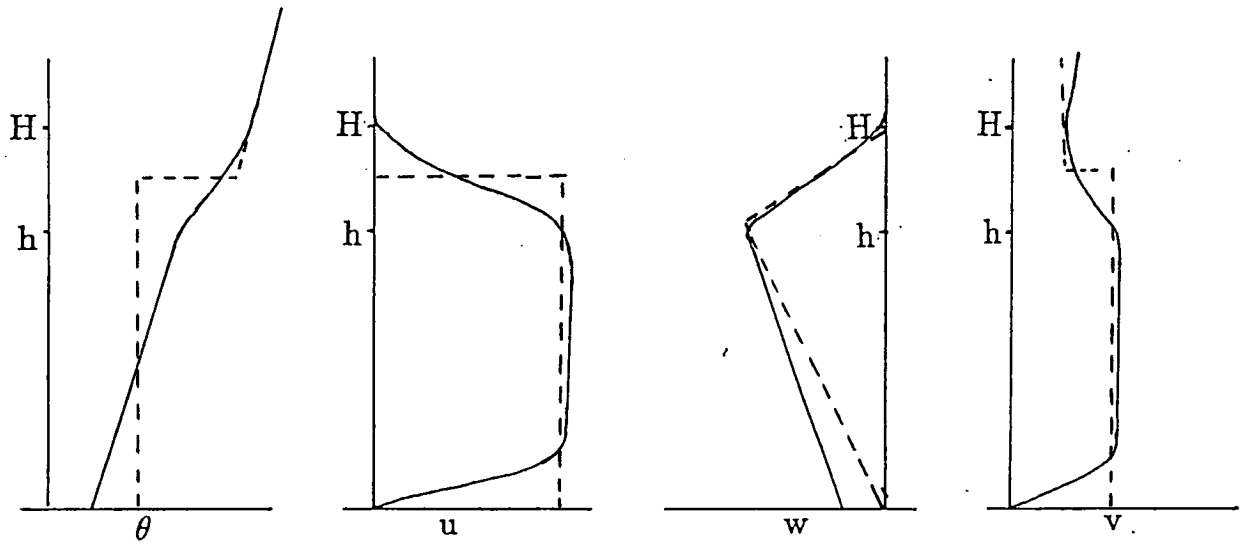

Figure 4.7: Schematic profiles of u,v, θ, and w, within the boundary layer. (—) Profiles used in the model (- - -)

is generally small as turbulence within the boundary layer, causes the profile to tend towards that of a well-mixed layer. For the purposes of the slab model the layer will be assumed to have a constant value of $\Delta\theta$, which will be taken to be the average for the layer; for a linear actual profile this would be the value of θ at $\frac{h}{2}$. Deviations of the actual θ profile from well-mixed are compensated for in the use of the profile factor S_1, which will be explained in section 4.4.1

4.3.2 The Governing Equations

The model is based on the following set of equations for the steady state conservation of momentum, mass, and heat, using the nomenclature given in the previous section and taking $(p - p_a)$ as the pressure depth of the boundary layer.

Momentum

$$w\frac{\partial u}{\partial n} + u\frac{\partial u}{\partial s} = g\frac{\Delta\theta}{\theta_{br}}\sin\alpha - \frac{1}{\rho}\frac{\partial p}{\partial s} - fv + \frac{\partial\left(\frac{\tau_x}{\rho}\right)}{\partial n} \tag{4.13}$$

$$w\frac{\partial v}{\partial n} + u\frac{\partial v}{\partial s} = \frac{\partial Vg}{dn}\frac{\partial(uhy)}{ds} + fu + \frac{\partial\left(\frac{\tau_y}{\rho}\right)}{\partial n} \tag{4.14}$$

Hydrostatic balance

$$\frac{dw}{dt} = \frac{1}{\rho}\frac{\partial}{\partial n}(p - p_a) - g\frac{\Delta\theta}{\theta_{br}}\cos\alpha \tag{4.15}$$

Heat

$$w\frac{\partial\theta}{\partial n} + u\frac{\partial\theta}{\partial s} = -\frac{1}{\rho C_p}\frac{\partial R_n}{\partial n} - u\frac{\partial\left(\overline{w'\theta'}\right)}{\partial n} \tag{4.16}$$

Mass

$$\frac{\partial u}{\partial s} + \frac{\partial w}{\partial n} = 0 \tag{4.17}$$

The wind above the boundary layer is assumed to be geostrophic and exclusively in the y direction, so that the first term on the right hand side of equation 4.14 allows for the velocity gradient above the boundary layer. It is assumed that this is a linear profile so that $\frac{\partial Vg}{\partial n} \approx \frac{Vg}{h}$. The second term on the right hand side of equation 4.13 can be replaced by the pressure gradient force of the free atmosphere and the effect of the thermal wind, between the free atmosphere and the boundary layer, so that

$$-\frac{1}{\rho}\frac{\partial p}{\partial s} = fVg - \frac{1}{\rho}\frac{\partial}{\partial s}(p - p_a) \tag{4.18}$$

Neglecting vertical accelerations with respect to the pressure variation, the hydrostatic equation can be rewritten as follows;

$$\frac{1}{\rho}\frac{\partial(p - p_a)}{\partial n} = -g\frac{\Delta\theta}{\theta_{br}}\sin\alpha \tag{4.19}$$

This can be integrated with respect to n and substituted into equations 4.13 using 4.18. Equations 4.13 to 4.17, can then be integrated in the n direction to height H which is assumed to be unaffected by katabatic flow, and in the y direction around the circumference, y_i, of the ice sheet replacing $\left(\frac{\partial\theta}{\partial n}\right)$ and $\left(\frac{\partial\theta}{\partial s}\right)$ with $\left(\frac{\partial\theta}{\partial z}\right)$, according to fig. 4.5 and neglecting second order derivatives, so that,

$$\begin{aligned}\frac{d}{ds}\int_{y_i}\int_0^H u^2\,dn\,dy_i &= \int_{y_i}\int_0^H g\frac{\Delta\theta}{\theta_{br}}\sin\alpha\,dn\,dy_i - \frac{d}{ds}\int_{y_i}\int_0^H\int_0^H g\frac{\Delta\theta}{\theta_{br}}\sin\alpha\,dn\,dn\,dy_i \\ &+ \int_{y_i}\int_0^H fVg\,dn\,dy_i - \int_{y_i}\int_0^H fv\,dn\,dy_i \\ &+ \int_{y_i}\int_0^H \frac{d}{dn}\left(\frac{\tau_x}{\rho}\right)dn\,dy_i \end{aligned} \tag{4.20}$$

$$\begin{aligned}\frac{d}{ds}\int_{y_i}\int_0^H uv\,dn\,dy_i &= -\int_{y_i}\int_0^H \frac{Vg}{h}W_e\,dn\,dy_i + \int_{y_i}\int_0^H fu\,dn\,dy_i \\ &+ \int_{y_i}\int_0^H \frac{d}{dn}\left(\frac{\tau_y}{\rho}\right)dn\,dy_i \end{aligned} \tag{4.21}$$

$$\begin{aligned}\cos\alpha\frac{d\theta}{dz}\int_{y_i}\int_0^H w\,dn\,dy_i - \sin\alpha\frac{d\theta}{dz}\int_{y_i}\int_0^H u\,dn\,dy_i = \\ -\int_{y_i}\int_0^H \frac{d}{dn}\frac{R_n}{\rho C_p}\,dn\,dy_i - \int_{y_i}\int_0^H \frac{d}{dn}\left(W_e\Delta\theta\right)dn\,dy_i \end{aligned} \tag{4.22}$$

$$-W_e y = d\frac{(uhy)}{ds} \tag{4.23}$$

4.3.3 The Profile Factors

Profile factors S_1, S_2 and S_3 have been introduced to scale the integrals in order to account for the shape of the velocity and density profiles such that (Manins and Sawford 1979):

$$S_1 g h^2 \frac{\Delta\theta}{\theta} = 2\int_0^H gn\frac{\Delta\theta}{\theta}\,dn \tag{4.24}$$

$$S_2 g h \frac{\Delta\theta}{\theta} = \int_0^H g\frac{\Delta\theta}{\theta}\,dn \tag{4.25}$$

$$\int_0^H w\,dn = W_e H - S_3 W_e h \tag{4.26}$$

h is the depth of the boundary layer, scaled using the profile factors in equations 4.24 to 4.26. If there was no entrainment h would be at the same height as H (Gosink, personal communication 1991), and there would be a discontinuity at the top of the boundary layer. The profile factors account for the distribution of the density relative to the buoyancy profiles, and arise because integrating each according to average characteristics of the layer, is not strictly equivalent to summing the integrals of each of the sub-layers within the boundary layer. For well-mixed katabatic flow $S_1 = S_2 = S_3 = 1$. There are very little data available to assess the values of the profile factors and sensitivity studies in the next section will show the development of the boundary layer to be relatively insensitive to variations in their value. This is also verified by Manins and Sawford (1979).

The Profile Factor S_1.

The pressure distribution associated with the thermal wind, described by S_1 in equation 4.24 is probably the most complex profile factor, because it must consider

that $\Delta\theta$ and θ are both functions of n. Ellison and Turner (1959) in laboratory experiments estimated S_1 to lie between 0.2 and 0.3, but on the glacial slopes the flow is of a much larger scale and has been observed to be more well mixed. Gosink (1989) observed Reynolds numbers on the glacial slope to be 5 orders of magnitude greater than those produced either in the laboratory experiments of Ellison and Turner, or in the later glacial valley study by Manins and Sawford (1979). Taking this into account and the fact that as the flow becomes more well mixed the profile factors should take on values closer to unity, S_1 would be expected to take on a slightly larger value than that used by Ellison & Turner. This was also suggested by Manins & Sawford (1979) and Gosink (1989). A value of 0.5 has been taken as a basis for the sensitivity studies.

The Profile FactorS_2.

Equation 4.25, defining S_2 is the least complex of the integrations, it governs the distribution of buoyancy throughout the layer. S_2 will deviate from unity because the value of θ in each sub layer is not constant throughout the layer. However, variations in the ambient density are likely to be relatively small compared to the other terms, and on this basis the value of S_2 would be expected to lie close to 1. Indeed laboratory experiments by Ellison and Turner (1959) found that S_2 varies from 0.6, to 0.9 at higher Reynolds numbers (more turbulent flow). Therefore in the well-mixed flow of the glacial slopes, 0.9 seems a reasonable value for S_2.

The Profile Factor S_3.

S_3 is associated with the vertical velocity within the boundary layer. Rather than defining a mean value for the layer, the value at H is used in accordance with entrainment theory (Manins & Sawford 1979). Entrainment of air from above the boundary layer into the katabatic flow will induce a vertical velocity, W_e, in the ambient air which will ultimately result in a velocity parallel to the isotherms in a stabily stratified environment (Manins and Sawford 1979). For horizontal isotherms this small horizontal velocity, U_H, is related to W_e by the following equation,

$$U_H \sin\alpha = W_e \cos\alpha \tag{4.27}$$

This should be taken into account in the integration of the flow speed U, as follows,

$$\int_0^H u\, dn = Uh + U_H H \tag{4.28}$$

Unless H is much larger than h, $U_H \ll U$ so that the second term on the right hand side of equation 4.28 can be neglected, except in the integration of the buoyancy equation 4.22. Substituting equations 4.26 and 4.28 into the left hand side of equation 4.22, produces a $\left[-U_H H \sin\alpha \frac{\partial\theta}{dz}\right]$ term and a $\left[W_e H \cos\alpha \frac{\partial\theta}{\partial z}\right]$ term which add to zero according to equation 4.27. There are no data with which to assess the value of S_3, which is associated with the vertical velocity in the n direction. In past studies, as in this study, it has been taken to be 1. Sensitivity studies later in this chapter will show that the evolution of the boundary layer is fairly insensitive to the value of S_3.

Gosink (1989) also included a fourth profile factor S_4 which was associated with the coriolis term in equation 4.13. This was used because V was not resolved explicitly, measured values were used at a specific height, and S_4 was included as a weighting factor for V, the mean layer velocity, compared to v, the velocity at

a specific height (Gosink, personal communication 1991). S_4 will not be included in this model since V is resolved for the layer.

4.3.4 Parameterisation of Surface Friction

Surface Stress, τ, is parameterised as

$$-\frac{\tau}{\rho} = C_d U^2 \tag{4.29}$$

This follows Dalrymple et al (1966), who define a drag coefficient independent of bulk stability as $\frac{\tau}{\rho}^{0.5}/V_4 = 0.039$. This is equivalent to $C_d = 0.0015$. Inoue (1989), also found that for $\frac{Z}{L} \leq 0.2$ the stability dependence is small and found values of C_d to vary according to wind direction, having a value of 0.0008 in the smoothest direction and 0.0015 in the roughest direction. Ball (1956) has used a value for C_d of 0.005, on the basis that true katabatic flow nearer the ice sheet margin† will be retarded more than the quasi-geostrophic winds of the interior because of additional drag at the upper interface. In an entraining model such as this the entrainment terms themselves account for this drag in the momentum equation.

The flow in the y direction is perpendicular to the orientation of the mountains and valleys of the ice sheet, and as such the assumption of a uniform slab in this direction is not strictly true. Flow across valleys induces gravity waves which retard the flow. This has been suggested by James (1989) to be important for the flow above the boundary layer, and Mobbs & Rees (1989) suggest that the drag force due to gravity waves at Halley Station on the Brunt Ice Shelf attains values of $10ms^{-1}$/day. In addition to this there are smaller scale undulations on a scale of approximately 5m caused by wind and ablation. Sastrugi, which are a kind of snow dune are prevalent over the whole of the ice sheet in Antarctica and because

they are formed by the action of the wind, they result in additional roughness of the surface perpendicular to the prevailing wind direction, in this case, along the y axis of flow. In order to account for these potentially large decelerative forces in the y direction the drag coefficient is prescribed a value greater than that in the s direction.

4.3.5 Entrainment with an Inverse Richardson Number Dependence

In these sensitivity studies entrainment is parameterised according to a Richardson number formulation after Manins and Sawford(1979). This has been derived from laboratory experiments of Ellison & Turner (1959). Alternative parameterisations will be investigated in chapter 5. The entrainment process is defined by the following equations:

$$W_e = -E\mathbf{U} \tag{4.30}$$

$$E = \frac{A_c}{S_1 Ri + A_k} \tag{4.31}$$

$$Ri = gh\frac{\Delta\theta}{\theta_{br}\mathbf{U}^2}\cos\alpha \tag{4.32}$$

Where $\mathbf{U}^2 = U^2 + V^2$

The Evolution of U, V $\Delta\theta$ and h.

Substituting equations 4.24, 4.25, 4.26, 4.28 and 4.29 into equations 4.20-4.23, gives the following equations describing the evolution of U,V,h and $\Delta\theta$.

$$\frac{dU}{ds} = S_2 g \frac{\Delta\theta}{\theta_{br} U} \sin\alpha + \frac{f}{U}(Vg - V) - S_1 \frac{1}{U h y_i} \frac{d}{ds}\left[g \frac{\Delta\theta}{\theta_{br}} \frac{h^2}{2} y_i \cos\alpha \right] + \frac{W_e}{h} - \frac{C_d U}{h} \tag{4.33}$$

$$\frac{dV}{ds} = f - \frac{W_e}{Uh}(Vg - V) - \frac{C_d V^2}{hU} \tag{4.34}$$

$$\frac{d\Delta\theta}{ds} = \frac{R_n}{\rho C_p h U} - \frac{d\theta}{dz}(\sin\alpha - S_3 E \cos\alpha) + \frac{\Delta\theta W_e}{hU} \tag{4.35}$$

$$\frac{dh}{ds} = -\frac{W_e}{U} - \frac{h\,dU}{U\,ds} - \frac{h\,dy}{y_i ds} \tag{4.36}$$

4.3.6 Initialisation of the Model

Equations 4.33 and 4.36 may be combined to produce a linear first order differential equation for the evolution of U down the slope as follows;

$$\frac{dU}{ds}(1 - Ri_c) = S_2 \frac{g\Delta\theta}{\theta_{br} U} \sin\alpha - S_1 \frac{g}{\theta_{br} U} \cos\alpha \left[\Delta\theta E - \frac{\Delta\theta h \pi}{y_i} + \frac{h d\Delta\theta}{2\,ds} \right] + \frac{f}{U}(Vg - V) - \frac{C_d U}{h} + \frac{W_e}{h} \tag{4.37}$$

$$Ri_c = S_1 \frac{gh\Delta\theta}{\theta_{br} U^2} \cos\alpha \tag{4.38}$$

From equations 4.37 and 4.38 it is apparent that if the Richardson number is unity then the equations become unstable. Therefore it is necessary to assume that the

flow is shooting at all points along the glacial slope. The definition of shooting flow requires that the layer velocity is greater than the velocity of propagation of small amplitude gravity waves (N in equation 4.12) so that $Ri_c < 1$. The flow is therefore characterised as having strong mixing by entrainment and breaking interfacial waves and is determined exclusively by conditions upstream.

In each run initial values of the variables U_1, V_1, h_1 and $\Delta\theta_1$ have been chosen according to observations and ensuring that the criteria for a critical Richardson number is met. Therefore h_1 is assumed to lie between 300m and 350m, U_1 between $6ms^{-1}$and $8ms^{-1}$, V_1 between $3ms^{-1}$and $8ms^{-1}$and $\Delta\theta_1$ between 8K and 12K. The model was run and the value of U_1 adjusted iteratively to eliminate any abrupt changes in gradient of U,V,h or $\Delta\theta$. This is necessary in a forward stepping model of this nature because boundary layer characteristics at each point along the slope are determined exclusively by upstream conditions. In the real atmosphere this may occur through the action of gravity waves propagating upstream which this model cannot incorporate due to the assumption of shooting flow.

4.4 Sensitivity Studies

Table 4.1 shows the initial conditions and parameters used in each experiment of the sensitivity studies. The prescribed boundary conditions of radiative cooling, geostrophic wind and stability and the parameterisation of entrainment will all be investigated in chapter 5, and have therefore been held constant in these studies. The value of B is $0.03\text{K}.ms^{-1}$which is equivalent to a surface heat loss of around $30Wm^{-2}$, which seems reasonable in comparison to the observed longwave heat flux in July (table 2.3). This value was used by Gosink(1989) and Manins & Sawford (1979) as a typical cooling rate over the slopes of Antarctica. The ambient

name	U	V	H	$\Delta\theta$	S_1	S_2	S_3	C_{du}	C_{dv}	Vg	$\frac{d\theta}{dz}$
std	8.5	3.0	300	8	0.5	0.9	1.0	0.0015	0.04	3	1.7
s125	8.5	3.0	300	8	0.25	0.9	1.0	0.0015	0.04	3	1.7
s19	9.5	3.0	300	8	0.9	0.9	1.0	0.0015	0.04	3	1.7
s25	7.5	3.0	300	8	0.5	0.5	1.0	0.0015	0.04	3	1.7
s35	8.5	3.0	300	8	0.5	0.9	0.5	0.0015	0.04	3	1.7
s35g67	8.5	3.0	300	8	0.5	0.9	0.5	0.0015	0.04	3	6.7
snov	10.5	0.0	300	8	0.5	0.9	1.0	0.0015	0.04	3	1.7
cdu008	10.0	3.0	300	8	0.5	0.9	1.0	0.0008	0.04	3	1.7
cdv2	8.0	4.0	300	8	0.5	0.9	1.0	0.0015	0.02	3	1.7
cdred	9.0	4.0	300	8	0.5	0.9	1.0	0.0008	0.02	3	1.7
cdx2	7.5	2.0	300	8	0.5	0.9	1.0	0.003	0.08	3	1.7
cdv8	9.5	2.0	300	8	0.5	0.9	1.0	0.0015	0.08	3	1.7
cdv3	7.5	3.0	300	8	0.5	0.9	1.0	0.003	0.04	3	1.7
cdu4[a]	7.5	3.0	300	8	0.5	0.9	1.0	0.004	0.04	3	1.7
cdv1[a]	8.5	4.0	300	8	0.5	0.9	1.0	0.0015	0.01	3	1.7

[a] Ri_c becomes too big

Table 4.1: Initial condition for the sensitivity studies.

stability of the air is taken to be 1.7°C/100m and the geostrophic wind speed $3ms^{-1}$, following the discussion of section 4.1.1. Entrainment has been halved from the Gosink case to prevent excessive growth of the b.l; A_c has been given a value of 0.0002 and A_k a value of 0.02. Initial values of the profile factors have been chosen according to the discussion in the previous section.

The model reproduces the results of Lalaurette and Andre (1985) with V set to 0. However this, and other similar models (eg Gosink 1989) appears to result in a

b.l which deepens excessively downslope. Work by Parish et al (1984/86/87/91) suggests that the acceleration of air to large speeds observed on the coast is only possible where the air converges in a valley. There are many stations on the coast of Antarctica with recorded speeds of less than 10m/s such as McMurdo and Halley. Unusually large wind speeds are particularly apparent in Adelie land where Cape Denison and Port Martin have average wind speeds of $19.8ms^{-1}$and $18ms^{-1}$respectively. The high speeds are largely a consequence of the topography not only in the immediate vicinity of the station but also for a considerable distance upwind (Parish 1984, Parish & Wendler 1991). The suggestion by the data of high velocities off the coast of Antarctica may well be a facet of the specific sites at which observations have been made rather than a generalisation that is true of the whole continent. A model such as this therefore, with average topography will not reproduce the very strong winds observed at these stations on the coast of Antarctica. The effect of more realistic topography will be investigated in chapter 5.

The following sensitivity studies will assess the variations in U, V, h and $\Delta\theta$ with each of the profile factors and C_d. Chapter 5 will then go on to look at the prescribed boundary conditions, the parameterisation of entrainment, the effect the surface topography, and the way in which the constraints on the model differ for past ice sheets.

4.4.1 Profile Factors $[S_1, S_2, S_3]$

As S_1 increases, the Richardson number defined in equation 4.38 increases linearly at approximately the same rate, so in order to maintain subcritical flow, U also increases. Once the model has been initialised, the effect of the large Richardson

number is compensated for by the inverse Richardson number dependence in the entrainment equation 4.31; a more stable layer has a much lower rate of entrainment and so a slower rate of growth of the boundary layer depth. The reduction in entrainment also reduces the drag at the top of the layer which helps to maintain a Richardson number of less than 1. The overall effect shown in fig. 4.8 is that as S_1 increases the Richardson number (Ri_c) increases and so does the speed of the boundary layer; the rate of growth of the boundary layer, is less because entrainment is reduced. Thus low values of S_1 tend to produce a boundary layer which grows downslope and high values result in a thinning of the layer downslope. The additional entrainment when S_1 is low produces a higher surface temperature gradient due to the incorporation of warmer air from above the boundary layer. Without the dependence of entrainment on the Richardson number the effects of S_1 are much less; a halving of S_1 and a doubling of A_c in the same run showed almost no difference to the speed, depth and temperature evolution of the flow, but obviously the Richardson number (Ri_c) was greater when the profile factor was greater. The value of S_1 chosen by previous authors has been 0.5, which seems reasonable in this case, preventing excessive boundary layer growth of the low S_1 case but also maintaining the flow as subcritical, without requiring wind velocities to be too large at the top of the slope.

The effects of S_2 are slightly more straightforward and are shown in fig. 4.9. From equation 4.33 it can be seen that reducing S_2 lessens the effective buoyancy force which as depicted in fig. 4.9 results in a slower, deeper flow which, because of the reduction in entrainment of warm air, is slightly colder, and with a lower temperature gradient along the surface of the ice.

The results of the sensitivity studies of S_3 are not shown as they were found to have almost no effect on the evolution of the flow, even if $\frac{\partial \theta}{\partial z}$ is increased to

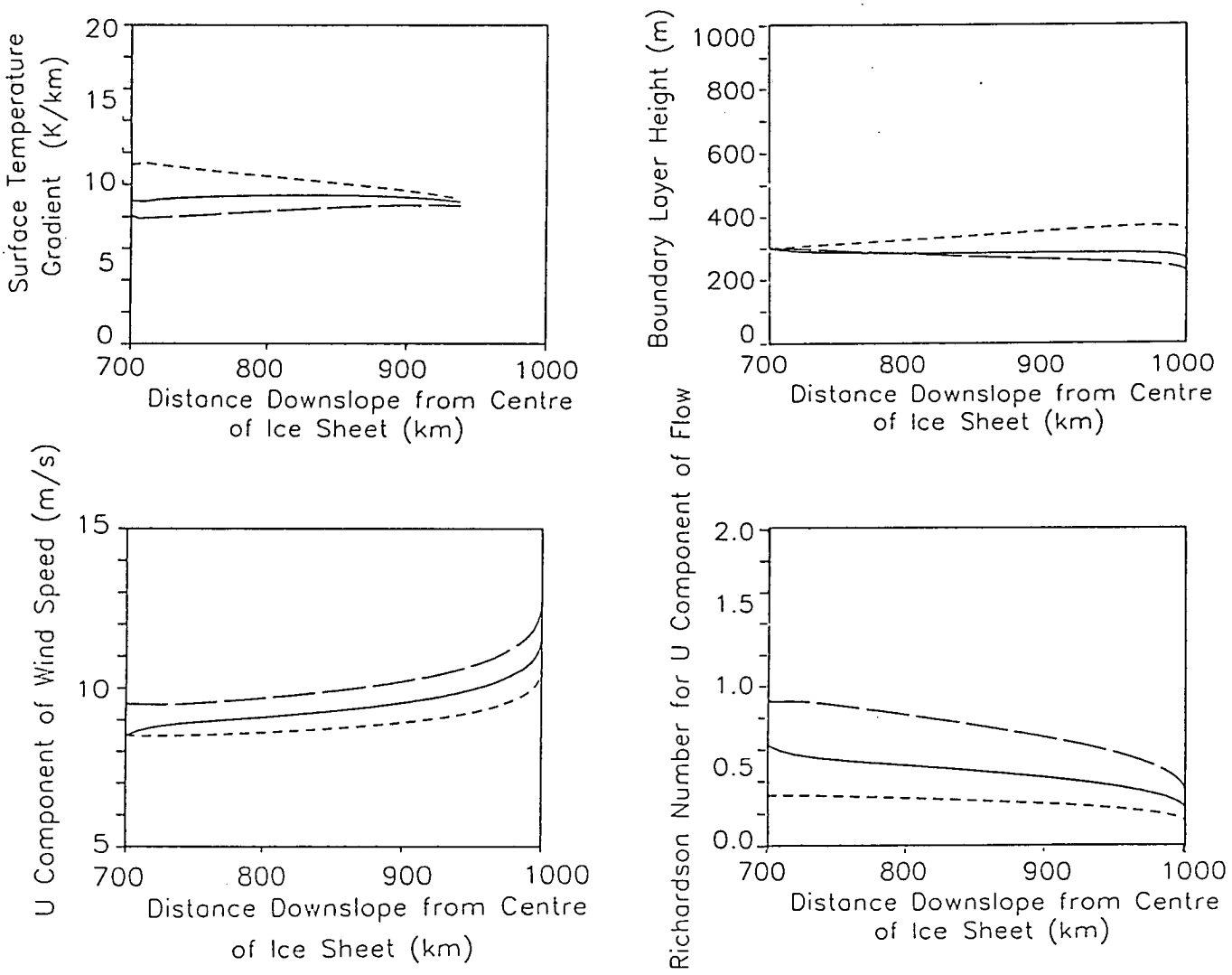

Figure 4.8: The variation in boundary layer characteristics for several values of S_1: $S_1 = 0.25$(- - - - -); $S_1 = 0.5$(———); $S_1 = 0.9$(— —).

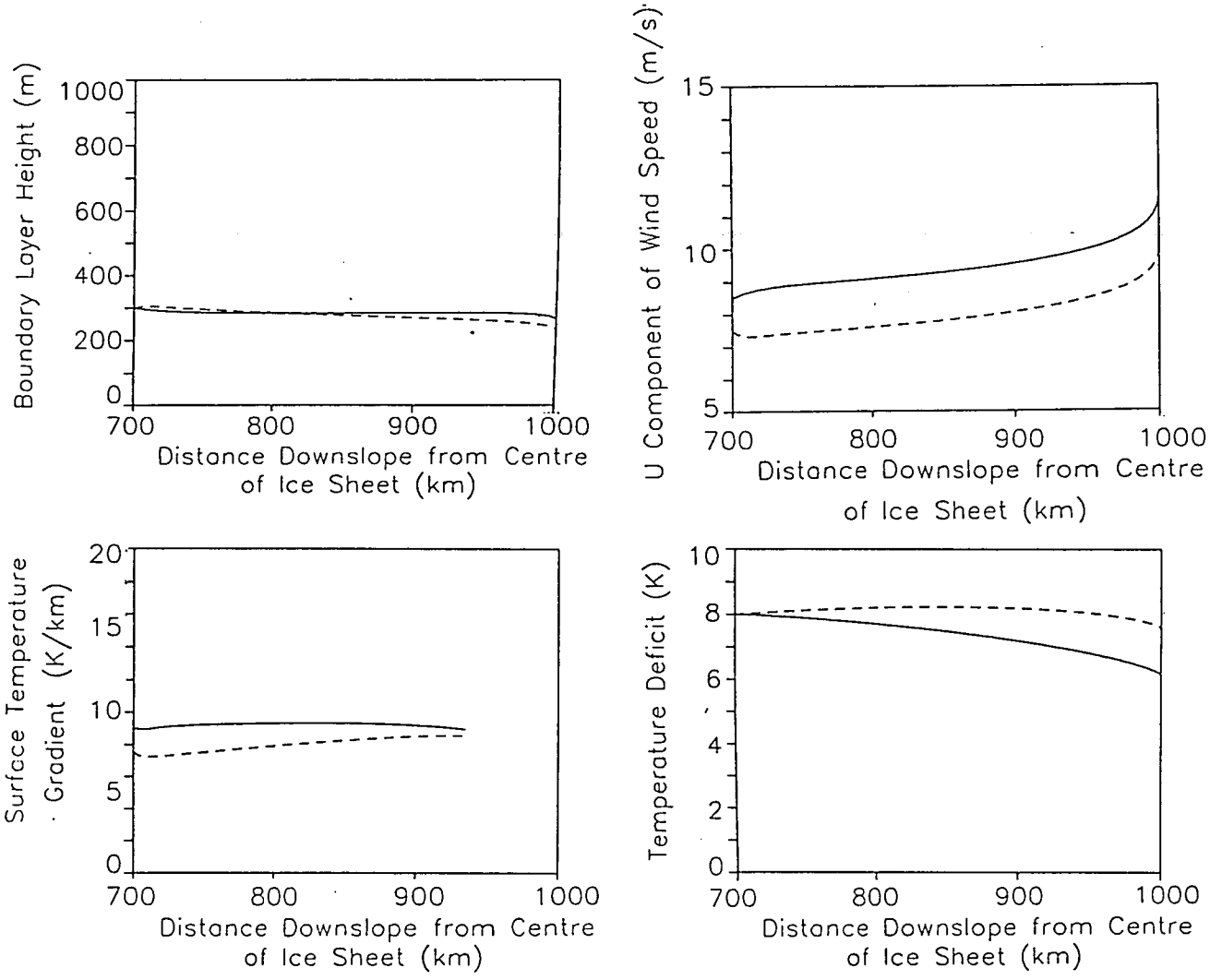

Figure 4.9: The sensitivity of the model to variations in S_2: $S_2 = 0.5$(– – –); $S_2 = 0.9$(———).

6.7K/km. This insensitivity arises because the entrainment and radiative terms tend to dominate the temperature evolution of the boundary layer, as shown in fig. 4.10, which shows the components of the temperature equation 4.35 for the 'std' case in table 4.1.

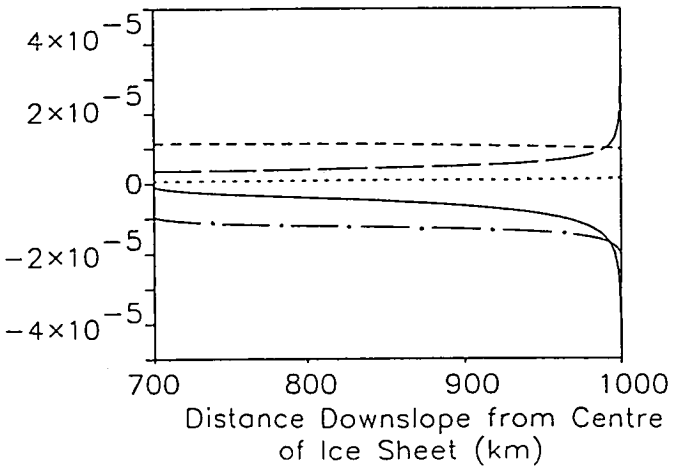

Figure 4.10: The components of the equation governing the rate of change of $\Delta\theta$: $\frac{d\Delta\theta}{ds}$(———); radiative term(- - - -); temperature gradient along the slope due to stability ($\frac{d\theta}{dz}\sin\alpha$)(— —); ($\frac{d\theta}{dz}S_3E\cos\alpha$)(·····); entrainment term ($\frac{\Delta\theta W_e}{hU}$)(—·—).

4.4.2 The Resolution of V

If the velocity in the y direction is not resolved, the flow downslope increases, because the retarding effect of the coriolis force is removed. The low Richardson number which this results in, causes more entrainment so that $\Delta\theta$ decreases and h increases more rapidly than the case when V is resolved, (fig. 4.11).

4.4.3 Drag coefficient$[C_d]$

The depth of the boundary layer is relatively insensitive to variations in C_d; the main variations in the boundary layer evolution occur due to the effect that the change in velocity has on the temperature evolution, via entrainment. Fig. 4.12 shows that if the drag coefficient is halved in both directions the velocity increases, most noticeably in the y direction of flow, which has an increase of

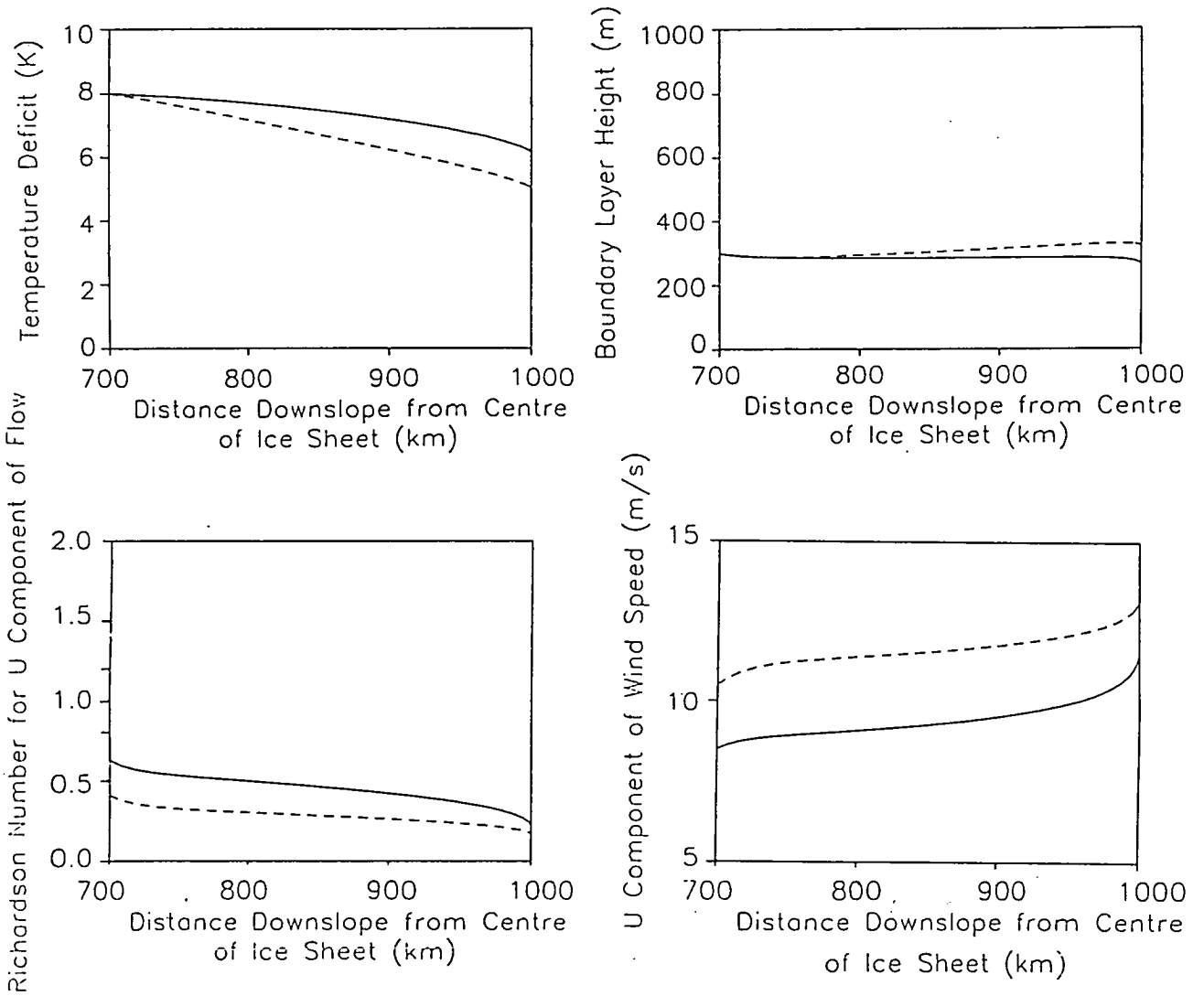

Figure 4.11: The effect of resolving the velocity in the y direction. with V(———); without V (- - - -).

$\approx 1.25 ms^{-1}$compared to a trivial increase in the U component. This occurs primarily because C_{dv} is greater than C_{du} and so when it is halved the effect is much greater, but also because an increase in the V component of flow places additional drag on the U component, which opposes the effect of the smaller drag coefficient. The increase in entrainment which occurs because of the faster flow is not sufficient to significantly alter the depth of the boundary layer. The decrease in temperature deficit, although small, is more significant and results in a slightly higher surface temperature gradient. A doubling of the drag coefficient has the reverse effect, resulting in much higher Richardson numbers and a lower surface temperature gradient. If the drag coefficient is reduced in the U direction only, the increase in the U component of flow produces a lower Richardson number and more entrainment and consequently a higher surface temperature gradient. This contrasts with the case where C_{dv} is small, which has a much smaller effect on the boundary layer evolution. The change in the V component of flow, is of minimal consequence for the depth and temperature of the boundary layer, the main effect is through the additional drag this exerts on the U component. If the retarding forces on the U component of flow become too great, either due to an increase in C_{du} or a decrease in C_{dv} the layer becomes super critical, which places bounds on the possible values for the drag coefficient.

4.4.4 Sensitivity to Changes in the Initial Conditions

If the initial values of U, V or h are changed, then the model adjusts itself within the first few tens of metres to the original value. Therefore in the sensitivity studies here, U, V and h at the top of the slope have been chosen to reduce any rapid changes in gradient at the beginning of the profile. If the temperature deficit is reduced as shown in fig. 4.13 the buoyancy of the air is less, so that the initial

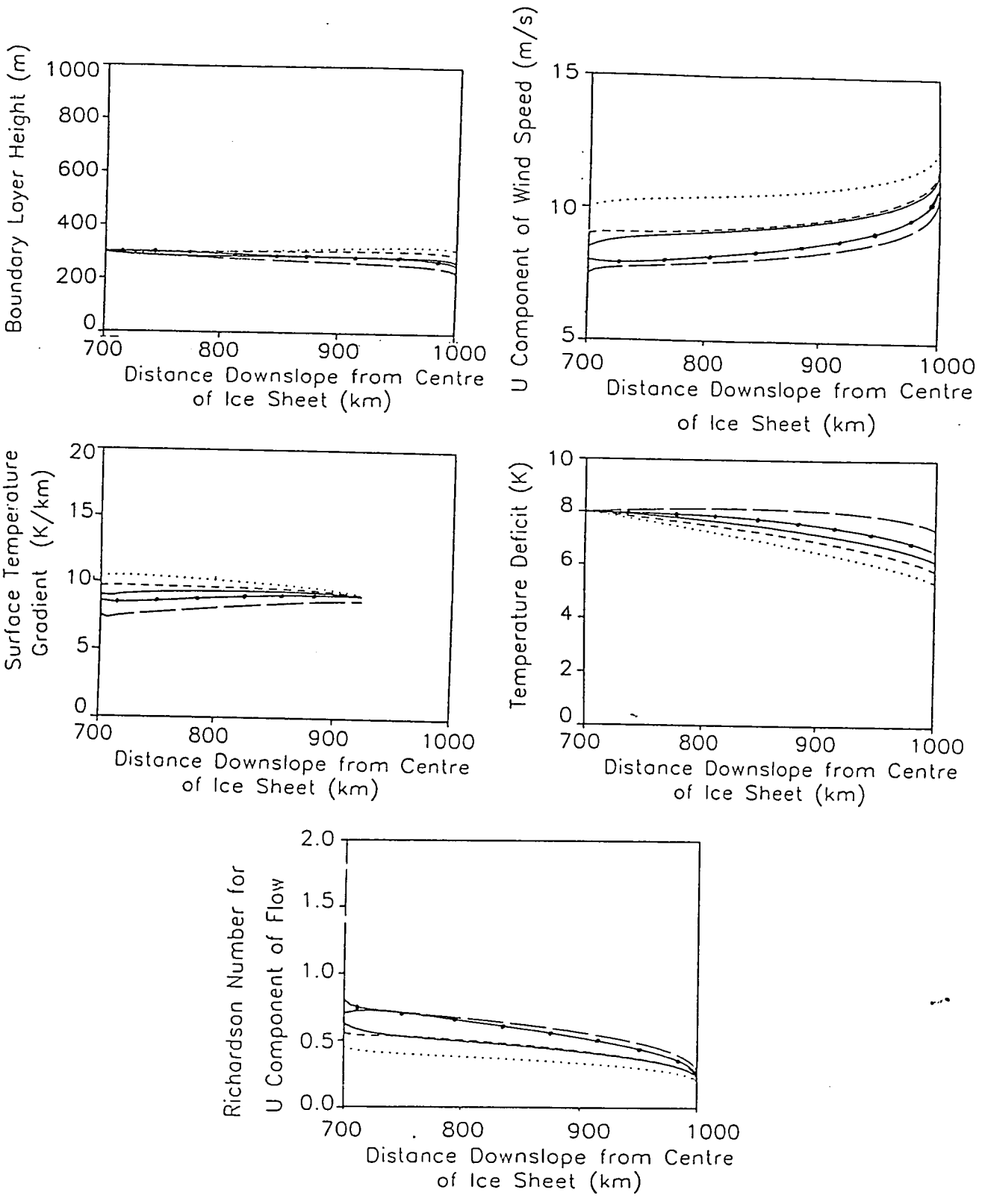

Figure 4.12: The sensitivity of the boundary layer to variations in C_d: $C_{du} = 0.0008$, $C_{dv} = 0.04$(·····); $C_{du} = 0.0008$, $C_{dv} = 0.02$(- - - -); $C_{du} = 0.0015$, $C_{dv} = 0.04$(———); $C_{du} = 0.0015$, $C_{dv} = 0.02$(—·———); $C_{du} = 0.003$, $C_{dv} = 0.08$(— —).

velocity is smaller and the effect on the Richardson number of the boundary layer is almost negligible. The entrainment velocity is only slightly reduced at the lower wind speed, so there is little difference in the depth of the boundary layer for the 2 cases. The reduction in the temperature gradient can partially be accounted for by the slight reduction in entrainment velocity. A larger effect is the fact that for lower values of $\Delta\theta$, the temperature of air which is entrained into the boundary layer, is closer to that of the boundary layer, and therefore its effect on the heat budget of the boundary layer is smaller.

4.5 Summary and Conclusions

This chapter has described a slab model to investigate the boundary layer over an ice sheet and shown the results of experiments used to test the sensitivity of the model to the various parameters. This is necessary for any meaningful interpretation of the experiments presented in the next chapter. The main points of the chapter can be summarised as follows

- Ice sheets are most sensitive to the ablation component of the mass balance and therefore a slab model has been developed as the most simple method to investigate the atmospheric boundary layer of this region more closely.
- Observations complemented by the results of models have been used to constrain the model.
- Following the work of Ellison & Turner (1959) and Manins & Sawford (1979), profile factors were introduced in order to account for the fact that the layer is not well-mixed.

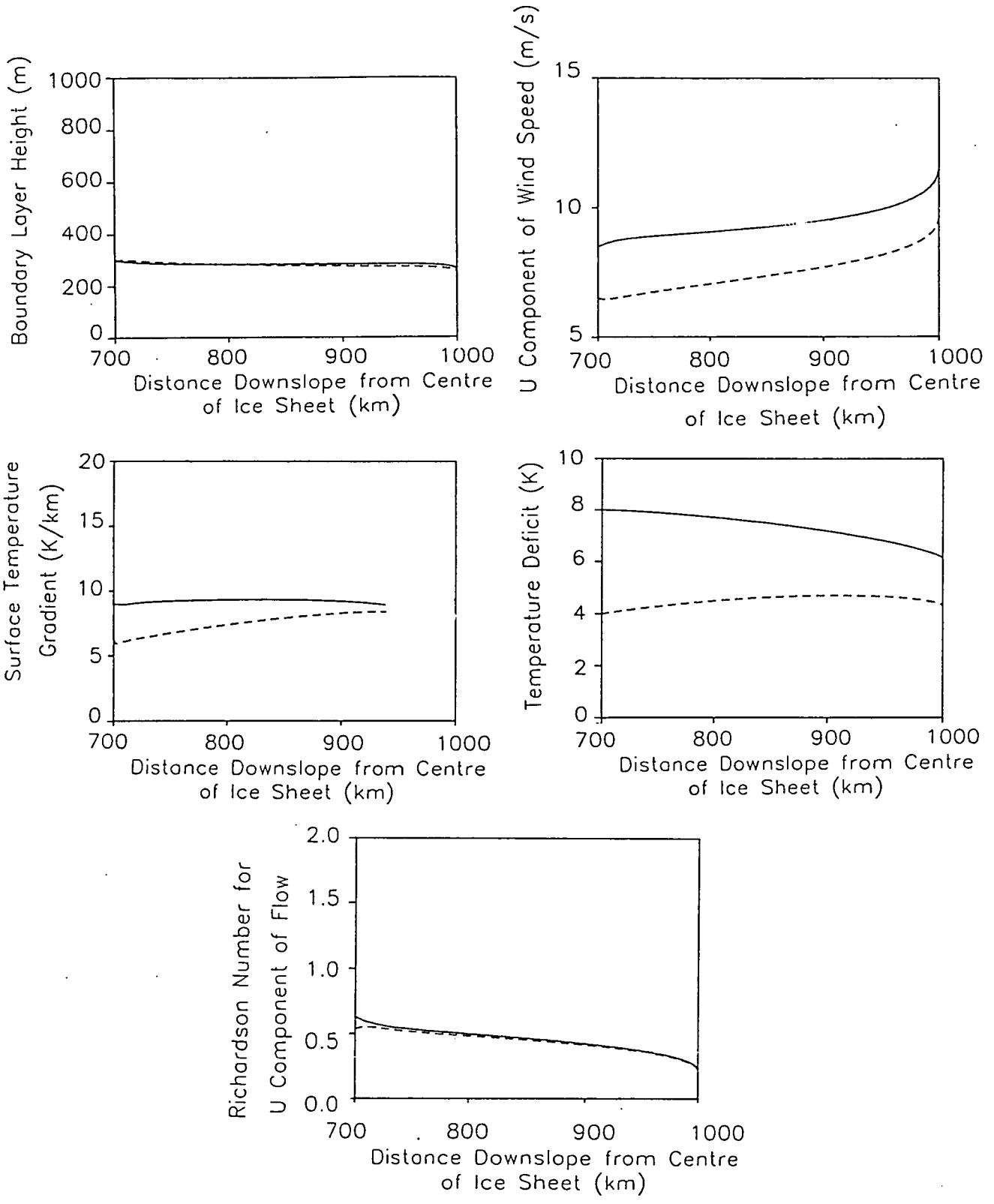

Figure 4.13: The effect of reducing $\Delta\theta$: $\Delta\theta = 8K$(——);$\Delta\theta = 4K$(- - - -).

- The model is fairly insensitive to the values of the profile factors, particularly S_3.
- A constant value for the drag coefficient in the U and V components produces high values of V, which causes the flow to become critical due to the increase in coriolis term in the U component of the momentum budget.
- The drag in the V direction has been increased considerably, to represent the effect of topographically induced gravity waves and the retarding effect on the flow of smaller undulations such as sastrugi.
- As long as C_{dv} remains large the model is relatively insensitive to its value.
- Changing C_{du} affects the temperature evolution of the boundary layer via entrainment. The effect on h is small.
- If $S_1 = 0.5$, $S_2 = 0.9$ and $S_3 = 1.0$ then C_{du} must be smaller than 0.004 and C_{dv} larger than 0.01 in order to prevent the flow slowing down and becoming critical.

The extent to which externally imposed changes on the boundary layer affect its evolution is dependent on the parameterisation of entrainment. Thus, as shown in the studies described above, variations in the profile factors or drag coefficient may have a direct effect on the layer velocity, but it is via entrainment that this alters the evolution of temperature or depth of the boundary layer. The parameterisation of entrainment therefore requires further investigation. This will be carried out in the next chapter along with sensitivity studies of the model to the climatological boundary conditions, (geostrophic wind speed, ambient stability and radiative cooling).

Chapter 5

Results of the Experiments with the Slab Model

This chapter will use the slab model introduced in chapter 4 to investigate the boundary layer over ice sheets of the present day and in the past. The first half of the chapter will look at the sensitivity of the model to changes in the boundary conditions. The prescribed boundary conditions such as the geostrophic wind speed† (Vg), stability of the ambient air (γ) and the surface cooling rate ($\frac{gR_n}{\theta\rho C_p}$) will be covered in section 5.1, and section 5.2 will be concerned with the parameterisation of entrainment.† Entrainment is important because of its strong influence on the wind speed and temperature evolution of the boundary layer; previous authors have noted a tendency for the Ellison & Turner (1959) type entrainment[1] to produce a boundary layer which is too deep (Lalaurette & Andre 1985, Gosink 1989). Section 5.3 will look at the lower boundary conditions at the ice sheet surface, particularly the surface profile, by considering profiles measured over present day ice sheets as well as those that have been reconstructed from the past, specifically the Laurentide ice sheet. This final section will also aim to look

[1]from now on referred to as ET type entrainment

C_{du}	C_{dv}	Vg (ms^{-1})	γ ($^{o}C/km$)	S_1	S_2	S_3	V_1 (ms^{-1})	h_1 (m)
0.0015	0.04	3	1.7	0.5	0.9	1.0	3	300

Table 5.1: The initialisation values of the parameters for the model experiments

at the way in which the prescribed atmospheric boundary conditions may have been different during the last glacial maximum (18kya), and the way in which this may have affected the boundary layer. The results will be used to determine the properties of the boundary layer which are most sensitive to the ice sheet boundary conditions, particularly those characteristics which may in turn affect the evolution of the ice. Thus providing a means of identifying the key atmospheric processes which should be incorporated into coupled ice-atmosphere models.

Unless otherwise stated the values of the initialisation conditions will always be the same for each of the experiments in this chapter. The values are given in table 5.1. U_1 varies between experiments and is adjusted iteratively to prevent excessive acceleration or deceleration at the start of the profile.

5.1 Sensitivity to Prescribed Boundary Conditions

5.1.1 The effect of the Geostrophic Wind [Vg]

Vg represents the overriding pressure gradient force. As shown in fig. 5.1, smaller values initially produce a more stable,† shallower, slower moving boundary layer

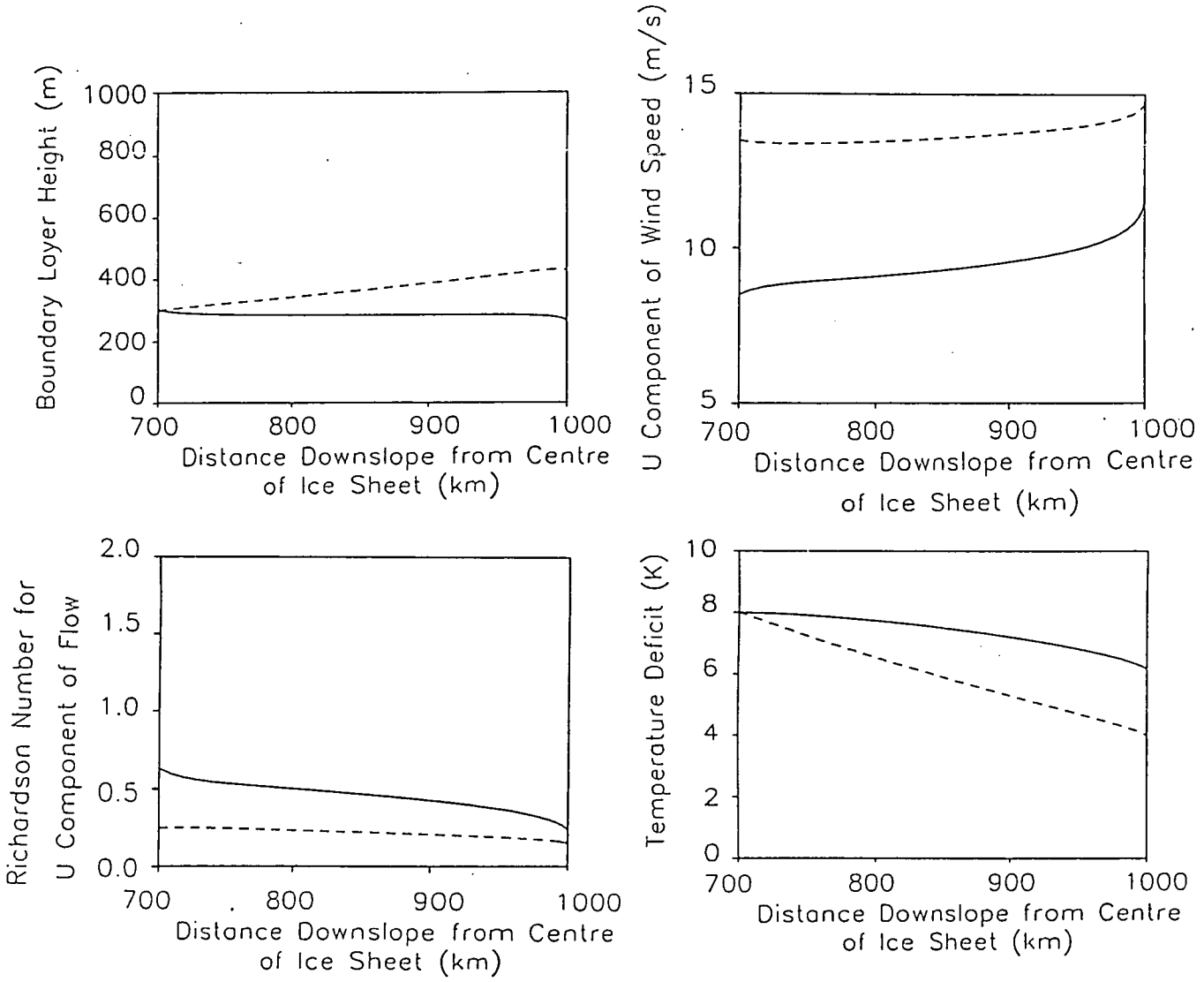

Figure 5.1: The sensitivity of the boundary layer to variations in geostrophic wind: Vg=3(———);Vg=5(- - - -).

with flow directed increasingly at right angles to the contours. If Vg becomes too small, at high S_1 and high C_d tranquil flow may develop because the pressure gradient force isn't sufficient to overcome the retarding forces on the flow. Conversely at high values of Vg the layer is faster, and as with the low C_{du} case the increase in entrainment causes an increase in $\frac{dh}{ds}$. A value for Vg of $3ms^{-1}$seems to produce reasonable results with a smooth surface profile, preventing excessive growth of the boundary layer which may occur if Vg is high, while producing a slight decrease in $\Delta\theta$, which would be prevented if Vg was too low.

5.1.2 The effect of Stability of the Air [γ]

Increased stability of the air tends to produce deceleration in the flow (Gosink 1989), which can be seen in fig. 5.2. In a more stable environment, air flowing down a slope is moving into progressively colder ambient air. Thus the temperature deficit and buoyancy of the air is much smaller further down the slope. In addition to this, in a more stable ambient environment, air which is entrained into the boundary layer at the bottom of the slope is colder that that being entrained further up, so the warming by entrainment is less effective closer to the margin;† this can be seen by the reduction in surface temperature gradient† for higher values of γ.

5.1.3 The effect of Radiative Cooling

Radiative cooling from the boundary layer is prescribed to be constant. The value used in most of the experiments is a radiative cooling rate of $0.0266 K m s^{-1}$ or $\approx 1 K hr^{-1}$ for a layer 100m deep, equivalent to a surface heat flux of approximately $30 W m^{-2}$. This is typical of the net (upward) flux at the surface in July over Antarctica (see table 2.3). This is the same as the lower range of the cooling rate used by Gosink (1989) of $0.001 m^2 s^{-3}$. Fig. 5.3 shows that the effect of doubling and halving this cooling rate on the depth of the boundary layer is small, the main effect is through the temperature deficit. A higher rate of radiative cooling maintains a large temperature deficit within the boundary layer, which reduces the surface temperature gradient to sub-adiabatic values and increases the wind speed due to the additional buoyancy force.

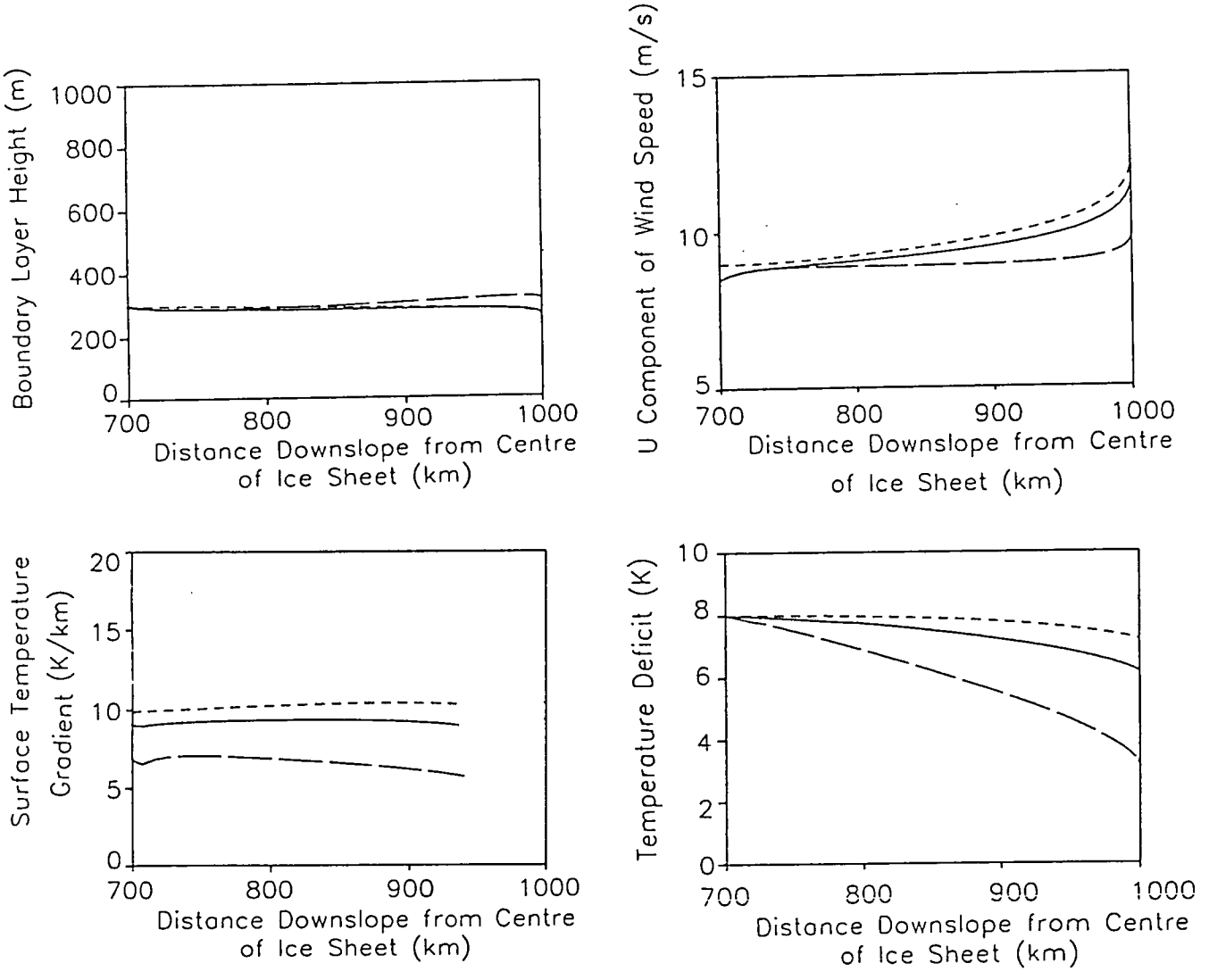

Figure 5.2: The effect of the stability of the ambient atmosphere on the flow: $\gamma = 6.7°C/km$(— —); $\gamma = 1.7°C/km$(———); $\gamma = 0.0$(-----).

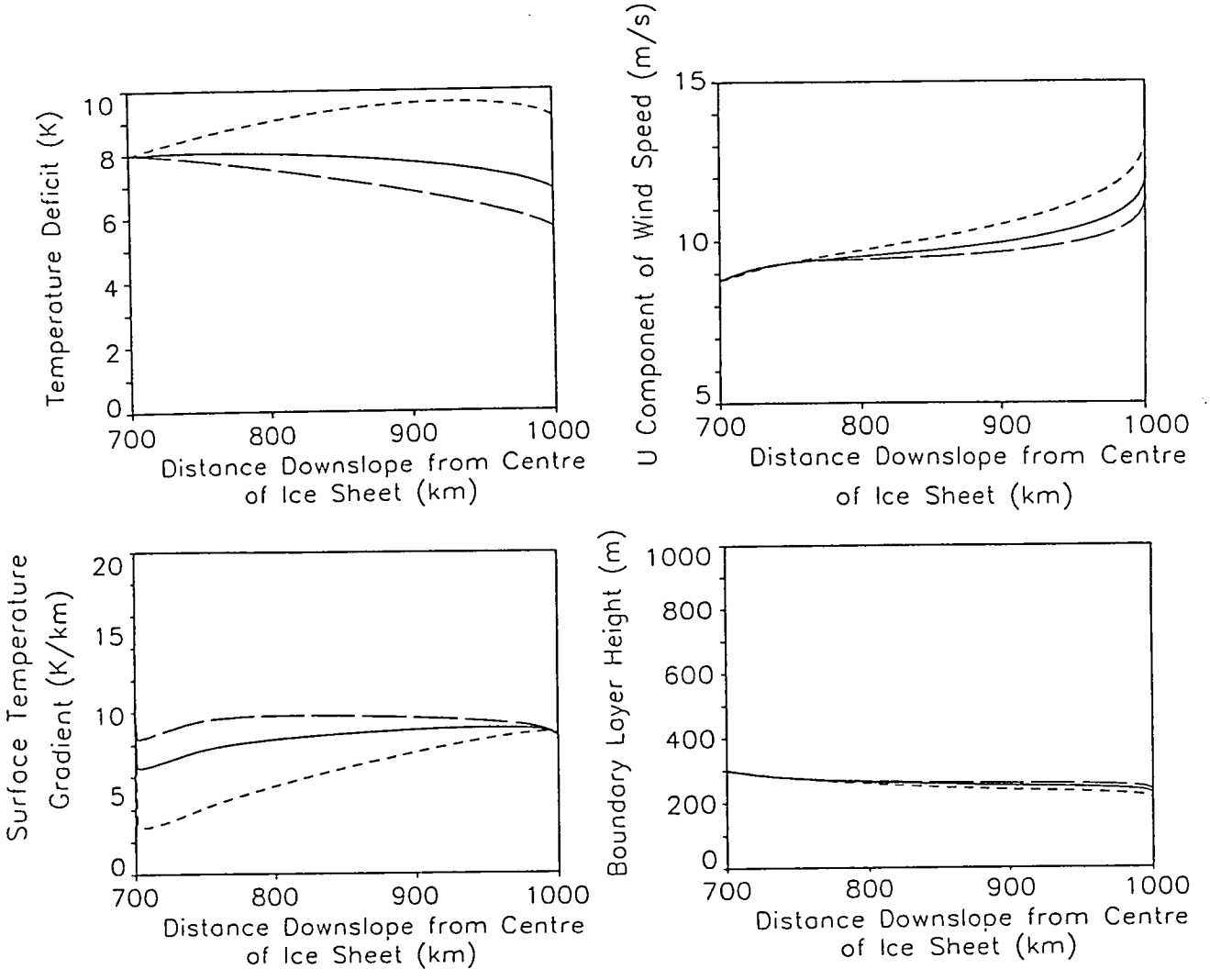

Figure 5.3: The sensitivity of the boundary layer to changes in $B = \frac{R_n}{\rho C_p}$:
$B = 0.0133 K m s^{-1}$(— —);$B = 0.0266 K m s^{-1}$(———);
$B = 0.0532 K m s^{-1}$(- - - -).

5.2 The Parameterisation of Entrainment

The above sensitivity studies investigated the effect of fixed boundary conditions on the evolution of the boundary layer. The precise evolution of the boundary layer however, is very much dependent on the parameterisation of entrainment, which modifies the depth, velocity and temperature of the boundary layer as it moves downslope. It was stated in the introduction to the chapter, that previous authors have found the parameterisation of entrainment to be a limitation of slab models (Lalaurette & Andre 1985), producing boundary layers which are too deep and too warm. This suggests that the extrapolation of empiricisms derived in the laboratory, such as that of Ellison & Turner (1959), to the much larger scale glacial slopes are not reliable. A lack of observational data makes it difficult to determine the exact contribution of entrainment to the boundary layer, yet as a key upper boundary condition to the boundary layer, it is an important process demanding further investigation. The following is an assessment of the evidence for entrainment over Antarctica, which provides a basis for an investigation of the parameterisation of entrainment in the atmospheric boundary layer over ice sheets.

Evidence for Entrainment.

If the principle of mass continuity is applied to the observational data, it becomes apparent that there must be entrainment into the boundary layer of the air above. The characteristics of the boundary layer, reviewed in chapters 2 and section 4.2, may be used to calculate an order of magnitude approximation of the entrainment velocity as follows. For a circular ice sheet of 1000km radius;

300km from the coast

$$h = 400m \qquad U = 6.5ms^{-1}$$

volume flux= $2\pi \times 700 \times 10^3 \times 400 \times 6.5 = 1.14 \times 10^{10}m^3s^{-1}$

at the coast

$$h = 400m \qquad U = 10ms^{-1}$$

volume flux= $2\pi \times 1000 \times 10^3 \times 400 \times 10 = 2.2 \times 10^{10}m^3s^{-1}$

So that $W_e \approx 0.007ms^{-1}$

Thus, the entrainment velocity must be of the order of $7 \times 10^{-3}ms^{-1}$. This compares well to the approximation made by Parish and Waight(1987) of $2 \times 10^{-3}ms^{-1}$in the interior and on the glacial slope, increasing to $2 \times 10^{-2}ms^{-1}$at the coast, based on results from a 2-dimensional primitive equation model.

The concept of entrainment is consistent with the assumption of shooting flow on the glacial slopes, and its parameterisation is a critical constraint on the upper boundary of the model. It determines the downslope evolution of the depth, temperature and velocity of the flow. For deep boundary layers entrainment is minimal, but if the b.l becomes excessively thin, entrainment responds by increasing the mass flux into the b.l, which at the same time will exert a drag at the

upper interface. (W_e/h term in the momentum flux equations 4.33 & 4.34). This feedsback to further enhance the thickening process via the inverse dependence of height and velocity, required to maintain mass continuity (equation 4.36).

The amount of entrainment depends on the available turbulent energy for conversion to potential energy within the boundary layer. Realistic parameterisation requires detailed observations of turbulent processes within the boundary layer as verification. Discussion and observations of turbulent boundary layers in the literature tends to focus on convective cases, where buoyancy production is the dominant term in the turbulent kinetic energy† budget (eg.Ball 1960, Carson 1973, Driedonks & Tennekes 1984, Manins & Turner 1978, Randall 1984, Rayment & Readings 1974, Stull 1976a,b, Tennekes & Driedonks 1981,Yamada & Mellor 1975, Zeman & Tennekes 1977). In a stable boundary layer, turbulence is generated mechanically by wind shear. Mechanical generation has been discussed in studies of stable boundary layers (eg. Andre et al 1978, Brost & Wyngaard 1978, McEwan 1983, Turner (1973), Zeman 1979), but it is more commonly referred to within the context of a convective case (eg.Stull 1976a,b). The limited availability of studies of mechanically generated turbulence in the stable boundary layer leads to uncertainties in the parameterisation of entrainment under these conditions. Two approaches will be discussed in this study, the first considers the turbulent kinetic energy budget of the whole boundary layer, and expands on the theory presented by Stull (1976a,b). The second is based on the assumption that it is the energy available at the top of the boundary layer that is important, in particular the rate of diffusion of energy towards the entrainment zone. This is a new parameterisation for the stable boundary layer, based on the concept used by Curran (1975) in the convective boundary layer. Idealised wind, temperature and heat profiles for the parameterisations are shown in fig. 5.4.

5.2.1 Type 1 Entrainment - The Turbulent Kinetic Energy Budget of the Whole Boundary Layer.

Theory

The turbulent kinetic energy budget of the boundary layer is described by equation 5.39 (Stull 1988), where q^2 is the turbulent kinetic energy (TKE) per unit mass in $m^2 s^{-2}$;

$$\overline{\frac{dq^2}{dt}} + \overline{\frac{\partial}{\partial z} w' \left(\frac{p'}{\rho_o} + q^2 \right)} = \frac{\tau}{\rho_o} \frac{\partial u}{\partial z} + \frac{g}{\theta_{br}} \overline{w'\theta'} - \epsilon, \qquad (5.39)$$

Storage & advection	pressure correlation & eddy transport	mechanical production	buoyancy production	viscous dissipation

For steady state conditions equation 5.39 assumes that TKE generated within the boundary layer at a particular point is either consumed by the mixing process of entrainment, which converts kinetic energy to potential energy by incorporating warm air from above the interface into the b.l., or it is removed by downslope advection, consumed in gravity waves, or dissipated locally by friction. The equation cannot be solved explicitly, and for this reason, following the work of Stull (1976a,b) the components of the budget are integrated through the depth of the boundary layer, and divided into the production, consumption and loss terms and each parameterised appropriately. The main production mechanisms in the

boundary layer are wind shear and buoyancy, represented by terms 1 and 2 on the RHS of equation 5.39. The following sections will describe the parameterisations which have been applied in this instance. They differ from that of Stull (1976a) so that the final equation requires no assessment of the depth of the entrainment zone, which is largely unknown for the stable boundary layer over ice sheets.

Parameterisation of Mechanical Generation Term

Mechanical energy is generated by wind shear within the boundary layer. The idealised profile of the wind velocity in the boundary layer is shown in fig 5.4a. The method described by Stull (1976a) has been used to divide the integral of the mechanical generation term in equation 5.39 into 3 sections; the surface layer, where the friction is assumed to produce a linear increase in wind velocity with height (up to h_s), the zone of constant wind velocity, which in this case corresponds to the low level jet in the stable boundary layer (between h_s and h_b), and the shear layer at the top of the boundary layer (from h_b to H) where wind speeds decrease to the geostrophic value at H. This is zero for the U component of the model which assumes the geostrophic flow to be exclusively in the y direction above the boundary layer. Thus

$$\int_0^H \frac{\tau}{\rho}\frac{\partial \mathbf{U}}{\partial z}dz = \int_0^{h_s} \frac{\tau}{\rho}\frac{\partial \mathbf{U}}{\partial z}dz + \int_{h_s}^{h_b} \frac{\tau}{\rho}\frac{\partial \mathbf{U}}{\partial z}dz + \int_{h_b}^{H} \frac{\tau}{\rho}\frac{\partial \mathbf{U}}{\partial z}dz \qquad (5.40)$$

The shear between h_s and h_b is assumed to be zero, and the generation of turbulence at the surface is assumed to depend on the roughness of the surface. Since this concerns the roughness of the surface it is parameterised using C_{du}, as opposed to C_{dv} which refers to the roughness of the terrain on a larger scale. So

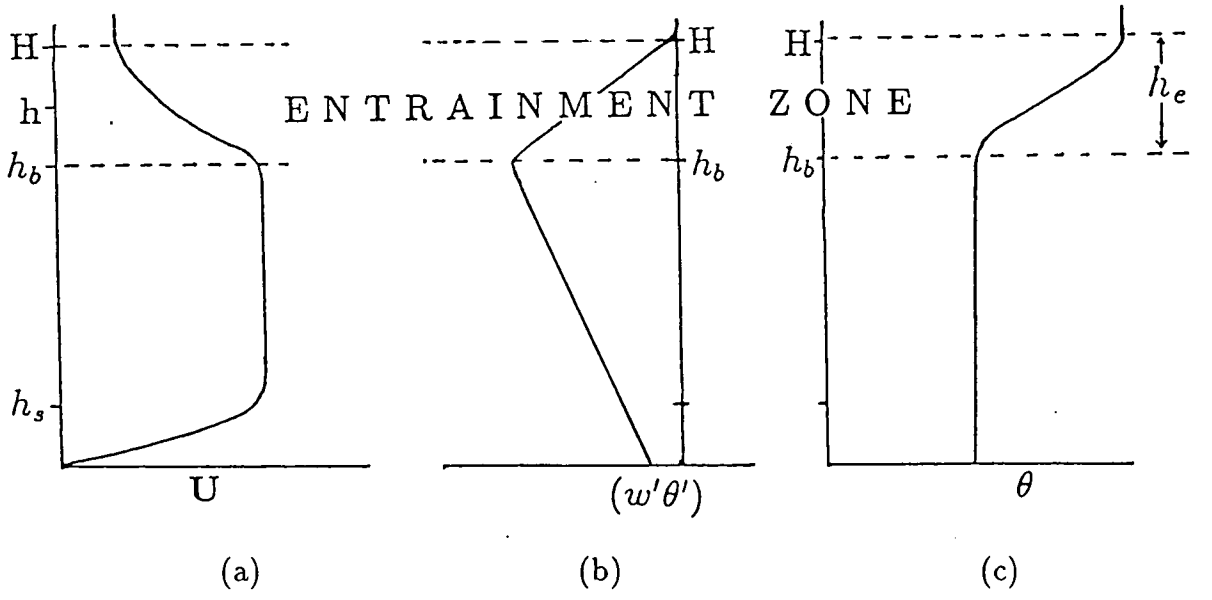

Figure 5.4: Idealised wind and heat flux profiles within the boundary layer.

that

$$\int_0^{h_s} \frac{\tau}{\rho} \frac{\partial \mathbf{U}}{\partial z} dz = C_{du} \mathbf{U}^2 \left| \overline{\mathbf{U}} \right| \tag{5.41}$$

where, C_{du} is the drag coefficient for the u component of flow, and $\left| \overline{\mathbf{U}} \right|$ is the wind velocity at the top of the surface layer (above h_s). This is taken as the average layer velocity such that $\left| \overline{\mathbf{U}} \right| = \sqrt{U^2 + V^2}$. The stress and wind shear at the top of the layer are parameterised using the relations given in the set of equations 5.42, after Tennekes & Driedonks (1981);

$$\frac{\tau}{\rho} = -W_e(\mathbf{\Delta U}_H) \qquad \frac{\partial U}{\partial z} = \frac{(\mathbf{\Delta U}_H)}{h_e}$$

where

$$(\mathbf{\Delta U}_H)^2 = (\Delta U_H)^2 + (\Delta V_H)^2 = U^2 + (V - Vg)^2 \tag{5.42}$$

$\mathbf{\Delta U}$, represents the velocity change from h_b to H, assuming that the wind above the boundary layer is geostrophic, and exclusively in the y direction, and h_e is the

depth of the entrainment zone shown in fig. 5.4. Hence the shear production at the top of the layer is parameterised as follows;

$$\int_{h_b}^{H} \frac{\tau}{\rho} \frac{\partial \mathbf{U}}{\partial z} dz = -W_e \left(\Delta \mathbf{U}_H\right)^2 \tag{5.43}$$

Parameterisation of the Buoyancy Term

The integral of the buoyancy term in equation 5.39 can be divided into two components, the TKE converted to potential energy via the entrainment of warmer air from above the boundary layer, and the TKE consumed by the negative turbulent heat flux due to surface cooling. The actual boundary layer over the glacial slopes is not well mixed. From fig. 5.5 it seems that there is a small negative flux which removes heat from a thin layer of the boundary layer close to the surface. It can be shown that in the stable boundary layer over an ice sheet, such as that in Antarctica, the consumption of turbulent kinetic energy by this negative turbulent heat flux at the surface, is sufficiently small compared to the shear generation terms that it can be neglected. The depth of the negative turbulent heat flux is uncertain. If it is assumed in fig. 5.5 that the heat is being removed from the surface layer by the turbulent heat flux into the surface, then the vertical extent of the heat flux profile is approximately 100m. This is in reasonable agreement with the findings from the model simulations of the nocturnal boundary layer by Brost & Wyngaard (1978). Therefore if we assume a linear profile extending to 100m above the surface, with a magnitude of $(Q_0) = 0.02 K m s^{-1}$ (Rusin 1964), and if $\mathbf{U} = 8.5 m s^{-1}$, $(\Delta \mathbf{U}_H) = 8.0 m s^{-1}$, $W_e = -0.007 m s^{-1}$ and $C_{du} = 0.0015$, the total rate of consumption of TKE is $ghQ_0/2\theta_{br} = 0.04 m^3 s^{-3}$, which compares to a rate of shear generation of $C_{du}\mathbf{U}^2 \left|\overline{\mathbf{U}}\right| - W_e \left(\Delta \mathbf{U}_H\right)^2 = 1.4 m^3 s^{-3}$. Thus it seems reasonable to neglect the consumption of TKE by the turbulent heat flux.

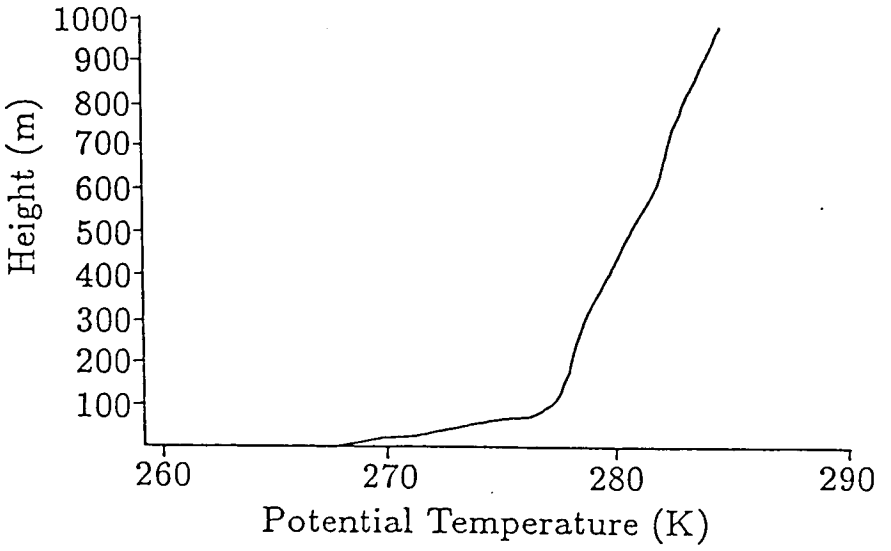

Figure 5.5: The temperature profile of the stable boundary layer over Antarctica in Adelie Land taken from Zbigniew et al (1986).

The remaining component of the buoyancy term, the conversion to potential energy at the top of the layer is parameterised using the relation $(w'\theta')_H = W_e\Delta\theta$. This flux is downwards and therefore negative; it is assumed to decrease linearly to zero through the depth of the boundary layer according to the Eulerian partioning (Manins & Turner 1978, Randall 1984), shown in fig 5.4b. The heat flux at the surface is neglected and remembering that W_e defined in equation 4.23, is positive upwards then;

$$\frac{g}{\theta_{br}}\int_0^H (w'\theta')_H\, dz = \frac{g}{\theta_{br}}\frac{h}{2}W_e\Delta\theta \tag{5.44}$$

Parameterisation of the Pressure Correlation Term

The pressure correlation and eddy transport term accounts for the redistribution of TKE due to peturbations in the pressure field. This is generally associated with vertically propagating gravity waves, which in convective layers arise through the action of buoyant plumes which penetrate the upper limit of the boundary layer.

The gravity waves observed in the boundary layer over ice sheets propagate at right angles to the orientation of the axes of the ridges and valleys, ie. along the v direction of flow (Mobbs & Rees 1989). The net contribution to the redistribution of TKE downslope is therefore assumed to be small in this case. Stull (1976a) suggests that where TKE is mechanically generated by shear, the gravity wave term is zero. Randall (1984) suggests an allowance for storage in gravity waves should be incorporated into the dissipation term and this will be discussed later. In this case, due to a lack of data and without a clear understanding of the role of gravity waves in the boundary layer over ice sheets, it is assumed that any net loss due to gravity wave storage is small and the the pressure correlation term is ignored.

Parameterisation of the Storage & Advection and Dissipation Terms.

For steady state, there is no change of TKE in time so the $\frac{dq^2}{dt}$ term in equation 5.39 becomes the advection term $\mathbf{U}\frac{dq^2}{ds}$. This advection term can be combined with the dissipation term in equation 5.39 to produce the following equation for the remaining terms;

$$L = \mathbf{U}\frac{dq^2}{ds} + \epsilon_t \tag{5.45}$$

The advection term is small; this can be illustrated by comparing the available energy converting TKE into PE at the top and bottom of the glacial slope. At the top of the slope, where $W_e = -0.002ms^{-1}$, h=400m,$\Delta\theta = 8$, then $-ghW_e\Delta\theta/2\theta = 0.1$, and 300km away at the coast $W_e = -0.02ms^{-1}$, h=400m, $\Delta\theta = 4K$ and $-ghW_e\Delta\theta/2\theta = 0.6$, so that $\mathbf{U}\frac{dq^2}{ds} \approx 10^{-5}$. Therefore it seems reasonable to assume that the frictional dissipation term is most important, and

that the term (L) accounts for the loss of TKE from the boundary layer. After Randall (1984), this can be represented as some fraction of the production term (P) so that $L = (1 - a_e)\,P$. This assumes that the rate of dissipation is directly proportional to the rate of production, although Randall suggests that this may not be strictly true, as mentioned earlier in the discussion of the pressure correlation term; he suggests that the loss of energy may be dependent on Richardson number in order to allow for storage in gravity waves. Using equations 5.41 & 5.43, the integral of the loss term becomes

$$L_i = (1 - a_e)\left[C_{du}\left(U^2 + V^2\right)\left|\overline{\mathbf{U}}\right| - W_e\left(\Delta \mathbf{U}_H\right)^2\right] \tag{5.46}$$

The Final Equation

Equations 5.41, 5.43, 5.44 & 5.46 can now be substituted into the integral of equation 5.39 to produce the following equation;

$$-\frac{gh\Delta\theta}{2\theta}W_e = a_e[C_{du}\mathbf{U}^2\left|\overline{\mathbf{U}}\right| - W_e(\Delta \mathbf{U}_H)^2] \tag{5.47}$$

This can be rearranged to produce an expression for the entrainment velocity so that,

$$-W_e = \frac{C_{du}\left|\overline{\mathbf{U}}\right|}{\mathbf{Ri}\left[\frac{1}{A_e} - \left(\frac{(\Delta \mathbf{U}_H)^2}{\mathbf{Ri}\mathbf{U}^2}\right)\right]} \tag{5.48}$$

where

$$\mathbf{Ri} = \frac{gh\Delta\theta}{\theta\mathbf{U}^2} \tag{5.49}$$

and $$\mathbf{U}^2 = U^2 + V^2 \text{ and } A_e = 2a_e$$

This method is based on that given by Stull (1976a), however the parameterisation of shear at the top of the layer has been changed from being proportional to

$(\Delta \mathbf{U}_H)^3$ as given by Stull, to the relation in equation 5.43. Stull considers the case where turbulent energy is generated by wind shear across the top of the boundary layer and proposes that entrainment velocity is governed by the following relation:

$$We \propto \frac{\Delta \mathbf{U}_H}{Ri_B} \text{ where } Ri_B = \frac{g\frac{\Delta\theta}{\theta}d_1}{(\Delta \mathbf{U}_H)^2},$$

where d_1 is the depth of the shear layer. Thus the entrainment increases with the shear at the top of the boundary layer since the greater the shear the more turbulence is generated. The theory presented in this work described in equation 5.48, incorporates a dependence on $(\Delta \mathbf{U}_H)^2$, such that as the shear at the top of the layer increases, the denominator of equation 5.48 becomes smaller. This formulation is therefore expressed in terms of the Richardson number of the whole boundary layer given by equation 5.49, as opposed to that of the shear layer as in the formulation of Stull. In a slab model, this has the advantage of being much easier to determine, without having to introduce further parameterisations for the depth of the entrainment zone which increases uncertainties yet further (Driedonks & Tennekes 1984). The empirical formula of Ellison and Turner (1959) is similar in its inverse Richardson number dependence. The differences lie in the introduction of term allowing for shear at the top of the boundary layer, the reduction in total TKE by the dissipation coefficient A_e and the dependence on C_{du}. Thus the terms in this work are more closely associated with actual processes occuring in the boundary layer such as the dissipation rate and roughness of the surface, rather than purely empirical adjustment to the Richardson number using a single empirical coefficient A_c as in the Ellison and Turner case.

The value of A_e

Exact values of a_e are uncertain. Stull (1976a) suggests a value for a_e of 0.02 so that A_e has a value of 0.04. As previously stated, Randall (1984) argues that

as stability increases the value of A_e should decrease to allow for the storage of shear generated energy in the form of gravity waves, but a lack of experimental and observational data makes this difficult to determine. McEwan (1983) found a_e for shear generated turbulence to be much higher, 0.2 from experiments using a stratified salt solution. Experiments of the sensitivity of the model to variations in A_e will be carried out in a later section.

Constraints on the Entrainment

The treatment of the shear generated energy at the top of the boundary layer, (equation 5.43) leads to the requirement of the entrainment equation that

$$A_e \frac{(\Delta \mathbf{U}_H)^2}{\mathbf{Ri}\mathbf{U}^2} < 1 \tag{5.50}$$

This criteria is not met if Ri becomes too small. Driedonks and Tennekes (1984) noted a similar problem and chose to incorporate the shear generation at the top of the layer with the shear generation at the ground. Stull (1976a) avoids this by parameterising the generation of shear at the top of the layer as $a_3(\Delta \mathbf{U}_H)^3$. However both Driedonks & Tennekes and Stull based their investigations in the daytime atmospheric boundary layer, when wind shear is less important in the production of turbulent kinetic energy. Laboratory experiments of shear generated turbulence by Turner (1973) found that as Ri tends to zero, the entrainment coefficient, defined as $\left(-E = \frac{\overline{w_e}}{|\overline{\mathbf{U}}|}\right)$, tends to 0.1. Therefore a constant K can be introduced to the denominator of equation 5.48. If it is assumed that there is no vertical shear in the V component of the wind speed then, $\frac{(\Delta \mathbf{U}_H)^2}{\mathbf{U}^2} \approx 1$ because the U component is always assumed to be zero above the boundary layer. Then equation 5.48 can be used to write an expression for the entrainment coefficient,

$$E = \frac{C_{du}}{\frac{\mathbf{Ri}}{A_e} - K} \tag{5.51}$$

h	U	V	U	$\Delta\theta$	C_{du}	Ri
300	8.5	3.0	9.014	8	0.0015	1.113

Table 5.2: The values of the variables used to construct fig. 5.8

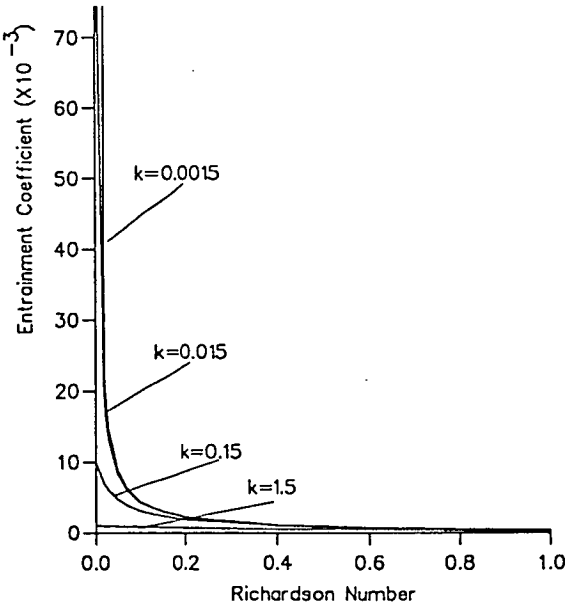

Figure 5.6: The variation of the type 1 entrainment coefficient with Richardson number for different values of the coefficient K. ($A_e = 0.5$)

So that if E=0.1 as $Ri \rightarrow 0$ then

$$K = -\frac{C_{du}}{0.1} \tag{5.52}$$

This can be incorporated into equation 5.48 assuming that the effect of K on the entrainment is small for Richardson numbers much greater than zero. This has been investigated in fig. 5.6 using equation 5.51. The height, velocity, temperature deficit, and drag coefficient are given the values of table 5.2 so that Ri can be calculated as 1.113.

K has been given a value of 0.015, and increased 10 fold to 0.15, and it can be seen

from the figure that the entrainment coefficient is insensitive to the value of K except when $Ri \rightarrow 0$. The curves show large divergence only when the Richardson number is less than 0.2 which is when the value of $\frac{\mathrm{Ri}}{A_e}$ approaches K. Therefore as long as $\frac{(\Delta \mathrm{U}_H)^2}{\mathrm{U}^2}$ never deviates far from unity, which is true for small V compared to U, it seems reasonable to introduce the parameter K into the general equation 5.48 such that,

$$-W_e = \frac{C_{du}\left|\overline{\mathrm{U}}\right|}{\mathrm{Ri}\left[\frac{1}{A_e} + \left(\frac{C_{du}}{0.1}\right)\left(\frac{(\Delta \mathrm{U}_H)^2}{\mathrm{RiU}^2}\right)\right]} \tag{5.53}$$

Sensitivity to A_e.

The sensitivity of the model to the value of A_e is shown in fig. 5.7. It can be seen that as A_e increases so does the entrainment. A_e has an approximately linear relationship with W_e, which can be investigated in more detail by inserting K into equation 5.51, and assuming $\frac{(\Delta \mathrm{U}_H)^2}{\mathrm{U}^2} \approx 1$, so that,

$$-W_e = \frac{C_{du}\left|\overline{\mathrm{U}}\right|}{\left[\frac{\mathrm{Ri}}{A_e} + \frac{C_{du}}{0.1}\right]} \tag{5.54}$$

For a typical value of K=0.015, the second term in the denomitor of equation 5.54 is relatively small compared to the Richardson number, so that the entrainment relation has a linear dependence on A_e and an inverse relationship with Richardson number. Using the values given in table 5.2, the sensitivity of entrainment to the Richardson number at different values of A_e have been investigated and the results shown in fig. 5.8. The inverse relationship means that the sensitivity of entrainment to the Richardson number is greatest for low values of Ri, but as shown in the fig. 5.8, the sensitivity in the range of Richardson numbers typical of the model (between ~ 0.6 and ~ 1.2) increases significantly with A_e.

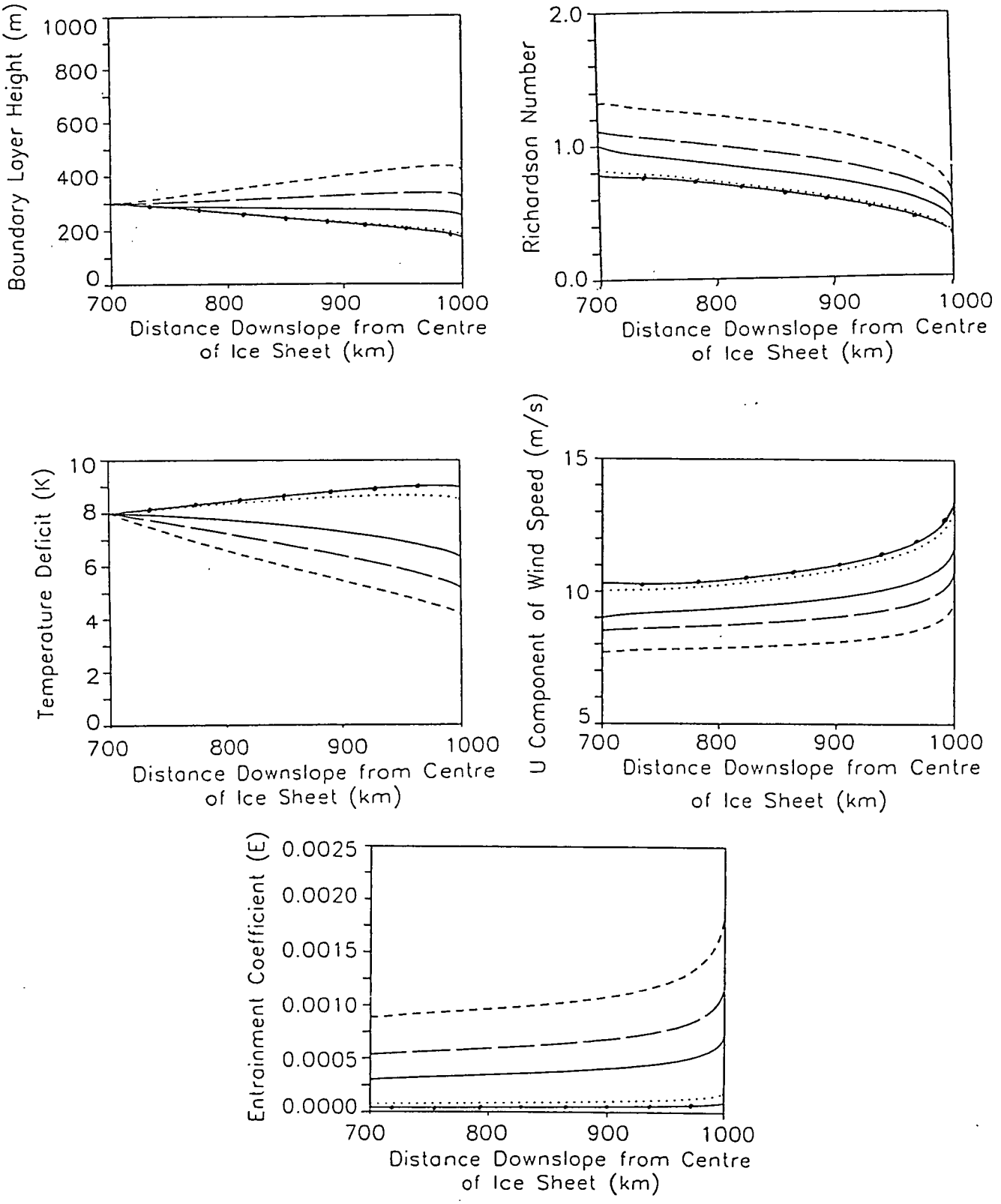

Figure 5.7: Sensitivity of the model to variations in the entrainment parameter A_e: $A_e = 0.8$(- - - -); $A_e = 0.4$(— —); $A_e = 0.2$(———); $A_e = 0.04$(.....); $A_e = 0.02$(—•—)

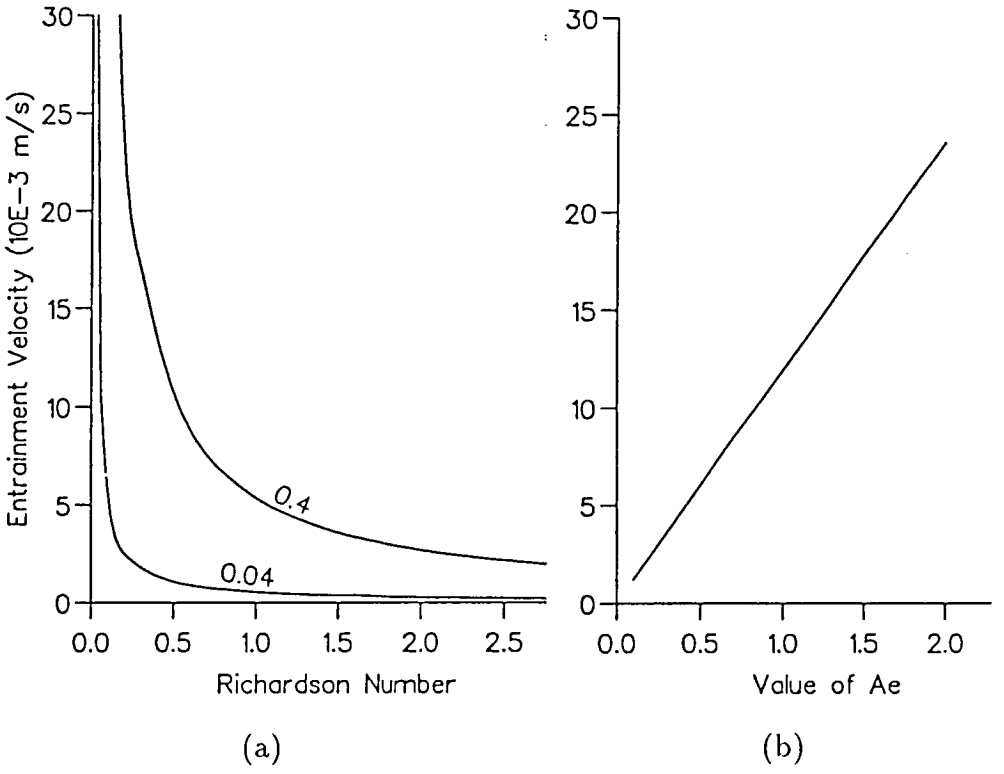

Figure 5.8: The Sensitivity of the type 1 entrainment to A_e and Ri

The entrainment is prevented from increasing too rapidly with A_e because more entrainment produces a deeper boundary layer, with a higher Richardson number, which has the effect of reducing the entrainment. This can be illustrated using figs 5.7 and 5.8. Fig. 5.7 shows an increase in the Richardson number from approximately 0.8 to 1.1 between $A_e = 0.04$ and $A_e = 0.4$. If the Richardson number had remained at the lower value when A_e was increased, fig. 5.8a shows that entrainment would have been 7×10^{-3} rather than 5×10^{-3}. Therefore in this case, the increase of Richardson number which accompanies an increase in A_e reduces the entrainment by approximately $\frac{1}{3}$.

5.2.2 Type 2 entrainment - Entrainment Governed by Diffusion.

Theory

The second approach to entrainment theory considers the amount of turbulent energy at the inversion. Curran (1975) suggests that the entrainment rate, or alternatively the rate of mixing of warm air downwards, is primarily determined by the rate of diffusion of turbulent kinetic energy to the top of the boundary layer. Curran (1975) used this theory to investigate convectively driven entrainment. In this work the theory will be applied to develop a new parameterisation for shear generated turbulence. A diffusion equation similar to that used by Curran (1975) is assumed to describe the profile of TKE diffused from the surface using the rate of production of TKE, $\varepsilon m^2 s^{-3}$, rather than the TKE per unit mass which was used in the energy budget equation 5.39. Thus

$$\frac{\partial \varepsilon}{\partial t} = K_m \frac{\partial^2 \varepsilon}{\partial z^2} - \frac{\varepsilon}{\tau_f} \tag{5.55}$$

where

$$\varepsilon = \frac{dq^2}{dt}$$

The last term on the righthand side of equation 5.55 was not used by Curran. It allows for frictional dissipation of TKE, using a timescale for frictional dissipation, τ_f in seconds and K_m is a vertical diffusion coefficient in $m^2 s^{-1}$. The equation has boundary conditions defined by a rate of generation of TKE at the surface ε_0, which decreases exponentially to zero at infinite height so that,

$$\varepsilon = \varepsilon_o \text{ at } z = 0$$

$$\varepsilon = 0 \quad as \quad z \rightarrow \infty$$

so the solution for a steady rate of production (ie $\frac{\partial \varepsilon}{\partial t} = 0$) is

$$\varepsilon(z) = \varepsilon_0 \, exp - \left[\left(\sqrt{\frac{1}{K_m \tau_f}} \right) z \right] \tag{5.56}$$

This represents energy generated at the surface reaching height z in the boundary layer by diffusion. It is this energy at height h, and the energy generated locally at the interface by wind shear that must be balanced against the downward flux of potential energy across the top of the inversion (Rayment & Readings 1974) so that,

$$-\frac{g}{\theta_{br}} \int_0^h (w'\theta')_H dz = \int_0^{h_s} \varepsilon_0 \, exp - \left[\left(\sqrt{\frac{1}{K_m \tau_f}} \right) h \right] + d \int_{h_b}^H \frac{\tau}{\rho} \frac{\partial U}{\partial z} dz \tag{5.57}$$

Between H and h_b is the entrainment zone shown in fig. 5.4. h in the diffusion term should strictly represent the height just below the zone of shear generation rather than the average boundary layer depth since the rate of diffusion above h_b will be altered by the local generation of energy. However it seems reasonable to assume that $h_e \ll H$ so that the depth of diffusion is h. Equation 5.57 also assumes that the locally generated energy at the boundary layer is not diffused downwards to any great depth, but that frictional dissipation acting locally reduces the amount of shear generated energy by a fraction (1-d).

The Final equation

Using the parameterisations of equations 5.43 and 5.44 for the shear generation and the downward flux of potential energy respectively and parameterising ε_0 according to equation 5.58 so that,

$$\int_0^{h_s} \varepsilon \, dz = \int_0^{h_s} \frac{dq^2}{dt} dz = \int_0^{h_s} \frac{\tau_\cdot}{\rho} \frac{\partial \mathbf{U}}{\partial z} dz = C_{du}(U^2 + V^2) \left| \overline{\mathbf{U}} \right| \tag{5.58}$$

Equation 5.57 becomes

$$-\frac{g}{\theta_{br}} \frac{h}{2} W_e \Delta\theta = C_{du}(U^2 + V^2) \left| \overline{\mathbf{U}} \right| \exp - \left[\left(\frac{1}{K_m \tau_f} \right)^{\frac{1}{2}} h \right] - dW_e \left(\mathbf{\Delta U}_H \right)^2 \tag{5.59}$$

and can be rearranged to give an expression for the entrainment velocity as follows:

$$-W_e = \frac{C_{du} \left| \overline{\mathbf{U}} \right| exp - (ah)}{\frac{\mathrm{Ri}}{2} \left[1 - \frac{D}{\mathrm{Ri}} \left(\frac{(\Delta \mathbf{U}_H)^2}{(\mathbf{U})^2} \right) \right]} \tag{5.60}$$

where $a = \sqrt{\frac{1}{K_m \tau_f}}$

and $D = 2d$

Value of parameters K_m, τ_f

There are no direct measurements of K_m or τ_f for the glacial slopes. Their values therefore are uncertain and a range of values suggested as reasonable by those observed elsewhere will be investigated in this section. Brost and Wyngaard (1978) use a turbulent timescale of $3000s$; this represents a lower limit for the timescale of frictional dissipation of turbulence τ_f. If τ_f is less than the turbulence timescale,

the turbulence would be dissipated before it is fully developed throughout the boundary layer. Timescales for frictional dissipation can be obtained by studying the 'spin-down' time for daytime atmospheric boundary layers. In the evening after sunset and when wind speeds decrease, the source of turbulent energy, (primarily surface heating but also wind shear), is removed and the rate of frictional dissipation determines the time it takes for turbulence to disappear. Wyngaard (1975) estimated this at between 3 and 4 hours, from model results compared to Minnesota data. Fig 5.9 shows the evolution of turbulent energy in a numerical model of the surface boundary layer described in Yamada and Mellor (1975). The temperature in the model decreased rapidly after 1600hours, therefore it is assumed there is no further generation of turbulence after this time, and the turbulence in the boundary layer is negligible by 1800hours, suggesting a value for τ_f of 2 hours.

K_m has been measured at Plateau station as $0.1m^2s^{-1}$ (Schwerdfeger 1984), but this is an inland station with a very different turbulent structure within the boundary layer to the region of greater momentum flux on the glacial slopes. Brost and Wyngaards' model study of a stable boundary layer found that the average value of K_m for the layer can be approximated to $K_m \approx 0.03kC_{du}\mathbf{U}^2h$, where k is the von karman constant, 0.4. Therefore if $C_{du}\mathbf{U}^2 = 0.1$ and $h = 400m$ then $K_m \approx 0.5m^2s^{-1}$ and its range can be determined as between $0.19m^2s^{-1}$ and $2.0m^2s^{-1}$. Other authors have suggested values greater than this. James(1989) for example used a value of $10m^2s^{-1}$, which is in closer agreement with the values given by Clarke (1970). Clarke constructed profiles of scaled values of the diffusion coefficient

$$\hat{K}_m = \frac{K_m}{(C_{du}U^2/f)} \tag{5.61}$$

From observations in a stable atmospheric boundary layer he obtained average

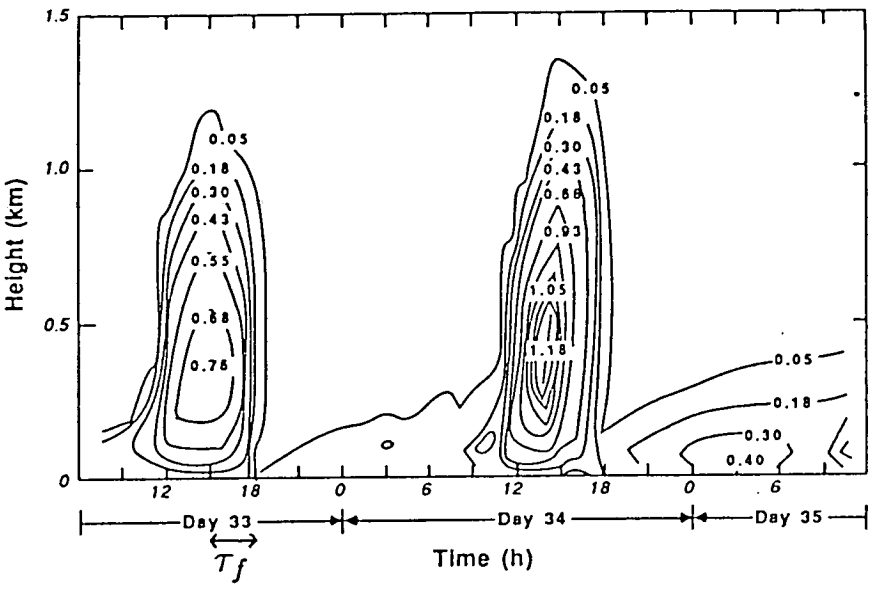

Figure 5.9: Evolution of tke (Yamada & Mellor 1975)

values for $\hat{K}_m$ of 0.006. If $C_{du}\mathrm{U}^2 = 0.1$ and $f = 1.4 \times 10^{-4}$ then $K_m \approx 4m^2s^{-1}$, possibly reaching $10m^2s^{-1}$ at higher wind velocities. The range of possible values for both K_m and τ_f is therefore large; $0m^2s^{-1} < K_m < 10m^2s^{-1}$ and $3600s < \tau_f < 14400s$. For a boundary layer 400m deep this gives a range in exp-(ah) of 7.5×10^{-5} to 0.44. Most of the evidence suggests that $K_m < 5$ and τ_f is between 2 and 3 hours. However, in order for this entrainment to produce a similar boundary layer to that using the ET type entrainment with A_c set to 0.0004, then K_m must have a higher value of $6.5m^2s^{-1}$ and $\tau_f = 7200s$. For comparison with the ET entrainment in the following experiments $K_m\tau_f$ will be given a value of 4.68×10^4; this will be reassessed in a later section.

Constraints on the Parameterisation

Equation 5.60 must be constrained in a similar manner to equation 5.48. Therefore taking $\frac{(\Delta \mathrm{U}_H)^2}{\mathrm{U}^2} \approx 1$, and introducing a constant K_{dif} to equation 5.60 the

entrainment coefficient can be defined when $\mathbf{Ri} = 0$ as,

$$E = \frac{C_{du} \exp -(ah)}{\frac{DK_{dif}}{2}} \tag{5.62}$$

So that if $E = 0.1$ when $\mathbf{Ri} \rightarrow 0$

$$K_{dif} = \frac{C_{du} \exp -(ah)}{0.05D} \tag{5.63}$$

If this is inserted into equation 5.60, then D cancels to give the following equation for the entrainment velocity;

$$-We = \frac{C_{du} \left|\overline{\mathbf{U}}\right| \exp -(ah)}{\frac{\mathbf{Ri}}{2}\left[1 + \frac{C_{du} \exp -(ah)}{0.1\mathbf{Ri}}\left(\frac{(\Delta \mathbf{U}_H)^2}{\mathbf{U}^2}\right)\right]} \tag{5.64}$$

The sensitivity of the entrainment to the value of $\frac{C_{du}exp(-ah)}{0.05}$ can be investigated in a similar manner to K in the previous section. For values of $K_m\tau_f$ of 4.68×10^4, assuming $\frac{(\mathbf{U}_H)^2}{\mathbf{U}^2} \approx 1$ and using the initial boundary layer given in table 5.2, fig. 5.10 shows the model to be relatively insensitive to the value of $\frac{C_{du}exp(-ah)}{0.05}$, unless the Richardson number becomes very low.

Sensitivity of the Model to Variations in $K_m\tau_f$

The sensitivity of the entrainment to the product of $K_m\tau_f$ is shown in fig. 5.11. When $K_m\tau_f$ increases so does the amount of entrainment. The additional drag at the upper interface combined with the reduction in buoyancy downslope produces a much slower layer with higher Richardson number. Fig. 5.12 shows the relationship between $K_m\tau_f$ and the entrainment velocity; it can be seen that the model is most sensitive when $K_m\tau_f$ is less than 1.5×10^5. So that in fig. 5.11, although increasing $K_m\tau_f$ from 9.36×10^4 to 1.87×10^5 is a larger increase that from 2.34×10^4 to 4.68×10^4, the relative changes in velocity and depth of the boundary layer are almost the same. In the same manner as for A_e in the type 1

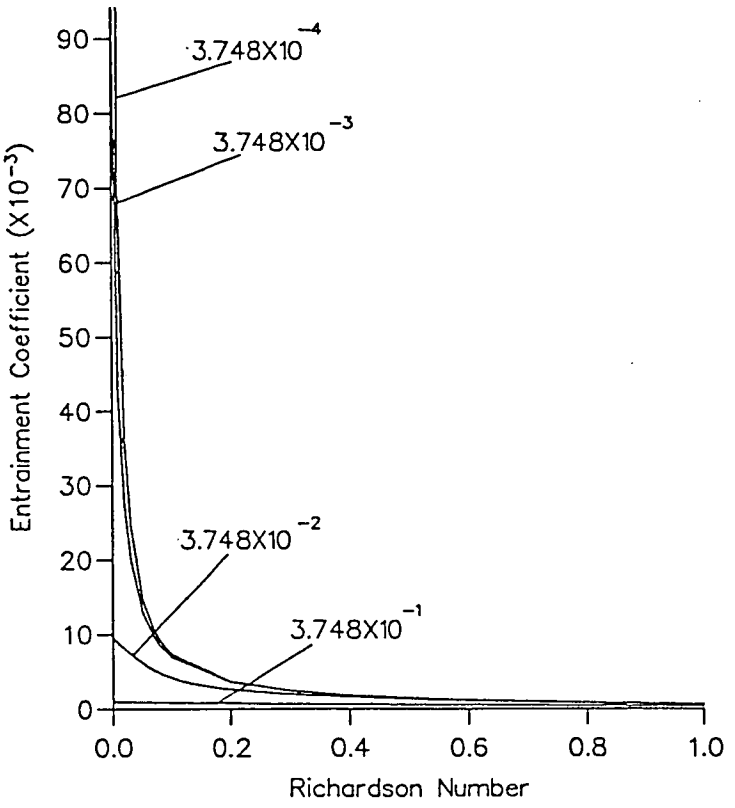

Figure 5.10: The variation of the type 2 entrainment coefficient with Richardson number for different values of $\left(\frac{C_{du}exp(-ah)}{0.1Ri}\right)$. $K_m\tau_f = 4.68 \times 10^4$

entrainment the increase in entrainment at high values of $K_m\tau_f$ is reduced by the corresponding increase in Richardson number.

5.2.3 The Effect of Entrainment on the Evolution of the Boundary Layer

When there is more entrainment, it may be expected that the depth of the boundary layer will increase, and that the additional warm air will cause the temperature deficit to become smaller, assuming that there are no corresponding changes in U or $\Delta\theta$. This is clearly shown in fig. 5.7. Manins & Sawford (1979) noted the effect of entrainment drag at the upper interface, which tends to slow down the speed of the boundary layer. Fig. 5.7 shows a decrease in the velocity of the boundary layer for higher values of A_e which produce more entrainment, but from

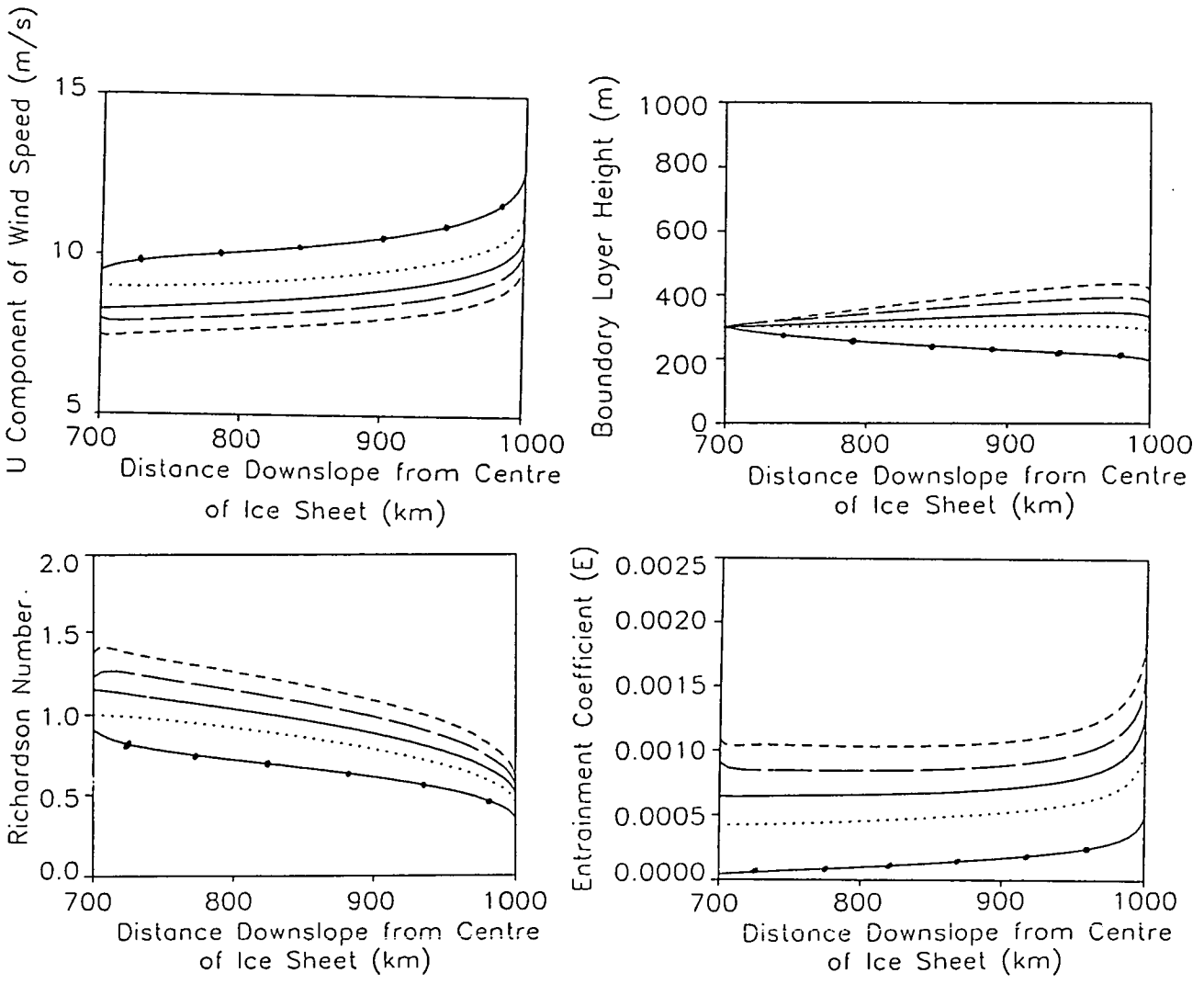

Figure 5.11: The evolution of the boundary layer for different values of $K_m\tau_f$: 1.87×10^5(- - - -); 9.36×10^4(— —); 4.68×10^4(———);2.34×10^4(·····); 4.68×10^3(—•—•—).

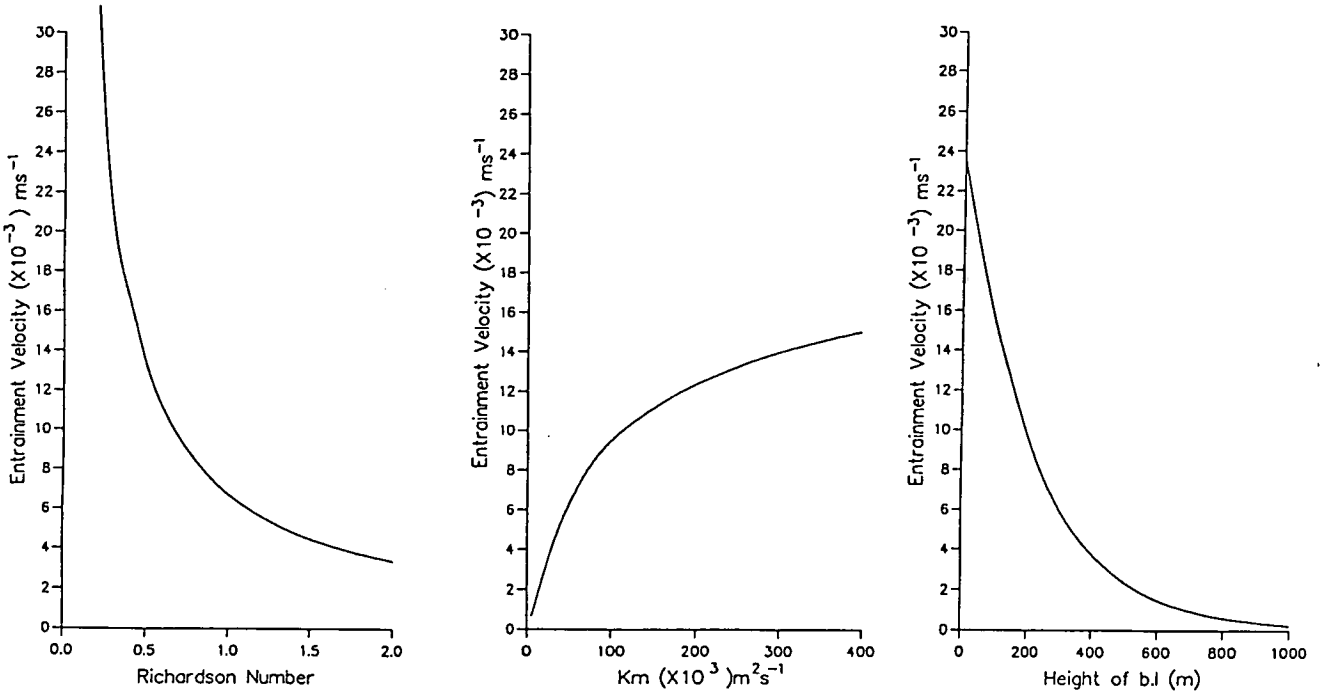

Figure 5.12: The sensitivity of the diffusion equation to variations in K_m, h and Ri.

fig. 5.13 it can be seen that the decrease in the buoyancy force is comparable to the increase in the drag force at the top of the layer. The decrease in velocity as entrainment increases, combined with the increase in depth of the boundary layer acts as a negative feedback on entrainment, via the Richardson number. In this way the parameterisation prevents large changes in the velocity or depth of the boundary layer.

5.2.4 Comparison of the two methods

The model was run to compare the boundary layer under 3 types of entrainment. The standard for comparison with the type 1 and type 2 parameterisations presented in sections 5.2.1 and 5.2.2, was the ET type entrainment used by previous authors, and presented in section 4.3.5. with A_c given a value of 0.0004. This is the value used by Gosink (1989), reduced from the value of 0.002 which Manins

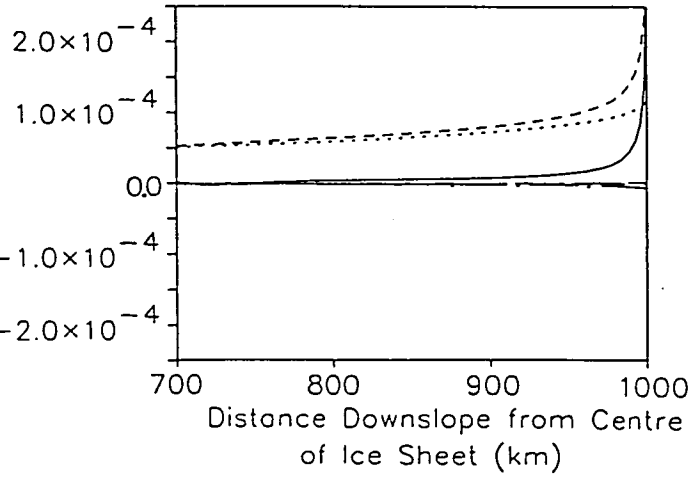

(a)$A_e = 0.04$

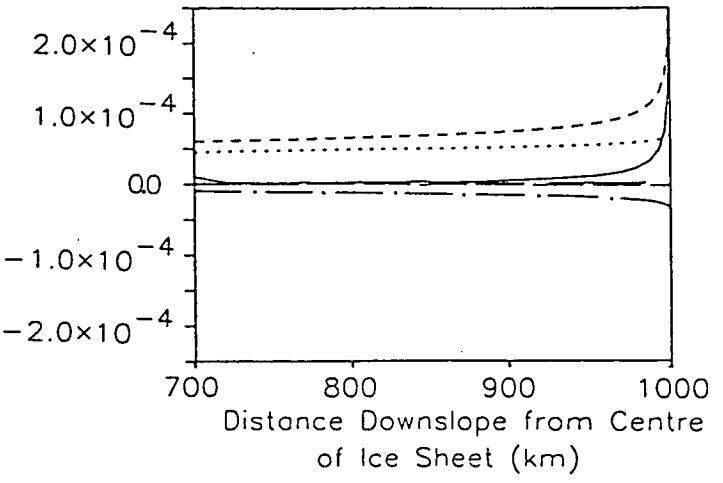

(b)$A_e = 0.4$

Figure 5.13: The components of the downslope momentum budget equation 4.33 for different values of A_e:
$\frac{du}{ds}$(———);buoyancy(- - - -); coriolis(— —);thermal wind(——-);entrainment drag(—·—);surface drag(·····).

& Sawford (1979) used, based on the laboratory experiments of Ellison & Turner (1959). Gosink (1989) assumed 0.0004 to be a more appropriate value over the glacial slopes, where Reynolds numbers are greater, but did not investigate the reliability of extrapolating the relationship derived in the laboratory to the much larger scale glacial slopes. If A_e and $K_m\tau_f$ are given values which produce entrainment of a similar magnitude to the ET case, then $A_e = 0.5$ and $K_m\tau_f = 4.68 \times 10^4$. These values are higher than those suggested in the previous discussion, which suggests that even the reduced ET entrainment is too high. The values of each of the parameters will be reassessed in a later section.

Air moving downslope over a dome shaped ice sheet accelerates as the buoyancy force becomes greater over the larger slopes. From equation 4.36 it can be seen that acceleration and divergence of the air will result in a reduction in the rate of growth of the boundary layer depth. Entrainment compensates for this tendency

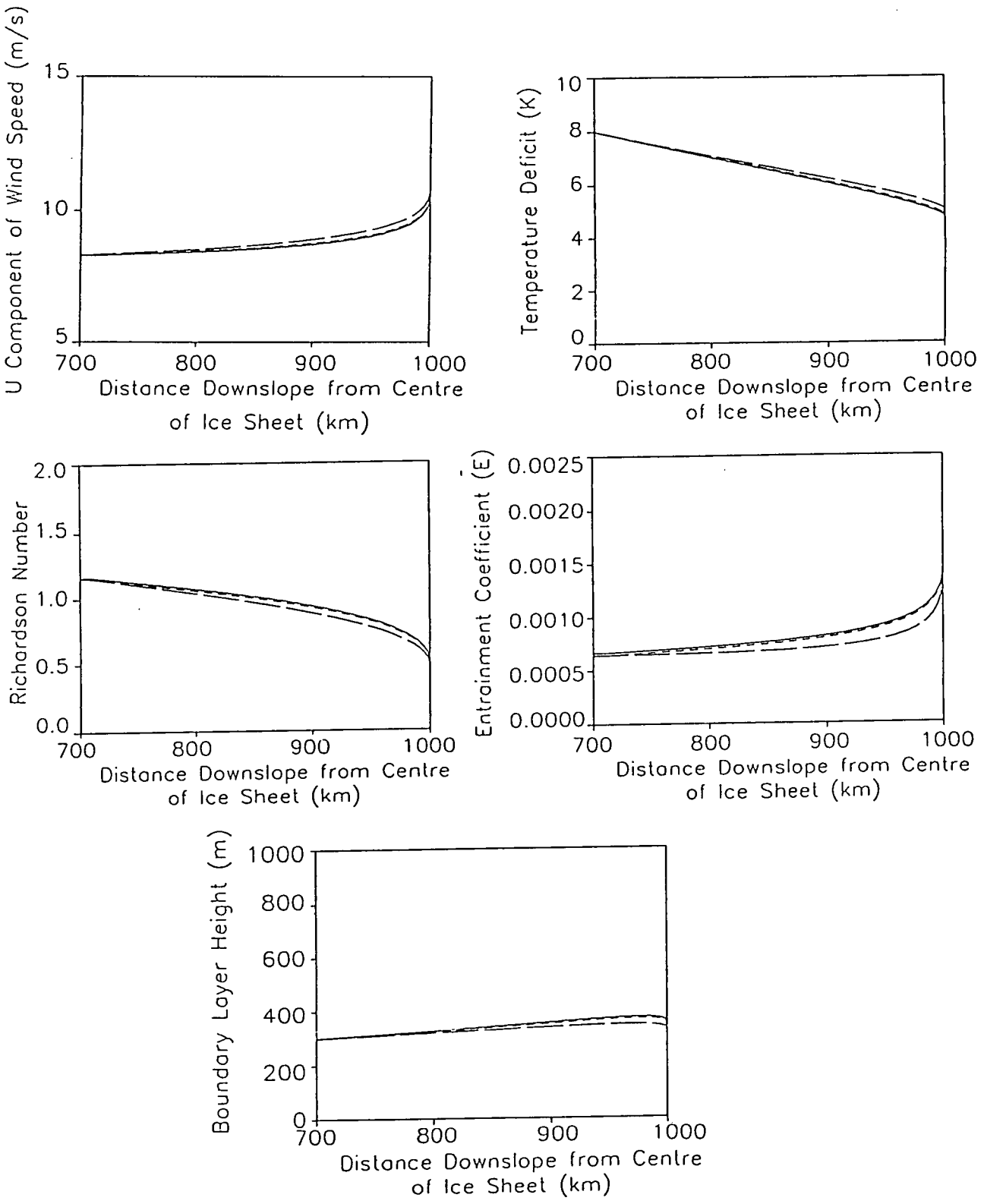

Figure 5.14: A comparison of the 3 parameterisations of entrainment: Type ET [$A_c = 0.0004$](———); Type 1 [$A_e = 0.5$](– – –); Type 2 [$K_m \tau_f = 4.68 \times 10^4$](— —).

for h to decrease, preventing h from becoming very small. Conversely if the depth of the boundary layer begins to increase too rapidly, and if all other factors remain unchanged, this will result in less entrainment, because one of the the sources of TKE (shear at the surface) is further away from the entrainment zone, and energy will tend to be dissipated before it reaches the top of the boundary layer. In this manner the boundary layer is prevented from becoming too deep. The effect of the increase in height of the boundary layer downslope, is to some extent offset in the boundary layer over an ice sheet with increasing slopes, because the increase in downslope momentum tends to increase the production of TKE both from shear at the surface and shear at the top of the boundary layer. All 3 methods of parameterisation have an inverse Richardson number dependence which reduces the entrainment as h increases, and increases entrainment for larger values of U. However as observed by Lalaurette & Andre (1985) and Gosink (1989), the ET type entrainment tends to produce a boundary layer which is too deep, even with the value of A_c reduced from 0.002 to 0.0004. Therefore it would seem that the Richardson number dependence isn't sensitive enough to the characteristics of the boundary layer. Fig. 5.14 shows the evolution of the entrainment coefficient E, for each parameterisation. The behaviour of the ET entrainment and the type 1 entrainment parameterisations is almost identical, as would be expected from the formulations. The entrainment coefficient of the type 2 entrainment equation however, increases at a slightly lower rate, because as well as the Richardson number dependence it also has an exponential dependence on the height of the boundary layer h. This is shown in figure 5.12c and shows the sensitivity to be greatest when the boundary layer is less than 500m which is the case over most of the boundary layer over Antarctica. The results shown in fig. 5.14 do not suggest that the the additional sensitivity introduced by the diffusion equation is sufficient to significantly affect the evolution of the boundary layer. This will be investigated further in the following sections.

5.3 A Look at the Boundary Conditions from Different Ice Sheets

The discussion so far has focused on the formulation and atmospheric boundary conditions of the slab model. This section is intended to consider the role of the ice sheet. The main driving force of the winds over the ice sheet is the buoyancy force. The ice sheet may potentially be a large influence on the magnitude of this force via the slope of the surface. Therefore it would be expected that the effect ice sheet shape has on the evolution of the boundary layer is potentially large, and under different circumstances the parameterisation of entrainment may become more important. Profiles taken from ice sheets of the present day will be used to test the hypothesis, which will then be used to look at ice sheets in the past. In this way it is hoped to be able to identify the key components of the boundary layer which are affected by the shape of the ice sheet, particularly those which may subsequently affect the evolution of the ice sheet itself.

5.3.1 Changing the Surface Profile.

Effect on the Boundary Layer

The effect that changing the profile of the ice sheet has on the evolution of the boundary layer, has been investigated using two profiles taken from present day ice sheets. The first profile is taken along a streamline in Adelie Land, Antarctica shown in fig. 5.15a (Drewry 1983), the second is from the Greenland ice sheet as shown in fig. 5.15b (Bindschadler et al 1989). The shape of these profiles are shown in figure 5.16. Greenland has been assumed to be a semi-infinite slab and therefore

has no geometric component in the mass continuity equation, the last term in equation 4.36. The evolution of the boundary layers for each of the profiles with $A_c = 0.0004$, $A_e = 0.5$ and $K_m\tau_f = 4.68\times10^4$ are shown in figs 5.17 and 5.18. If the topographic profiles shown in fig. 5.16 are compared with the velocity profiles it can be seen that the velocity is largely governed by surface slope, which then affects the entrainment coefficient, the boundary layer depth, and the temperature deficit. This is illustrated by fig. 5.19 which shows the components of the U velocity for the Greenland profile with the type 2 entrainment ($K_m\tau_f = 4.68 \times 10^4$). The evolution of $\frac{du}{ds}$ (shown by the continuous line) is dominated by the variations in the buoyancy force (the upper dashed line) of the layer, which responds to the changes in magnitude of the slope. Generally as the slope increases so does the velocity, and the subsequent reduction in the Richardson number causes more entrainment. The depth of the boundary layer tends to respond to the acceleration of the air rather than the increase in entrainment and thus tends to deepen most when the slope is reduced and the air slows down, rather than when entrainment is large. This is confirmed by fig. 5.20, which shows the accelerative $\left(\frac{du}{ds}\right)$ term to dominate over the entrainment term (W_e) in the depth evolution. The increase in entrainment with slope is accompanied by a decrease in the temperature deficit, which tends to produce high surface temperature gradients, as noted by Fortuin & Oerlemans (1990) in their study of the surface temperature over Antarctica. The increase in surface temperature gradient with additional warm air is offset slightly because as the air flows downslope in a stably stratified environment, the boundary layer moves into progressively colder ambient air, in the manner discussed in section 5.1.2. Thus at the end of the profile where the gradient $\frac{d\Delta\theta}{ds}$ is greatest, the surface temperature gradient remains slightly less than it is further upslope where the gradient of $\frac{d\Delta\theta}{ds}$ is smaller.

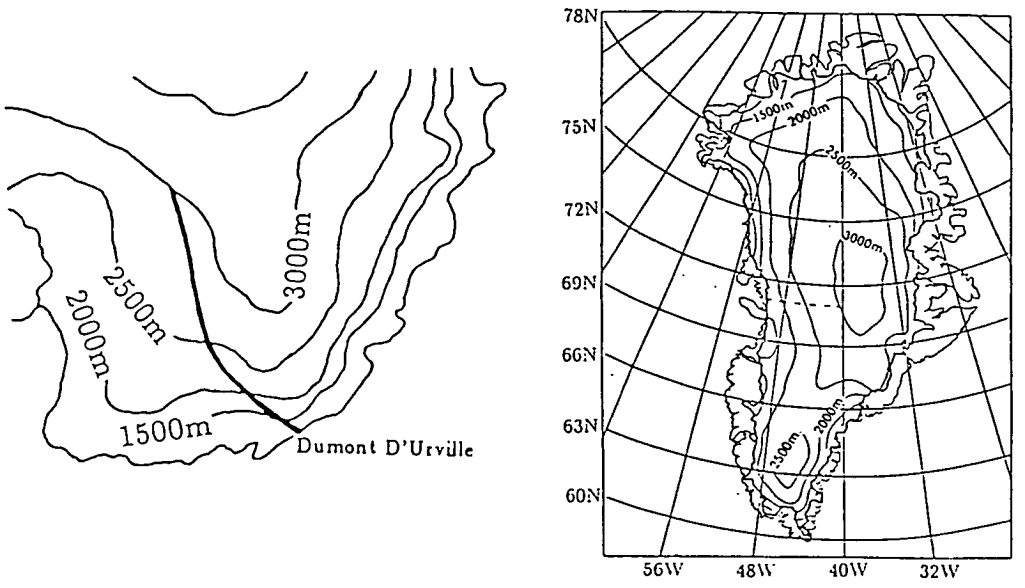

(a) Adelie Land (b) Greenland

Figure 5.15: The location of the profiles used for the model runs shown in 5.17 and 5.18.

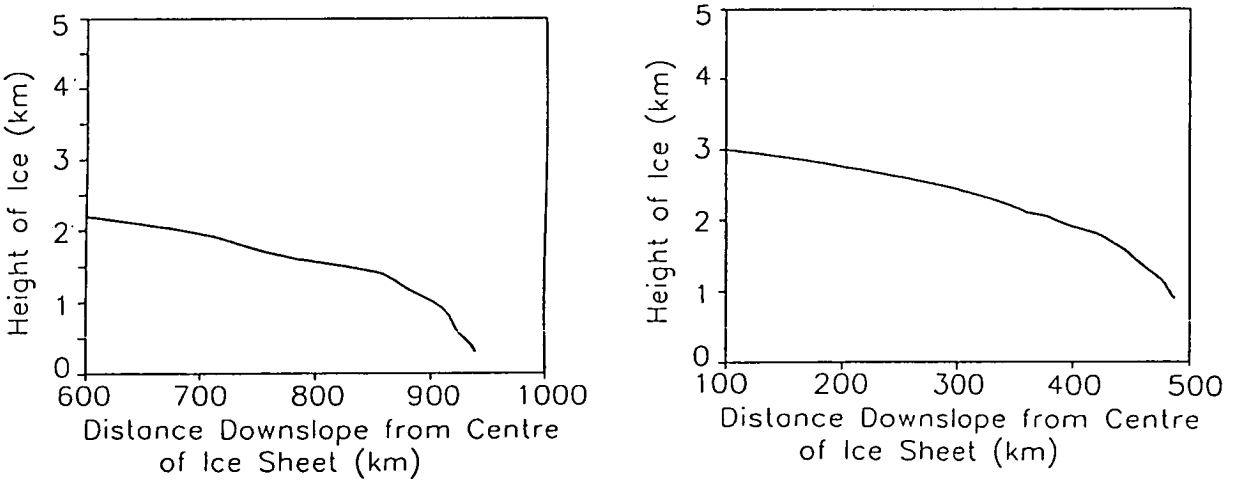

(a) Adelie Land (b) Greenland

Figure 5.16: The surface profiles shown in fig. 5.15.

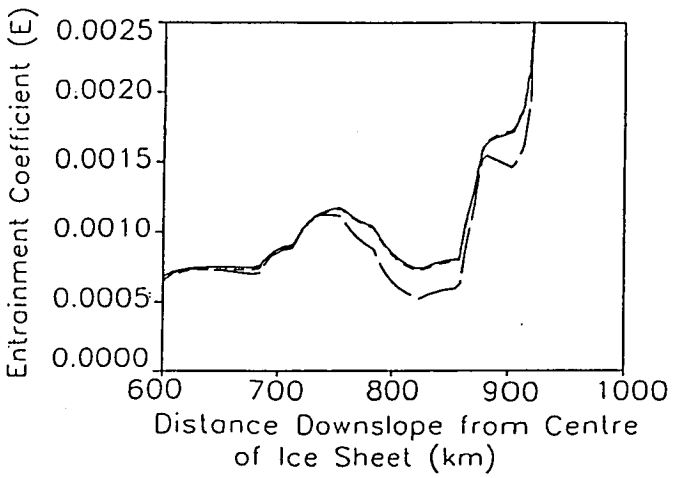

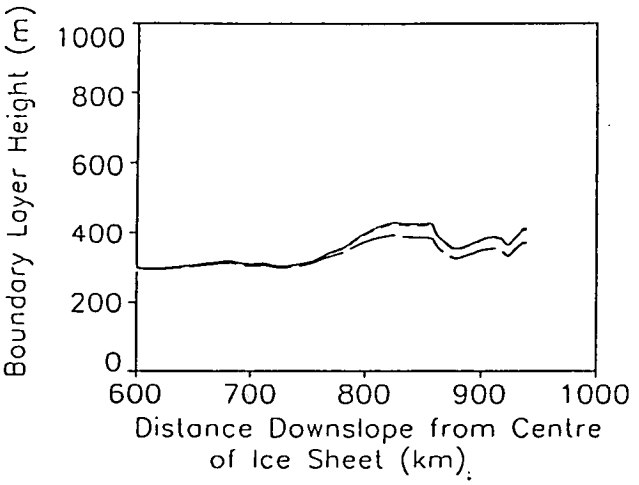

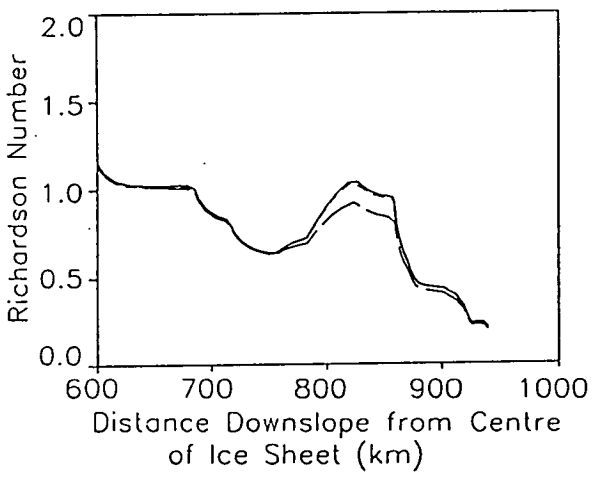

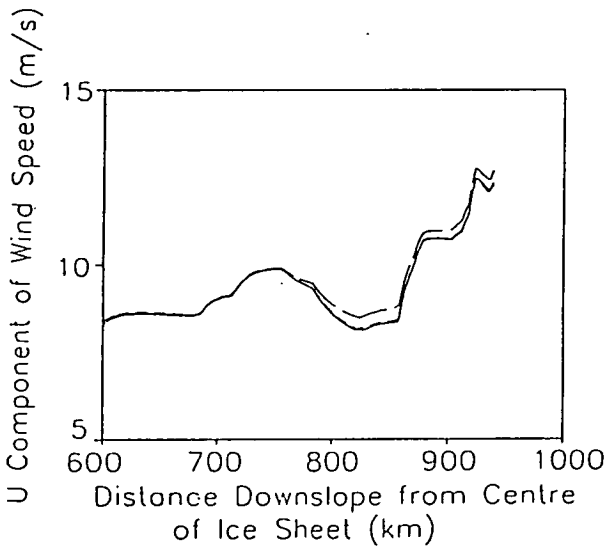

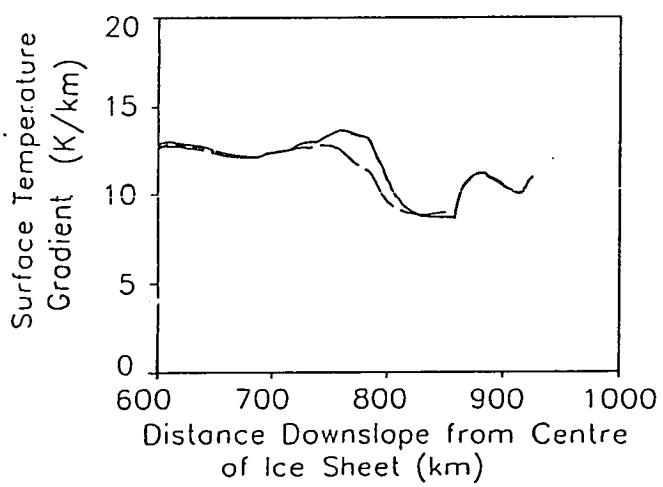

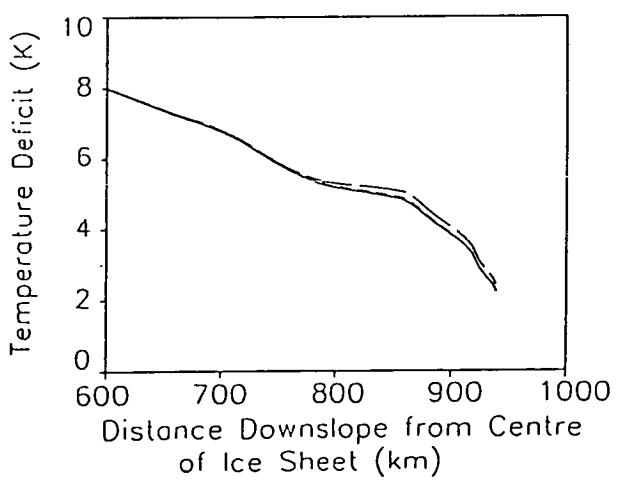

Figure 5.17: The effect of surface profile on the evolution of the boundary layer, using the profile from Adelie Land Antarctica. Fig. 5.15a:
Type ET($A_c = 0.0004$(———); Type 1($A_e = 0.5$)(- - -);
Type 2($K_m \tau_f = 4.68 \times 10^4$)(— —).

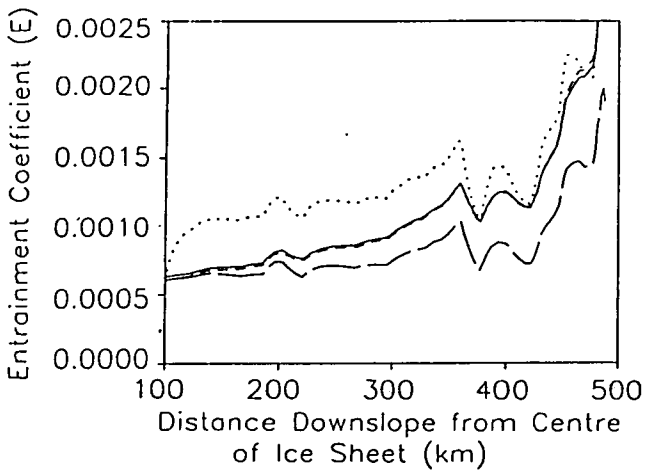

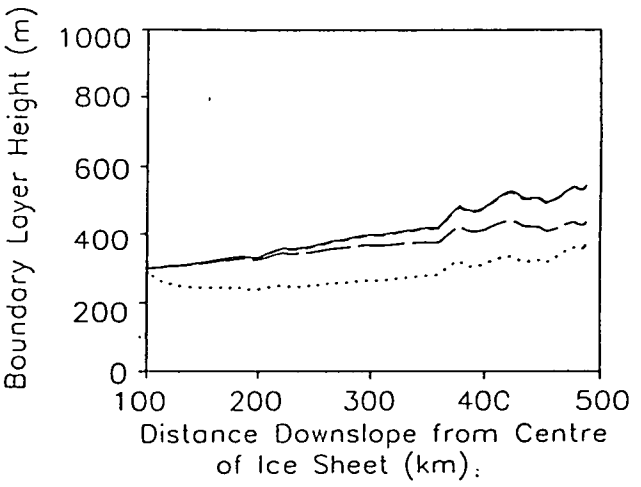

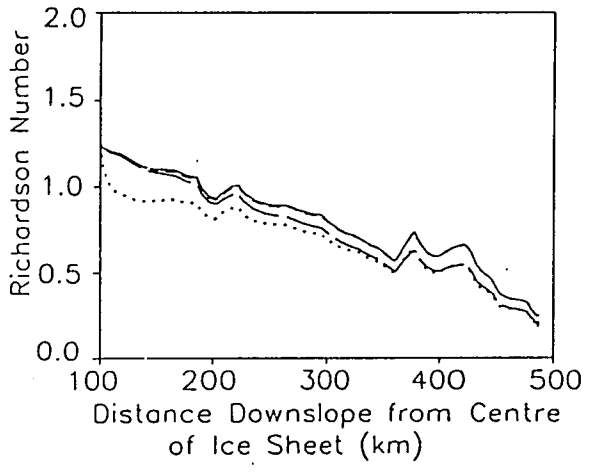

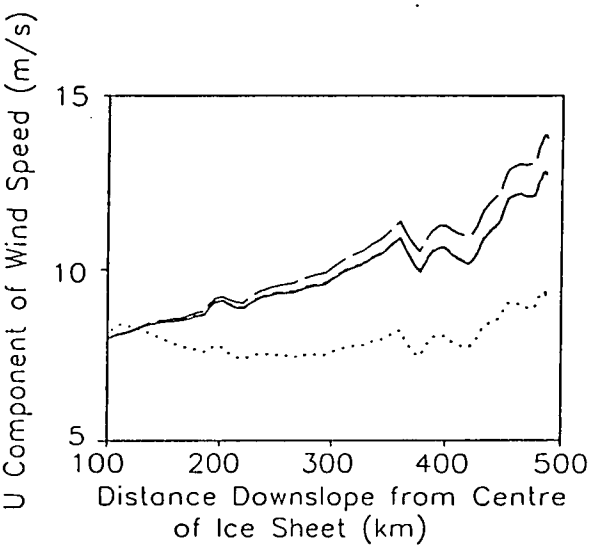

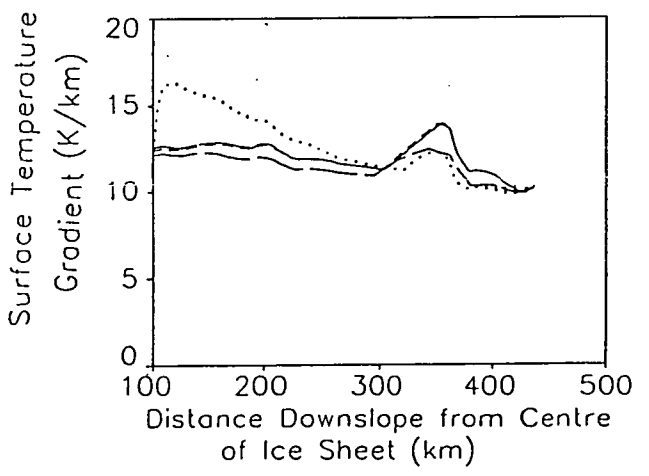

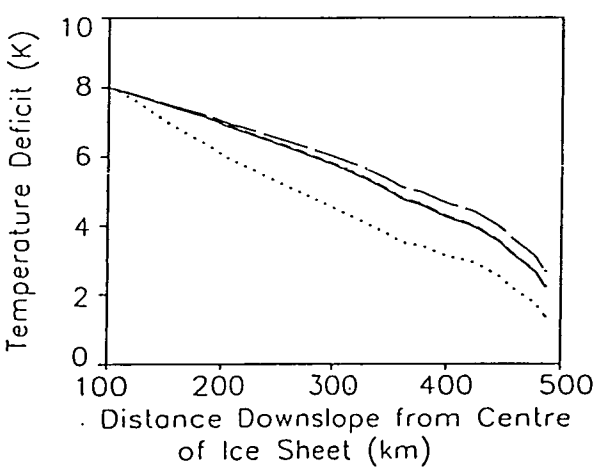

Figure 5.18: The effect of surface profile on the evolution of the boundary layer using the Greenland profile of fig. 5.15b:

Type ET($A_c = 0.0004$)(———); Type 1($A_e = 0.5$)(- - - -);

Type 2($K_m \tau_f = 4.68 \times 10^4$)(— —); with geometry - see text(·····).

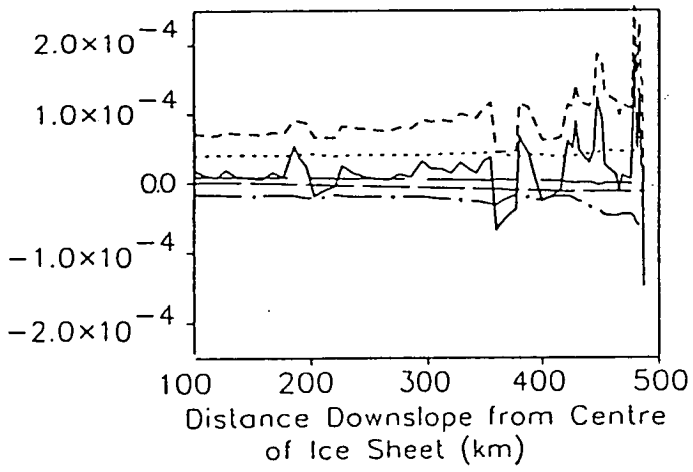

Figure 5.19: The components of the momentum budget equation 4.33 for the Greenland profile using type 2 entrainment:
$\frac{du}{ds}$(———); buoyancy(- - - -); coriolis(— —);thermal wind(—— -);entrainment drag(— · —);surface drag(·····).

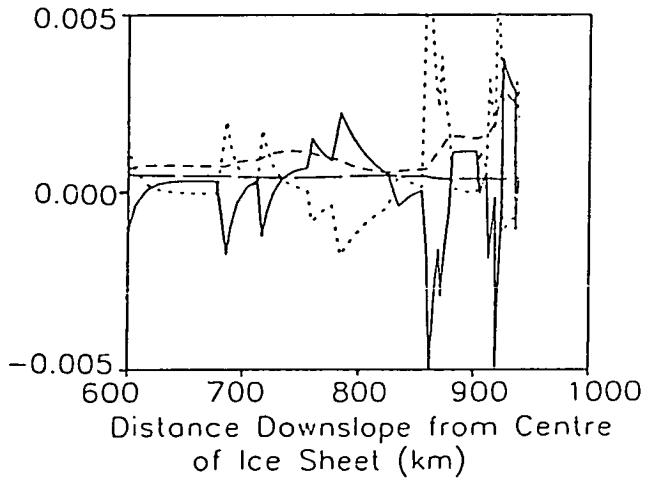

Figure 5.20: The components of the depth evolution for the boundary layer over Adelie Land, with type 2 entrainment: $\frac{dh}{ds}$(———); entrainment(- - - -); geometry(— —); acceleration(·····).

Geometry

Fig. 5.18 has an additional run. This shows the effect of including geometry. This is particularly noticeable on a small ice sheet such as Greenland where the geometric divergence is large. The shape of the Greenland ice sheet means that in the southern portion, south of the Arctic Circle, air flow radiates from the southern dome. Further north the ice sheet can be considered to be a semi-infinite slab the contours aligned in straight lines parallel to the coast and central ridge. The profile used in this example is at $71°N$, and therefore lies somewhere between the two. The figure shows the effect of geometry is very important on an ice sheet of this scale. The additional divergence produces a more shallow boundary layer which, because the Richardson number is lower, increases entrainment. However the increase in entrainment is not sufficient to increase the mass flux (Uh) along a streamline, to the no geometry case. The addition of warm air to the boundary layer decreases the temperature deficit, a process which is enhanced because the air is incorporated into a more shallow boundary layer.

The Geostrophic Wind

In these experiments Vg was given a value of $3ms^{-1}$which is the value typical over the Antarctic ice sheet. In Greenland, however the geostrophic flow above the boundary layer fluctuates. On average there is a high pressure situated over the ice sheet, which produces a clockwise geostrophic wind above the boundary layer. Superimposed on this is the mean meridional flow of an upper atmospheric westerly jet stream. The meridional flow may weaken the glacial anticyclone, destroying the boundary layer. This occurs in the slab model when Vg is reduced in the y direction as shown in the experiments in section 5.1.1. On the western flanks

of the ice sheet therefore downslope flow may often be absent, or weak whereas on the east the meridional flow may enhance the downslope flow, producing the cold air outbreaks which are common on the east coast of Greenland (Radok et al 1982).

The Significance of the Parameterisation of Entrainment.

Figs. 5.17 and 5.18 show that the way in which entrainment is parameterised seems to have little effect on the characteristics of the boundary layer (U, $\Delta\theta$, h & Ri). The entrainment coefficient E, using the type 2 entrainment, shows a slightly greater response to the increase in the boundary layer height, and offsets the increase in entrainment that occurs when the air accelerates over larger slopes. Between 750km and 850km downslope on the Adelie Land profile it can be seen that the entrainment for the type 2 entrainment is slightly lower than the other parameterisations. From this it would be expected that if the acceleration of the air was much greater or persisted for much further downslope the difference between the parameterisations would be more apparent. On this scale, however the effect these small variations have on the wind speed, temperature and depth of the boundary layer is small.

A Reassessment of the Entrainment Parameters

It has already been noted that the ET type entrainment tends to produce over deep boundary layers and the values of A_e and $K_m\tau_f$ required to produce comparable entrainment coefficients are much greater than suggested by the observational data. Therefore the values of A_e, K_m and τ_f have been reassessed on the basis of the discussion in sections 5.2.1 and 5.2.2. The boundary layer for the Adelie Land

and Greenland profiles for $A_e = 0.3$ and $K_m \tau_f = 2.16 \times 10^4$ with A_c adjusted to 0.00025 for comparison are shown in fig. 5.21 and 5.22. It can be seen that the boundary layer depth remains lower and the velocity higher while the reduction in $\Delta\theta$ is less, which results in a lower surface temperature gradient, around 10K/km. These are all characteristics which are closer to the observations. As discussed in chapter 2, the wind speed over Adelie Land is consistently around $10ms^{-1}$and rapidly accelerates at the coast. The surface temperature gradients over the slope are just over the DALR and the temperature deficit decreases from over 8K in the interior to 1 or 2K at the coast. This suggest that the entrainment processes on a scale as large as the boundary layer over an ice sheet cannot simply be extrapolated from empiricisms derived in the laboratory. The dissipation is in fact much greater than the laboratory experiments suggest, which may be actual dissipation or the results of additional storage of TKE in gravity waves.

5.3.2 Past Ice Sheets

Past ice sheets have been reconstructed from paleoevidence, such as that given by Denton & Hughes (1981). Two profiles have been taken from the late Wisconsin-Weichselian maximum reconstruction of the Laurentide ice sheet, as shown in fig. 5.23. The profiles have been smoothed using the idealised profile given in equation 4.11, n_g has been given a value of 2.5, profile A has a span† and height of 2050km and 3800m respectively, profile B a span of 1700km and height of 3700m. The model was initiated at the top of the glacial slope, which is assumed to be where the gradient begins to increase, at an elevation of approximately 2500m. Comparisons between the actual and smoothed profiles are shown in fig. 5.24. Runs with these surface profiles but the remaining boundary conditions unchanged are shown in figs 5.26 and 5.25. The only small difference which

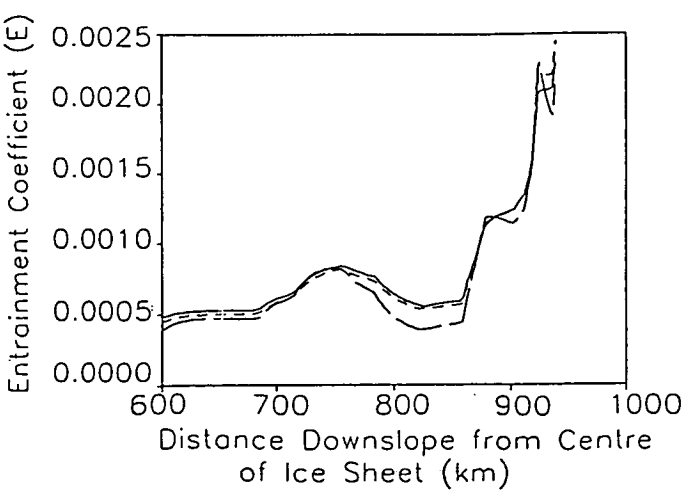

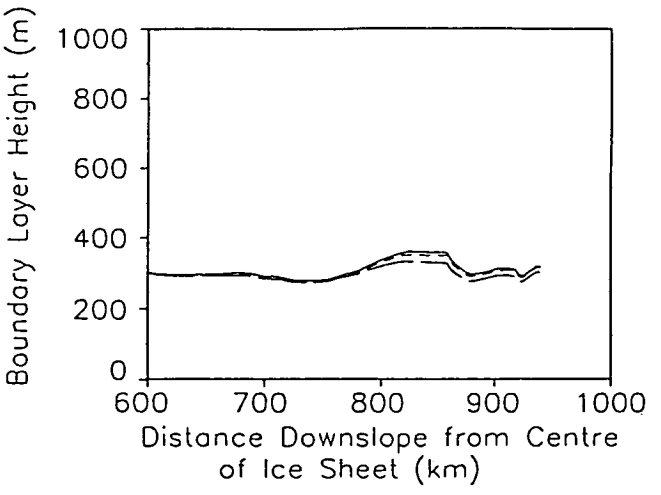

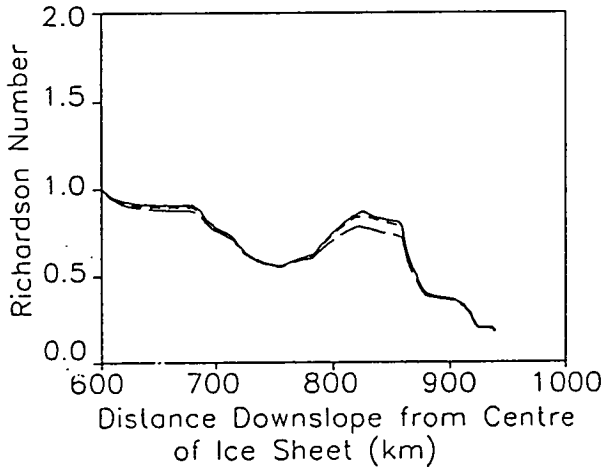

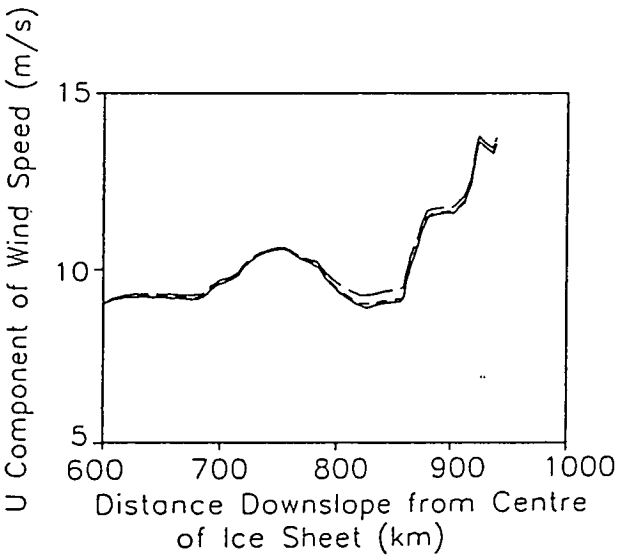

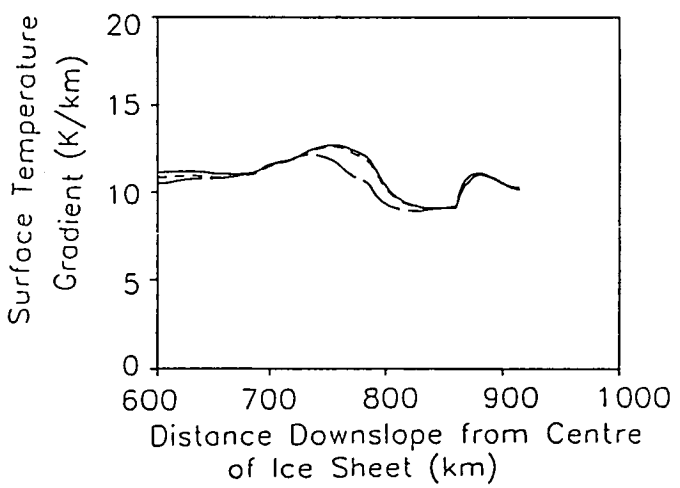

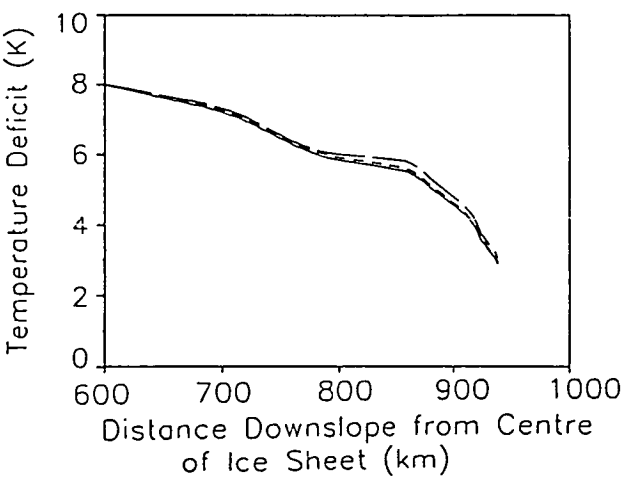

Figure 5.21: The effect of surface profile on the evolution of the boundary layer, using the profile from Adelie Land Antarctica, Fig. 5.15a:
Type ET(A_c = 0.00025)(——); Type 1(A_e = 0.3)(- - - -); Type 2($K_m\tau_f = 2.16 \times 10^4$)(— —).

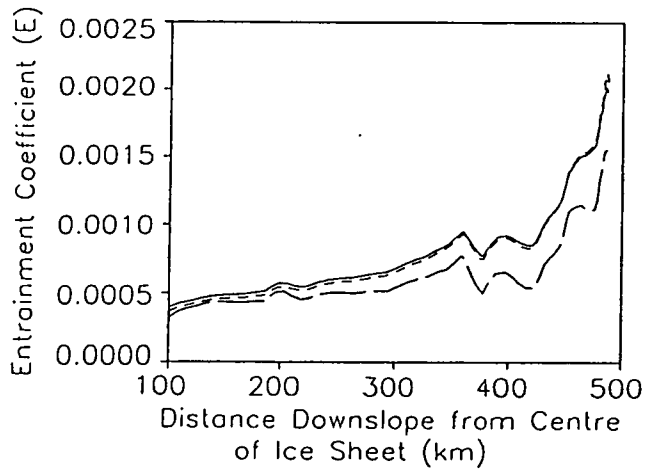

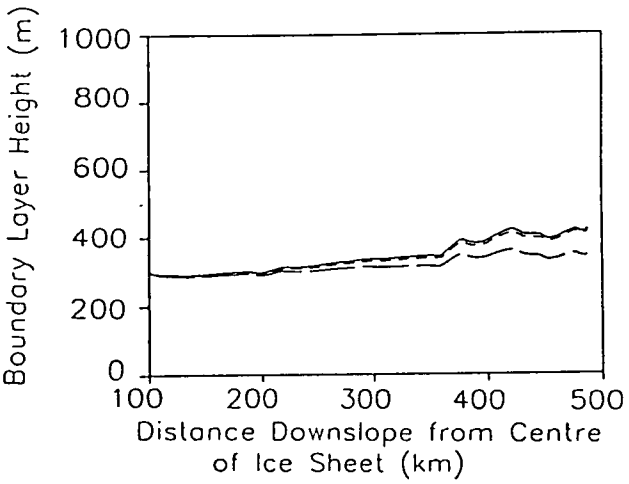

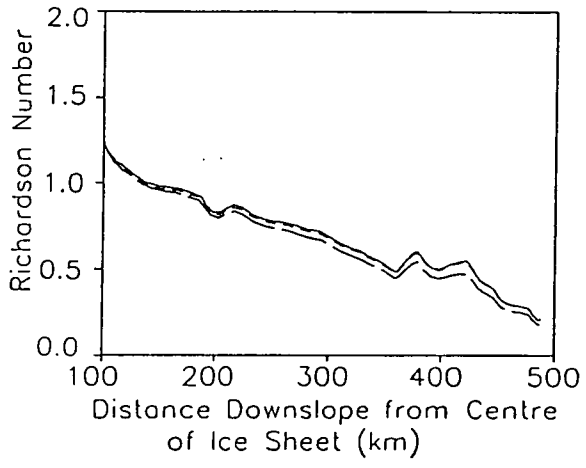

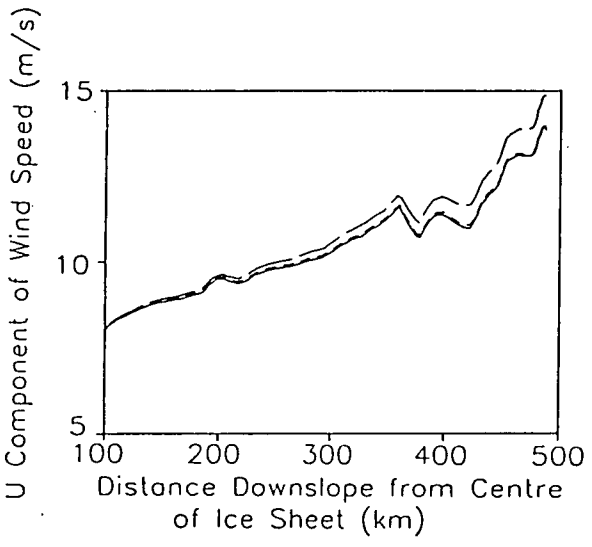

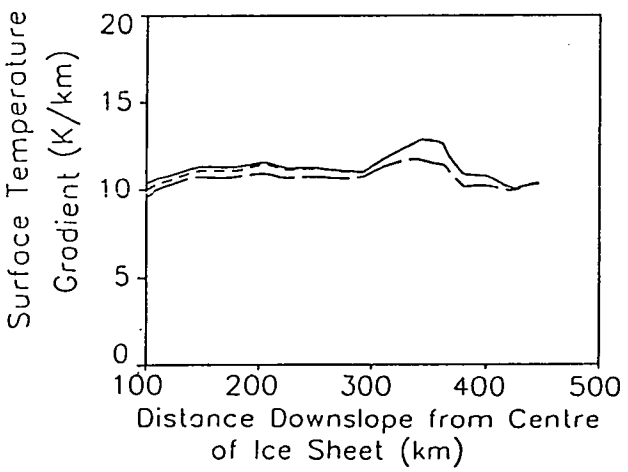

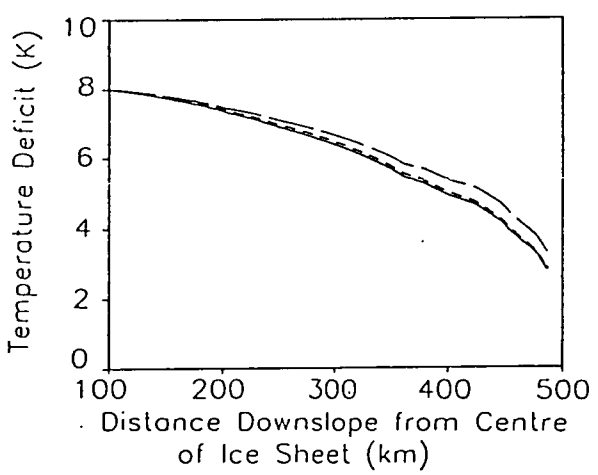

Figure 5.22: The effect of surface profile on the evolution of the boundary layer using the Greenland profile of fig. 5.15b:

Type ET($A_c = 0.00025$)(———); Type 1($A_c = 0.00025$)(- - - -); Type 2($K_m \tau_f = 2.16 \times 10^4$)(— —).

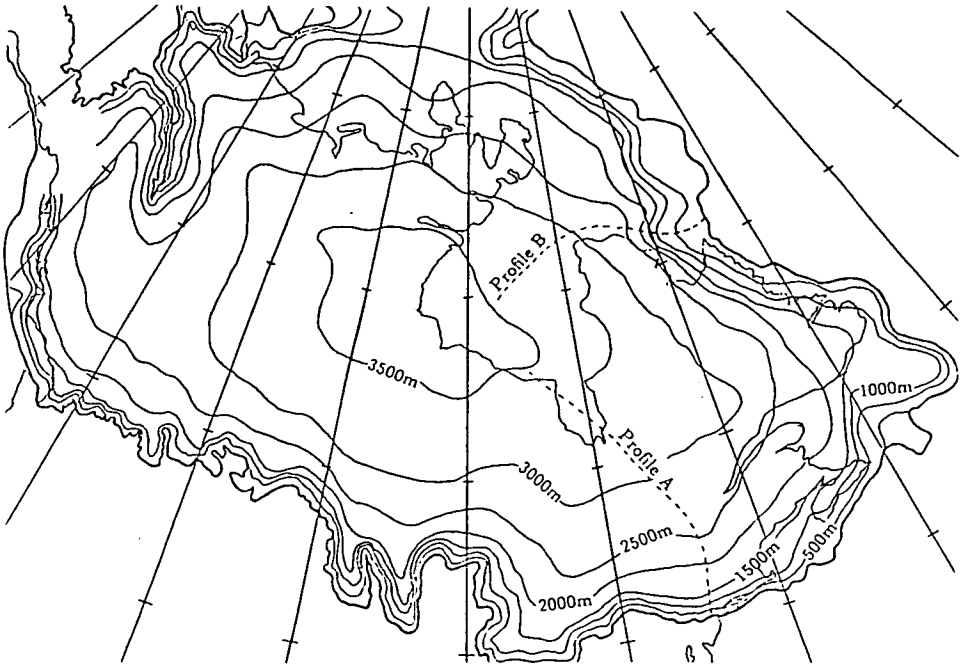

Figure 5.23: The location of the profiles taken from the reconstruction of the Laurentide ice sheet.

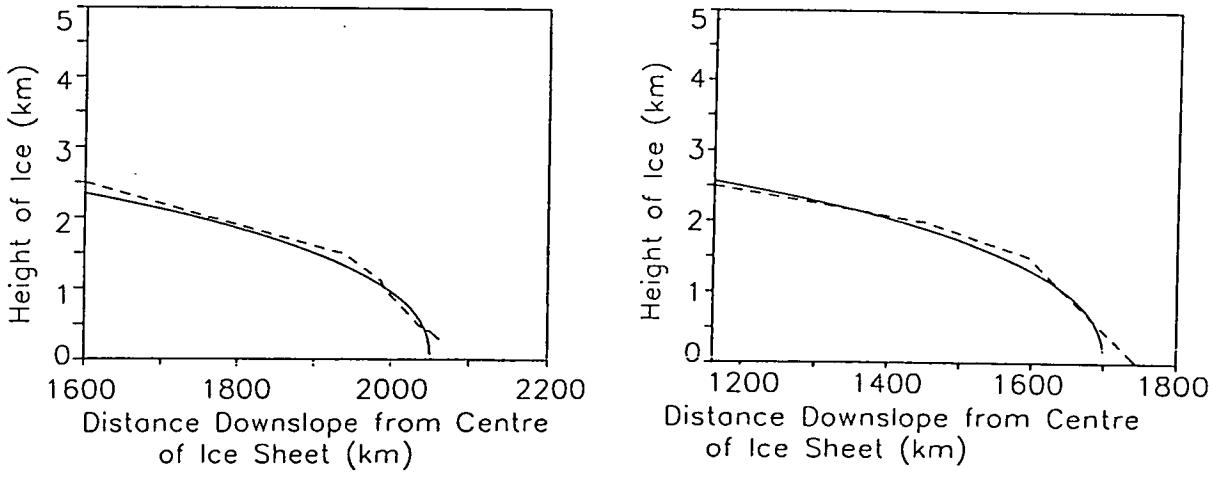

(a) Profile A

(b) Profile B

Figure 5.24: The effect of smoothing the profiles over the Laurentide ice sheet:Actual profile(- - - -);Smoothed profile(———).

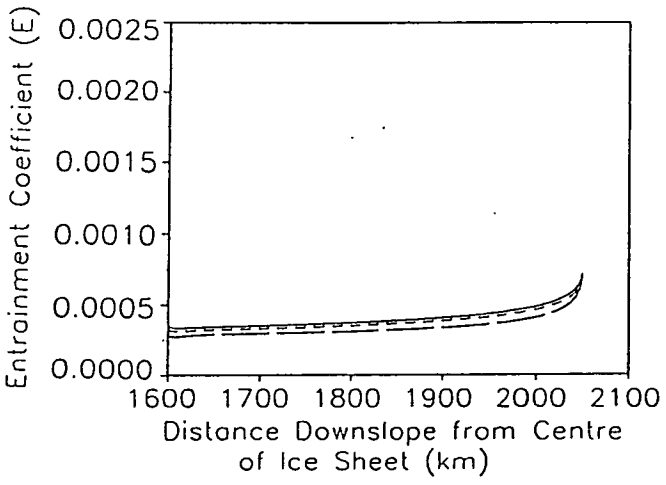

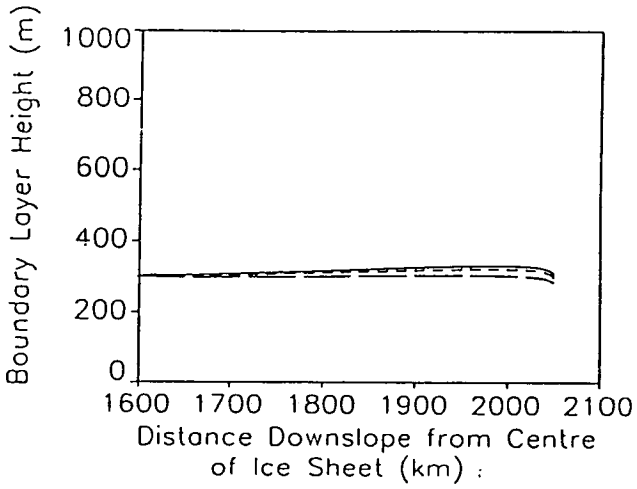

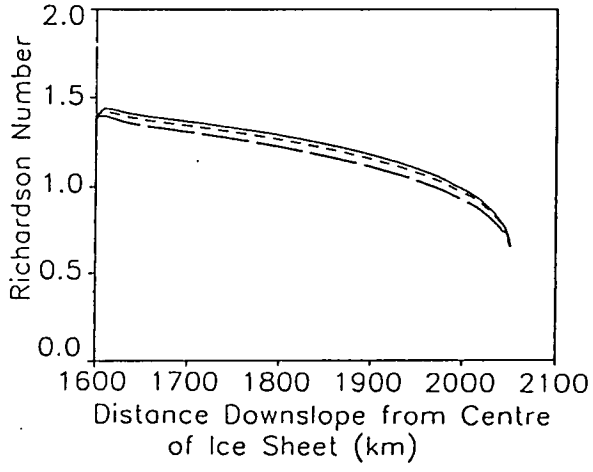

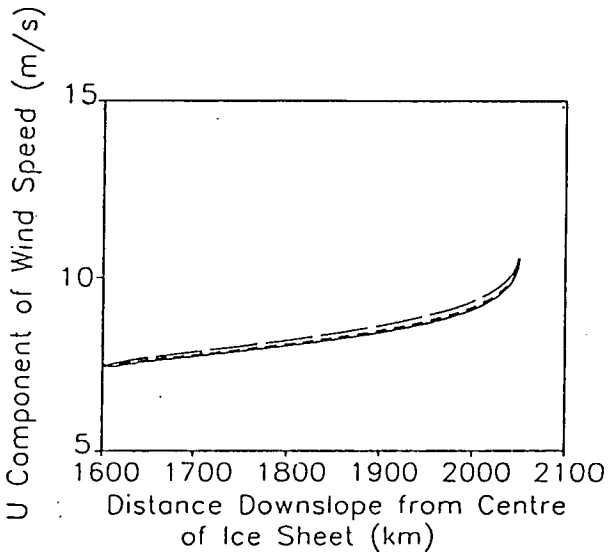

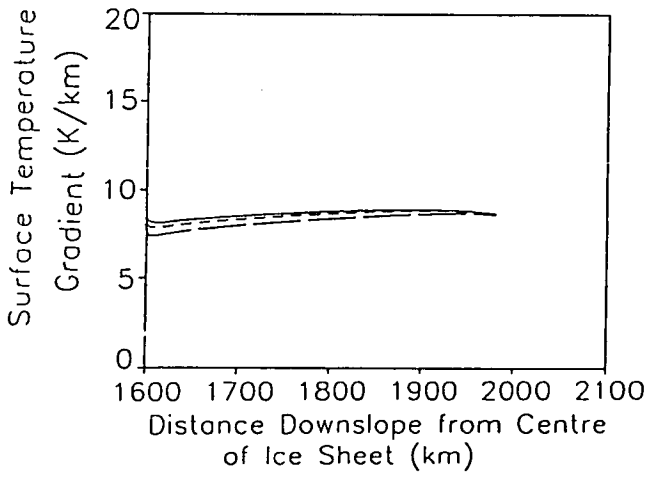

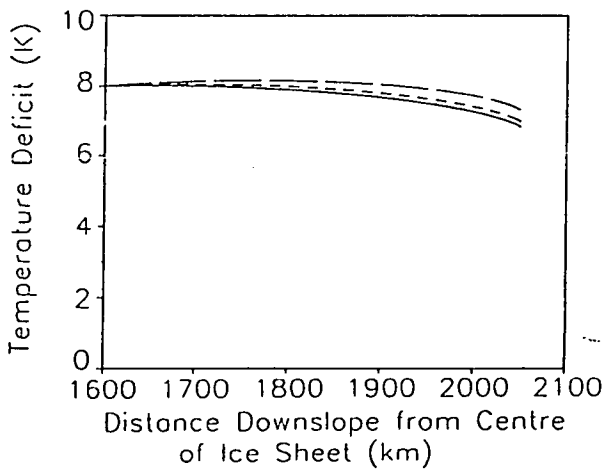

Figure 5.25: The evolution of the boundary layer with the surface profiles from the Laurentide ice sheet:Type ET(A_c = 0.00025)(———); Type 1(A_e = 0.3)(- - - -); Type 2($K_m\tau_f = 2.16 \times 10^4$)(— — —), [Profile A].

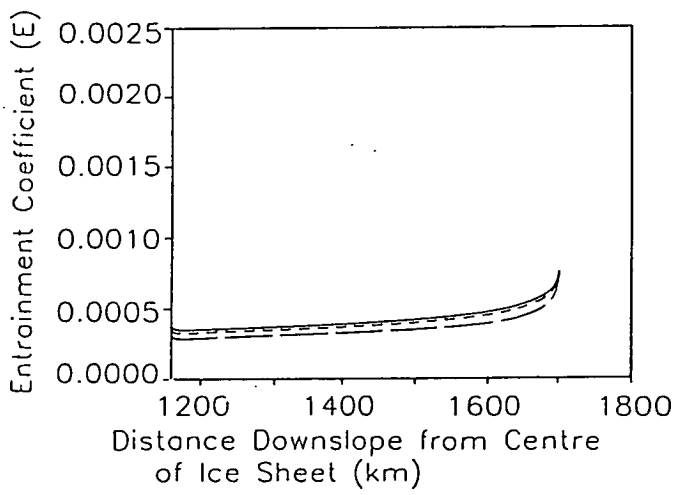

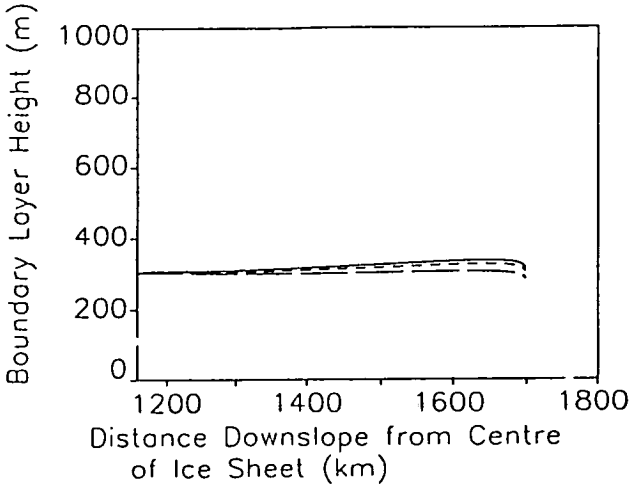

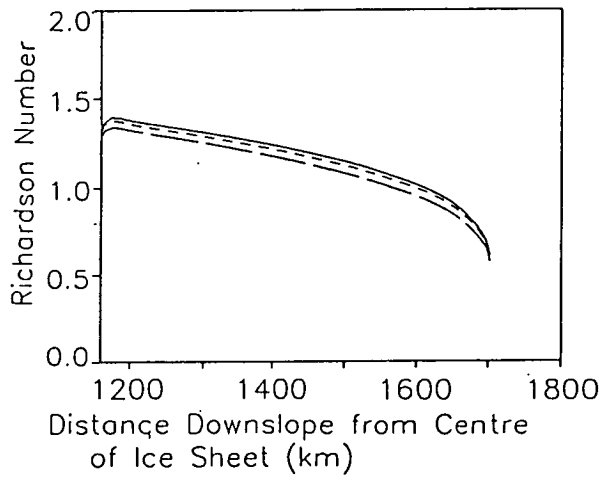

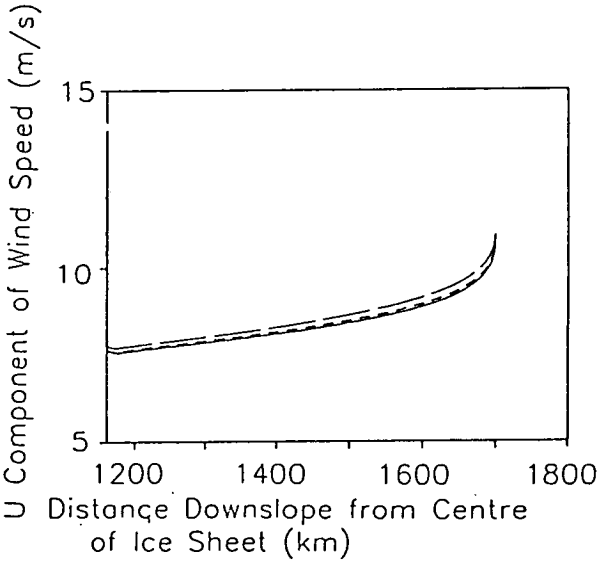

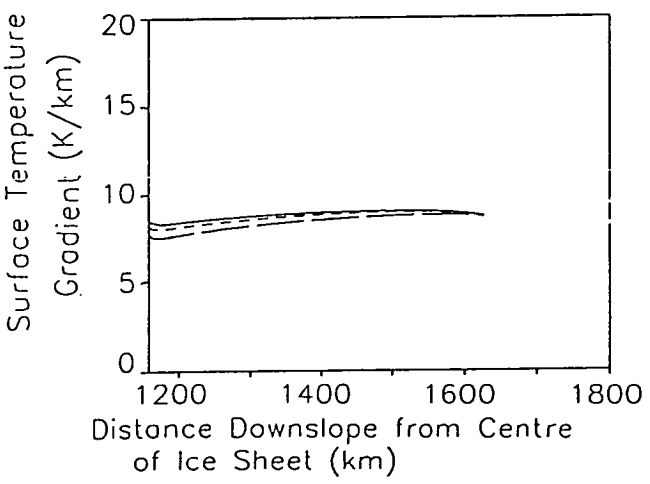

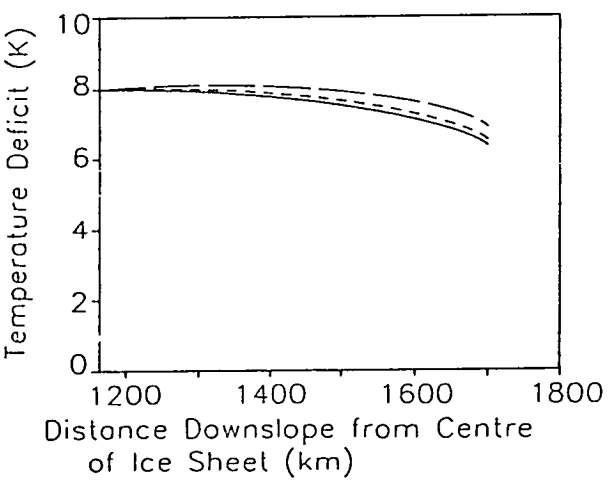

Figure 5.26: The evolution of the boundary layer with the surface profiles from the Laurentide sheet: Type ET($A_c = 0.00025$)(———); Type 1($A_e = 0.3$)(- - - -); Type 2($K_m \tau_f = 2.16 \times 10^4$)(— —), [Profile B].

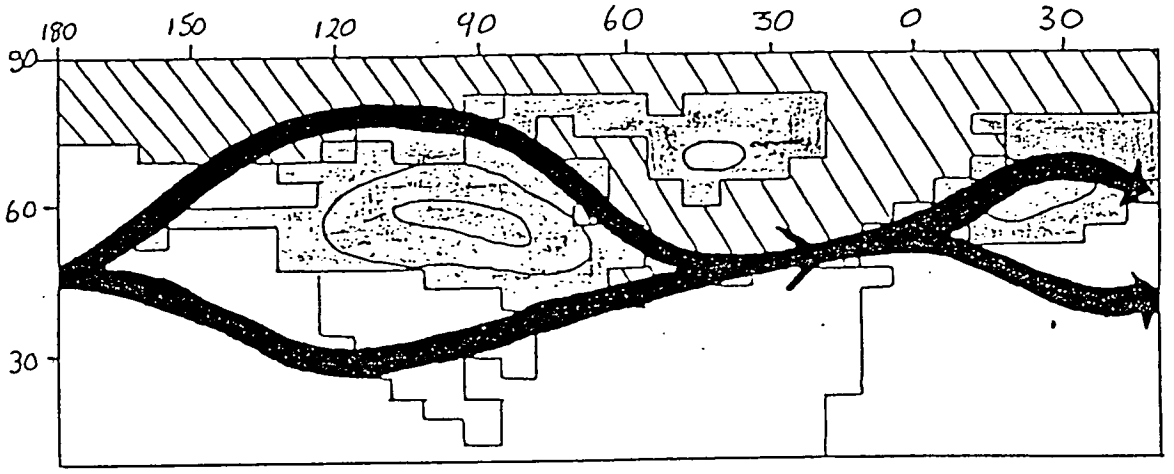

Figure 5.27: The split in the jet stream over the Laurentide ice sheet according to Kutzbach & Wright (1985).

arises between the parameterisations of entrainment is the slightly slower rate of growth of the boundary layer when the diffusion type equation is used.

The Geostrophic Wind.

Past ice age boundary conditions are likely to have been very different to those of the present day. One of the largest differences seems to be in the value of Vg. Experiments with GCMs suggest that the jet stream divided into 2 around the Laurentide ice sheet (eg. Kutbach & Wright (1985), Manabe & Brocolli (1985)), as shown in fig. 5.27. Thus the mean zonal flow is superimposed onto the anticyclone created by the presence of the ice sheet. Over the northern flank the mean meridional pressure gradient force enhances the downslope flow, but over the south facing slopes, the upper atmospheric pressure gradient force opposes the flow closer to the surface. Increasing Vg in the model produces a much deeper and faster boundary layer, primarily because the increase in U increases the entrainment coefficient, and more entrainment leads to a deeper boundary layer, as shown in fig. 5.28. It is interesting to see that the type of entrainment becomes much

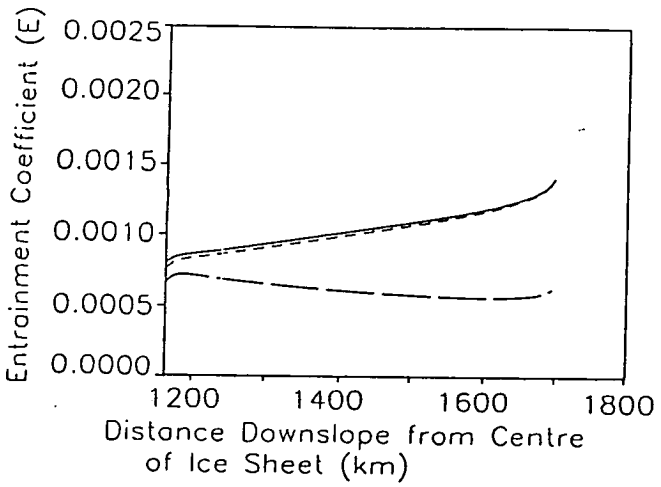

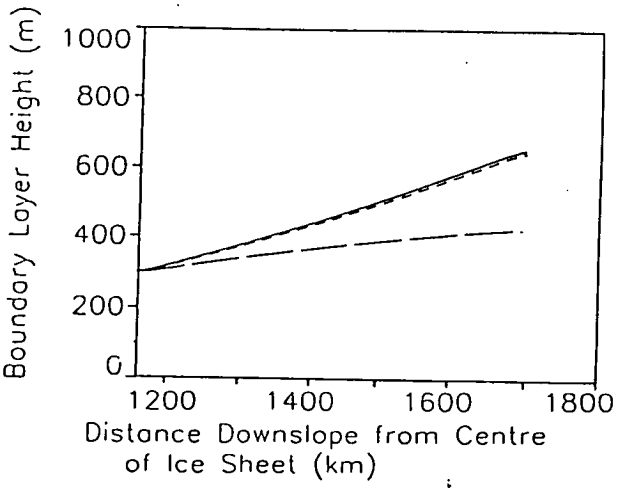

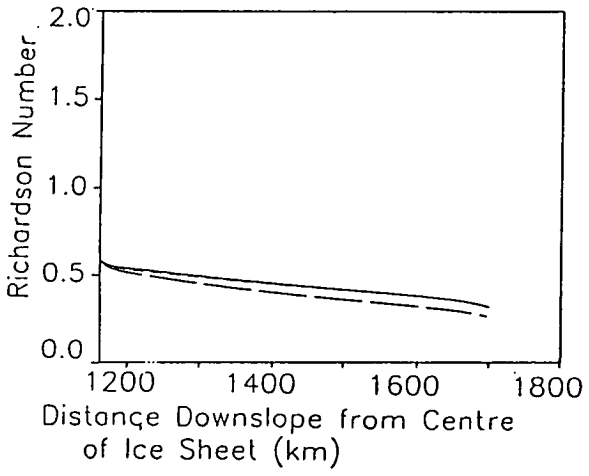

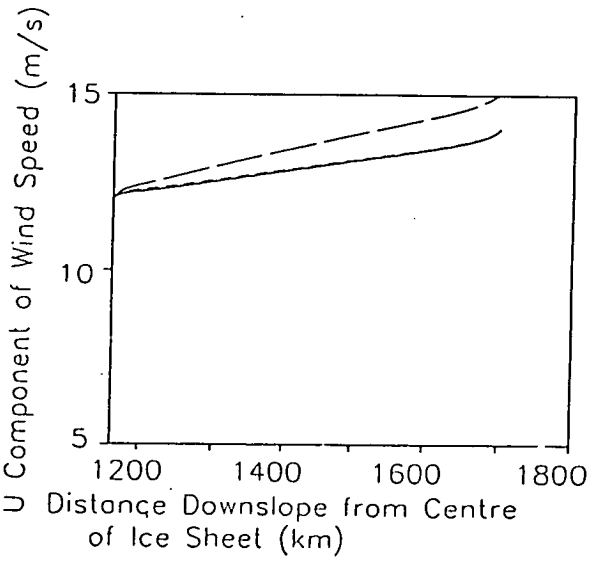

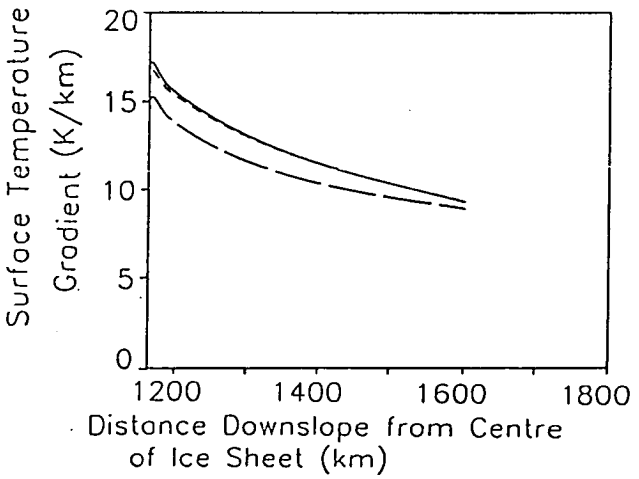

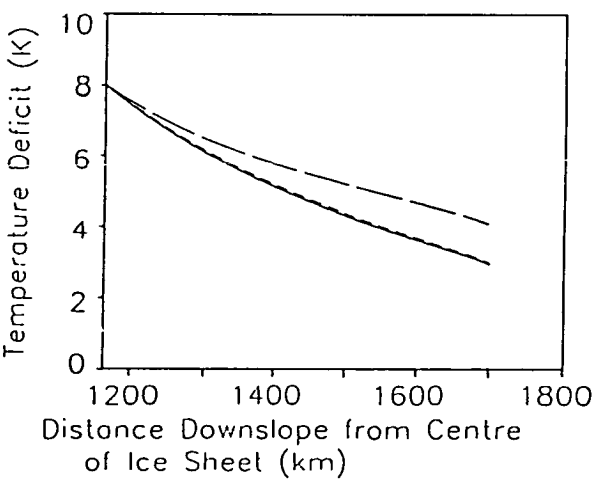

Figure 5.28: The evolution of the boundary layer with the profile B from fig. 5.23 with $Vg = 10ms^{-1}$: Type ET[$A_c = 0.00025$](——); Type 1[$A_e = 0.3$](- - - -); Type 2[$K_m\tau_f = 2.16 \times 10^4$](— —).

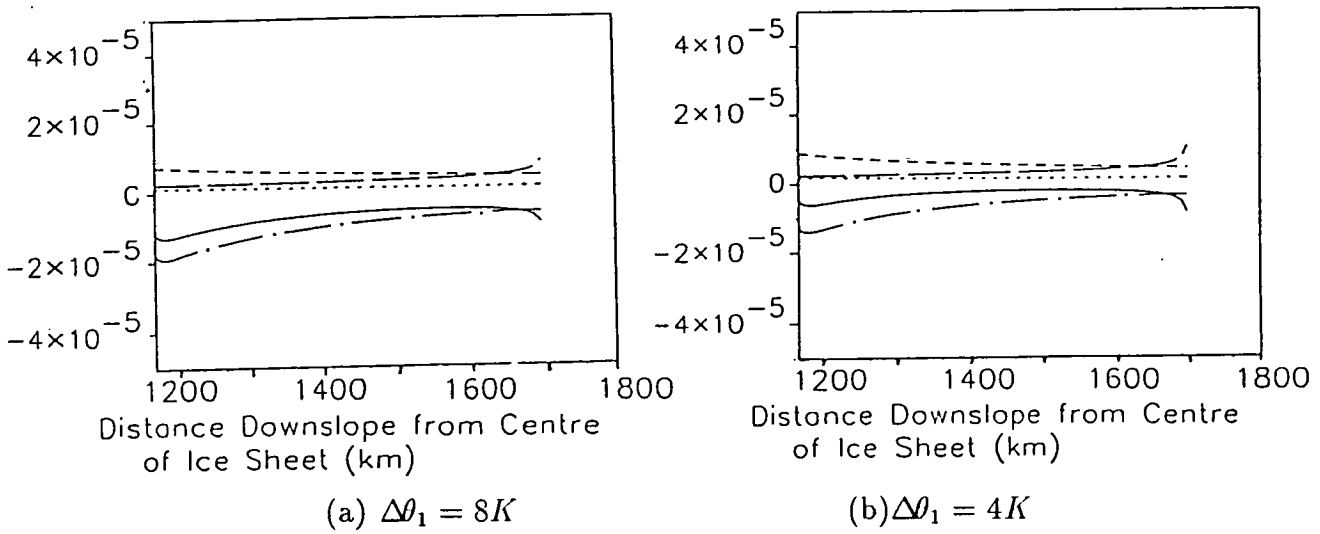

Figure 5.29: The components of the heat budget equation 4.35 for Vg=10; $\frac{d\Delta\theta}{ds}$(———); radiative term(- - - -); temperature gradient along the slope due to stability ($\frac{d\Delta\theta}{dz}sin\alpha$)(— —); ($\frac{d\theta}{dz}S_3E\cos\alpha$)(·····); entrainment term ($\frac{W_e}{hU}$)(— · —).

more significant under these conditions. Using the diffusion equation, the layer remains colder, the surface temperature gradient smaller, and the velocity greater, suggesting a very fast moving, cold layer of air flowing north off the ice sheet. To the south of the Laurentide ice sheet, because the mean flow opposed the direction of geostrophic flow initiated by the presence of ice, the glacial anticyclone may have been weakened absent.

Kutzbach & Wright (1985) discuss the evidence for anticyclonic flow over the Laurentide ice sheet. Evidence of palaeo-wind directions are preserved in sand dunes in the rocks and the distribution of Loess deposits, although it is important to recognise that the geological dune evidence of wind direction may only be recording the strongest winds which are not necessarily the prevailing winds. The geological evidence suggests a northerly to north westerly flow off the southern margin of the Laurentide ice sheet between Montana and Washington state at the time of the glacial maximum. It is uncertain as to whether this represents

the actual orientation of the prevailing palaeo wind field or whether the record has been distorted by the occurrence of less frequent but stronger winds. True anticyclonic flow would have an easterly component. The results of the slab model presented here suggest that with a strong westerly upper air flow, it is likely that the surface anticyclonic drainage flow will be weakened, if not destroyed, resulting in prevailing surface westerlies. Drainage flow may only occur when the strength of the upper jet is reduced. Kutzbach & Wright note more evidence for anticyclonic flow off the margins of the ice sheet during its retreat. It is unclear from the geological evidence whether this indicates an actual increase in anticyclonic flow as the ice sheet retreats, or simply that the evidence for the glacial maximum has been somehow obscurred. The GCM experiments of Shinn & Barron (1989), show a decrease in the strength of the jet over North America and the North Atlantic for a smaller Laurentide ice sheet. If this is the case then the weaker westerly upper flow may allow the anticyclonic, drainage flow to develop, aided by the strong temperature gradient across the margin of the ice, making it possible for a glacial anticyclone to become prevalent as the ice retreats.

The northerly component of the flow at the glacial maximum may not have been drainage flow produced by the boundary layer mechanisms which drive the the slab model, it is possible these apparent drainage winds were the product of the complex dynamics of the air at the ice sheet margin, producing a surface flow with a northerly component. One such mechanism occurs over Antarctica during the summer. Kodama et al (1989) observed that the mesoscale temperature gradient between the cold ice and relatively warm open ocean produces a low level geostrophic wind which operates in a similar manner to the katabatic wind during the polar night. Model simulations of the glacial maximum and paleo-evidence of surface temperatures suggest that there was a very strong horizontal temperature gradient across the margin of the Laurentide ice sheet, which may be expected to

operate in a similar manner. A second mechanism which may induce a northerly component in the surface wind is from the GCM results presented by Kutzbach & Wright (1985). They show a strengthening of the northerly component of the surface winds due to a presence of a jet core over the North Atlantic sea ice margin. The upper level flow at the southern margin of the ice sheet is at the entrance to this jet and therefore accelerating and encouraging southward drift at the surface.

Temperature Deficit. The increase in entrainment with higher values of Vg, implies the air will be more well mixed and possibly a lower value of $\Delta\theta_1$ is appropriate. Fig. 5.30 has been run with $\Delta\theta = 4K$, which as explained in chapter 4 results in a reduction of U. This halves the Richardson number, so entrainment is increased and so is the depth of the boundary layer. It may be expected that an increase in entrainment would also lead to a bigger $\frac{d\Delta\theta}{ds}$ but because the air is mixed into a slightly deeper layer and the temperature discrepancy between the ambient and boundary layer air is much smaller, the effect that entrainment has on the temperature of the boundary layer is less, so surface temperature gradient is reduced, and closer to the DALR.† This is confirmed by fig. 5.29 which shows the components of the temperature equation, 4.35. Thus it is the increase in the size of the component associated with the entrainment, the 4th term on the right hand side of equation 4.35 which dominates the evolution of, and produces the decrease in (increase in negative), $\frac{d\Delta\theta}{ds}$.

The Effect of Geometry

The importance of including some geometry of the ice sheet in the model was clearly shown for the Greenland ice sheet in section 5.3.1. This section looks at the difference between the boundary layer of profile B (figs. 5.23 and 5.24), and

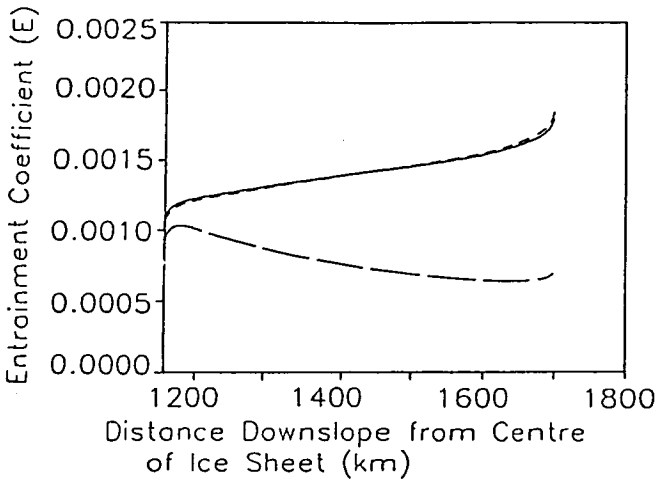

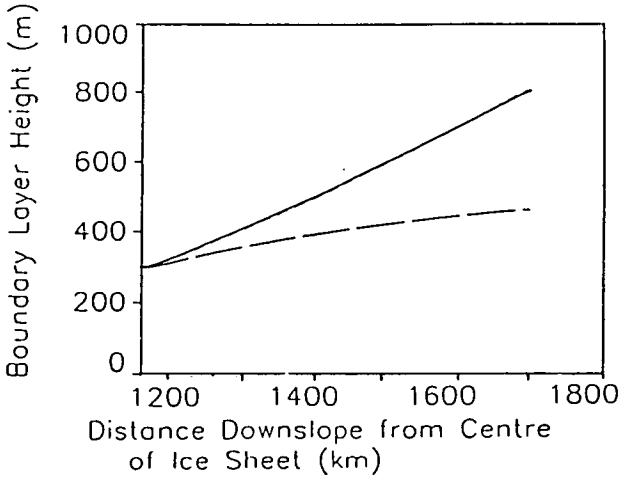

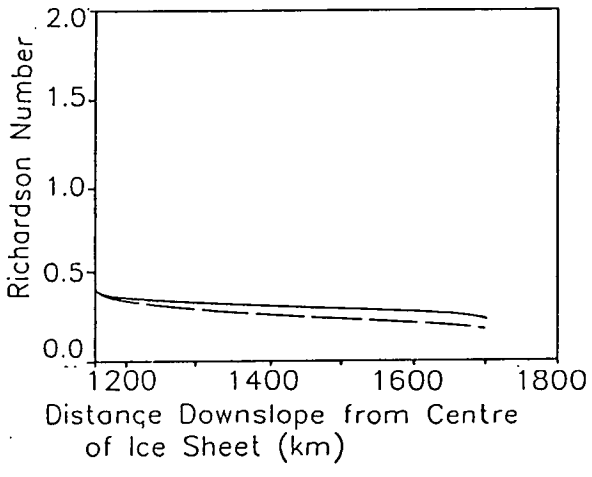

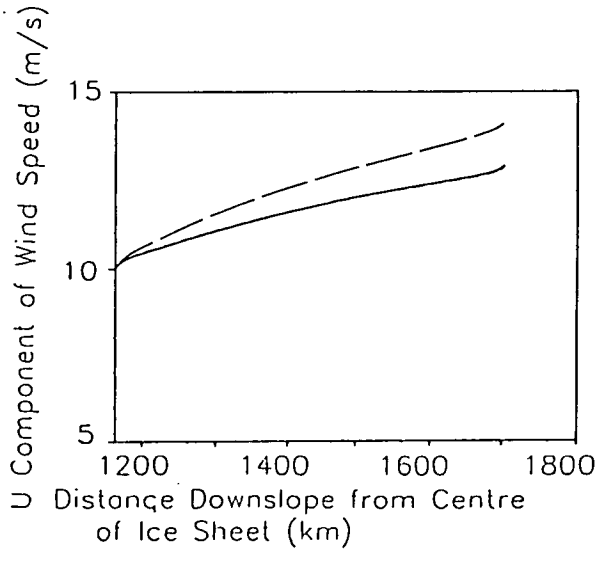

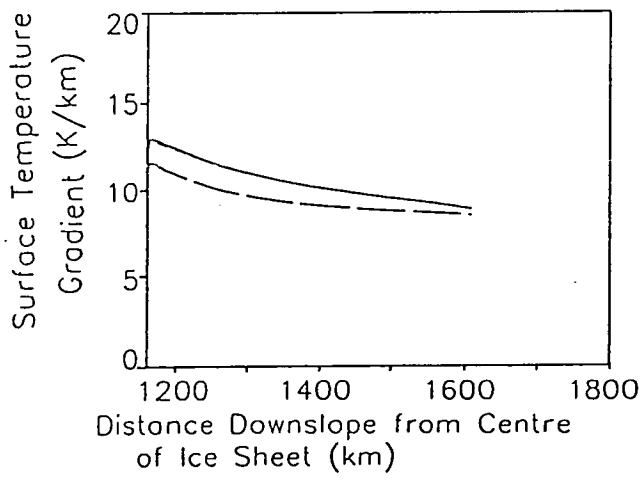

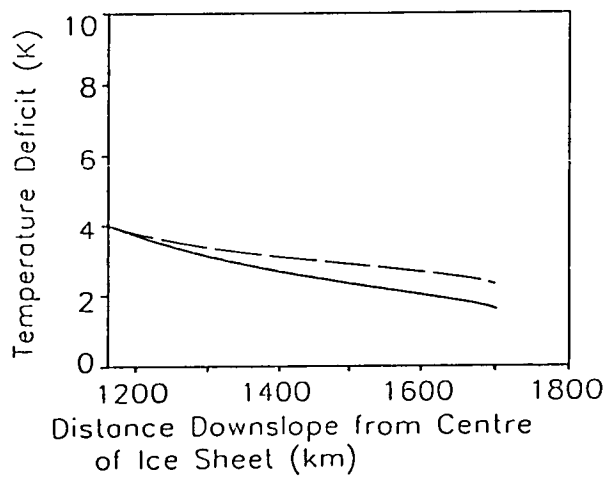

Figure 5.30: The evolution of the boundary layer if $\Delta\theta_1 = 4K$ and $Vg = 10ms^{-1}$: Type ET [$A_c = 0.00025$] (——); Type 1 [$A_e = 0.3$] (- - - -); Type 2 [$K_m\tau_f = 2.16 \times 10^4$] (— — —).

that of a smaller ice sheet. The smaller ice sheet is given a profile using equation 4.11 with a height at the divide† of 3000m, a span of 1000km and a value for n_g of 2.5. The evolution of the boundary layer for the smaller ice sheet is shown in fig. 5.31, results are shown for the type 1 and type 2 entrainment with Vg given values of $3ms^{-1}$and $10ms^{-1}$. The figure can be compared to figs. 5.26 and 5.28. Over the smaller ice sheet the geometric divergence is greater and that the depth of flow is considerably reduced, so the velocity is only slightly increased and the mass flux for the small ice sheet is much smaller. This, combined with a slight increase in entrainment results in a bigger horizontal gradient in the temperature deficit, so that $\Delta\theta$ is similar at both margins, although the air over the smaller ice sheet has travelled a much shorter distance. It is possible that the initial temperature deficit over a smaller ice sheet will be smaller and therefore so will the deficit at the margins, added to the fact that absolute temperatures over a smaller ice sheet are likely to be higher, the results suggest that as the ice sheet retreats the air flowing off the ice sheet becomes warmer which would be expected to enhance melting and retreat of ice. An important factor in the maintenance of high wind speeds, is the steepening of the profile as the ice sheet retreats. If the small ice sheet is given a flatter profile then the acceleration of air is not so great and there is less entrainment of warm air. Therefore it would seem that an ice sheet that steepens as it retreats will induce a positive feedback on ablation.†

5.4 Conclusions

This chapter has looked at experiments with the slab model that was developed in chapter 4. Firstly exploring the prescribed boundary conditions, namely the geostrophic wind speed, the stability of the air and the surface cooling rate, and secondly taking a detailed look at the parameterisation of entrainment, in order to

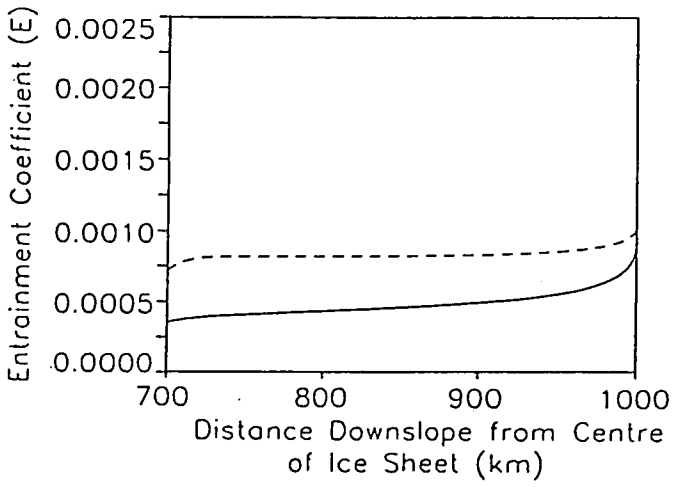

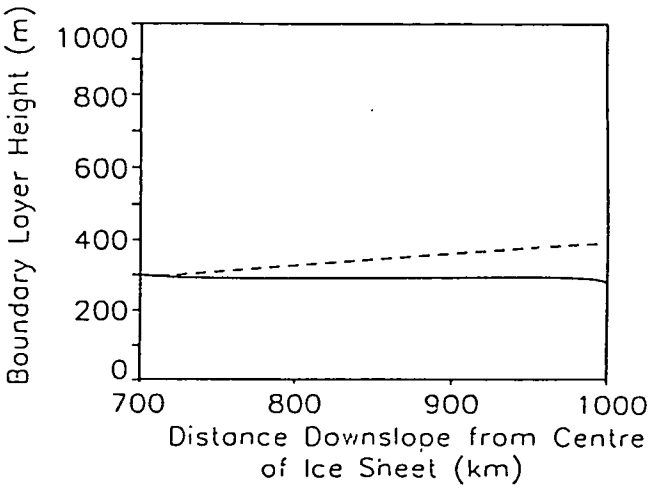

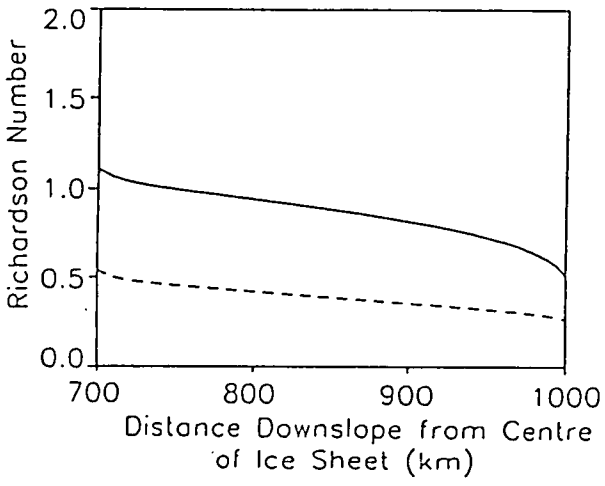

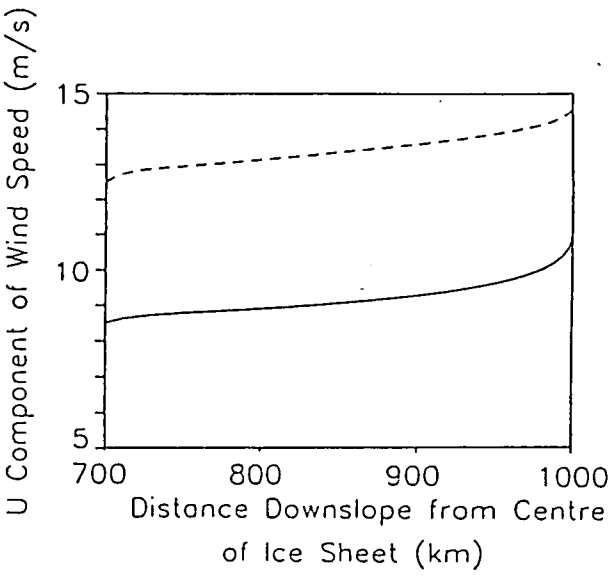

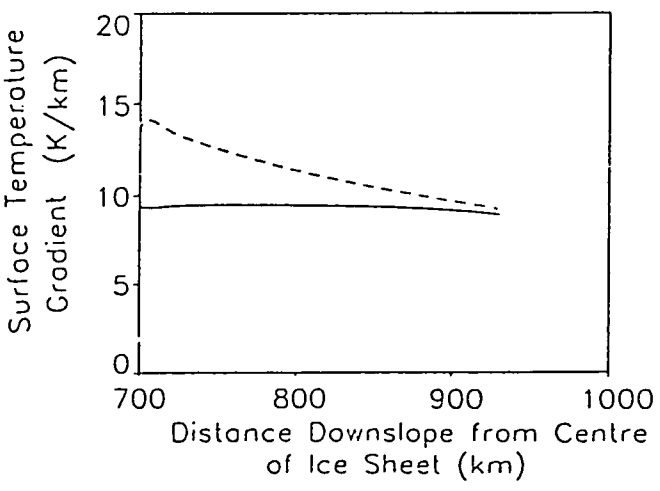

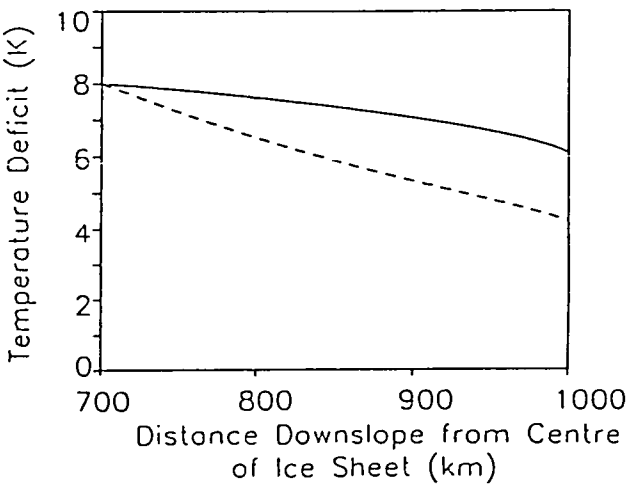

Figure 5.31: The effect of geometry on the boundary layer evolution for the Laurentide ice sheet(n_g=2.5), [h_d = 3000m,span=1000km]:Vg=3ms^{-1}(——); Vg=10ms^{-1}(- - - -).

improve on that used by previous authors. The fixed boundary condition which is most likely to be influenced by the growth of large northern hemisphere ice sheets is the geostrophic wind field. The stability of the air and surface radiation budget may also change but their effect on the boundary layer evolution, as long as drainage flow remains, will be less than the presence of a strong upper jet stream. The orientation of the mean meridional flow, relative to the glacial anticyclone is important in determining the effect of the geostrophic wind. It seems that a slab model is useful when combined with the results of GCM, in order to explain why there may have been no glacial anticyclone at the glacial maximum.

The results of this chapter suggest that the method of parameterising entrainment is unimportant unless there are large increases in geostrophic wind speed. If this occurs the type 2 entrainment which considers the rate of diffusion of TKE to the top of the boundary layer is more sensitive to the change in height of the boundary layer and prevents the b.l from becoming excessively deep. This chapter has shown that the coefficient of 0.002 suggested by Ellison & Turner (1959) and used by Manins & Sawford (1979) is too high for the glacial slopes, and that under conditions which produce excessive acceleration of the layer and very deep boundary layers, the simple inverse Richardson number relationship is an inadequate descriptor of entrainment. In the case of a large ice sheet the acceleration may be a consequence of an enhanced pressure gradient force, given in the geostrophic wind speed of the slab model. Inclusion of the geometry of the ice sheet is also important in preventing the formation of a boundary layer which is too deep over an ice sheet which cannot be approximated to a semi-infinite horizontal slab.

Small ice sheets will have a smaller central plateau and therefore air flowing from the centre will have less time under the dominant influence of radiative cooling

before it accelerates. The depth and strength of the inversion is therefore likely to be less. The rate of reduction ie. the warming rate of the boundary layer depends on the slope of the ice sheet. For a broad flat ice sheet with small slopes the rate of warming will be less due to a reduction in entrainment. Work by Oerlemans & Hoogendoorn (1989) suggests that the effect of global warming on the mass balance† field over Greenland decreases with altitude, this is supported by the findings of Braithwaite & Olesen (1990c) who also state that the ice sheet profile will steepen as it retreats. It would be expected that the acceleration of the air, and increase in entrainment over steeper slopes will lead to a deeper layer of warmer air flowing off the margin of the ice, thus introducing a positive feedback. The dynamics of the atmospheric boundary layer are more important for the ablation zone† so the boundary layer is less likely to be an important component of an advancing ice sheet, when accumulation† and the dynamics of the ice are more important.

5.4.1 Summary

- The geostrophic wind has most influence on the growth of ice compared to other fixed boundary conditions.
- The method of parameterisation of entrainment is unimportant unless the geostrophic wind becomes large, in which case the Type 2 entrainment prevents excessive growth of the boundary layer depth.
- The new parameterisations of entrainment give best results when $A_e = 0.3$ and when $K_m \tau_f = 2.16 \times 10^4$.
- ET type entrainment cannot be extrapolated directly from the results of laboratory experiments to the glacial slopes. Analysis of the Types 1 and

2 entrainment suggest that the losses of TKE are much greater on a scale as large as an ice sheet, therefore the coefficient A_c should be much smaller (0.00025).

- The effect of the boundary layer evolution on the ice sheet will vary according to the ice sheet slope.
- A retreating ice sheet which is steepening, will induce a positive feedback via entrainment of warm air.
- A broad flat ice sheet will tend to be colder due to stagnation of air.
- The effect of the boundary layer on the evolution of the ice, depends on the balance between ice sheet size and topography and the geostrophic wind and radiational cooling, this will be returned to in the final chapter.

Chapter 6

Conclusions

The aim of this thesis was to look at the components of the climate to which an ice sheet is most sensitive, in order to understand the way in which the climate of ice sheet models may be more interactive. The approach taken was to look at the climate over present ice sheets in chapter 2, and use it as a standard with which to compare the climate simulated by models in chapter 3. The findings of these two chapters were then used to look at the climate over ice sheets in more detail, in order to determine the climatic parameters which are most sensitive to the evolution of the ice sheet, and the extent to which these characteristics of the climate feedback, and influence the way in which the ice sheets themselves evolve.

6.1 Main Findings

Chapter 1 reviewed the work to date on the coupling of climate and ice sheets, and the main mechanisms of interaction that have been put forward. The different approaches of climatologists and glaciologists were outlined in order to assess ways

in which research may progress. From the results of ice sheet models it seems that the ice is most sensitive to the climate in the ablation zone. Ablation is dominated by boundary layer processes, yet few studies by climatologists have looked at the nature of the boundary layer in the ablation zone. In chapter 2 the sparse distribution of observations over ice sheets became apparent. This leads to large gaps in our understanding of the climate over ice sheets. However, it is still possible to produce an overview of the climate, which although not ideal, is able to provide boundary conditions and verification for models which can be used to understand more about the dynamics of the climate. A brief look at the simulations from GCM's in chapter 3, showed that their resolution is a major limitation to providing any detailed boundary conditions for ice sheet models. They extend up to the top of the atmosphere with 9 or 11 layers and are unable to model the boundary layer processes with sufficient accuracy to produce a realistic surface climate, which determines ablation. The main problem of GCM's seemed to be in the radiation scheme and parameterisation of clouds which, having been developed for the cloud and radiation typical of the whole globe is not appropriate over ice sheets. Details of cloud and radiation balance over ice sheets are still largely unknown due to a lack of data, although advances in satellite technology are changing this.

Chapters 4 and 5 looked at the climate of the ablation zone more closely. A slab model of the atmospheric boundary layer over an ice sheet was used to investigate the way in which temperature, wind speed, surface temperature gradient and depth of the boundary layer respond to different ice sheets. The results were used to predict the way this may feedback to affect the evolution of the ice.

6.1.1 Model Findings

Sensitivity studies showed the model to be relatively insensitive to the model parameters, the profile factors S_1, S_2 and S_3. The coriolis force is an important component of the velocity evolution in the boundary layer, requiring the resolution of flow perpendicular to the slope as well as parallel to the maximum slope. However, in order to maintain downslope flow, a large drag coefficient is required for the V component of the flow. This is necessary because additional retarding forces may be acting on the flow in this direction at a wide variety of spatial scales. These may be accounted for by any one, or a combination of, the following factors.

(i) Assuming a semi infinite slab in the y direction does not allow for the pressure variations which occur in this direction (personal communication Gosink 1991). Over Antarctica these are mainly initiated by the Trans Antarctic Mountains, and also by smaller cross-valley undulations.

(ii) Gravity waves which may be topographically induced have been observed to retard the flow over Antarctica (Mobbs & Rees 1989).

(iii) At a much smaller scale, sastrugi orientated in the direction of prevailing flow, cause additional roughness of the surface perpendicular to their lineation; they may be of the order of 5m in size, which could impose a significant drag force on the flow.

Sensitivity to Climatic Boundary Conditions

The sensitivity of the model to climatic boundary conditions varies. The model is generally insensitive to the radiative cooling rate, and the stability of the atmosphere has a retarding influence on the flow. The boundary condition most likely

to vary over a large ice sheet to the extent it significantly affects the boundary layer evolution, is the geostrophic wind. The presence of an ice sheet cools the lower atmosphere leading to subsidence and a glacial anticyclone, with a pressure gradient force which reinforces the downslope flow. In this model the pressure gradient force is included as the geostrophic wind above the boundary layer. It was shown in chapter 2, that the geostrophic wind is important for the maintenance of consistent downslope flow. The experiments of chapter 5 showed that the stronger the geostrophic wind (in the positive y direction), the faster and deeper the boundary layer flow. In certain circumstances the geostrophic wind due to the mean meridional pressure field, superimposed on the glacial anticyclone, may disrupt the anticyclonic geostrophic flow. In the present day this occurs over Greenland where the jet stream has an east-west component over the ice sheet. Therefore when the zonal flow is strong, the drainage flow is destroyed on the western slopes, but may be reinforced on the east, producing cold air outbreaks in the Denmark Strait. In chapter 5 this was shown to be important for past ice sheets, located in the mid-high latitudes of the northern hemisphere. GCM simulations of the Laurentide ice sheet (eg. Shinn & Barron 1989), show that the strength of the mid latitude jet stream, originating from the mean meridional temperature gradient, varied as the ice sheet grew. Over the southern margin of the ice the jet stream opposed the anticyclonic flow of the glacial anticyclone and it is therefore likely to have weakened the drainage flow in this region. At the northern margin however, an east-west jet stream reinforces the downslope flow.

Sensitivity to Ice Sheet Boundary Conditions

The model was used in chapter 5 to look at the way in which the shape of the ice sheet affects the evolution of the boundary layer. The results showed the slope

of the ice sheet to be important, and to a lesser extent the geometry of the ice sheet, depending on whether the ice forms a semi-inifinite slab or a dome. As a dome shaped ice sheet becomes smaller, the slopes tend to increase more rapidly, producing higher wind speeds in the boundary layer, and more entrainment in order to compensate for the additional divergence of flow over a smaller dome.

Work by Braithwaite & Olesen (1990c) and Oerlemans & Hoogendoorn (1989) suggests that the Greenland ice sheet is becoming steeper as it retreats, and that the largest changes in mass balance occur at the margin; the radiation balance and accumulation at higher elevations is relatively unchanged. Experiments with this slab model carried out in chapter 5, suggest that under these conditions, the velocity of the boundary layer will increase with the additional buoyancy force on the slopes; this will lead to more entrainment and a deeper, warmer boundary layer, with a surface temperature gradient above the dry adiabatic lapse rate. In this manner the retreat of ice may be enhanced due to the positive feedback, via increased entrainment. The following experiments investigate this further.

Fig. 6.1 shows the effect on the boundary layer of ice sheets which are successively smaller but maintaining a constant profile, defined by;

$$\left(\frac{H_i}{h_d}\right)^2 = \left(1 - \frac{x}{s_p}\right) \tag{6.65}$$

where H_i is the height of the ice, h_d the height of ice sheet at the divide, x the distance from the centre of the ice sheet, and s_p the span of the ice sheet. The values of h_d and s_p are changed for each profile in fig. 6.1, so that for profile 1, $h_d = 2.4km$ and $s_p = 500km$, for profile 2, $h_d = 1.75km$ and $s_p = 360km$ and for profile 3, $h_d = 215km$ and $s_p = 125km$. The boundary conditions are the same as those used in section 5.3.2, with only the surface profile changed in each instance. The initial depth is taken to be the same in each case (110km), since the profiles at the centre are almost identical; differences in the boundary layer development

are therefore only noticeable as the air begins to flow downslope. As explained above, over a smaller ice sheet the slopes become large much more rapidly, and the figure shows the boundary layer becoming faster and warmer in response to this. The geometry of the dome shaped ice sheet is important in preventing the boundary layer becoming too deep, but as shown in fig. 6.2, the effect is only large near the centre of the ice sheet and therefore does not vary significantly as the ice sheet shrinks from 500km to 215km radius. These results show that a retreat of an ice sheet without a steepening of the profile is sufficient to warm the boundary layer, such that for profile 3, the temperature deficit decreases from 6K to 2K in 100km, compared to a similar decrease over 400km for the larger ice sheet of profile 1 (fig. 6.1a). Over a smaller ice sheet, it is likely that absolute temperatures will be warmer, increasing the significance of the warming, since it is more likely to exceed 0°C. The divergence of the curves in the evolution of the temperature deficit shows that the extent of warming increases downslope, since this is where entrainment is greatest. This is consistent with the findings of Braithwaite & Olesen (1990c), that ablation increases most at low elevations; a process which leads to a steepening of the profile which will enhance the process yet further, as explained in the following section.

Fig. 6.3 shows the effect of a change in slope of the profile. The profiles are defined by equation 6.65. Profile 1 is as in fig. 6.1, for profile 4, $h_d = 1.75km$ and $s_p = 500km$ and profile 5, $h_d = 1.25km$ and $s_p = 500km$. As the profile becomes flatter, the boundary layer becomes shallower, slower and colder. Fig. 6.3a shows a difference of over 2K betweeen the temperature deficit at the margin of profile 1, compared to that of profile 5, for both types of entrainment. If the ice sheet is very flat, so that the flow is slow, then the temperature deficit associated with profile 5, shows that the radiation regime begins to dominate the temperature evolution. The figure shows an increase in the temperature deficit of the boundary layer, but

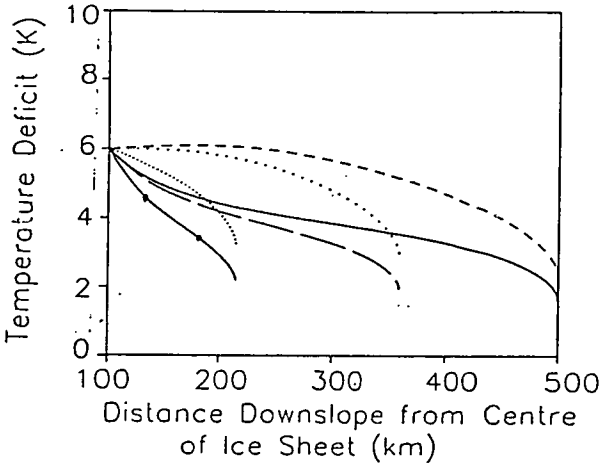

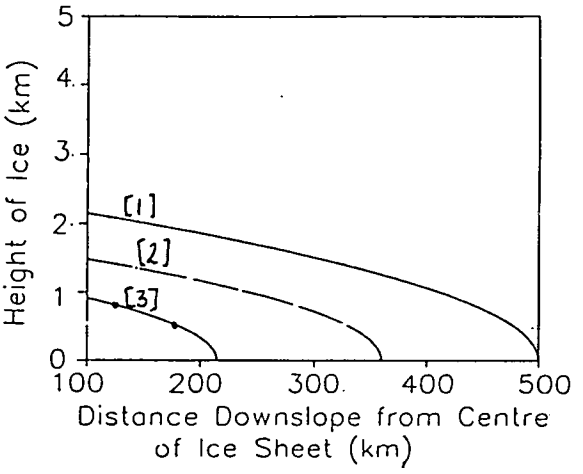

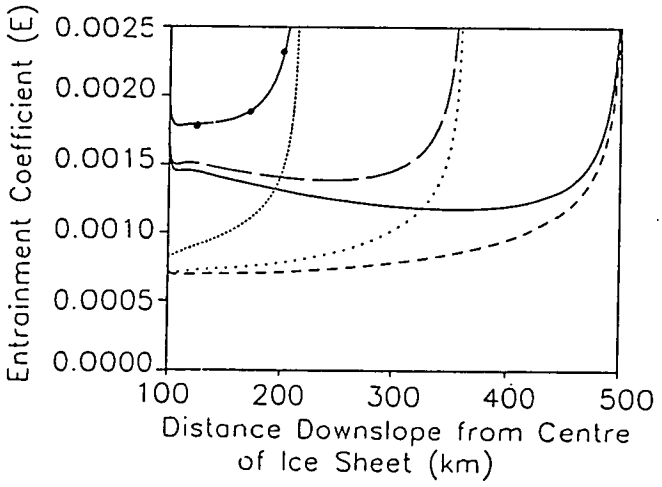

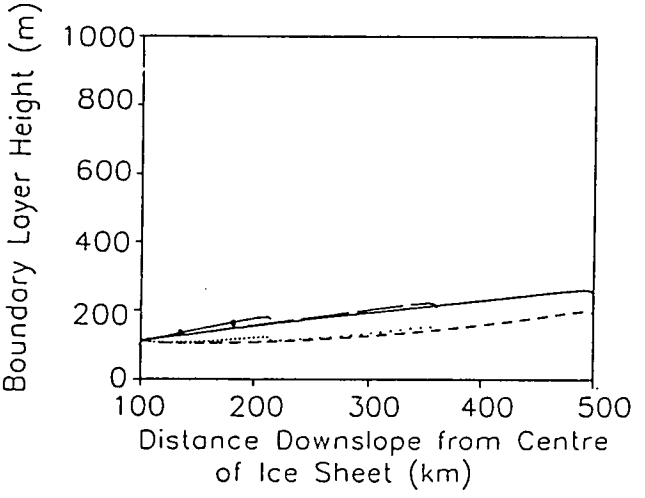

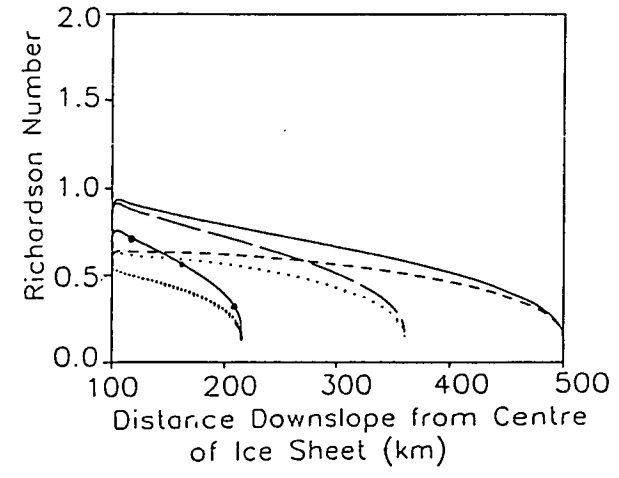

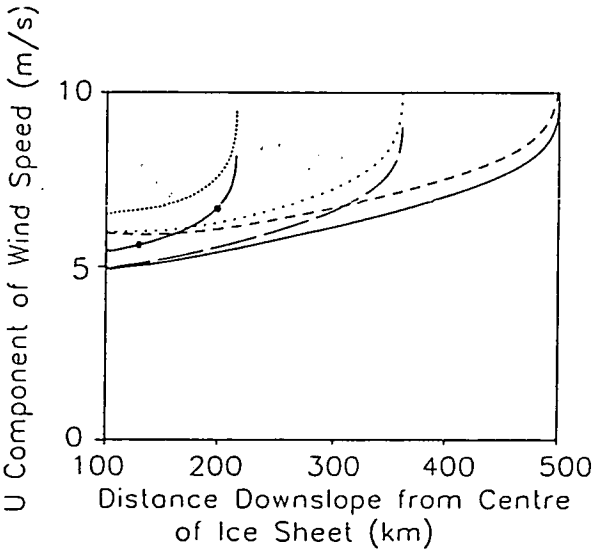

but the same profile. [numbers in square brackets indicate profile number from the text]: Type 1 entrainment ($A_e = 0.3$); [1](- - - -); [2](·····); [3](———); Type 2 entrainment ($K_m \tau_f = 2.16 \times 10^4$); [1](———); [2](— —); [3](—•—•—).

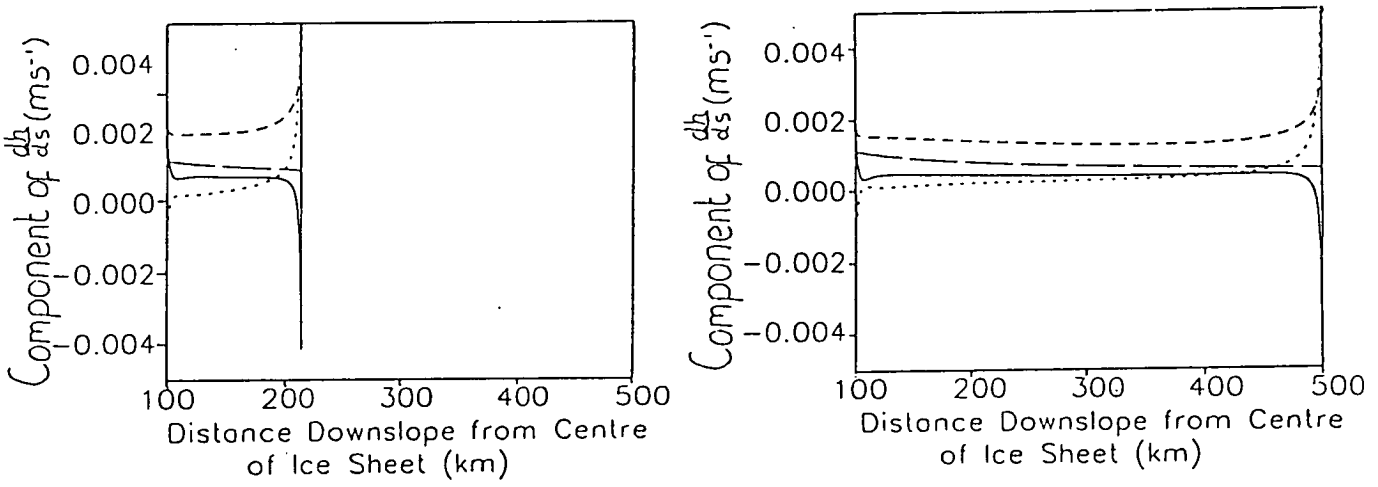

Figure 6.2: The depth evolution of the boundary layer for the small and large profiles shown in fig. 6.1. $\frac{dh}{ds}$(———);entrainment(- - - -). geometry (— —); acceleration (-------) Type 2 entrainment $K_m\tau_f = 2.15 \times 10^4$.

this may arise because the cooling is prescribed to be constant in the model. In order to investigate this further, requires a more sophisticated radiation scheme such as could be provided by a semi-interactive grey body model responding to changes in boundary layer depth. The evolution of a flat ice sheet as shown in fig. 6.3, requires a deformable bed, and may occur where the ice sheet lies over tills. It is unlikely that a large continental ice sheet will rest exclusively on a deformable bed, more commonly the centre of the ice sheet overlies solid bedrock which acts as an undeformable bed. The Laurentide ice sheet is likely to have been such a mixed bed, producing lobes as shown in fig. 6.4 where the bed becomes softer. In this instance the boundary layer would develop over the initial steep slopes but air would then stagnate over the lobe. Here the radiation budget will dominate boundary layer evolution, until the air finally flows off the margin. The effect of this on the ice sheet evolution would vary with location. If the ice sheet is far north, the net radiation budget is likely to be negative, but the further south, the more positive the radiation budget, which will lead to melting of ice. It is possible

that at some point, once the radiation budget is sufficiently large, retreat will be initiated causing removal of the lobe, accompanied by steepening of the slopes which will enhance retreat. The actual effect would depend on the comparative timescales of ablation and advection of ice into the ablation zone.

Entrainment

The response of the boundary layer to changes in boundary conditions, imposed either from the climate, or the shape of the ice sheet is to a large extent dependent on the parameterisation of entrainment. This determines the amount of warm air from above that is incorporated in the boundary layer, and therefore affects the depth, temperature and velocity of the flow. Chapter 5 looked at two new parameterisations of entrainment, to use as an alternative to the empirical relation derived in the laboratory by Ellison & Turner (1959). The first parameterisation solved the TKE budget for the whole of the boundary layer, following a similar method to that derived by Stull (1976a). The final equation is similar to that of Ellison & Turner (1959), but with smaller coefficients related to boundary layer characteristics. The second parameterisation considered the rate of diffusion of TKE through the boundary layer becoming available in the entrainment zone. This is a new parameterisation for the shear generation of turbulence, adapted from the principle put forward by Curran (1975). This parameterisation has an exponential dependence on boundary layer height, and therefore responds much more quickly to changes in depth of the boundary layer. Experiments with the parameterisation suggest that caution is required when applying laboratory derived parameterisations to the larger scale climate. Both new parameterisations suggest that the coefficients of Ellison & Turner are too high, resulting in boundary layers which are too deep. This problem was also noted by Gosink (1989)

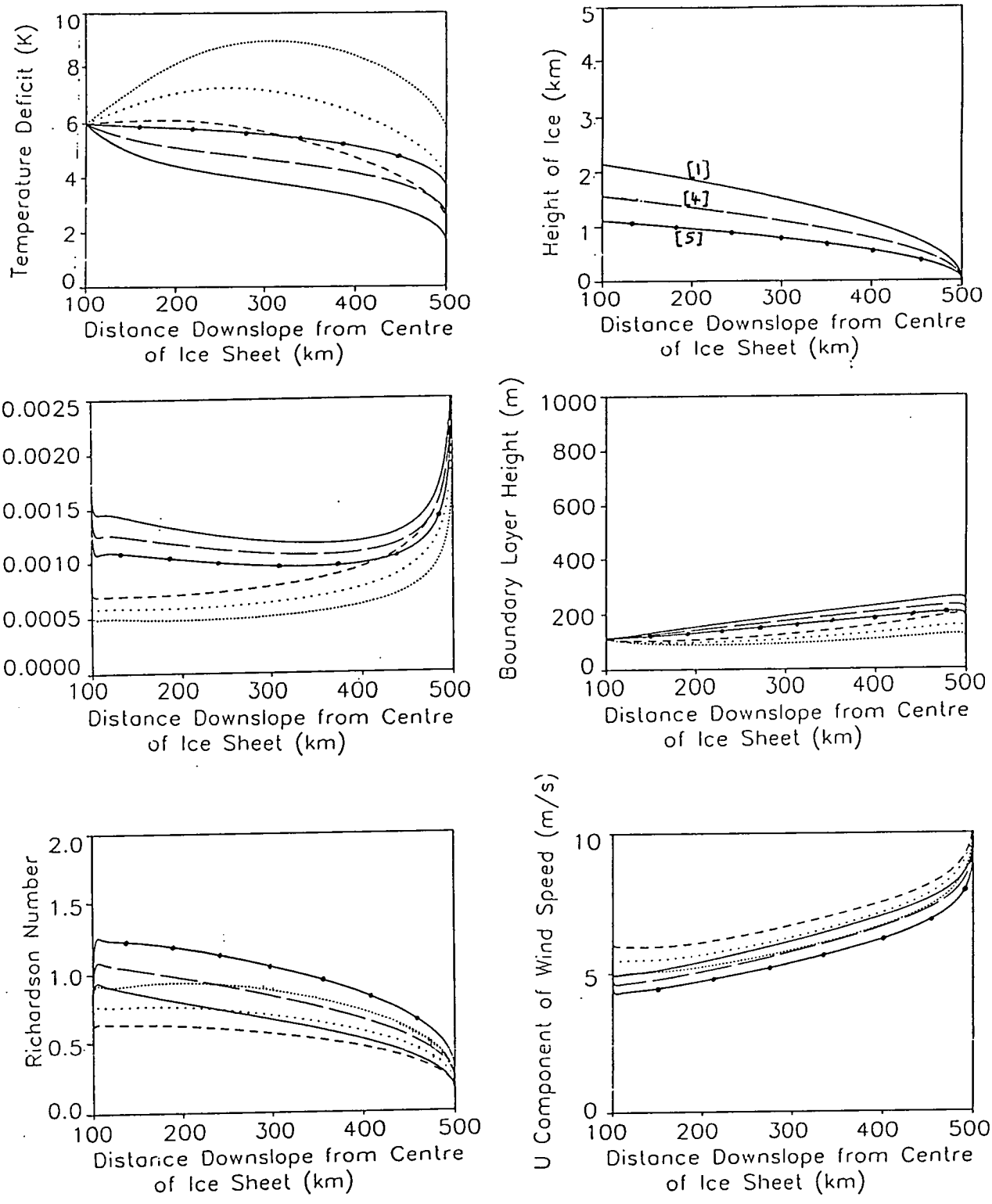

Figure 6.3: The evolution of the boundary layer for ice sheets of a deformable bed, producing ice sheets of the same size but different profiles. [Numbers in square brackets indicate profile number from text]: Type 1 entrainment $A_e = 0.3$; [1](- - - -); [4](·····);[5](——·——); Type 2 entrainment $K_m \tau_f = 2.16 \times 10^4$; [1](———); [4](— — —); [5](—•—•—).

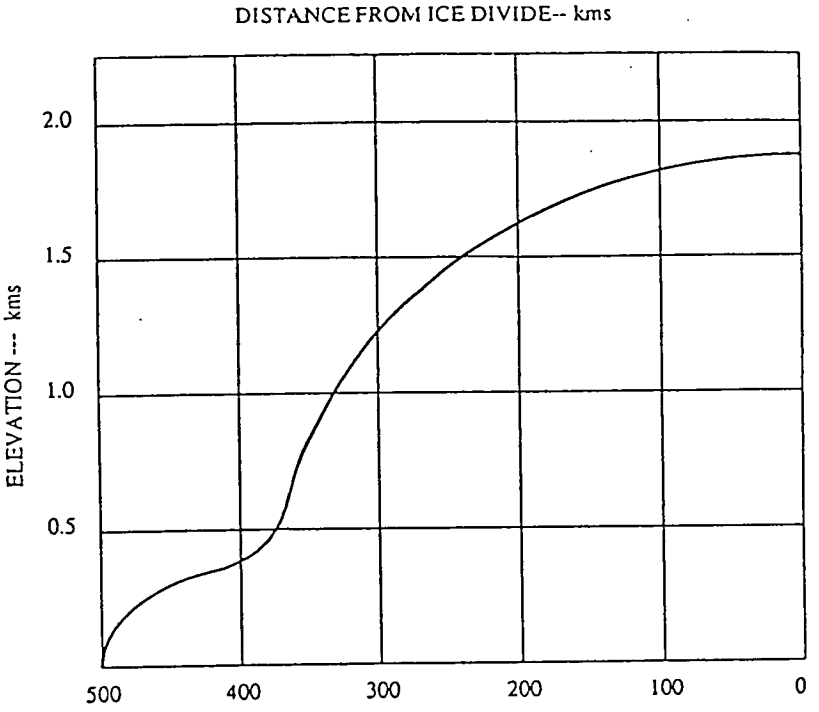

Figure 6.4: The shape of an ice sheet formed over a mixed deformable and non-deformable bed.

and Lalaurette & Andre (1985). It seems that the loss of turbulent kinetic energy from the boundary layer is much greater on a larger scale, than from small scale experiments in the laboratory, but it is uncertain whether this is due to additional dissipation or storage in gravity waves; Randall (1984) suggests that the loss term should have an inverse dependence on Richardson number in order to account for storage in gravity waves. To be more specific, further model investigations in combination with the aquisition of experimental data are required. If the coefficients of Ellison & Turner are reduced, there is little difference in the parameterisations unless there are conditions which cause large changes in the depth of the boundary layer. In chapter 5 it was shown that this may occur if the geostrophic wind speed increases by a large amount. This causes an enhanced flow speed which increases the amount of entrainment. If the other components of the depth evolution remain relatively unchanged, such that there is no change in the geometry of the ice sheet or the acceleration of the flow, the ET and type 1 entrainment produce boundary layers which are much deeper than that of the type 2 entrainment which has greater ability to stabilise boundary layer depth. Following on

from this, it would be expected that if other components of the depth evolution change then the method of parameterisation is again important. In figs. 6.1 & 6.3, as the ice sheet becomes smaller, or the slopes become greater, the acceleration of air increases, shown by the divergence of the curves in fig. 6.1f and the convergence of the profiles in fig. 6.3f. When air accelerates, the boundary layer becomes more shallow; in this case the type 2 entrainment, which tends to offset changes in boundary layer depth, maintains a deeper and slower boundary layer than the ET or type 1 entrainment, which are less able to respond to compensate for changes in the components of the depth evolution. As seen from the figs. 6.1 & 6.3 the increase in depth at the margin is between 50 and 100m and the decrease in velocity associated with the type 2 entrainment is around $0.5ms^{-1}$; this results in a boundary layer which is over 1°C warmer for the type 2 entrainment at the margins (fig. 6.1a and fig. 6.3a). This is a significant amount in terms of ablation if the temperatures are fluctuating around freezing.

6.2 Future Work

This thesis has shown that the evolution of ice is influenced by a complex interplay between the boundary layer evolution and entrainment, the radiation budget, ice sheet shape and the overriding pressure gradient force signified by the geostrophic wind. As an ice sheet grows, it tends to produce a strengthening in the jet stream. For the northern flanks of the Laurentide ice sheet, this would enhance the downslope drainage of cold air, spilling out into the Polar Basin and Davis Strait. This air would encourage cyclogenesis at the margins as it undercuts the relatively warm air. This may have acted to feed the ice sheet as it advanced. On the southern flanks the geostrophic wind opposed the anticyclonic drainage flow, although the presence of a jet core over the SE margin and the Atlantic may

have encouraged some southward drift of air (Kutzbach & Wright 1985), enhanced by a large temperature gradient across the margin. In this region the ice would be subject to the influence of air advected from elsewhere, the encroachment of cyclones over the ice more frequent and as the ice sheet moved further south an increased tendancy to be affected by warm air masses, which may have ultimately played a role in the ice retreat.

The experiments of Shinn & Barron (1989) show a weakening of the geostrophic wind associated with the mean meridional pressure field as the ice sheet retreats. Over the southern flanks of the Laurentide ice sheet this means that there would be less opposition in the larger scale climate to the development of a glacial anticyclone, so that the pressure field of the ice sheet would dominate the region allowing drainage flow to prevail. The rate of retreat of the ice then would depend on the shape of the ice sheet which will vary according to the bed and surface temperature gradient. A deformable bed or low surface temperature gradient ($< 1°C100m^{-1}$), produces a flat ice sheet over which the atmospheric boundary layer will be slow moving and the radiation balance will dominate the ablation. A solid bed, or a high surface temperature gradient ($> 1°C100m^{-1}$) however, will tend to produce an ice sheet with steeper slopes, which will encourage the development of a more fast flowing, deeper and warmer boundary layer, which may in turn enhance the steepening process as the entrainment, and therefore the warming is greatest at the foot of the ice. In this way the boundary layer development may act as a positive feedback on the ice retreat.

Further work is required in order to look at the interplay between geostrophic wind, boundary layer development and ice sheet shape. The work of glaciologists suggest that ablation is an important component of the climate. This work shows the boundary layer development to be an important consideration for ablation

and that the climatic boundary conditions imposed on ice sheet models, of either an idealised climate surface, or an energy balance model which does not allow for the entrainment of warm air into the boundary layer, are not adequate predictors alone for ablation. Work in the future should be concentrated in two areas.

(i) The development of models should consider constructing a simple model of the boundary layer climate to predict ablation which can be run in conjunction with an ice sheet model. The model could be 'switched on' at specific intervals in the ice sheet evolution and used to provide an ablation function with which to drive the ice sheet. The atmospheric model should incorporate entrainment, the geostrophic wind and a grey body radiation scheme.

(ii) The aquisition of more reliable data over ice sheets is required in order to verify the models. For the large scale climate this should include radiation budgets and cloud cover. Observations of the boundary layer evolution at intervals along the glacial slopes are also needed. These would ideally include observations of boundary layer depth, temperature structure, wind speed and turbulence, this would allow a more reliable assessment of the parameterisations of entrainment and which scheme represents the actual case most closely.

The work presented in this thesis has drawn together the ideas of climatologists and glaciologists and provided a basis for further study, through both modelling and fieldwork. By accepting that fully coupled models of climate and ice sheets are unrealistic, given the complicated nature of the ice-atmosphere system, the disparate timescales of the atmosphere and ice, and limited computer power, this thesis has aimed to determine the climatic parameters which are most important to include when providing mass balance conditions to drive an ice sheet model.

Bibliography

[1] Ambach, W (1979): Zum Wärmehaushalt des Grönländischen Inlandeises: Vergleichende studie im akkumulations - und ablationsgebiet. (Radiation Budget of Greenland Ice Sheet; comparitive study in areas of accumulation and ablation) *Polarforschung,* **49**, 44-54.

[2] Ambach, W (1989): Effects of climatic peturbations on the surface ablation regime of the Greenland ice sheet, West Greenland. *J. Glaciology,* **35**(121), 311-316.

[3] Andre, J.C et al (1978): Modelling the 24-hour evolution of the mean and turbulent structures of the planetary boundary layer. *J. Atmos. Sci.,* **35**, 1861-1883.

[4] Bader, H (1961): The Greenland Ice Sheet. *U.S Army CRREL,* **I-B2**.

[5] Ball, F.K (1956): The theory of strong katabatic winds. *Aust. J. Phys.,* **9**, 373-386.

[6] Benson, C.S (1962): Stratigraphic studies in the snow and firn of the Greenland ice sheet. *U.S Army Snow and Ice and Permafrost Research Establishment. Corps of Engineers.* Research Report 70.

[7] Bindschadler, R.A & H.J Zwally (1989): Surface topography of the Greenland ice sheet from satellite radar altimetry. *NASA Goddard Space Flight*

Center NASA SP:503.

[8] Braithwaite, R.J & O.B Olesen (1990a): Response of the energy balance on the margin of the Greenland ice sheet to temeperature changes. *J. Glaciology,* **36**(123), 217-221.

[9] Braithwaite, R.J & O.B Olesen (1990b): A simple energy balance model to calculate ice ablation at the margin of the Greenland ice sheet. *J. Glaciology,* **36**(123), 222-228.

[10] Braithwaite, R.J & O.B Olesen (1990c): Increased ablation at the margin of the Greenland ice sheet under a greenhouse effect climate. *Annals of Glaciology (IGS),* **14**, 20-22.

[11] Broecker, S & G.H Denton (1990): What Drives Glacial Cycles? *Sci. Am.,* **262**(1), 43-50.

[12] Brost, R.A & J.C Wyngaard (1978): A model study of the stably stratified planetary boundary layer. *J. Atmos. Sci.,* **35**, 1427-1440.

[13] Budd, W.F & I.N Smith (1979): The growth and retreat of ice sheets in response to orbital radiation changes. *Proc. of Canberra Symposium, Sea level and climate change convention. Dec 1979.*

[14] Carson, D.J (1973): The development of a dry inversion-capped convectively unstable boundary layer. *Q.J. Roy. Met. Soc.,* **99**, 450-467.

[15] Cattle, H & D.L Roberts (1988): The performance of atmospheric circulation models in polar regions. *In: Report of the 3rd session of the working group on sea-ice and climate, Oslo, 31 May - 3 June 1988, WMO/ICSU/WMO.* Report No. 5 WMO/TD/272, or WCRP 18.

[16] Clarke, R.H (1970): Observational studies in the atmospheric boundary layer. *Q.J Roy. Met. Soc.*, **96**, 91-114.

[17] Curran, J (1975): Physiological and synoptic-scale influences on diurnal humidity variations over vegetation. *PhD Thesis, Dept Meterology, University of Edinburgh.*

[18] Dalrymple, P.C (1966): A physical climatology of the Antarctic Plateau. *In: Studies in Antarctic Meterology, M.J Rubin (ed.) Antarctic Research Series, American Geophysical Union.* **19**, 195-231.

[19] Dalrymple et al (1966) South Pole Micrometerology Program: data analysis. *In: Studies in Antarctic Meterology, M.J Rubin (ed.) Antarctic Research Series, American Geophysical Union.* **19**, 13-57.

[20] Denton, G.H & T Hughes (1981): The Last Great Ice Sheets. *John Wiley & Sons, New York.*

[21] Diamond, M (1960): Air temperature and precipitation on the Greenland ice sheet. *J. Glaciology,* **3**(27), 558-567.

[22] Drewry, D.J (1983): The surface of the Antarctic ice sheet. *Sheet 2 of: Antarctica: Glaciological and Geophysical folio. D.J. Drewry (ed.), Scott Polar Research Institute, Cambridge.*

[23] Driedonks, A.G.M & H. Tennekes (1984): Entrainment effects in the well mixed atmospheric boundary layer. *Bound. Lay. Met.,* **30**, 75-105.

[24] Ellison, T.H & J.S Turner (1959): Turbulent entrainment in stratified flows. *J. Fluid. Mech.,* 6, 423-448.

[25] Fortuin, J.P.F & J. Oerlemans (1990): Parameterisation of surface temperature and mass balance of Antarctica. *Annals of Glaciology, (IGS)* **14**, 78-84.

[26] Glen, J.W (1955): The creep of polycrystalline ice. *Proc. Roy. Soc. London. Set A.* **1175** 519-538.

[27] Gosink, J.P (1982): Measurement of katabatic winds between Dome C and Dumont d'Urville. *Pure & Appl. Geophys.*, **120**, 503-526.

[28] Gosink, J.P (1989): The extension of a density current mdoel of katabatic winds to include the effects of blowing snow and sublimation. *Bound. Lay. Met.*, **49**, 367-394.

[29] Hays, J.D et al (1976): Variations in the earths orbit: Pacemaker of the ice ages. *Science*, **194**, 1121-1132.

[30] Henderson-Sellers, A & K. McGuffie (1987): A Climate Modelling Primer. *Research and developments in climate and climatology series, John Wiley & Sons Ltd.* 217pp.

[31] Hindmarsh, R.A et al (1989): Modes of operation of thermomechanically coupled ice sheets. *Annals of Glaciology, (IGS).* **12**, 57-69.

[32] Hyde, W.T & W.R Peltier (1985): Sensitivity experiments with a model of the ice age cycle: The response to harmonic forcing. *J. Atmos. Sci.*, **42**(20), 2170-2188.

[33] Imbrie, J.N et al (1984): The orbital theory of Pleistocene climate: support froma revised chronology of $\delta^{18}O$ record. *In: Milankovitch and Climate, A. Berger (ed.)* **1**.

[34] Inoue, J. (1989a): Surface drag over the snow surface of the Antarctic Plateau. 1. Factors controlling surface drag over the katabatic wind region. *J. Geophys. Res.*, **94**(D2), 2207-2217.

[35] Inoue, J. (1989b): Surface drag over the snow surface of the Antarctic Plateau. 2. Seasonal change of surface drag in the katabatic wind region. *J. Geophys. Res.*, **94**(D2), 2219-2224.

[36] James, I.N (1989): The Antarctic drainage flow implications for the hemispheric flow on the southern hemisphere. *Antarctic Science,* **3**, 279-290.

[37] Kodama, Y et al (1989): The diurnal variation of the boundary layer in summer in Adelie Land, East Antarctica. *J. App. Met.*, **28**(1), 16-24.

[38] Kutzbach, J.E & P.J Guetter (1986): The influence of changing orbital parameters and surface boundary conditions on climate simulations for the past 18000 years. *J. Atmos. Sci.*, **43**(16), 1726-1759.

[39] Kutzbach, J.E & H.E Wright (1985): Simulation of the climate of 18,000 years B.P: Results for the North American/ North Atlantic/ North European Sector and comparison with the geologic record of North America. *Quat. Sci. Rev.*, **4**, 147-187.

[40] Lalaurette, F & J.C Andre (1985): On the integral modelling of katabatic flows. *Bound. Lay. Met.*, **33**, 135-149.

[41] Langway, C.C. Jr. (1959): Accumulation and temperature on the inland ice of Northern Greenland. *J. Glaciology,* **3**(30), 1017-1044.

[42] Letregully, A. et al (1991): Steady state characteristics of the Greenland ice sheet under different climates. *J. Glaciology,* **37**(125), 149-157.

[43] Lettau, H.H (1966): A case study of katabatic flow on the South Polar Plateau. *In: Studies in Antarctic Meteorology, Antarctic Research Series, Rubin (ed.),* **9**.

[44] Lettau, H.and W. Schwerdfeger (1967): Dynamics of the Surface-Wind regime over the interior of Antarctica. *Antarctic Journal of the U.S,* **2**(5), 155-158.

[45] Lettau H.H et al (1977): Air temperature and two dimensional wind profiles in the lowest 32 meters as a function of bulk stability. *In: Meteorological studies at Plateau Station Antarctica, Paper 6 Antarctic Research Series,* **25,** 77-91.

[46] Lindeman, M & J. Oerlemans (1987): Northern hemisphere ice sheets and planetary waves - a strong feedback mechanism. *J. Clim.,* **7**(2), 109-117.

[47] Manabe, S & A.J Broccoli (1985): The influence of continental ice sheets on the climate of an ice age. *J. Geophys. Res.,* **90(D1)**, 2167-2190.

[48] Manins, P.C & B.L Sawford (1979): A model of katabatic winds/ *J. Atmos. Sci.,* **36**, 619-630.

[49] Manins, P.C & J.S Turner (1978): The relation between the flux ratio and energy ratio in convectively mixed layers. *Q.J Roy. Met. Soc.,* **104**, 39-44.

[50] Mather, K.B & G.S Miller (1967): Notes on the topographical factors affecting the surface in Antarctica, with special reference to katabatic winds; and bibliography. *Technical Report, University of Alaska,* UAG-R-189.

[51] McEwan, A.D (1983): Internal mixing in stratified fluids. *J. Fluid Mech.,* **128**, 59-80.

[52] Mitchell, J.F.B et al (1988): Climate simulations for 9000 years B.P: Seasonal variations and effect of the Laurentide ice sheet. *J. Geophys. Res.,* **93**(D7), 8283-8303.

[53] Mobbs, S.D and J.M Rees (1989): Studies of atmospheric internal gravity waves at Hadley station Antarctica, using radiosondes. *Antarctic Science,* **1**, 65-75.

[54] North, G.R et al (1981): Energy Balance Climate Models. *Rev. Geophys. Space Phys.,* **19**(1), 91-121.

[55] North, G.R et al (1983): Simple energy balance model resolving the seasons and the continents: Application to the astronomical theory of the ice ages. *J. Geophys. Res.,* **88**(C11), 6576-6586.

[56] Nye, J.F (1959): The motion of ice sheets and glaciers: *J. Glaciology,* **3**, 493-507.

[57] Oerlemans, J (1980): Some model studies on the ice age problem. *Koninklijk Netherlands Meterologisch Instituut, De Bilt,* Publicatie No. 158.

[58] Oerlemans, J. (1981): Modelling of Pleistocene European ice sheets: Some experiments with simple mass balance parameterisations. *Quat. Res,.* **15**, 77-85.

[59] Oerlemans, J & N.C Hoogendoorn (1989): Mass balance gradients and climate change. *J. Glaciology,* **35**(121), 399-405.

[60] Oerlemans, J & C.J Van der Veen (1984): Ice Sheets and Climate. *D. Reidel Publ. Co., Dordrecht, Netherlands.*

[61] Oerlemans, J & A.D Vernaker (1981): A model study of the relation between northern hemisphere glaciation and precipitation rates. *Cont. Atmos. Phys.,* **54**, 352-361.

[62] Ohmura, A & N. Reeh (1991): New precipitation and accumulation maps for Greenland. *J. Glaciology,* **37**(125), 140-148.

[63] Parish, T.R. (1984): A numerical study of strong katabatic winds over Antarctica. *Mon. Weath. Rev.,* **112**(3), 849-555.

[64] Parish, T.R & D.H Bromwich (1986): The inversion wind pattern over West Antarctica. *Mon. Weath. Rev.,* **114**, 849-860.

[65] Parish, T.R & D.H Bromwich (1987): The surface wind field over the Antarctic ice sheets. *Nature,* **328**, 51-54.

[66] Parish, T.R and K.T Waight (1987): The forcing of Antarctic katabatic winds. *Mon. Weath. Rev.,* **115**, 2214-2226.

[67] Parish, T.R and G Wendler (1991): The katabatic wind regime at Adelie Land Antarctica. *Int. J. Climatology,* **11**, 97-107.

[68] Paterson, W.S.B (1981): The Physics of Glaciers. *Pergamon Press, Oxford.* 380pp.

[69] Phillpot, H.R & J.W Zillman (1970): The surface temperature inversion over the Antarctic continent. *J. Geophys Res.,* **75**, 4161-4169.

[70] Pitcher, E.J et al (1983): January and July simulations with a spectral GCM. *J. Atmos. Sci.,* **40**(3), 580-604.

[71] Putnins, P (1970): The climate of Greenland. *In: World Survey of Climatology, H.E Landsberg (ed.), Climates of the Polar Regions, S. Orvig (ed.),* Vol.**14**, Ch.2, 3-128.

[72] Radok, U et al (1982): Climatic and physical characteristics of the Greenland ice sheet. *Co-operative Institute for Research in Environmental Sciences, University of Colorado, Boulder, Co.,* Parts **I, II, & III.**

[73] Randall, D.A (1984): Bouyant production and consumption of TKE in cloud-topped mixed layers. *J. Atmos. Sci.*, **41**, 402-413.

[74] Rayment, R & C.J Readings (1974): A case study of the structure and energetics of an inversion. *Q. J. Roy. Met. Soc.*, **100**, 221-233.

[75] Rusin, N.P. (1964): Meteorological and radiational regime of Antarctica, (translated from Russian), *Jerusalem, Israel Program for Scientific Translations.*

[76] Schwerdfeger, W. (1970): The climate of the Antarctic. *In: World Survey of Climatology, H.E Landsberg (ed), Climates of the Polar Regions, S. Orvig (ed.), Elsevier* Vol.**14**, Ch.4, 253-335.

[77] Schwerdfeger, W (1984): Weather and Climate of the Antarctic. *Amsterdam: Elsevier*, 261pp.

[78] Schwerdfeger, W. and L.J. Mahrt (1968a): The relation between terrain features, thermal wind, and surface wind over Antarctica. *Ant. J. U.S,* **3**, 190-191.

[79] Schwerdfeger, W. and L.J. Mahrt (1968b): The relation between the Antarctic temperature inversion in the surface layer and its wind regime. *Proc. of the Int. Symp. on Antarctic Glaciological Exploration, September,* 308-315.

[80] Shinn, R.A & E.J Barron (1989): Climate senstitivity to continental ice sheet size and configuration. *J. Am. Met. Soc.,* **2**(12), 1517-1537.

[81] Slingo, A (1985): Handbook of the meteorological office 11-layer atmospheric general circulation model: Model description. *Met.O 20,* Vol.**1**, DCTN 29.

[82] Stull, R.B (1976a): The energetics of entrainment across a density interface. *J. Atmos. Sci.*, **33**, 1260-1267.

[83] Stull, R.B (1976b): Mixed layer depth model based on turbulent energetics. *J. Atmos. Sci.*, **33**, 1268-1278.

[84] Stull, R.B (1988): An Introduction to Boundary Layer Meteorology. *Kluwer Academic Publishers, The Netherlands.* 666pp

[85] Sugden, D.E (1977): Reconstruction of the morphology, dynamics and thermal characteristics of the Laurentide ice sheet at its maximum. *Arc. & Alp. Res.,* 9(1), 21-47.

[86] Tennekes, H & A.G.M Driedonks (1981): Basic entrainment equations for the atmospheric boundary layer. *Bound. Lay. Met.,* **20**(4), 515-531.

[87] Turner, J.S (1973): Buoyancy effects in fluids. *Cambridge University Press,* 367pp.

[88] Vowinckel, E & S. Orvig (1970): The climate of the North Polar Basin. *In: World Survey of Climatology, H.E Landsberg (ed), Climates of the Polar Regions, S. Orvig (ed.), Elsevier* Vol.**14**, Ch.3, 129-252.

[89] Watson, R.T et al (1990): Greenhous gases and aerosols. *In: Climate change the IPCC scientific assessment., J. Houghton et al (ed.), WMO/UNEP/IPCC, Cambridge University Press.*

[90] Wendler, G (1989): On the blowing snow in Adelie Land, Eastern Antarctica. *In: Glacier Fluctuations and Climate Change, J. Oerlemans (ed.), Kluwer Ac. Press, Dordrecht, Netherlands.* 261-279.

[91] Williamson, D.L et al (1987): Description of the NCAR Community Climate Model (CCM1). *Climate and Global Dynamics Division, National Center for Atmospheric Research, Bouler, Colorado.*

[92] Wyngaard, J.C (1975): Modelling the planetary boundary layer - extension to the stable case. *Bound. Lay. Met.,* **5**, 441-460.

[93] Yamada, T & G Mellor (1975): A simulation of the Wangara atmospheric boundary layer data. *J. Atmos. Sci.*, **32**, 2309-2329.

[94] Zbigniew, S et al (1986): Observational Study of the atmospheric boundary layer over Antarctica. *J. Clim. App. Met.*, **25**, 641-651.

[95] Zeman, O (1979): Parameterisation of the dynamics of stable boundary layers and nocturnal jets. *J. Atmos. Sci.*, **36**, 792-804.

[96] Zeman, O & H Tennekes (1977): Parameterisation of the turbulent energy budget at the top of the daytime atmospheric boundary layer. *J. Atmos. Sci.*, **34**, 111-123.

Appendix A

Glossary of Terms

Ablation The loss of snow or ice from an ice mass, by eg. melting and runoff, evaporation, sublimation, wind erosion, iceberg calving.

Ablation zone The zone of an ice sheet in which the net annual ablation exceeds net annual accumulation.

Accumulation The gain in snow or ice on an ice mass, by eg. precipitation, blown snow from another location, sublimation.

Accumulation zone The zone of an ice sheet in which the net annual accumulation exceeds net annual ablation.

Baroclinic A baroclinic zone exists where lines of constant pressure intersect lines of constant density. Lines of constant density generally coincide with the isotherms, there is thus a temperature gradient along the surface of constant pressure which leads to advection of heat. Mid-latitude cyclones develop in regions of strong baroclinicity.

Climate point The point at which the climate surface intersects with sea level.

Climate surface A theoretical line in the atmosphere along which the mass balance of an ice sheet is zero. The point at which this line intersects the surface of an ice sheet is the ELA.

Dry adiabatic lapse rate The rate of change of temperature of an unsaturated air parcel displaced vertically and adiabatically in the atmosphere. (9.8°C/km).

Elevation desert effect The effect of continentality on precipitation over an ice sheet, which causes accumulation to decrease towards the centre of an ice mass.

Entrainment The mixing of air from above down into the boundary layer.

Environmental lapse rate The rate of decrease of temperature in the atmosphere with height.

Equilibrium Line Altitude (ELA) A theoretical height on an ice sheet at which net annual accumulation equals net annual ablation. It therefore separates the accumulation zone from the ablation zone, (sometimes referred to as the snowline).

Foehn A warm dry wind which flows down the lee side of mountains. It occurs because as the air flows over the mountain, it cools as it rises. This causes condensation and the air continues to cool at the saturated adiabatic lapse rate. Precipitation may occur causing a loss of moisture from the air, so that as it sinks on the lee side of the mountain it warms at the higher dry adiabatic lapse rate

(9.8°C/km)

Geostrophic wind A theoretical wind which blows at a speed which produces a the balance between the coriolis force and the pressure gradient force.

Ice divide The line of the highest points on an ice sheet delineating the ice drainage basin. Ice flows away from the ice divide in more than one direction.

Ice span The distance between the ice divide and the ice margin.

Ice margin The edge of an ice sheet.

Isostasy The equilibrium between the lithosphere (the Earths' crust and upper mantle) and the more fluid asthenosphere below. This causes land masses to rise and fall relative to each other, and relative to sea level, under the influence of large loads, such as may be caused by a large ice sheet or mountain chain.

Lapse rate The rate at which the temperature of an air parcel or at a particular point in the atmosphere, decreases with height.

Mass balance The difference between the ablation and accumulation at a point or for a region or for the whole ice sheet over a specified time interval.

Pit Sites A site on a glacier where a pit is dug, generally a few metres deep a core taken from the base of a pit enables investigation at greater depths. The stratigraphy of the ice is then used to obtain information about glaciological and climatological characteristics such as, the structure of the ice, density, grain size, hardness, annual accumulation, the extent of ablation, and temperature (it has

been shown that the temperature 10m below the surface represents the mean annual air temperature).

Saturated adiabatic lapse rate The rate of change of temperature of a saturated air parcel displaced vertically and adiabatically in the atmosphere. ($\approx$6.7°C/km).

Stable environment An environment which will cause an air parcel which is forcibly lifted, to return to its original position. This requires that the environmental lapse rate is less than the dry adiabatic lapse rate, or less than the saturated adiabatic lapse rate if it is saturated.

Surface temperature gradient This has been used to replace the term 'lapse rate' used in the glaciological literature. It refers to the rate of change in temperature moving downwards along the surface of the ice.

Turbulent Kinetic Energy (TKE) The kinetic energy associated with turbulence, as opposed to the mean kinetic energy that is associated with the mean velocity of flow.

Appendix B

Key to Mathematical Symbols

a	Constant in the parameterisation of mass balance (after Oerlemans 1981).
A	Empirical constant accounting for the radiative properties of the atmosphere.
A_c	Empirical constant in the ET entraiment parameterisation.
A_k	Empirical constant in the ET entraiment parameterisation.
a_e	Fractional loss term due to frictional disipation in the type 1 entrainment.
A_e	$2.a_e$.
Å	Ångström ratio.
B	Empirical constant accounting for the radiative properties of the atmosphere.
B	radiative cooling in the slab model in $K.ms^{-1}$, $\left[\frac{R_n}{\rho C_p}\right]$.
b	Constant in the parameterisation of mass balance (after Oerlemans 1981).
C_{du}	Drag coefficient for the U component of flow.
C_{dv}	Drag coefficient for the V component of flow.
C_f	Temperature at the base of the ice sheet after Hindmarsh et al (1989)¿
C_p	Specific heat capacity (used by North et al 1983).
$C(\hat{r})$	Effective heat capacity.
d	Fractional loss term due to frictional disipation of shear generated

turbulence in the type 2 entrainment.

d_1 Depth of the shear layer for the Stull (1976a) entrainment.

D 2.d.

D_c Diffusion coefficient for heat transport.

E Entrainment coefficient.

E_r Radiant emittance.

f Coriolis parameter.

G Mass balance.

h_b Height of the lower boundary of the entrainment zone.

h_d Height of ice sheet at the divide.

h_s Height of the surface shear layer.

h Scaled depth of the boundary layer.

h_e Depth of the entrainment zone.

h_1 Initial depth of the boundary layer at the top of the slope.

H Height above the surface which is unaffected by katabatic flow.

H_e Distance from the ELA in Hindmarsh (1989).

H_i Height of ice above the level of the margin.

H^* height of ice above sea level, (Oerlemans 1981).

k Von karman constant.

K Constant in type 1 parameterisation of entrainment.

K_{diff} Constant in type 2 parameterisation of entrainment.

K_m Vertical diffusion coeficient.

L Total loss term for TKE.

L_i Integral of L over the boundary layer depth h.

m Mass of air parcel.

n axis normal to the $s - y$ plane.

n_g Constant defined by Glens' Flow Law for ice.

N^2 Brunt-Vaisalla buoyancy frequency.

$\delta^{18}O$ Ratio of the concentration of heavy oxygen $18O$ to the lighter isotope ^{16}O.

p_* Surface pressure of the Met.O model.

$p - p_a$ Pressure depth of the boundary layer.

q^2 Turbulent kinetic energy per unit mass in $m^2 s^{-2}$.

$Q(H_e)$ Accumulation function from Hindmarsh et al (1989).

Q_0 Turbulent heat flux from the ground.

δQ Milankovitch radiation variations.

r unit vector position on the Earths' surface.

R_N Net LW radiation.

$R_\downarrow$ downward SW radiation.

$R_\uparrow$ upward LW radiation.

Ri_c Critical Richardson number for the U component of flow.

$\mathbf{Ri}$ Richardson number for the layer.

s axis of slab model parallel to line of maximum slope.

s_p Span of an ice sheet.

S Solar constant.

S_d Solar insolation distribution function.

S_1 Profile factor associated with the thermal wind in the boundary layer.

S_2 Profile factor associated with the distribution of buoyancy in the boundary layer.

S_3 Profile factor associated with the vertical velocity in the boundary layer.

t Time.

T Temperature.

u Flow component along the s-axis.

U Mean layer velocity along the s-axis.

$|\overline{\mathbf{U}}|$ Mean layer resultant velocity.

U_1 Initial mean layer velocity along the s-axis at the top of the slope.

$\Delta \mathbf{U}_H$ Resultant velocity change between h_b and H.

v Flow component along the y-axis.

V Mean layer velocity along the y-axis.

V_1 Initial mean layer velocity along the y-axis at the top of the slope.

Vg Geostrophic wind speed along the y-axis above the boundary layer.

W_e Entrainment velocity.

x horizontal distance.

δx Change in position of the climate point.

y axis perpendicularly to the left of the s-axis.

y_i Circumference of the ice sheet.

α Albedo.

α_f Meteorological feedback parameter (after Hyde & Peltier 1985).

γ stability of the atmosphere. $\left[\frac{d\theta}{dz}\right]$.

ϵ Emissivity of the atmosphere.

ε Rate of production of turbulent kinetic energy in $m^2 s^{-3}$.

ε_0 Rate of generation of turbulent kinetic energy in the surface layer.

θ Potential temperature.

θ_{bl} Average temperature in the boundary layer.

θ_{br} Average reference temperature within the boundary layer. (see fig. 4.5)

θ_r Reference temperature at the top of the slope.

$\Delta\theta$ Temperature deficit in θ_{br} in the boundary layer.

λ_s Sine of the latitude.

ρ Density.

σ Vertical co-ordinate of the Met.O model.

σ_{sb} Stefan Boltzman constant.

τ Shear stress.

τ_a Transmissivity of the atmosphere.

τ_f Timescale of frictional disipation.